Remote sensing of the Northwest African upwelling

and its production dynamics

Dissertation zur Erlangung des

Doktorgrades der Naturwissenschaften

am Fachbereich 5 – Geowissenschaften

der Universität Bremen

Gutachter:

Herr Prof. Dr. Gerold Wefer

Herr Prof. Dr. Venugopalan Ittekkot

vorgelegt von Peer Helmke

Bremen, Dezember 2003

Tag des Kolloquiums: 2 Februar 2004

Gutachter:

Herr Prof. Dr. Gerold Wefer

Herr Prof. Dr. Venugopalan Ittekkot

Prüfer:

Herr Prof. Dr. Helmut Willems

Frau Prof. Dr. Katrin Huhn

Inhaltsverzeichnis

Abstract

The North Atlantic off NW Africa is characterized by the trade wind induced upwelling of cold and nutrient rich waters. As one of most strongest eastern boundary upwelling areas it is marked by low sea surface temperature and high bio-production, both subject to strong seasonal and interannual variations.

Satellite measurements of sea surface temperature (SST) and chlorophyll-*a* (Chl-*a*) in the upper water-column were used to (a) recognize the upwelling of deep water and its distribution and mixing in the surface, (b) identify the development of phytoplankton blooms and (c) provide further insights in the characteristics of its variations.

The spatial structure of the Cape Ghir filament – a recurring patterns of westward transported high Chl-*a* concentration – was classified and correlated to distinct pattern of wind forcing. This was done to evaluate the usability of the Cape Ghir filament as a proxy parameter for variations in wind forcing and climate.

Measurements of surface Chl-*a* were compared to deep-sea fluxes of organic carbon in order to determine the relationship between both parameters and to further calculate the export of C_{org} and the export variation strength.

The upwelling intensity and variation were studied from the oscillation of SST and Chl-*a*. Each parameter was used with its own allocated definition-set for 'upwelling'. In the SST-based study, upwelling was defined as the area where the near-coast SST was 3.5 K below an off-shore reference temperature at the corresponding latitude. When using chlorophyll-*a* as a proxy for upwelling, the area with a Chl-*a* concentration $> 1\text{mg m}^{-3}$ was defined as a high chlorophyll-*a* zone (HCZ). To find the link between surface and deep ocean the source area was determined where the concentration of Chl-*a* in the surface ocean has the highest correlation with C_{org}-flux in the deep sea as measured by the sediment trap. The regression between the Chl-*a*-signal in the area of highest correlation, assumed to be an approximation to the source region of marine particles sampled with the sediment trap, and the trapped C_{org}-concentration served as an empirical export model for organic carbon. The export model was applied to the HCZ off Northwest Africa to calculate upwelling-driven export of organic carbon.

We used 9 and 1 km-resolution satellite data in order to categorize mesoscale patterns and processes such as the Cape Ghir upwelling filament. From this data-base five major groups of filament structures were established on the basis of filament extension, filament axis and types of vortices.

Abstract

The off-shore extension of SST-defined upwelling from 1988 through 1999 between 18° and 25°N shows maxima in January and May/June with an average area of 140,000 km^2 (standard deviation of 20,000 km^2). Minima in August exhibit an extension of 43,000 km^2 (15,000 km^2 standard deviation). A correlation between SST and North Atlantic Oscillation (NAO), previously found in global studies from the North Atlantic, was not discovered in this local-to-regional investigation. On a small-scale-view the upwelling development exhibits a highly variable nature. Local patches of low upwelling intensity exist even in above average years of upwelling. The time period fall 1998 - summer 1999 stand out because of unparalleled strong upwelling not correlated with strong positive NAO, although the opposite should be expected. An intense El Niño-event followed in the Pacific Ocean whose long-distance effects are assumed to have influence, for instance, on the SST in the Atlantic. The period of strong upwelling in 1998-99 is recognized in the SST record and Chl-a-concentration, and also calculated with the C_{org}-export model. The yearly mean value of C_{org} exported from the HCZ is ca. 1.5 Tg while increased to ca. 2.62 Tg from August 1998 to July 1999. The export increase was caused by an expansion of the HCZ rather than by an increase of the mean Chl-a-concentration in the surface water. During this outstanding period, the derived C_{org}-export from the HCZ to a 1000 m-depth level did not significantly differ from the four year mean (20.6 mg m^{-2} d^{-1}).

The correlation analysis between C_{org}-export and its relationship to the sea-surface Chl-a reveals a region which more accurately represents variations in C_{org}-flux (r = 0.74) than rectangular boxes in the vicinity of trap locations elsewhere do (r = 0.52). The enhanced relation increased the export-model quality.

Different structure-types of the Cape Ghir filament were assigned to distinct forcing situations. It was recognized that the main axis of the filament moved from southwest westward during enhancing along-shore wind-stress. The spatial filament distribution agrees with the enhanced abundance of the upwelling-indicator foraminifer *Globigerina bulloides* in underlying surface sediments. This indicates that the actual upwelling spatial dynamics resembles that of the last 500 – 1000 years.

The spatial upwelling pattern reacts sensitively to changes in forcing and can therefore be used as a qualitative indicator for changes in the wind-system.

Zusammenfassung

Der Nordatlantik vor der Küste Nordwest Afrikas wird durch den von Passatwinden induzierten Auftrieb kalten, nährstoffreichen Wassers gekennzeichnet. Als eins der weltweit aktivsten Ostküsten-Auftriebsgebiete, ist es geprägt durch niedrige Temperaturen an der Meeresoberfläche und hohe Bioproduktion, wobei beide Merkmale starker saisonaler und interannueller Schwankung unterliegen.

Satellitenmessungen der Oberflächenwassertemperatur (SST) und des Chlorophyll-*a* (Chl-*a*) Gehaltes der oberen Wasserschicht wurden verwendet um den Zustrom von Tiefenwasser und dessen Verteilung an der Oberfläche zu erkennen, die Entstehung von Planktonblüten zu identifizieren und weitere Einblicke in die Charakteristik der Variationen zu gewinnen.

Die räumlichen Strukturen des Kap Ghir Filamentes – eines wiederkehrenden Musters nach Westen transportierter hoher Chl-*a*- Konzentration – wurden klassifiziert, mit Windantriebsmustern und Sedimentverteilungen verglichen. Es sollte damit die Nutzbarkeit des Filaments als Anzeiger für Wind- bzw. Klimaänderungen untersucht werden.

Messungen von Oberflächen Chl wurden mit dem Fluss organischen Kohlenstoffs in die Tiefsee in Verbindung gesetzt, um das Maß des Zusammenhanges zu bestimmen, die Menge des C_{org}-Exports zu kalkulieren und die Stärke der Export-Variation zu ermitteln. Die Stärke und Variation des Auftriebs wurde dann anhand der Schwankungen der beiden Parameter, SST und Chl-*a*, betrachtet. Für beide Parameter wurden eigene Bedingungen für die Definition von Auftrieb genutzt. Bei der SST-basierten Untersuchung wurde Auftrieb als der Bereich definiert, in dem die küstennahe SST 3,5 K unter der des offenen Ozeans auf gleicher Breite lag. Bei der Untersuchung der Chl-Konzentration wurde ein Bereich von über 1mg m^{-3} als Auftrieb bzw. Zone hoher Chlorophyll-Konzentration (HCZ) definiert.

Um Aussagen über die Verbindung von Ozeanoberfläche und Tiefsee treffen zu können, wurde die Zone bestimmt, an der die Chl-Konzentration der Wasseroberfläche am besten mit C_{org}-Fluss in der Tiefsee, gemessen an Sedimentfallenproben, korreliert. Die Regression zwischen dem Chl-Signal dieser als Quellregion angenommenen Fläche und der C_{org}-Reihe der Sedimentproben, diente als Exportmodell organischen Kohlenstoffs. Das Exportmodell wurde auf die HCZ vor Nordwestafrika angewendet um den auftriebsgesteuerten Kohlenstoffexport zu kalkulieren.

Für die Einstufung mesoskaliger Muster und Prozesse, wie dem Kap Ghir Filament, wurden nicht nur 9 km Chl Daten, sondern auch Messungen in 1 km Auflösung genutzt. Das

Kap Ghir Filament wurde anhand seiner Ausdehnung, der Ausdehnungsachse und der Struktur von Wirbeln in fünf Hauptgruppen klassifiziert. Die Ausdehnung des SST-definierten Auftriebs in den Jahren 1988 bis 1999 zwischen 18° N und 25° N, zeigt Maxima im Januar und Mai/Juni von durchschnittlich 140.000 km^2 bei einer Standardabweichung von 20.000 km^2. Das Minimum von 43.000 km^2 (Standardabweichung 15.000 km^2) liegt im August. Eine Korrelation zwischen SST und Nordatlantischer Oszillation (NAO), wie sie in globalen Untersuchungen für den Nordatlantik gefunden wird, konnte auf lokaler bis regionaler Skala nicht festgestellt werden. Die Entwicklung des Auftriebs zeigt bei kleinräumiger Betrachtung eine hohe Variabilität, so dass auch in Jahren überdurchschnittlich intensiven Auftriebs lokale Felder geringen Auftriebs existieren. Die Periode Herbst 1998 bis Sommer 1999 zeichnet sich durch außergewöhnlich starken Auftrieb im Sinne der oben genannten Definition aus. Sie liegt zwar nicht in einer stark positiven NAO-Phase, während der man verstärkten Auftrieb annehmen würde, folgt jedoch einem starken El Niño-Ereignis, welches ebenfalls durch Fernwirkung Einfluss auf den Atlantik ausüben kann.

Diese Periode starker Auftriebsaktivität 1998/1999 zeigt sich ebenso in der Untersuchung der Chl-*a*-Konzentration und des abgeleiteten C_{org}-Exports. Dem durchschnittlichen jährlichen C_{org}-Export aus der HCZ von 1,5 Tg steht ein Export von 2,62 Tg C_{org} im Jahreszeitraum August 1998 bis Juli 1999 gegenüber. Die Steigerung des Exports kam in diesem Zeitraum durch eine Ausdehnung der HCZ zustande und nicht durch höhere durchschnittliche Chl-Konzentration. Der abgeleitete Export von C_{org} aus der HCZ auf ein Niveau von 1000 m Tiefe wich in diesem Zeitraum nicht signifikant vom Vierjahresmittel (20,6 mg m^{-2} d^{-1}) ab.

Durch die Korrelationsanalyse des Zusammenhangs von Wasseroberfläche und C_{org}-Sedimentation konnte eine Region gefunden werden, die die Variationen im C_{org}-Fluss besser repräsentiert (r = 0,74) als es rechteckige Regionen in Fallennähe tun, wie sie in bisherigen Untersuchungen als Quellregion angenommen wurden (r = 0,52). Dieses verbessert die Qualität des Export-Modells.

Die Strukturklassen des Kap Ghir Filaments konnten spezifischen Antriebssituationen zugeordnet werden. Es zeigte sich, dass die Hauptachse des Filaments mit steigendem küstenparallelen Windstress von SW auf W rotiert.

Die Verteilung der Filamente stimmt mit dem Muster erhöhter Konzentration der auftriebsanzeigenden Foraminiferenart *Globigerina bulloides* in Sedimentoberflächen überein. Dies ist ein Anzeichen dafür, dass das Auftriebsgeschehen in den letzten 500-1000 a ähnlich dem heutigen war.

Das Muster des Auftriebs reagiert sensibel auf veränderlichen Antrieb und kann deshalb als qualitativer Anzeiger für Änderungen des Windsystem genutzt werden.

Introduction

Geology has been dealing with the solid third of the earth's surface. Slowly it has been recognized that the complete picture of the Earth could not be drawn without taking into account the other two thirds, namely the oceans. In addition, it is evident that different life forms occure in certain regions of the oceans. Subtropical gyres for example have been compared with deserts due to their nutrient-limitation whereas upwelling areas have been declared as the 'rainforests of the sea'. Oceanic productivity has proved to be as variable as that of the Earth's surface. As more and more life is found in the deserts of the earth, the categorization into 'deserts' and 'rainforests' concerning oceans becomes even more relative, and the input of the gyres is taken into account for global marine production. Regions like gyres and upwelling areas are not strictly separated from each another. Fronts do exist in which the exchange is limited, but it does take place. Eddies penetrate [*Williams and Follows*, 1998] or jet streams cross these fronts, thus generating an exchange between the systems and influencing their biogeochemistry. The understanding of marine biogeochemical cycles is one focus of modern marine geology, although is not restricted to its own discipline. It interacts more and more with other disciplines, like meteorology, climatology and oceanography which help to understand biogeochemical cycles.

From today's point of view, important properties are the volume and speed of gas exchange between the water surface and atmosphere. This gas exchange, as well as the composition of species in surface waters and their growth is modulated by the strength and frequency of the variability of their habitat. Gas exchange and production of biomass are one part of the (marine) carbon cycle that will be portrayed in the following chapter.

The global carbon cycle

The ocean contains more than 90% of the carbon involved in the global carbon cycle. The concentration of atmospheric CO_2 is mainly controlled by the ocean. Two natural processes, the 'solubility pump' and the 'biological pump' keep the concentration of CO_2 in surface waters, and hence also in the atmosphere, lower than those in the deep ocean. Without these 'pumps' the CO_2 concentration in the atmosphere would be manifold higher than it is now. In the natural carbon cycle downward transport is balanced by the slow upward transport induced by diffusion and mixing of water masses. The largest part of the ocean deep water sinks in relatively small areas: on the edge of Antarctica and in the polar North Atlantic. The water sinks into deeper layers because of its low temperature and the high density resulting from it. Since CO_2 possesses a good solubility in cold water, concentrations of dissolved CO_2 are highest in deep water.

Through the 'solubility pump' the sinking water is transported into the deeper ocean. It takes between 500 and 1000 years before the deep water re-enters the ocean surface through global ocean circulation. For this time span the soluted CO_2 is excluded from the terrestrial-atmospheric carbon cycle.

During photosynthesis CO_2 is taken up by phytoplankton and transformed into organic carbon. This process is called 'primary production' because organic material is synthesised from inorganic compounds such as CO_2 and nutrients. The organic carbon passes through the marine food chain or is decomposed by bacterial respiration in near-surface layers into its inorganic compounds. As a global mean, 1-3 % of C_{org} sinks from the mixed surface layer into deeper parts of the ocean and is thus temporarily excluded from the carbon cycle. This process is known as the biological pump. Understanding and quantifying the export of organic carbon into the deep sea is an essential part in the comprehension of the carbon cycle.

The 'carbonate pump' is closely associated with the biological pump. It comprises the production of calcium carbonate through calcifying algae and animals like coccolithophorids and foraminifers. As a by-product of photosynthesis calcium carbonate is precipitated mainly in the form of calcite, aragonite and magnesium-calcite, and built into organism skeletons. The calcification uses bicarbonate ions for reduction resulting in the freeing of CO_2, following the equation:

$$Ca^{2+} + 2HCO_3^- <==> CaCO_3 + CO_2(g) + H_2O.$$
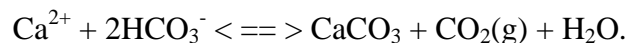
The calcium carbonate sinking into deeper layers is again dissolved and is converted into bicarbonate. The export of calcium carbonate to the deep sea therefore releases CO_2 at the ocean surface. The indirect transport of CO_2, which partly supersedes the effect of the biological pump, constitutes the carbonate pump. Because of this, budgeting of ocean surface CO_2 is not possible solely by observing organic carbon production. A way to explain this is by calculating the export ratio of organic to inorganic carbon (the 'carbon rain ratio').

In the carbon cycle CO_2 permanently moves from the atmosphere into the ocean and vice versa. Averaged over a whole-year cycle and the global ocean surface the total flux into and out of the ocean should be roughly in equilibrium. It is generally assumed that this was the case during pre-industrial times [*Indermuhle et al.*, 1999; *Sarmiento and Toggweiler*, 1984]. In some areas like the equatorial Pacific, the outgassing of CO_2 exceeds the dissolution while in temperate and higher latitudes of the Northern Hemisphere the flux into the ocean water predominates [*Gloor et al.*, 2003; *Takahashi et al.*, 2002]. In other regions the flux direction is

seasonally determined. Warmer temperatures promote outgassing while colder water supports the solution of CO_2. The rate of CO_2 uptake or emission also depends on the local wind velocity, the ocean surface roughness, and mixing of the surface ocean layer [*Volk and Hoffert*, 1985]. At the direct ocean-atmosphere interface, a submillimetre water layer exists which equilibrates very rapidly with the atmospheres CO_2-concentration. If the layer is disturbed, an ocean-atmosphere-gradient exists and outgassing or uptake can take place.

Carbon dioxide differs from other gases dissolved in the ocean water, such as N_2 and O_2, because of its capacity to react with water molecules to form bicarbonate and carbonate-ions. The solubility of these ions in water is much higher than that of CO_2. Due to this reaction sea water can take up ca. 100 times the amount of CO_2 than if the reaction did not take place.

The dynamic equilibrium of the natural carbon cycle was disturbed by anthropogenic influence. Since the early industrialisation period in the 1830s, the CO_2 concentration in the atmosphere increased from 280 to 373 ppm. The increase of 33 % means an enrichment of atmospheric carbon by 190 Pg carbon or 703 Pg CO_2 (1 Pg = 10^{15} g) [*Houghton et al.*, 2001; *Siegenthaler and Sarmiento*, 1993]. Today the ocean-atmosphere CO_2 concentration is in disequilibrium due to the anthropogenic emission of CO_2. Each year about 2 Pg carbon are taken up by the oceans, hence dampening the atmospheric CO_2 increase. Finding out in which direction the uptake capacity of the oceans develops in the coming decades and how the ocean biochemical cycles react to the increasing CO_2 concentration are key issues of current climate research.

Main objectives

The main goal of this thesis was to study upwelling dynamics and to examine the upwelling reaction to atmospheric forcing as apart of climate which, to an increasing degree is beeing recognized as highly variable. The analysis was combined with deep-sea particle flux measurements in order to determine conclusions on upwelling-induced carbon export.

Manuscript 1: Synoptic view on the Cape Blanc upwelling area on the basis of 12-years remotely sensed sea surface temperature

The characterization of seasonal and interannual variability was the aim of the evaluation of satellite-born SST measurement during a twelve-year period in the trade wind dominated upwelling off Northwest Africa. The observation of surface SST patterns provides insights about the physical effects of near-surface wind forcing. The impact of colder subsurface water is shown which is 'drawn' up to the surface from deeper parts of the water column by the wind

induced westward transport of surface waters. The mixing of cold, deep water with warmer surface water during turbulent mixing processes at the surface is also observable.

Since 1960 it is known that the winter circulation pattern of the subtropical atmosphere above the Atlantic in particular depends on the position and strength of the Iceland Low and Azores High [*Bjerknes*, 1964]. The influence of the rhythmically-appearing North Atlantic Oscillation (NAO) on the subtropical Atlantic SST has been demonstrated by several studies [*Frankignoulle*, 1999; *Osborn et al.*, 1999; *Paeth et al.*, 2003; *Peng et al.*, 2002].

In order to identify a possible NAO influence on the upwelling pattern by means of varying trade wind intensities, the small-scale empirical relation of NAO and winter SST was examined off Northwest Africa.

Manuscript 2: Dynamics of the Cape Ghir filament off Northwest Africa

The upwelling of deeper water at the west coasts of continents is normally not a uniform phenomenon. Short-term fluctuations of wind intensity and direction lead to temporary appearance of local upwelling cells, partly strong focussed surface currents and whirls. These phenomena can be observed particularly from the biological reaction to nutrient input by the upwelled water. When nutrient-rich, deep water mixes with warm surface water in the euphotic zone a phytoplankton bloom can develop. The increased plankton Chl-*a* can then be tracked with an ocean-colour sensor even if the SST contrast vanished and the upwelled water can not be differentiated by temperature sensors.

In this study rapid biophysical reaction of the upwelling system to the forcing situation was used as an indicator for short-term fluctuations in the trade wind system.

A wealth of current-patterns developing at the coast of Morocco at Cape Ghir was categorized and assigned to distinct wind-forcing situations.

Manuscript 3: Northwest African upwelling and its effect on off-shore organic carbon export to the deep-sea

A further objective was to quantify C_{org} sedimentation to the deep sea and its temporal and spatial variation, and to determine the degree of dependence of C_{org}-sedimentation patterns from the surface Chl-*a* concentration. Export of organic carbon from the surface to the deep sea is

another important section in the marine carbon cycle. Hence, the total amount of C_{org}-export to the deep ocean was calculated from a locally fitted regression model.

For an actualistic approach to interpret paleoceanographic results it is necessary to closely estimate the organic carbon export. A further important aspect is the possibility to sequestrate atmospheric CO_2 and to exclude it from the carbon cycle by sedimentation. These processes are significant when regarding anthropogenic CO_2 input into the atmosphere.

Study area

Topography
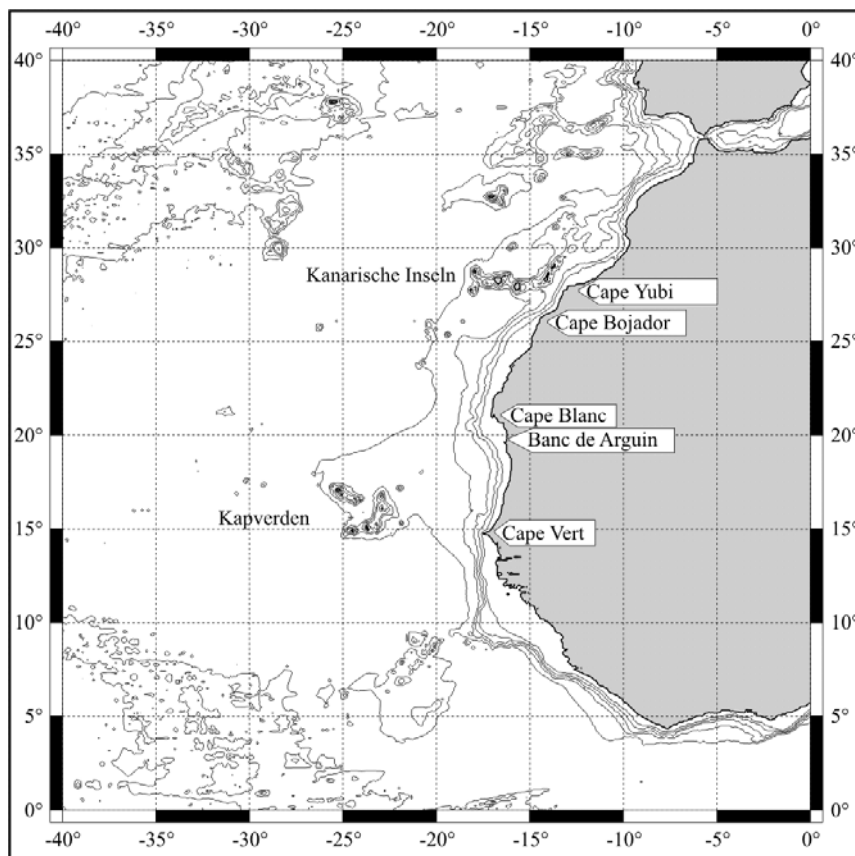
Figure 1. Study area

The study area is located off the coast of Northwest Africa between 5° - 36°N and 5° - 36°W. It includes the shelf, continental margin and the open ocean from Gibraltar in the north down to the southernmost tip of Liberia in the south. The coastline is structured by several capes, Cape Ghir (31°N), Cape Yubi (28°N), Cape Bojador (26°N), Cape Blanc (21°N) and Cape Vert at 15°N. Two groups of islands lie offshore, the Canary Islands at 27° - 29°N and the Cape Verde Islands at 14° - 18°N (Figure 1.).

Both archipelagos are of volcanic origin [*Thorne et al.*, 2003 in press]. The shelf – up to 200 km wide (south of Cape Vert) - and a gently sloping continental margin form the transition from the African continent to the Canary and Cape Verde Basins east of the mid-Atlantic ridge.

Wind-system

In the main part of the study area between 10° and 30°N, the near-surface wind system is controlled by the northeast trade winds as a part of the Hadley-Circulation. North of 30°N the exact position of a zonal belt of high pressure cells with low surface winds is determined by the location of the Azores High. The anticyclonic rotation of air out of the Azores High leads to north-easterly winds at the African coast even north of 30°N. South of 15°N the sphere of influence of the Intertropical Convergence Zone (ITCZ) begins, which describes the border between the northeast and southeast trade winds. In boreal summer, when the ITCZ is at 13°-15°N and the southeast trade winds are crossing the equator northwards, they are deflected by the Coriolis-force eastward and become the southwest monsoon [*Ramage*, 1971]. The coast south of Cape Vert is affected by southerly winds and upwelling is thus suppressed.

During boreal summer large amounts of dust are carried out of the Sahara and Sahelian in some 1.5 to 5 km height by the Saharan air layer (SAL) westward over the Atlantic ocean [*Swap et al.*, 1996; *Torres-Padrón et al.*, 2002]. A part of the dust enters the ocean and promotes phytoplankton growth due to the input of iron as an often limiting micro-nutrient [*Moore et al.*, 2002; *Sarthou et al.*, 2003].

Oceanography

The main current system in the open North Atlantic ocean is the North Atlantic subtropical gyre. The northern part, the Azores current, feeds the Canary Current which is a broad eastern boundary current moving at 10-30 cm s^{-1} along the African coast from Morocco equatorward [*Batteen et al.*, 2000; *Wooster et al.*, 1976]. At 15°N the Canary Current detaches from the coast and flows westward under the influence of the Equatorial Countercurrent coming from the south. Both currents flow in the same direction, but due to their different speeds an anti-cyclonic gyre exists south of the detachment. The size and position of the gyre is determined by the seasonally varying strength of Canary and Equatorial Countercurrents.

Along-shore winds in the trade wind belt lead to a 50-70 km wide band of intensive upwelling [*Hagen*, 1981]. North Atlantic Central Water of 200–400 m depth is the source for upwelling water north of Cape Blanc. South of Cape Blanc the source merges with the more

nutrient-rich, northward-flowing South Atlantic Central Water [*Barton*, 1998]. At the surface the upwelled water mixes with the Canary Current and is transported southwestward. Especially at the confluence of the Canary Current and Equatorial Countercurrent, upwelling signals in the form of plankton blooms can be transported far off-shore.

Material and Methods

Sea surface temperature data

Water surface temperatures used in this study where sensed by several infrared sensors operational since 1978 by several NOAA satellites (National Oceanic & Atmospheric Administration). On a plane nearly perpendicular to the equator plane, the satellites encircle the earth in 102 minutes or 14.1 times per day. The local solar time for the equator plane crossing remains approximately the same from day to day. On a time-scale of years, however, the solar time drifts and leads to changing irradiance conditions during the scan what makes the comparison of multi-year measurements more difficult [*Price*, 1991]. The orbital plane, on which the satellites circle the earth, rotates each orbit 25.5° relative to the 0° meridian. From an altitude of 833 km nearly each point of the earth is observed daily.

The actual orbital parameter varies slightly between the satellites of the NOAA series. Values cited here refer to the NOAA-15 launched at 13.05.1998.

The Advanced Very High Resolution Radiometer (AVHRR) onboard the satellites continuously scans a 2399 km wide swath. The satellite reflects the information as direct broadcasting in the highest possible resolution of 1.1 km near the equator (High Resolution Picture Transmission = HRPT). Ground receiving stations can receive data as long as they are in the transmission area of the satellite.

Onboard the satellite, the HRPT data volume is reduced numerically to 1/15 of global area coverage (GAC). A whole orbit of GAC data is saved until the satellite reaches one of the NOAA Command and Data Acquisition (CDA) stations located near Fairbanks, Alaska, and Wallops Island, Virginia, USA: Only about 11 minutes of one orbit can be saved onboard the satellite in highest resolution, to be read out later by a CDA. HRPT data which were not received and saved by one of the world-wide stationary or mobile ground receiving stations, such as the *RV Polarstern*, are definitely lost. This point is stressed here in detail to preclude the common misunderstanding that high resolution data would be available for each location; it is only the case if previously recorded. The same problem arises with the recording of Sea-viewing Wide Field-of-View Sensor (SeaWiFS) data (see below).

The AVHRR sensor detects radiation on six spectral bands from which one is in the range of visible light and five bands covering the infrared (Table 1, Figure 2). Position of channel 4 and 5 is selected to reside in the infrared (IR) where a determination of SST is possible and on the other hand to fit in 'windows' of atmospheric Transmission (Figure 2).

Table 1. Position and application of AVHRR channels

AVHRR/3 channels			
Channel	Resolution at Nadir	Wave-length(nm)	Typical use
1	1,09 km	580 - 680	Daytime cloud and surface mapping
2	1,09 km	725 - 1000	Land-water boundaries
3A	1,09 km	1580 - 1640	Snow and ice detection
3B	1,09 km	3550 - 3930	Night cloud mapping, sea surface temperature
4	1,09 km	10300 - 11300	Night cloud mapping, sea surface temperature
5	1,09 km	11500 - 12500	Sea surface temperature

Different algorithms to calculate SST from IR measurements have been established over the years but only the 'Pathfinder' algorithm is briefly mentioned here [*Evans and Podestá*, 1998; *Smith et al.*, 1996].
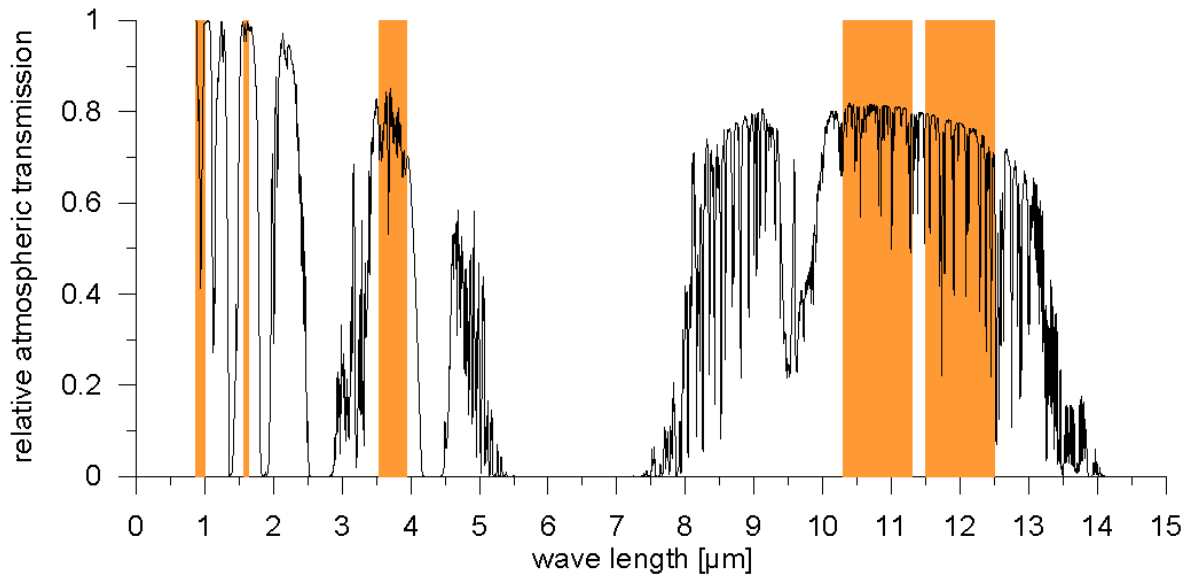
Figure 2. Position of AVHRR channels (orange boxes) and atmospheric transmission (solid line, Transmission pers. com. David Rabanus, I. Phys. Institut, Univ. zu Köln, 11.2003)

Mainly short-wave radiation enters the Earth's surface. The ocean receives the energy and emits long-wave radiation as near black-body radiation. Without the disturbance of the atmosphere, the SST could be calculated directly from the IR channels which detect the emitted long-wave radiation. Ozone, water vapour and aerosols in the atmosphere, however, attenuate the long-wave radiation and change their spectrum. It is the main task of the Pathfinder algorithm to correct for these alterations.

$$SSTsat = a + b\,T4 + c\,(T4 - T5)\,SSTguess + d\,(T4 - T5)\,(\sec(rho) - 1),$$

where SSTsat is SST derived from satellite measurements, T4 and T5 are the IR measurements of AVHRR-channels 4 and 5, SSTguess is an *a priori*-estimation of SST and rho is the zenith-angle of the satellite from which the distance from sensor to the point of measurement depends and is therefore the strength of perturbation. Coefficients a, b, c and d were determined by monthly regression analyses from satellite and *in situ* measurements [*Evans and Podestá*, 1998]. Water is nearly opaque for IR radiation, that means that the emitted long-wave radiation results only from the upper micrometers of the water surface and represent their temperature. Within wind velocities up to 10 m/s, a sub-millimetre thin laminar layer exists at the water/air boundary whose temperature can differ from the water bulk temperature (skin effect).

The mean deviation of the skin layer is given as 0.11 K [*Horrocks et al.*, 2003]or even smaller down to nearly zero for afternoon overpasses [*Minnett*, 2003]. Especially in upwelling

areas, frequent intense winds prevent a strong skin effect. Through atmospheric correction and permanent comparison with *in situ* measurements, the Pathfinder dataset reaches an average accuracy of 0.3 K [*Vazquez*, 1999].

SST data used in this study were exclusively received from the NASA Physical Oceanography Distributed Active Archive Center, Jet Propulsion Laboratory, California Institute of Technology, USA (po.daac, podaac.jpl.nasa.gov). They are available in certain different temporal and spatial resolutions from which the daily data were used (global coverage, 9 km nominal resolution, ascending node, type: Equal Angle Best SST data). At the po.daac the data files are stored in Hierarchical Data Format (HDF), which facilitates the storage of several data-sets along with meta-data such as pixel size, spatial resolution, algorithm version, processing date, and quality of information in one file. This makes it easier to keep track of the data source and quality. The software package Interactive Data Language (IDL®) and free available software from National Center for Supercomputing Applications, University of Illinois, USA (NSCA, hdf.ncsa.uiuc.edu) were used for data read out and processing.
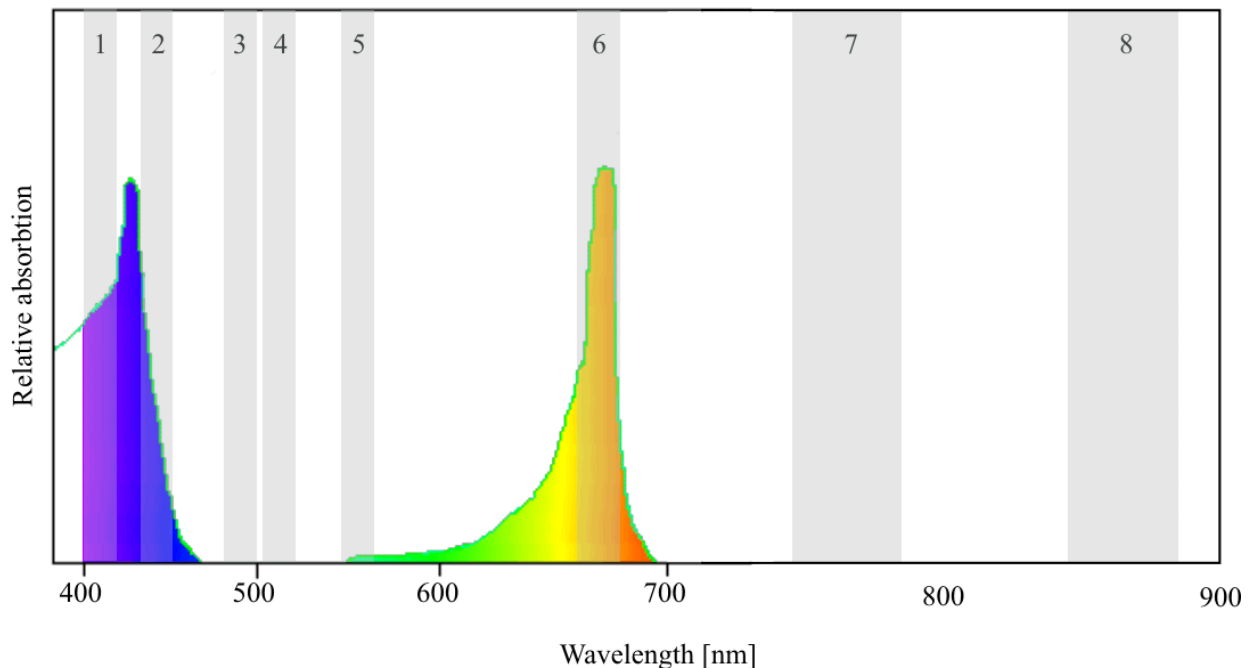

Figure 3. Position of SeaWiFS channels and Chlorophyll-*a* absorption spectrum

Chlorophyll-*a* -measurements and processing

Besides SST, the Chl-*a* concentration is an important parameter for characterizing upwelling. Along with carotene, lutein and phycocyanobilin, Chl-*a* is one of the most important

photopigments for photosynthesis. Chl -*a* absorbs light in the yellow/orange and blue spectral bands and produces glucose as a building block of organic matter.

Chl-*a* absorption results in a shift towards green of the light spectrum emitted by the ocean. The Chl-*a* algorithm 'OC4' applied to data used here calculates surface water Chl-*a* concentration from the differences between SeaWiFS channels 2, 3 and 4, and channel 5 [*O'Reilly et al.*, 2000].

The SeaWiFS sensor, operational since September 1997, is installed onboard the OrbView-2 satellite. Orbital parameters of OrbView-2 are similar to those of the NOAA series, likewise circular, sun-synchronous, near-polar orbit with 98.2° inclination and 705 km height. The time of equatorial plane crossing however does not undergo a drift but is kept constant to 12:00±20 local solar time which makes inter-year comparisons easier.

SeaWiFS detects radiation emitted by the earth on six spectral bands of 20 nm width in the visible spectrum and on 2 bands of 40 nm width in the near infra-red (Figure 3). Different spatial resolution products are calculated onboard the OrbView-2 as they are an the NOAA satellites. In direct picture transmission of HRPT data the nominal resolution is about 1.13 km. Recorded GAC data has 4.5 km resolution (for further description of HRPT, LAC and GAC format see chapter 'SST data' and *McClain* [1992]).

Table 2. Position und application of SeaWiFS channels

SeaWiFS channels			
Channel	Wave-length (nm)	Color	Primary Use
1	402-422	violet	Yellow substance and turbidity
2	433-453	blue	Chlorophyll absorption maximum
3	480-500	blue-green	Chlorophyll and other pigments
4	500-520	blue-green	Turbidity, suspended sediment
5	545-565	green	Chlorophyll, suspended sediment
6	660-680	red	Chlorophyll absorption
7	745-785	near IR	O_2 absorption
8	845-885	near IR	Aerosol optical thickness, vegetation, water vapor reference over the ocean

Chl-*a* data must be corrected for atmospheric effects of water vapour, aerosols and ozone in the same way that AVHRR IR measurements are. In contrast to IR, the signal for the determination of Chl-*a* concentration in the visible spectrum results not only from the water skin layer but from the uppermost 2–50 m of the water column.

Ocean colour is partly determined by Chl-*a* content, but other components are also involved, such as suspended sediment, coccolithophorids or cyanobacteria which overprint the spectral response of Chl-*a* with their own spectrum. Therefore, in addition to atmospheric correction, areas of high suspended sediment or coccolithophorid concentration are determined and excluded from Chl-*a* calculation when required [*Fargion and Mueller*, 2000].

Nearly all Chl-*a* calculations in this study were made from 9 km resolution, daily, global standard projections (Level-3 standard mapped images = SMI) and were available from the Distributed Active Archive Center (DAAC) NASA Goddard Space Flight Center Greenbelt, MD, USA (daac.gsfc.nasa.gov, Figure 4). The DAAC functioned as the archive, processing and distribution centre. HRPT data which were used for local studies were recorded at the local ground-stations: Universidad de las Palmas de Gran Canaria and Centro Espacial de Canarias (HCAN), Canary Islands, Spain, und Istituto di Fisica dell'Atmosfera (HROM), Rome, Italy.
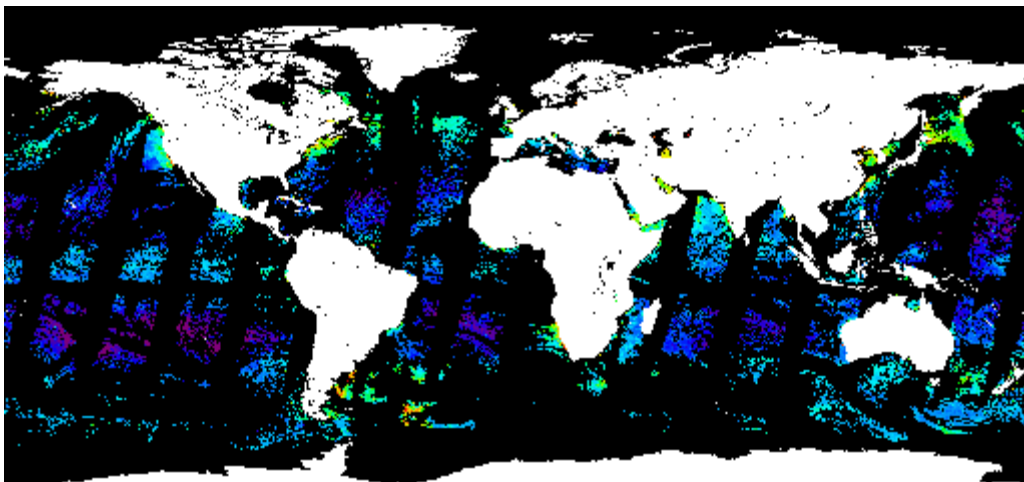
Figure 4. SeaWiFS coverage 25.10.2003

HRPT data are provided from the DAAC as level-1A HDF files. Level -1A is a compilation of raw radiation counts of the eight spectral bands plus additional information about satellite-telemetry, sensor calibration and navigation [*Patt et al.*, 2000]. Higher level formats were processed with the SeaDAS (SeaWiFS Data Analysis System) software package. For statistics and analysis SeaDAS was used in combination with self designed routines under IDL®.

SeaWiFS marginal note

The DAAC provides current SeaWiFS data for use in research under a contract between Orbital Image Cooperation, Dulles, USA, and NASA which expires on 19 December 2003. Currently NASA is not going to sign a new contract, so HRPT data can no longer be received from ground stations without direct license from Orbital Image Cooperation.

Onboard the NASA Earth Observing System satellites Terra and Aqua, the SeaWiFS follow-up sensor MODIS (Moderate Resolution Imaging Spectroradiometer) is operational. MODIS's primary spatial resolution of 250 m is 16 times better than that of SeaWiFS, while MODIS data processing is not yet implemented in the SeaDAS software. Therefore, the user has to rely on the currently provided MODIS 4.88 km resolution.

Trap data

Remote sensing results of the ocean surface were combined with *in situ* measurements to interpret internal processes in the Northwest African upwelling system. Deep-sea C_{org}-flux rates in combination with Chl-*a* data as an indicator for bio-production are presented to determine progression and quantities the of C_{org}-export.

Sedimentation and the associated organic carbon flux off the Northwest African coast was continuously monitored since the early 1990s with moored sediment traps. Particle flux was determined using large aperture time-series sediment traps of type SMT 234 Aquatec Meerestechnik, Kiel, deployed from 11.06.1998 to 07.11.1999 at 21,25°N; 20,70°W. The trap was moored at 3580 m water-depth, ca. 540 m above the sea-floor. The sampling interval was 18x27.5 days [*Balzer et al.*, 2000; *Fischer and crew-members*, 1999]. Validation of trap results is discussed in detail in the third manuscript.

Overview of own research

Manuscript 1: Synoptic view on the Cape Blanc upwelling area on the basis of 12-years remotely sensed sea surface temperature

Manuscript 2: Dynamics of the Cape Ghir filament off Northwest Africa

Manuscript 3: Northwest African upwelling and its effect on off-shore organic carbon export to the deep-sea

Synoptic view on the Cape Blanc upwelling area on the basis of 12-years remotely sensed sea surface temperature

PEER HELMKE[1], ROBERT DAVENPORT[2]

1 FB5 Geosciences, University of Bremen, Klagenfurterstraße, 28359 Bremen, Germany

2 DFG Research Center Ocean Margins University of Bremen, Klagenfurterstraße, 28359 Bremen, Germany

Abstract

The seasonal and interannual variation of upwelling off northwest Africa between 18°N and 25°N and its response to large-scale atmospheric variations was studied for the period 1988 through 1999 using NOAA-satellite Advanced Very High Resolution Radiometer (AVHRR) sea surface temperature (SST) data. The seasonal migration of pronounced upwelling, which follows the northward shift of the north-east trades in late spring and back in winter was confirmed. Strongest upwelling in terms of spatial coverage of a near-coast temperature deficit against the open ocean was observed in December-January and June-July. Westward extension of cold water was found to be the largest at 18° to 20°N in the period May - July caused by confluence and enhanced offshore entrainment through the Canary Current and cyclonic circulation south of Cape Blanc at 21°N. The interannual SST variation in the open northwest Atlantic Ocean shows a relationship to the North Atlantic Oscillation (NAO). The December to March NAO index was correlated to the corresponding four month SST mean. A broad band of negative correlation leads from the African coast at 20° to 27°N southwestwards to the open ocean. Within the area of significance better than 95%, about 50% of the year-to-year SST variation can be explained by the NAO. The regional response to a positive NAO phase, which was shown to be upwelling enhancement from former studies, was not found in our local scale analysis. The local scale upwelling response to the NAO is not predictable and ranges from positive to negative anomalies in upwelling occurrence. Even years of strongest upwelling ('88, '89, '98 and '99) reveal irregularly placed, mesoscale domains (50-200 km diameter) of negative upwelling anomalies.

1. Introduction

This study covers the northern subtropics along the west coast of Africa, focusing on the upwelling off Cape Blanc between 18° and 25°N latitude (Figure 1).

Off northwest Africa NE trade winds are a characteristic atmospheric pattern. As in other trade wind zones off California/Oregon, off Peru and off southwest Africa, the friction of equartorward to westward winds causes an offshore transport of surface water near the coast (Ekman transport). The mass deficit of surface water is substituted by subsurface water, which is mostly colder and enriched in nutrients. At the northwest African coastal upwelling area this subsurface water mass consists of North Atlantic Central Water with a southward transition to South Atlantic Central Water at around 20°N latitude [*Mittelstaedt*, 1991].
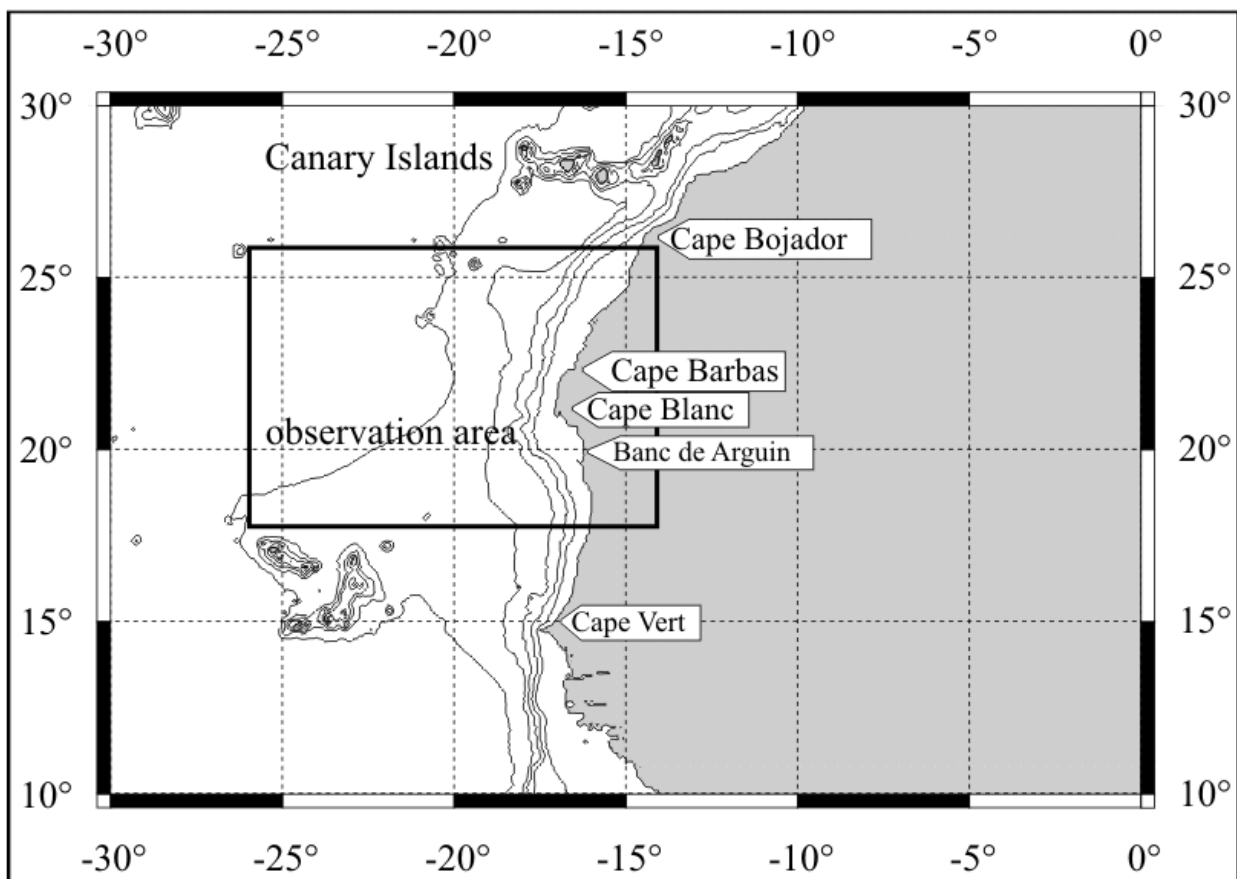
Figure 1. Location of investigation area (18°-26°N; 14°-26°W). Isobaths at 2000 m, 1000 m and 200 m are plotted, the latter tantamount to the shelf edge.

The center of the northwest African upwelling between 21° and 24°N latitude is exposed to the trade winds throughout the year and hence shows permanent upwelling. The adjacent coastal regions are marked by strong seasonality of trade winds and upwelling [*Hagen*, 1981; *Mittelstaedt*, 1991; *Peters*, 1976; *Schemainda et al.*, 1975]. The convergence of the Canary

Current and regional recirculations at Cape Blanc favor a strong western drift of the phytoplankton blooms induced by coastal upwelling of nutrients known as the "giant filament" after *Van Camp et al.* [1991] [see also *Fischer et al.*, 1996; *Gabric et al.*, 1993; *Hernández-Guerra and Nykjær*, 1997].

For this study we have analyzed remotely sensed SST and wind data to provide further insights into the seasonal and interannual variations of the upwelling at Cape Blanc. The objective was furthermore to study the possible influences of the North Atlantic Oscillation (NAO) on the upwelling pattern off northwest Africa.

2. Data and Methods

2.1. Pathfinder SST

Daily data and monthly averages of SST with a resolution of 9 km have been provided by NASA Physical Oceanography Distributed Active Archive Centre for the time period from January 1988 to December 1999 [*Vazquez et al.*, 1998]. Five-day composites have been made to reduce data gaps existing in the source data. Distance-weighted spatial interpolation was carried out for remaining gaps. For the interpolation the maximum distance was limited to fifteen pixels. Still missing data have been taken from Pathfinder 9 km resolution SST climatologies [*Casey and Cornillon*, 1999].

2.2. Upwelling definition

A simple definition of upwelling - exclusively based on SST - was used to facilitate the analysis of the approximately 4,700 images. The temperature difference against the open-ocean SST was calculated. As open-ocean reference temperature the SST averaged from 1,300-1,800 km offshore for the respective latitude was taken, using an approach comparable to that of *Wooster et al.* [1976], *Speth et al.* [1978], *Mittelstaedt* [1983], *Nykjær and Van Camp* [1994] and others. This method was employed to exclude data gaps in the reference temperature induced by cloud cover. The limiting value for the upwelling definition was set to 3.5 K difference against the open-ocean reference temperature. Tests with smaller (larger) temperature limits for the upwelling definition did not reveal any structural difference in the spatial pattern, apart from a greater/smaller offshore expansion of the area, which meets the criterion. The total amount of temperature difference above the threshold of 3.5 K was not taken into account in further analysis.

3. Results and Discussion

3.1. Seasonal upwelling variations

In order to show the seasonal variations in the upwelling location and its offshore extension, the percentage of coverage with upwelled water per season was calculated. In Figure 2 an area of nearly permanent upwelling (>70% coverage) was observed between 21° and 26°N throughout the seasons. South of 21°N the upwelling frequency decreased to <20% in summer. The frequency increased again from fall to winter towards the south.

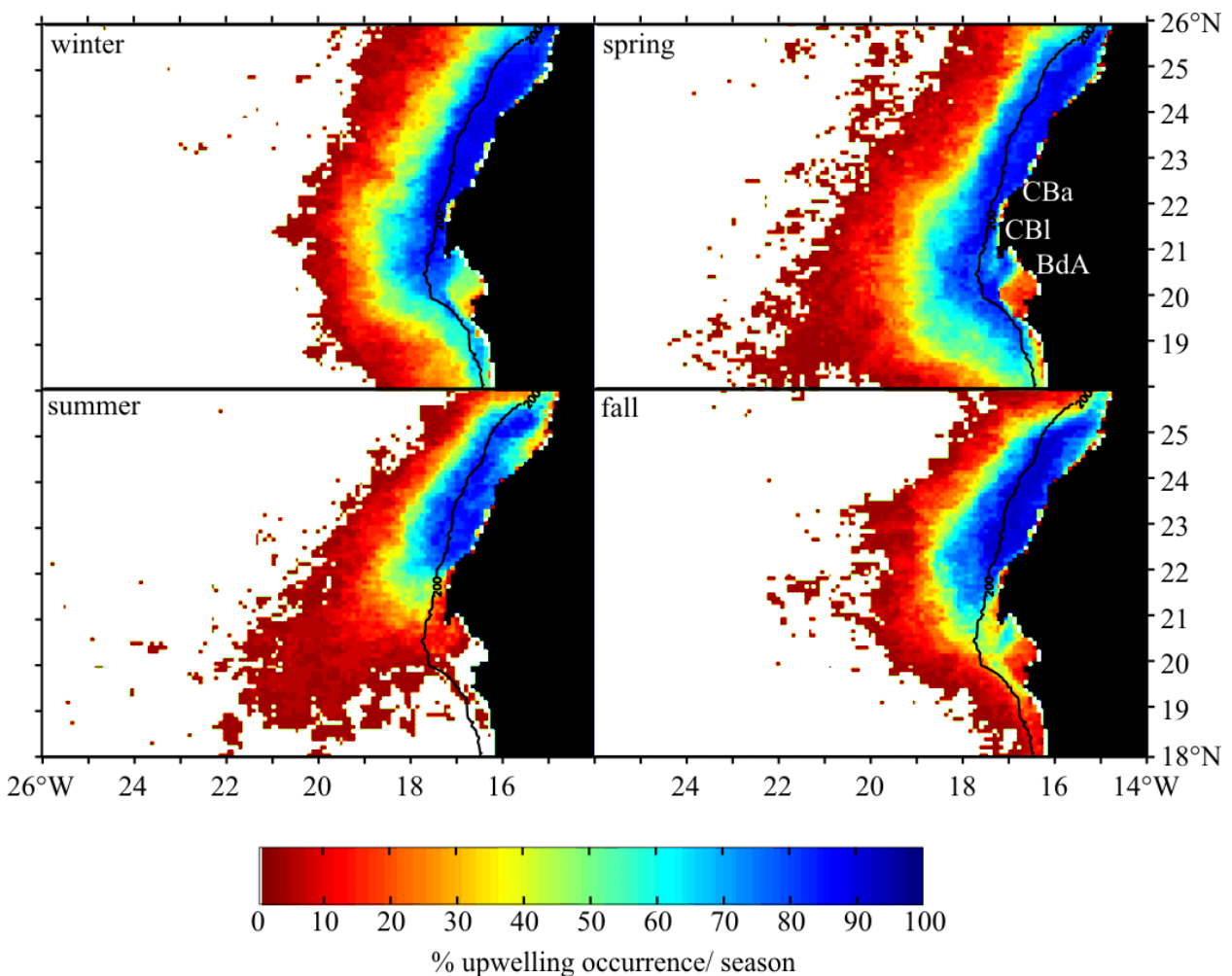**Figure 2.** Twelve-year (1988 – 1999) seasonal mean of spatial upwelling occurrence as percentage of coverage with SST lower than reference temperature (explained in chapter upwelling definition). The shelf-edge (200 m depth) is indicated (solid line).

The position of largest off-shore extension of upwelling occurrence does not simultaneously move with the maximum near-shore upwelling occurrence to the north, but

follows with a delay. During summer, when the southern boundary of >70% upwelling occurrence reaches its northernmost position, the tongue of offshore-transported upwelling water is still located between 18° and 21°N latitude, as in spring. The southward vector of the offshore transport disappears in fall, hence the cold tongue extends from the maximum upwelling occurrence at 21°-26°N westwards.

The seasonal distribution shows that the southern borderline of frequent upwelling followed the trade wind system in summer and fall towards the north. The strongest upwelling intensity expected for winter and spring is confirmed by a high upwelling frequency (>70%) detected north of 20°N in winter and north of 18.5°N in spring, respectively for at least 100 km offshore.

The climatological course of upwelling size during the year (Figure 3) shows a bimodal pattern with broad maxima in January and May/June and pronounced minima at the end of March and August. The size of the area covered by upwelled water varied from 46,000 km^2 in August to 145,000 km^2 in June. The standard deviation is largest in phases of a large upwelling area, particularly in January.
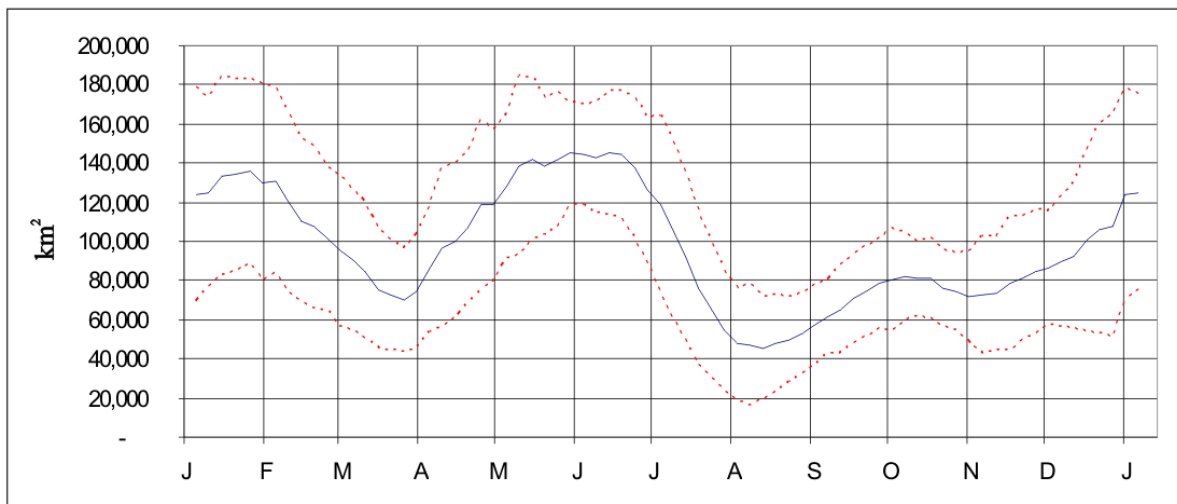
Figure 3. Running average (25 days) of twelve-year climatologies of upwelling size and standard deviations (dashed lines)

South of Cape Blanc towards 19°N, a pattern is detected on the Banc d'Arguin, which differs from the usual upwelling distribution. As illustrated in other studies [*Peters*, 1976], the upwelling continues southwards on the shelf, without including the shallow Banc d'Arguin. The southern bank area is minimally influenced by upwelled water, whereas the north-western part is greatly affected. In the northern part, cold upwelling water drifts onto the Banc d'Arguin, which is only about ten meters deep. Drifting towards the south, the cold water is warmed up on the bank by up to 5 K and mixes with the along-shore current. Therefore, no occurrence of upwelled

water was found at the southern part of the Banc d'Arguin in Figure 2, which confirms results of *Mittelstaedt* [1983] and *Peters* [1976].

3.2. Interannual upwelling variations

The accumulative size of upwelling, which is presented in Figure 4 shows maxima in January and May/June in '88 - '91, '93 – '95, '99 occasionally followed by a third, smaller peak in fall ('89, '91, '95). Although the peaks in winter and spring were well developed in eight out of twelve years, their time of occurrence was not exactly fixed but varied by about one month. The size of the upwelling area varied between 12,000 km^2 (1991) and 240,000 km^2 (1998). From 1988 to 1993 the upwelling size yearly running average seems to follow a biennial fluctuation, which changed into a three year depression from 1994 to 1996. In the meantime the yearly range of variation decreased significantly from 1995 to 1997. During 1994 and 1996 the twelve year mean of 97,000 km^2 was only seldom exceeded.
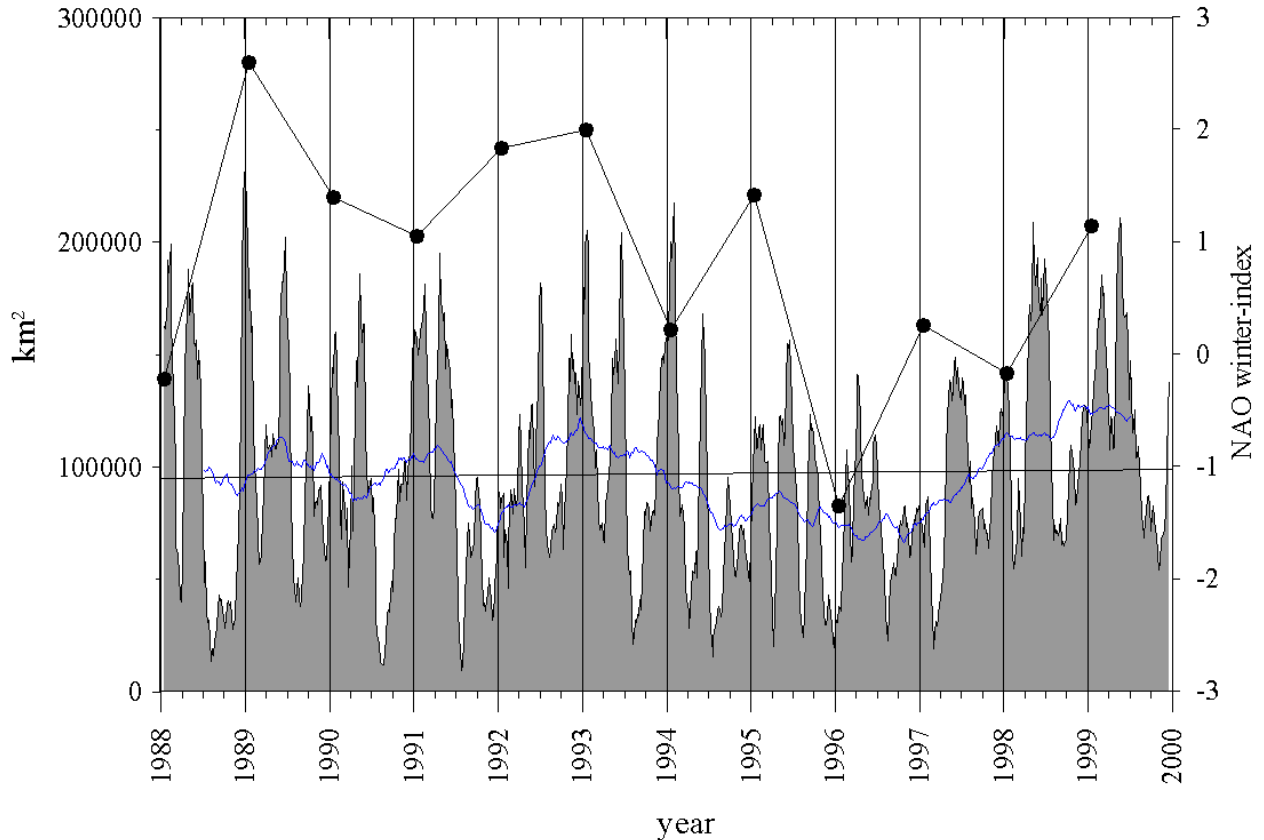
Figure 4. Upwelling occurrence area in square kilometers for the period of 1988 – 1999. Running average of 25 days (shaded area) and one year (blue, solid line) and the twelve year mean value (black, straight level) (96,900 km^2) are shown. The NAO winter-index is indicated for comparison (connected dots) [*Hurrell*, 1995].

The Northwest African upwelling is known to persist all the year at about 21° to 24°N and to undergo seasonal fluctuations poleward of this latitudinal range [*Hagen*, 2001; *Nykjær and Van Camp*, 1994; *Speth et al.*, 1978; *Van Camp et al.*, 1991]. From 20° to 24°N, upwelling is abundantly seen west of the shelf-edge, while north of 24°N the frequency >50% is confined to a narrow band on the shelf (Figure 5a). South of 20°N the maximal yearly occurrence of upwelled water decreases rapidly to less than 40%. In years of generally less upwelling, occurrence south of 20°N ('92, '94-'97) it is more confined to the shelf than in years of high upwelling frequency ('88, '90, '93, '98). The cold water signal is transported westwards to 20° to 23°W at a latitude of about 22°N, the western tip of the cold water tongue can be deflected southwards to 20°N ('88, '90, '91, '98). This deviation cannot be explained by an intensified Canary Coastal Current alone, since the intrusion of colder water from the north would be recognized in the north of the study area, which is clearly not the case in 1988 and 1990 instead intensified Ekman transport would result in an anomaly pattern, as shown in Figure 5b.
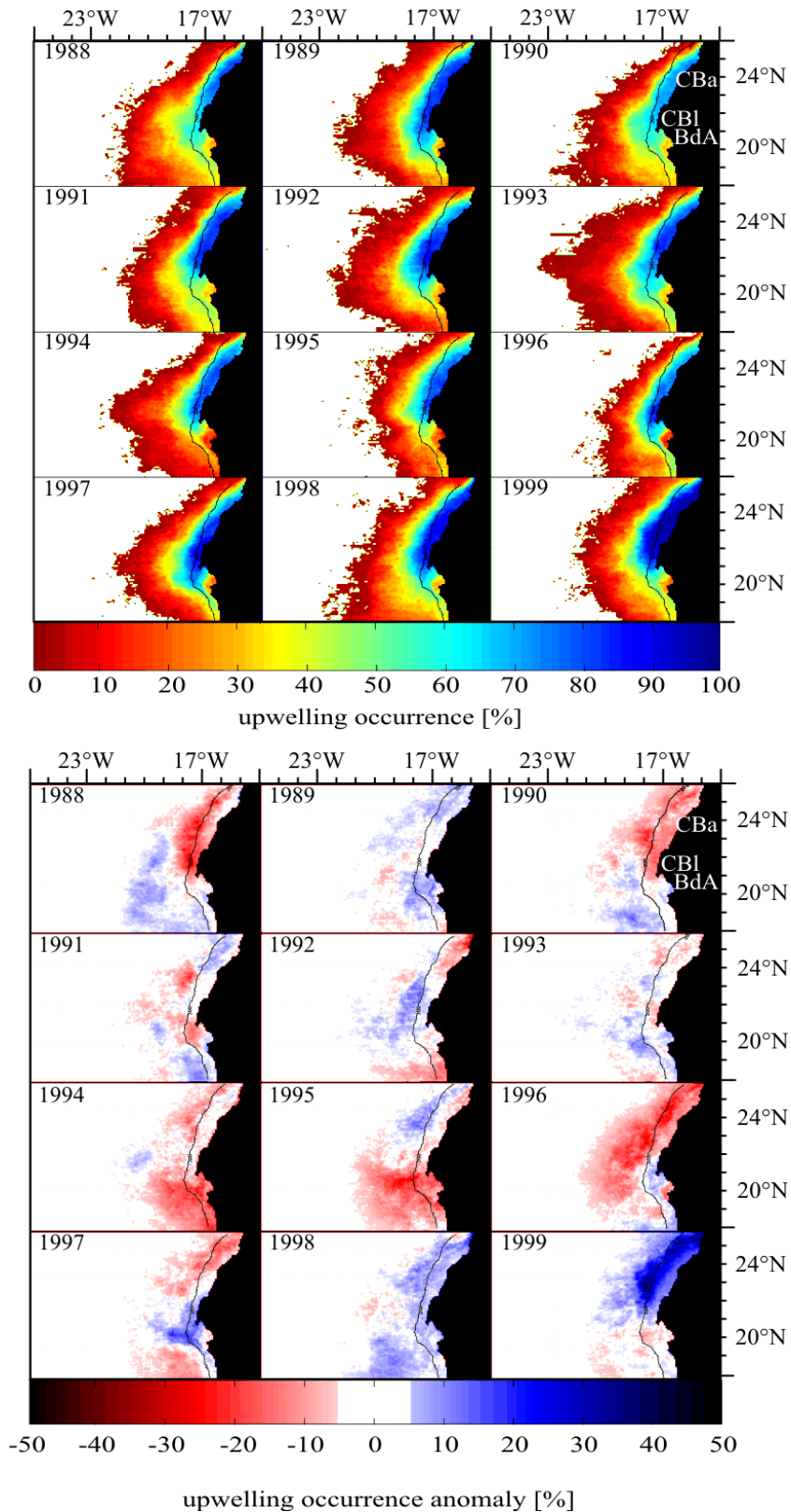
Figure 5. Yearly spatial pattern of upwelling occurrence (a) and anomalies from the 1988 – 1999 mean (b).

It is striking how irregularly and patcilyy the anomalies are distributed over the years (Figure 5b). Even years of strongest upwelling ('89', '98 and '99) reveal irregularly placed, mesoscale domains (50-200 km diameter) of negative upwelling anomaly and vice versa ('94-

'96). The borders of anomaly domains seem to be partially related to the shelf region in e.g. '92 and '95 where a negative on-shelf anomaly is separated from a positive off-shelf anomaly, or during '96 and '97 where a similar condition existed south of 20°N.

To examine the NAO impact as a possible source for interannual upwelling variation we correlated the NAO winter-index to the December to March satellite SST (Figure 6).
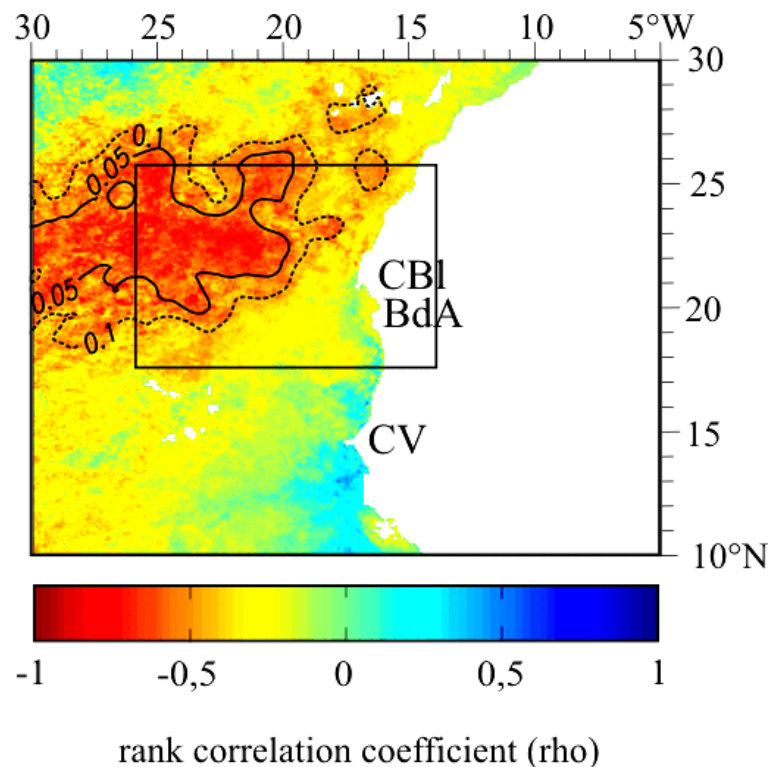

rank correlation coefficient (rho)

Figure 6. The rank-correlation between NAO winter season index as defined by [*Hurrell*, 1995] and the December to March satellite SST mean for the period of 1988-1999 in the region of 0°-40°N latitude and 0°-40°W longitude. The figure shows a broad band of NAO-SST association extending from the northern African coast to the south-west. The near-shore center of association is between Cape Blanc in the south and the Canary Islands in the north at 21°-27°N latitude. Labeled lines indicate smoothed significance levels at 0.05 and 0.1 respectively.

Preceding results of mostly coarse-scale hemisphere to worldwide studies found an interaction between NAO and Atlantic SST [*Frankignoulle*, 1999; *Osborn et al.*, 1999; *Paeth et al.*, 2003; *Peng et al.*, 2002]. Our calculation shows a broad band of negative correlation, which extends from the African coast at 20° to 27°N westwards to the open ocean. This pattern can by explained by increased latent heat transport during intensified trade winds in positive NAO phases [*Cayan*, 1992; *Hurrell*, 1995]. Off northwest Africa a strong sea level pressure gradient in the subtropical Atlantic (positive NAO phase) leads to intensified NE trade winds particularly in spring. Nevertheless, we did not find a near-shore signal of significant correlation. We assume, that in the 9 km resolution data we used, too much of the natural spatial variance is conserved to

reveal a good correlation as found in coarser scale data. Patches of mesoscale to submesoscale range in upwelling occurrence demonstrate this high spatial variance (Figure 5b).

According to *Hurrel* [1995] the year 1995 has a NAO-Index of 1.41, but increased upwelling was not observed. The reason for this might be the open ocean impact of the trade wind driven evaporation. Due to the strong air pressure gradient, the winds are moderate at this latitude. Strong surface winds result in a low reference SST due to latent heat transport into the atmosphere. The SST within the examined area must be even lower to comply with the definition for the upwelling, thus, upwelling events will not be recognized that easily.

The distribution of the upwelling was compared between two years of especially strong and weak upwelling (Figure 7). The time period from 1992 to 1995 was characterized by strong NE trades and intensive upwelling. Strongest upwelling in January 1993 was triggered by intensive trade winds during a high NAO phase. Therefore 1993 was chosen as a year of intensified upwelling activity within a four year long phase of positive NAO [*Hurrell*, 1995]. This choice should avoid the influence of a possible NAO precursor [*Halliwell Jr.*, 1998]. An equally long phase of negative NAO cannot be found within 1988 to 1999, therefore 1996 was chosen as the only year with clearly negative NAO.

The upwelling maximum in early summer 1993 was displaced 3° towards the south compared to 1996. With an upwelling threshold-temperature of 3.5 K below the reference temperature, the upwelling area in January 1993 is more than five times larger than in 1996. Additionally, the upwelling intensity in January-June 1993 was higher than average. For the period December-March the portion of total atmospheric variation of the northern hemisphere explained by the NAO reaches its maximum. From these examples we conclude that a positive NAO can generally intensify upwelling off Cape Blanc even though the multi-year correlation with relative fine-scale SST data is not significant.

A part of the upwelling variability can be explained by modifications in the wind system, which is triggered by the NAO as previously mentioned. Additionally, the El Niño/Southern Oscillation (ENSO) may influence the northwest African SST pattern. Other studies have underlined the effect of ENSO on the precipitation in Africa, north Brazil and the Caribbean [*Chiang et al.*, 2000; *Folland et al.*, 1986; *Moura and Shukla*, 1981] and also on the wind field above the subtropical North Atlantic and the Atlantic SST [*Enfield and Mayer*, 1997; *Roeckner et al.*, 1996; *Saravanan and Chang*, 2000].

It was found in previous studies that a strong ENSO cycle in the Pacific may result in a southward shift of the Intertropical Convergence Zone (ITCZ) [*Janicot*, 1997; *Rajagopalan et al.*, 1998] and weakened North Atlantic trade winds by displaced Walker circulation [*Hameed et*

al., 1993; *Wallace et al.*, 1990]. *Enfield and Mayer* [1997] showed that this connection also exists for the area of this study. The Niño-3 index (the SST mean at 5°S-5°N, 150°-90°W) and the wind field in the NE Atlantic display a significant interbasin correlation with a lag of one month. The SST-anomaly observed in this study off northwest Africa has the highest correlation with a lag of 4-5 months after a maximum of the El Niño in December. *Saravanan and Chiang* [2000] gave proof of a static relationship between El Niño-events and positive SST-anomalies in the subtropical North Atlantic with maximum regression in the east and especially at Cape Vert. Results from long-term studies show the connection of ENSO with wind- and SST-anomalies in the equatorial and mid-latitude Atlantic [*Chiang et al.*, 2000; *Enfield and Mayer*, 1997; *Gianinni et al.*, 2000; *Janicot*, 1997; *Saravanan and Chang*, 2000]. Considering this background, we suggest, the weak upwelling observed in January-June 1992 to be related to the El Niño/La Niña-event 1991-1992. A similar coincidence for El Niño in 1982-1983 and weak upwelling off Portugal was stated by *Barton* [1998].
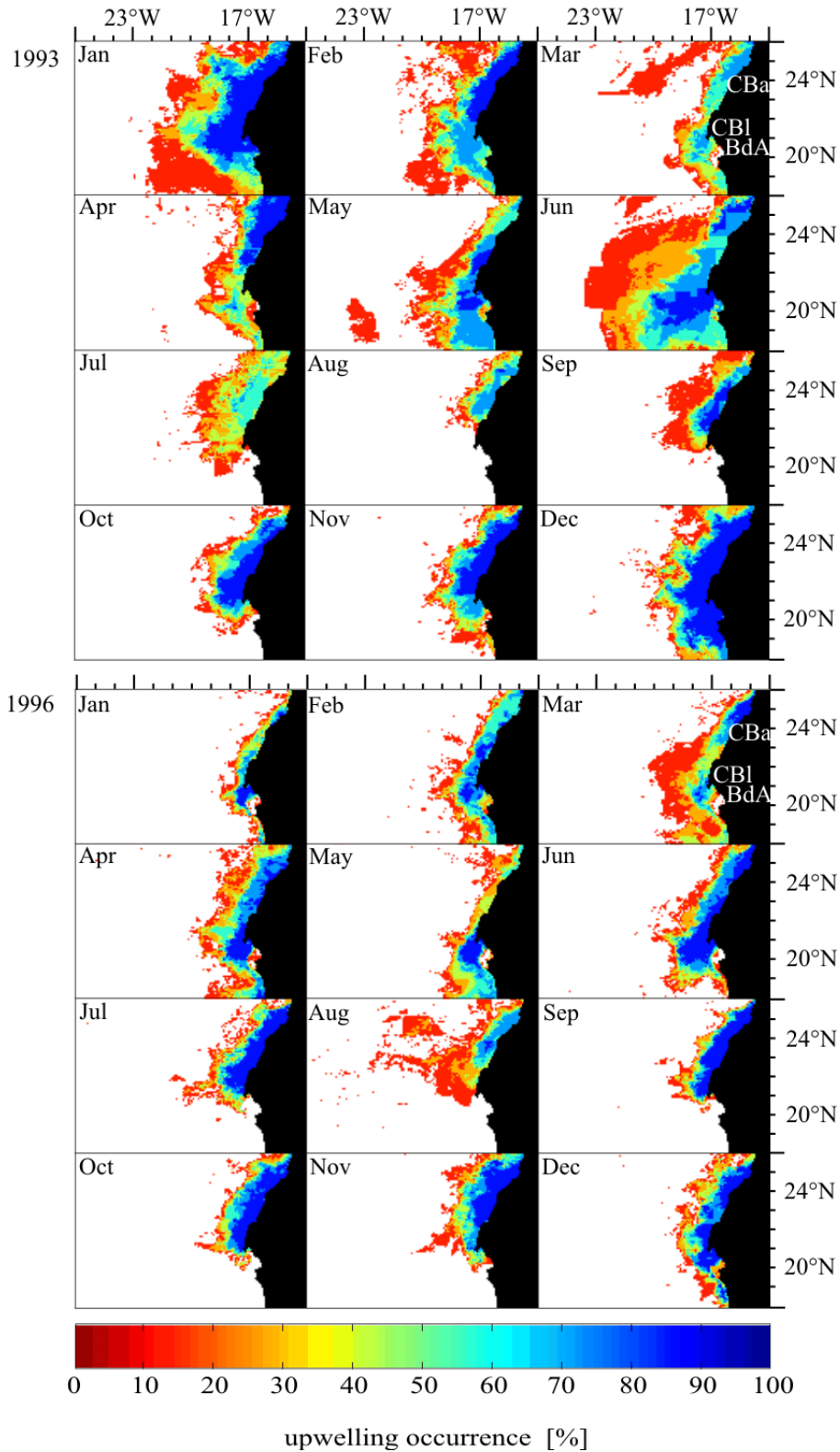
Figure 7. Monthly comparison of 1993 during positive NAO phase (a) and 1996 during negative NAO phase (b) in terms of upwelling occurrence. In contrast to other computations presented here, this is made out of five daily SST data composites, produced by averaging good values over time and filling residual gaps with nearest neighbor distance weighted average.

4. Conclusions

The seasonal pattern of upwelling size climatology shows peaks in January and June followed by a minimum in August and a weak period until December. We have confirmed that upwelling occurs throughout the whole year in the zone north of 21° to 26°N. The maximum intensity of the upwelling shifts southwards in winter and northwards in summer according to the season and the position of the ITCZ respectively. From April to June, intense upwelling is found far south. From July to September it tends to shift rapidly back to the north. The distribution of upwelling anomalies is largely irregular; maxima and minima of upwelling are displaced relative to their position in years without strong upwelling anomalies. The high energetic nature and strong internal variance of this eastern boundary upwelling system also account for the weak predictability of upwelling response to enhanced wind stress under positive NAO phases.

Strong El Niño/La Niña events as in 1992 and 1998 also influence the SST of the tropical Atlantic with a lag of a couple of months [*Enfield and Mayer*, 1997; *Saravanan and Chang*, 2000]. This might explain why the upwelling in 1992 was weak, although the NAO in that year was more intensive as in 1993, when strong upwelling occurred.

Wind stress-related filament structures off Cape Ghir, NW Africa

PEER HELMKE[1], ROBERT DAVENPORT[2], HOLGER KUHLMANN[2]

1 FB5 Geosciences, University of Bremen, Klagenfurterstraße, 28359 Bremen, Germany

2 DFG Research Center Ocean Margins, University of Bremen, Klagenfurterstraße, 28359 Bremen, Germany

Abstract

The SeaWiFS instrument has provided an unparalleled multi-year view of the pigment patterns and dynamics associated with the northwest African upwelling system. Although the general pigment features of this upwelling system have been well documented using historical CZCS imagery, the almost daily SeaWiFS images have given a completely new view of the daily, seasonal and interannual dynamics of the many filaments and other mesoscale features. We present a study of more than 4 years of SeaWiFS imagery of the filament off Cape Ghir, Morocco. The Cape Ghir filament can be seen throughout the year in SeaWiFS images with the exception of the annual late winter/spring bloom when the filament is visually suppressed by increased ambient pigment levels. We have categorised the various filament structural forms and attempted to correlate them on a seasonal and interannual scale with alongshore wind patterns. The study shows that although the filament displays significant variability both seasonally and annually, there are certain structural patterns that are repeated each year in specific seasons. The dominant pattern is associated with the main upwelling period in summer/fall, when alongshore wind stress increases due to strengthening trade winds. During this period, the filament progresses from a compact structure oriented NE-SW in June/July through to increasingly complex forms in August/September oriented E-W. It finally evolves into various structures, some oriented SE-NW in late fall. Significant upwelling though is found to take place over shorter periods in late-winter and spring, leading to complex filament structures; these are shown to be related to periods of increased alongshore wind stress. The interannual filament pattern observed by SeaWiFS is also reflected in the spatial distribution of sediment accumulation rates and the common upwelling foraminifer Globerina, off Cape Ghir implying a similar upwelling

system throughout the Holocene. The extension of the filament far offshore resulting from increased alongshore wind stress in late-winter and spring suggests that highly variable sedimentation events observed far offshore from Cape Ghir during the Last Glacial Maximum may be directly related to increased trade winds during this period. The study demonstrates that analysis of the relationship between alongshore wind stress and filament patterns may, in specific cases, provide a guide to interpretation of upwelling related events and strength as observed in surface sediments and sedimentation cores.

1. Introduction

The northwest African (NWAF) coastal upwelling is situated at the eastern boundary of the North Atlantic recirculation system. Along with those in the western coastal zones of the Americas, southwest Africa and the Iberian peninsula, it represents one of the world's major upwelling systems. The seasonal and latitudinal dependence of the NWAF upwelling system was first described by *Wooster et al.* [1976] based on historical ship's measurements of sea surface temperature (SST), wind stress and currents. The upwelling of cool, nutrient rich water along the northwest African coast is the result of alongshore wind forcing from the northeast trade winds. The strength of the trades is related to the position of the Intertropical Convergence Zone (ITCZ) and the associated Azores High both of which generally oscillate between northerly/southerly positions in summer/winter respectively, giving rise to a pattern of wind forcing which is highly seasonally and latitudinally dependent. This pattern of seasonal SST along the coast has been extensively described by several authors [*Mittelstaedt*, 1991; *Nykjær and Van Camp*, 1994; *Van Camp et al.*, 1991; *Wooster et al.*, 1976]. In general south of 20°N upwelling occurs during the winter; between 20°N and 25°N upwelling is persistent throughout the year with maximum intensity during spring and fall, while north of 25°N, upwelling occurs during summer and fall.
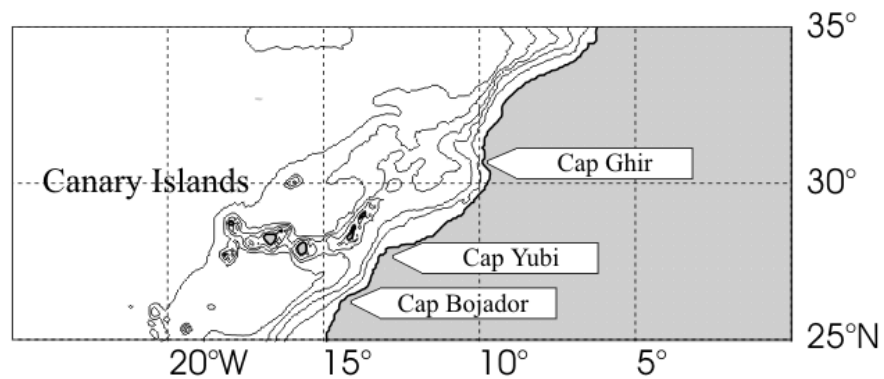
Figure 1. Study area

The colder upwelled water is observed in satellite SST imagery as a narrow coastal band extending up to 50 km offshore. The boundary between the upwelled water and the offshore water, the coastal transition zone, mainly follows the shelf edge and is the region where the seasonal picnocline intersects the sea surface, forming a frontal zone some 10 –20 km wide and 20-50 m deep [*Hagen*, 2001]. Embedded in this zone is an equatorward flowing coastal jet (Figure 2) [*Hagen*, 2001] which has also been observed for the North American coastal upwelling system [*Strub et al.*, 1991] and is probably characteristic for such coastal transition zones. The frontal zone should be a barrier to offshore transport of upwelled water and hence the cross-shelf biomass export. This is not always the case, and is evident from both SST and pigment images of coastal upwelling regions which often display filaments and complex mesoscale eddies migrating some distance offshore beyond the expected boundary of the coastal transition zone (see for example, Strub et al., 1991, for North America, Lutjeharms and Stockton, 1987, for southwest Africa; Kostianoy and Zatsepin, 1996, for northwest Africa). For NWAF *Kostianoy and Zatsepin* [1996]) identified 60 filaments over 1000 km of coastline from an analysis of satellite SST. The development of filaments is assumed to be related to a change in coastal and/or seabed topography. *Strub et al.* [1991] postulated several models for filament production off the Californian coast. 'Squirts' are one-way jets transporting coastally upwelled water to the deeper ocean which may terminate with a pair of counter-rotating vortices seen in pigment images as a 'mushroom' or 'hammerhead' shape. A second model consists of mesoscale eddies imbedded in a slow moving southward current which draw upwelled water offshore. The third model consists of a continuous southward jet meandering offshore and onshore. During the onshore transgression, the jet may entrain coastal upwelled water and then create filaments offshore in the next meander. From an analysis of velocity fields, water properties and SST imagery, *Strub et al.* [1991] concluded that for the Californian system a combination of the meandering jet and the mesoscale eddy models could best explain filament development (see

Figure 2.4 in Hill, 1998). In the meandering jet model it is probable that much of the cooler water transported offshore returns on the inshore leg of the meander. Nevertheless, there will be some turbulent mixing at the extreme offshore end. The offshore transport of upwelled water via such filaments may be a significant means of transporting organic carbon over the shelf to the deep ocean [*Gabric et al.*, 1993].
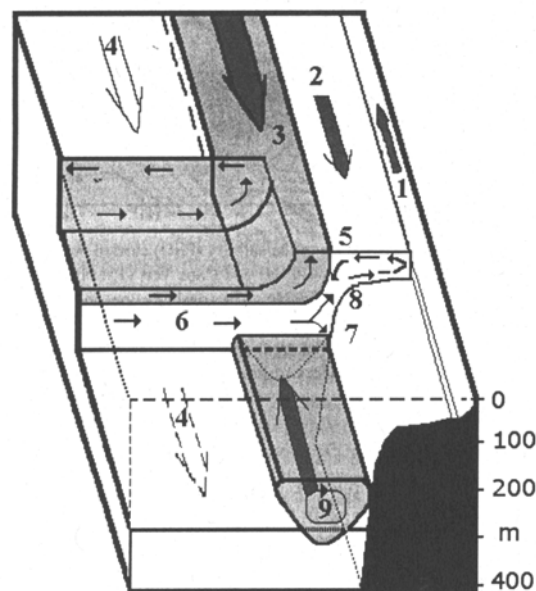

Figure 2. Taken from Hagen, 2001: Some aspects of the two-dimensional steady-state current system according to Hagen (1981). 1) Zone of a weak near-shore countercurrent; 2) Primary upwelling zone with wind-induced southward currents between the main frontal zone (3) and the coastline; 3) Main frontal zone along the shelf edge as a result of pycnoclines rising to the sea surface, with embedded coastal jet; 4) Canary Current as eastern branch of the anticyclonic gyre circulation (dashed lines indicate weak countercurrents alternating temporally); 5) Wind-generated offshore current induces downwelling at the frontal barrier and intense mixing with vertical temperature inversions; 6) Onshore compensation current of intermediate layers is the main source of upwelling water; 7) Downward branch of (6), as part of the divergence zone of zonal currents off the continental slope; 8) Upward branch of (6) feeding upwelling water into (2); 9) Poleward flowing undercurrent with a thickness of several hundred meters.

The question whether upwelling intensity responds to climate change was addressed by *Bakun* [1990] who analysed coastal wind stress over four decades for the upwelling systems off California, Peru, the Iberian Peninsula and Morocco. He concluded that in all cases wind stress has been increasing during the respective upwelling seasons. Although there was no evidence of interregional correlation between the various time series, they all nevertheless shared this same long-term trend. Bakun argued this is consistent with simulations that suggest that off northern California, for example, increased atmospheric CO_2 leads to increased southward wind stress. Bakun suggested several atmospheric and biological consequences as a result of increased upwelling intensity, such as increased coastal fog in summer and increased primary productivity.

In this study we compared the along-shore wind stress with the mesoscale structure and orientation of the Cape Ghir filament off the coast of Morocco at 31°N for the period of SeaWiFS operations from September 1997 to December 2001. From analysis of SeaWiFS images, we categorized the overall filament structures into 8 basic types and 6 sub-types and mapped these on a monthly basis for comparison with the mean along-shore wind stress to determine if there was any consistent causal relationship. We also investigated if present filament patterns are a guide to the filament's history during the Holocene and Last Glacial Maximum (LGM) by comparing present annual filament patterns with the distribution of the typical upwelling planktic foraminifera, *Globigerina bulloides,* found in surface sediments off Cape Ghir.

1.1. The Cape Ghir Filament

The Cape Ghir filament (31°N) is a more or less permanent filament associated with the NWAF upwelling system [*Hagen et al.*, 1996]. It generally extends some 200 km offshore but it has been observed to extend up to 500 km [*Davenport et al.*, 2002]. *Nykjær and Van Camp* [1994] investigated the correlation between upwelling as seen in SST and the Ekman wind forcing along the NWAF coast. They noted that at Cape Ghir there appears to be a 3-month lag between wind forcing in summer and the time of maximum upwelling and suggested that the lag was related to the changing coastal topography associated with Cape Ghir and local ocean floor topography. The only published study devoted to the Cape Ghir filament is that of *Hagen et al.* [1996] who conducted a mesoscale CTD survey in September-October 1992 and analysed remotely sensed SST images of the region. According to *Hagen et al.* [1996] the permanence of the filament cannot be explained only by the seasonal pattern of along-shore wind stress. It is instead proposed, that the filament probably develops as the result of the southwards coastal jet which bifurcates on the northern edge of the Cape Ghir Plateau (CGP) (Figure 1). The near-shore branch forms a cyclonic eddy-like structure over the eastern part of the plateau while the offshore branch feeds the filament with cold water. The offshore end of the filament may develop a pair of counter-rotating eddies which draw the upwelled water further offshore. In this study, we will demonstrate that although the filament may be predominately driven by bottom topography over the CGP, the surface mesoscale structure and axial orientation of the filament as seen in pigment imagery is partly correlated with the along-shore wind stress to the North of Cape Ghir. Indeed, the permanency of the filament makes it ideal for investigating the seasonal and interannual wind stress driven upwelling variability in this region. We will specifically attempt to answer the following questions:

How often and for how long do the various mesoscale structures of the Cape Ghir filament occur on a seasonal and interannual basis?

How do the various filament structures relate to wind forcing and how are seasonal and interannual changes in wind patterns reflected in changes in filament characteristics?

Can the long-term observation of such filaments from pigment data alone be used to monitor interannual regional and basin (North Atlantic Oscillation) climate changes?

Assuming we can answer these questions in the affirmative it is natural to further ask:

Is it possible to infer past regional and basin climate patterns from typical upwelling foram distribution in deep sea surface sediment patterns related to the Cape Ghir filament?

2. Data and Methods

2.1. SeaWiFS Data

We visually analysed all available daily 9 km resolution SeaWiFS Level 3 images covering the NWAF upwelling system for the period September 1997 to December 2001 provided by the DAAC at Goddard Space Flight Centre, NASA, and categorized the major mesoscale structures of the Cape Ghir filament. The images are provided as part of the CD available with this issue as a 'movie' showing the dynamics of the NWAF upwelling on a daily basis over the 52 month period. The daily binned 9 km resolution images were interpolated stepwise to fill gaps induced by cloud coverage or high aerosol concentration. As a first step, gaps were filled by an interpolation in space with an exponential inverse distance weighted mean up to the fifth neighbouring pixel. A rolling composite over eleven days was calculated using the same weighting approach in time (comparable to the SeaWiFS product http://seawifs.gsfc.nasa.gov/cgi/level3_rolling.pl?DAY=&PER=&TYP=chl). Finally, remaining missing data were filled with SeaWiFS chlorophyll-*a* monthly climatology data. For the video production the images were stacked to avi format, taking advantage of the freeware pjBmp2avi. To avoid cross platform problems, we used the older more widely distributed Radius® Cinepak® Codec version 1.10.0.6. The video may be displayed with Windows® Media Player, Quicktime® under Apple® OS or XAnim under any UNIX environment.

In SeaWiFS imagery the Cape Ghir filament displays a bewildering variability of structural forms described by *Nykjær* [1988] as consisting of complex squirts and mesoscale eddies. Nevertheless, by careful analysis of such imagery it is possible to identify some basic forms that are seen consistently from year to year. Many of these basic forms are relatively stable over

weeks although significant sub-scale variability is always present. We therefore categorised the various structural forms into 5 different types as follows (Figure 3):

Type I   Narrow, compact jet structure oriented towards the southwest.

Type II   Large, compact filament extending several hundred kilometres off-shore along an E-W axis

Type III   Small filament extending less than 100 km offshore, often with a complex outer edge.

Type IV/S   Narrow, meandering jet extending several hundred kilometres offshore in a westerly or north-westerly direction. A more complex form involves two such jets forming a double structure (Type IV/D).

Type V   A large partially compact, partially diffuse filament showing complex structure and no specific orientation.
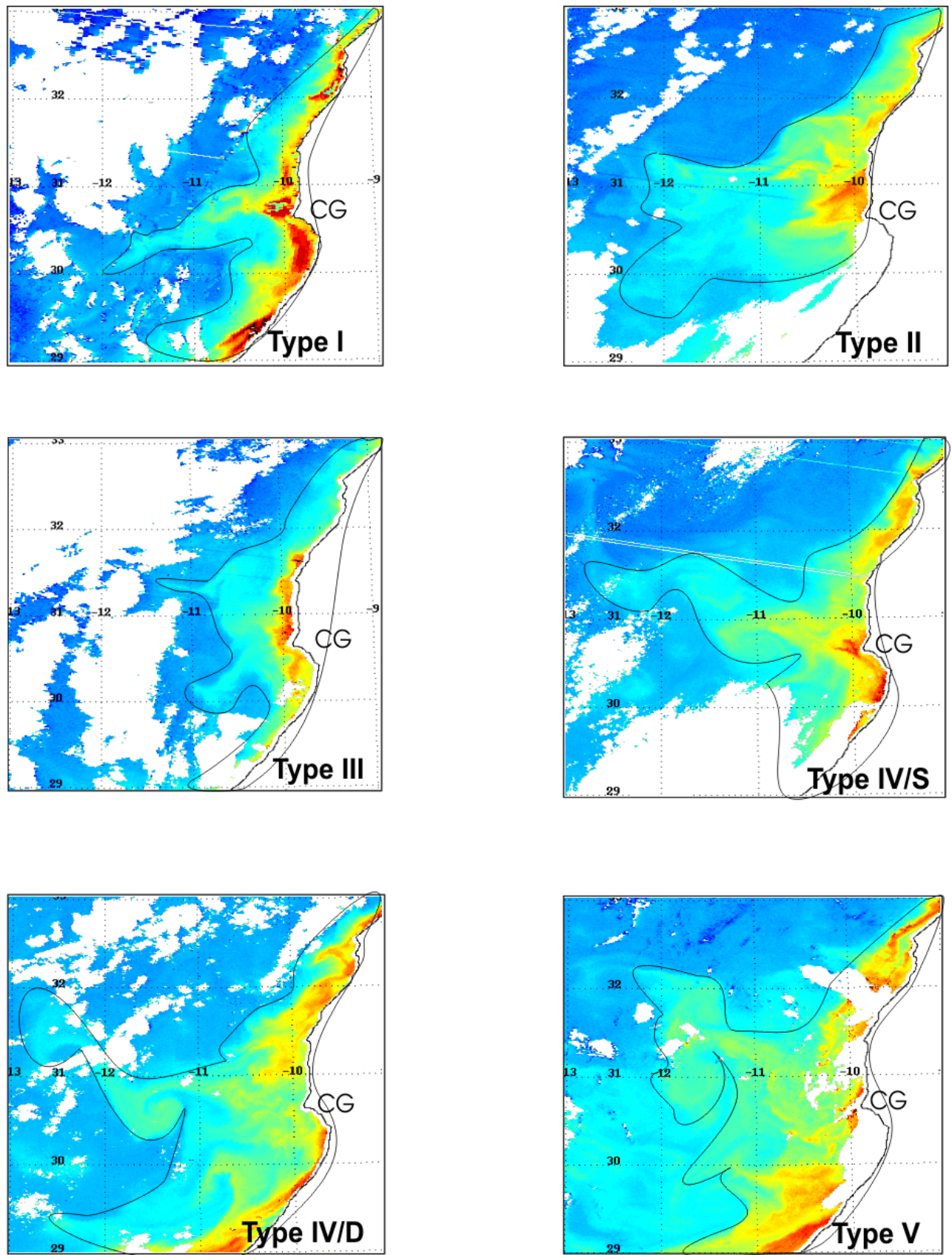
Figure 3. Classification of the Cape Ghir filament structures (for explanation see text)

Using daily SeaWiFS 9 km resolution data, we then identified the characteristic filament class or classes for each month over the period September 1997 to December 2001 (Figure 4). In some cases, where 9 km images were not sufficient to resolve the filament class, we used SeaWiFS Local Area Coverage (LAC) Level 1A imagery (also from NASA DAAC) of approximately 1 km resolution processed to Level 2 using the SeaDAS version 4.3.
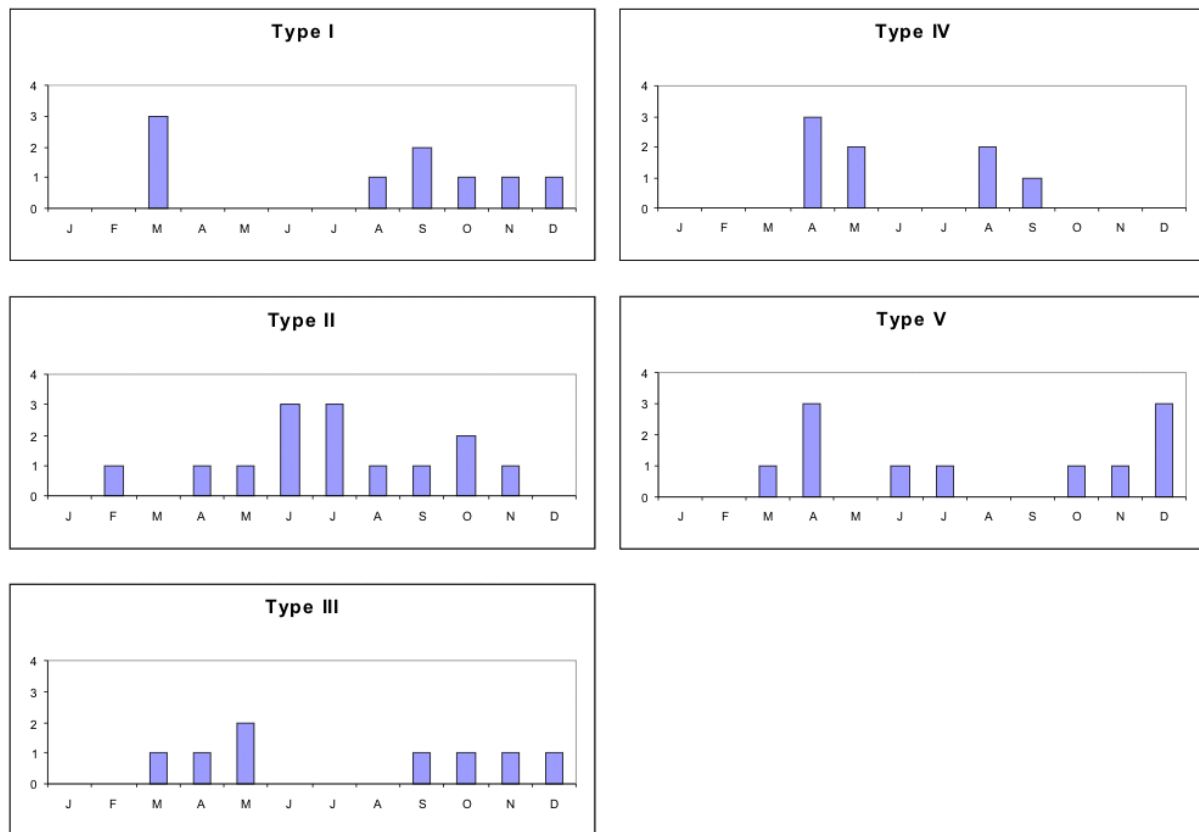
Figure 4. Monthly frequency distribution of the Cape Ghir filament types for the period September 1997 to December 2001

2.2. Wind data

We derived the mean monthly alongshore wind stress (Newtons m^{-2} Figure 5) as a proxy for upwelling off Cape Ghir [*Bakun*, 1990] for a region 30°N-32°N, 10°W-13°W. For this purpose we used meridional wind stress data from the ERs^{-1} and -2 radar satellites; the coast north of Cape Ghir runs approximately north-south and therefore it was assumed that the along-shore wind stress is the same as the meridional wind stress. The wind data were extracted from the CERSAT-IFREMER, Plouzane, France, database (http://www.ifremer.fr/cersat); the data are mapped into 1° x 1° cells. Errors in the wind stress were never more than ±0.01 Newtons m^{-2} (Figure 5). We investigated possible long-term trends in the along shore wind stress for the

period 1992 to 2000 (period of available ERS data) using mean values for periods July-October of each year. The monthly data for the period September 1997 (start of SeaWiFS data set) to December 2000 were used to investigate possible correlation with filament activity.
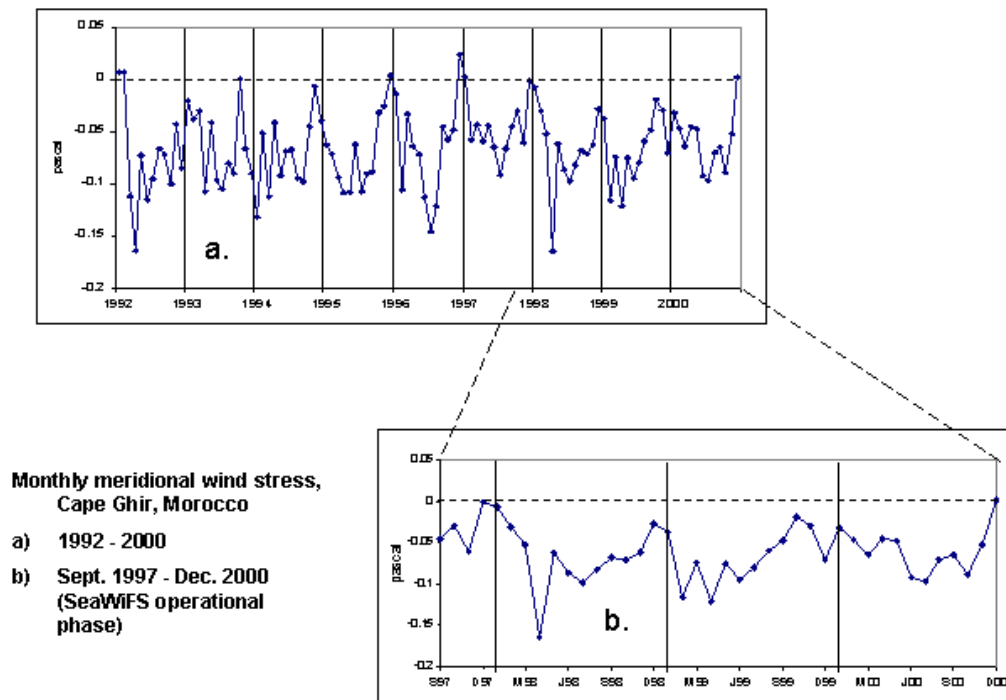
Figure 5. ERS meridional windstress off the coast of Cape Ghir

3. Results and Discussion

3.1. Wind stress – long term variability

Assuming that the period of maximum upwelling off Cape Ghir is from July-October [*Nykjær and Van Camp*, 1994; *Wooster et al.*, 1976], we investigated the 4-month mean along-shore wind stress for the period 1983 to 2000 (all available data from CERSAT-IFREMER) (Figure 5a). Although there is considerable interannual variability (range 0.07-0.11 Newtons m^{-2}), there is an overall decreasing trend over the period 1993-2000. *Bakun* [1990] showed that for eastern boundary upwelling systems, there has been a trend of increasing along-shore wind stress over approximately 40 years (1946-1988). During the upwelling season off Morocco at 28°N for a 35-year period from 1946-1981, there was an increase of approximately

0.08-0.14 Newtons m^{-2}. Comparison with the more recent Cape Ghir data should be treated with caution (Cape Ghir is further north (31°N), maximum upwelling season restricted to a 4-month period, only 9 years of data for Cape Ghir). Nevertheless, the data do suggest that the along-shore wind stress off NWAF probably cycles through decadal and longer periods of variability and it is not clear that the trend observed by *Bakun* [1990] is sustainable over the long term. Indeed direct comparison with the CERSAT-IFREMER data for the period 1992-2000 off Morocco at 28°N shows the same decreasing trend as at Cape Ghir.

For the period of SeaWiFS operations, the along-shore 4-month mean wind stress during the period of maximum upwelling (July-October) at Cape Ghir has shown little interannual variability (range 0.07-0.09 Newtons m^{-2} for 1997-2000). This implies that if wind stress modulates the filament then we should observe a consistent pattern for this period each year in the SeaWiFS imagery. When we examine the monthly data throughout 1992-2000 (Figure 5a) there is a consistent pattern of strengthening along-shore winds in July each year which then gradually ease through August/September before briefly strengthening again in October/November. Although the peak wind stress in July varied by a factor of 2 over the 8-year period (0.07-0.14 Newtons m^{-2}), during the SeaWiFS period from 1997-2000 it varied by only some 25% (0.08-0.1 Newtons m^{-2}). Outside of the main upwelling season, strengthening alongshore winds are seen in January-April each year and the wind stress can be even higher than for the 'classical' upwelling period (e.g. April 1998, 0.15 Newtons m^{-2}). That this can induce increased upwelling activity is clearly evident in SeaWiFS imagery e.g. April 1998 where the filament can be traced for an unprecedented 500 km offshore (Figure 6). Indeed we suggest that the upwelling pattern for Cape Ghir should really be described in terms of a broad upwelling in July-October each year with shorter but intense monthly upwelling periods anytime between January-May. It is precisely these winter/spring upwelling events that are not so obvious in SST imagery when the difference between upwelled and ambient water is at a minimum or even non-existent. Furthermore, such events were not observed by *Wooster et al.* [1976] and *Nykjær and Van Camp* [1994] both of whom used an upwelling index based on the difference between the SST over the continental shelf and a point at the same latitude further offshore. Such an index is heavily biased toward the summer months when the temperature difference between the upwelled water and that offshore is at a maximum. Therefore, pigment data may be a more sensitive indicator of upwelling events and subsequent filament growth throughout the year than SST. Although solar insulation and SST and hence biological activity is lower in winter, the nutrient rich upwelled water still promotes phytoplankton growth as it is carried offshore, as seen in SeaWiFS imagery.
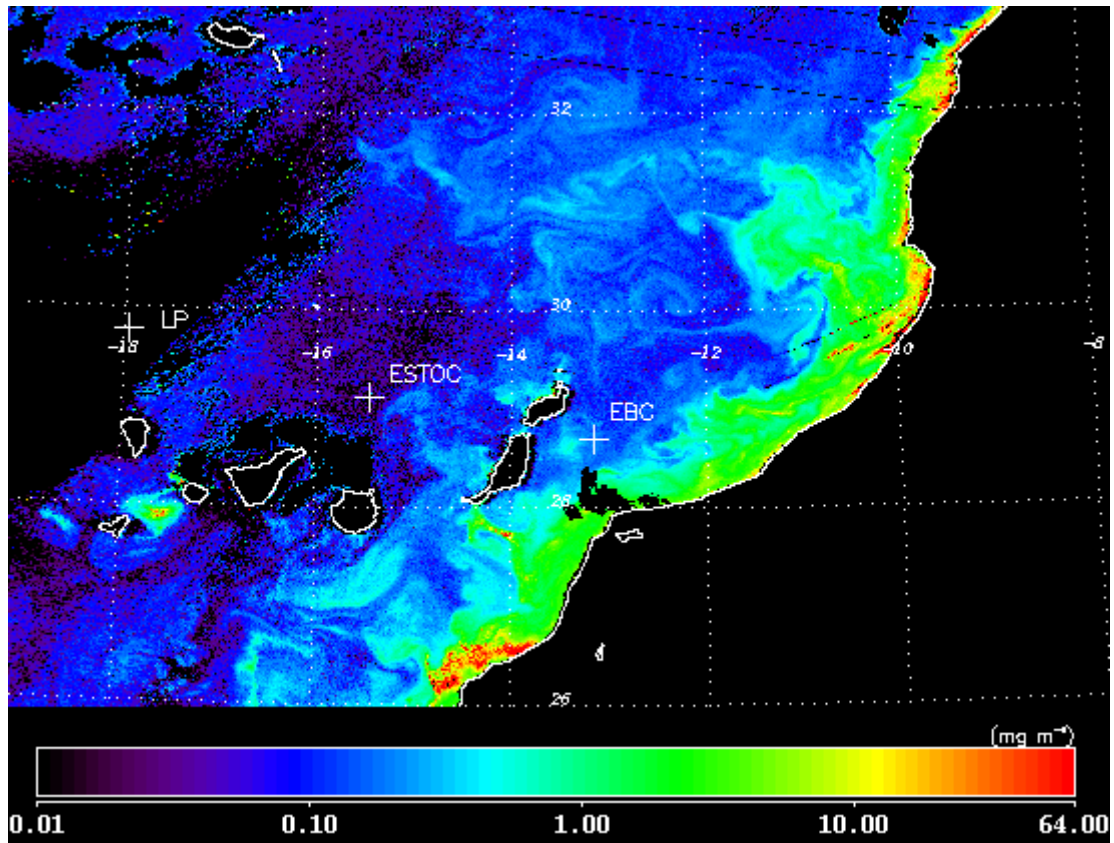
Figure 6. Large upwelling filament at Cape Ghir, 19 March 1998

3.2. Pigment Structures

The inspection of individual pigment images of the Cape Ghir filament often show a bewildering variety of structures. Nevertheless our analysis of the SeaWiFS images shows that certain structures are repeatedly observed both seasonally and interannually and can be related to specific wind patterns.

3.3. Summer upwelling period

Filament development during the main upwelling season from July to October showed a similar pattern each year. The onset of strengthening alongshore trade winds in July (Fig. 5) was observed as a compact filament structure with its major axis oriented southwest-northeast (Type A1, Figure 3) for three of the four years in the SeaWiFS data (July 1999, -2000, and -2001). The one exception was July 1998 which also showed a compact structure but with the major axis oriented east-west (Type A2). Nevertheless, a type A1 was observed in the previous month (June 1998); inspection of the meridional wind stress data (Fig. 5) shows that the summer trade winds had also started to strengthen one month earlier. During August, the filament's major axis tended to rotate clockwise into an east-west direction (Type A2) (August 1998, -2000, -2001) or became

more disrupted (Type A4) (August 1999, -2000) with no specific orientation. Through September-October the filament displayed a variety of forms ranging from compact structures oriented northwest-southeast (Type A3) throughto increasingly complex structures (Types A4 and A5). Occasionally meandering sub-filaments (Type F1) developed, stretching for several hundred kilometres offshore beyond the main filament (September 1998, September-October 1999, September 2001). These were also observed to develop compact eddies (Type F2) (August 1999, September 2001). The end of the main upwelling season was characterized by either a disrupted filament (Type A4) or the filament (Type A5) became part of a regional cyclonic circulation pattern in the Bay of Agadir to the south of Cape Ghir (November 1998, October 1999, December 2000, September-October 2001).

The consistent interannual pattern of filament development is correlated with the meridional wind stress data previously discussed i.e. peak meriodional wind stress in July each year decreasing through August-October, and implies a strong coupling between wind stress and the filament structure off Cape Ghir in the main upwelling season.

3.4. Winter/spring upwelling period

During the winter and early spring months the region off Cape Ghir is strongly influenced by the annual surface bloom off NWAF [*Davenport et al.*, 1999]. The filament structure was mostly suppressed in SeaWiFS imagery by the ambient pigment signal but was nevertheless visible during a weak annual bloom in February/March thus confirming that it is a permanent feature. In March/April the annual bloom receded revealing a diffuse filament structure extending several hundred kilometres off-shore (March 1998, April 1999, April 2000, April 2001). In March/April 1998 the filament also displayed a smaller compact structure (Type A4) but with an enormous diffuse structure extending some 500 km off-shore. It is possible that such extended structures are present each year but are generally not visible because of the annual bloom in this region.

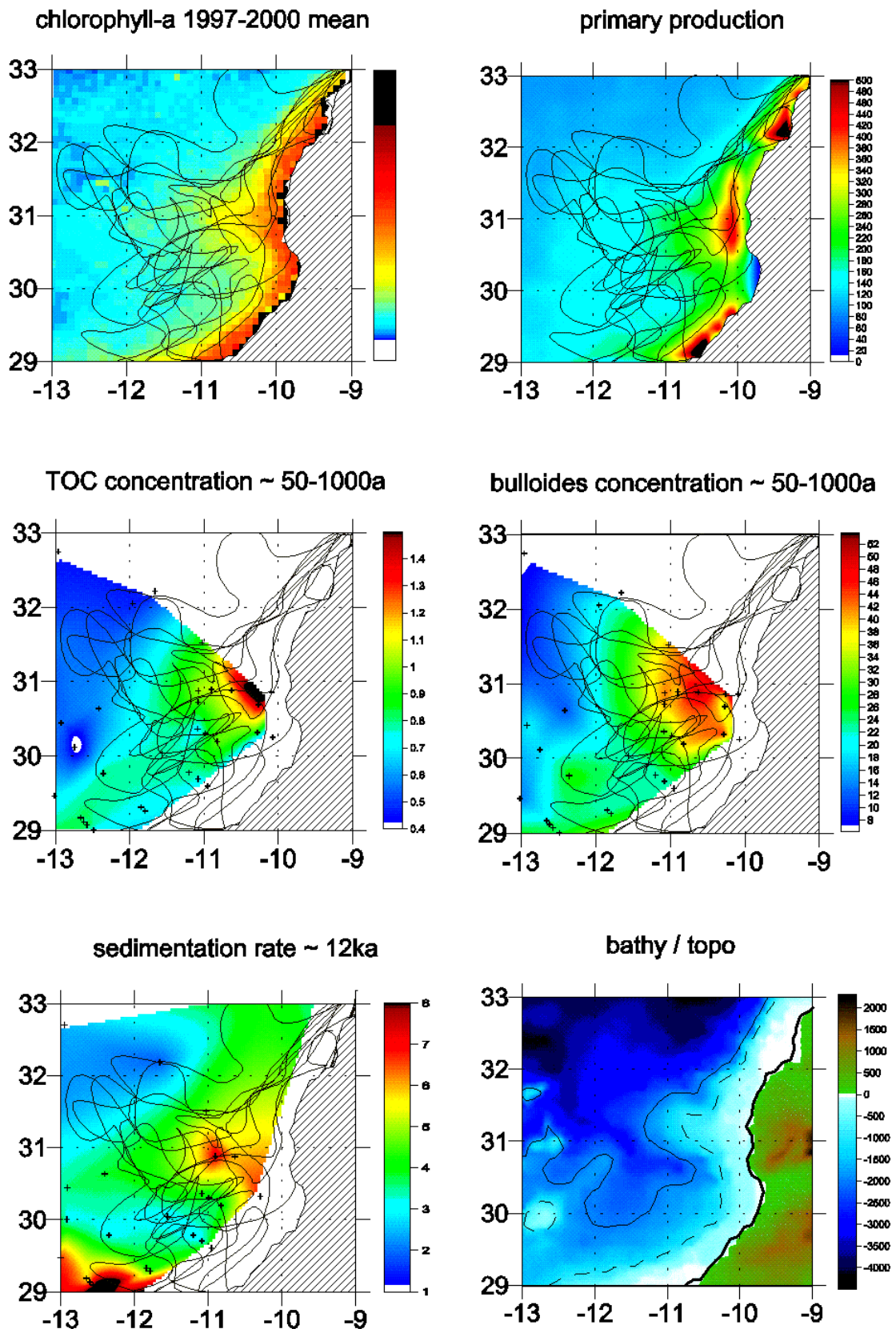**Figure 7.** Multiparameter comparison for the Cape Ghir region with main filament structures overlain: four year chlorophyll-*a* mean (upper left panel), yearly primary production (upper right panel), total organic carbon concentration in surface sediments (middle left panel), *G. bulloides* concentration in surface sediments (middle right panel), Holocene sedimentation rate (lower left panel) and bathymetry (lower right panel).

3.5. Cape Ghir upwelling signal in offshore surface-sediments

How would we expect the seasonal and interannual pattern of the surface biomass as seen in SeaWiFS imagery to be reflected in the surface-sediments off Cape Ghir? Total sediment accumulation rates off Cape Ghir have varied between about 4 cm ka^{-1} in the Holocene to 10 cm ka^{-1} in the Last Glacial Maximum based on analysis of the sediment core GeoB 4216 [*Henderiks et al.*, 2002]. The SeaWiFS data covers just over 4 years and it would seem unreasonable to make any prediction of long-term sediment accumulation rates and distribution of biomass associated with the filament given such a limited data set. We have demonstrated though, that the seasonal and interannual filament pattern is consistent over at least 4 consecutive years. Given that the trade wind system along the NWAF has been in place for at least 250 ka from analysis of marine sediments [*Freudenthal et al.*, 2002], we may assume that the same trade wind driven filament patterns observed today have also occurred in the past.

3.6. Holocene

The influence of the Cape Ghir filament on surface-sediments over the past 100-500 years is seen in the distribution of typical upwelling planktic foraminifera such as *Globigerina bulloides* (Figure 7) [*Meggers et al.*, 2002]. Although there is a low spatial resolution with the sediment core sampling approach, the influence of the Cape Ghir filament can be traced in a broad arc around Cape Ghir with its major axis zonally orientated (Figure 7). The lower concentration of *Globigerina bulloides* observed south of Cape Ghir (Figure 7) is reflected in the SeaWiFS data as to the initial southwesterly orientation of the filament during the onset of upwelling in July. Similarly, the orientation of the filament in a northwesterly direction during late fall leads to surface sediment deposition north of Cape Ghir.

During winter and spring, the filament may be oriented in any direction, but primary production is significantly reduced as a result of decreased solar insulation. That there appears to be a visual correlation between surface sediment distribution and seasonal filament patterns is not self-evident given the complex transportation mechanisms for surface particles through the water column. Nevertheless, we suggest that the trade wind pattern seen today appears to have driven the upwelling system off Cape Ghir in a consistent manner for at least the last 500 years and, apart from the brief glacial advance of the Younger Dryas, probably throughout the Holocene.

3.7. Last Glacial Maximum

It is generally assumed that during the glacial periods the trade winds intensified leading to increased alongshore wind stress off NWAF and intensified upwelling [*Sarnthein et al.*, 1982]. The lowering of sea level during the LGM by some 120 m [*Fairbanks*, 1989] moved the coastline off NWAF towards the edge of the shelf and hence the overall upwelling centre occured further west [*Freudenthal et al.*, 2002]. At Cape Ghir though the shelf edge is about 20 km offshore and hence the upwelling centre remained more or less where we see it today. Filament formation at Cape Ghir continued during the LGM according to results obtained with an eddy-permitting high resolution regional oceanographic model of the Canary Islands [*Freudenthal et al.*, 2001; *Johnson and Stevens*, 2000]. Given the higher trade wind stress it is therefore probable that the filament both intensified and extended further offshore than in the Holocene. The sediment core from site GeoB 4216 some 400 km west of Cape Ghir displays a highly variable productivity record over the last 250 ky. The core contains TOC concentrations with higher productivity, especially during the glacial periods as a result of increased upwelling at Cape Ghir [*Freudenthal et al.*, 2001]. In addidtion the sediment accumulation rate off Cape Ghir is higher in the Glacial than in the Holocene, particularly toward the southwest from Cape Ghir. Both these results are consistent with the SeaWiFS observations at the start of the main upwelling system in summer and the brief upwelling events in late winter/spring when the filament is oriented southwest and west due to elevated wind stress. Though the filament often develops a complex form during these periods, the overall consequence of increased wind stress in both cases is to extend the filament up to 500 km westwards as can be seen in the SeaWiFS image for 19 March 1998 (Figure 6).

4. Conclusions

The dynamic behaviour of the Cape Ghir filament as observed in SeaWiFS pigment imagery displays a consistent seasonal pattern which appears to be correlated with the strength of the alongshore wind. Although the filament often appears complex there is nevertheless a clear growth and progressive rotation of the filament axis from southwest to west in the main upwelling season. Typically, the filament tends to display an increasingly complex surface structure as the upwelling season progresses, with a non-resolvable orientation and elevated pigment patterns also in a northwest orientation from Cape Ghir. At other times of the year, particularly late winter/early spring, elevated wind-stress along the coast north of Cape Ghir may lead to substantial filament development, sometimes extending up to 500 km westwards. The main factor responsible for the development of the filament may be the forcing of the southward

coastal and offshore wind at Cape Ghir as a result of the shallower topography over the Cape Ghir Plateau (CGP) [*Hagen et al.*, 1996]. Nevertheless the observations from SeaWiFS imagery strongly suggest that once the filament has developed its surface manifestation is primarily modulated by the along-shore wind stress.

Acknowledgements

Northwest African upwelling and its effect on off-shore organic carbon export to the deep-sea

PEER HELMKE[1], OSCAR ROMERO[2], GERHARD FISCHER[1,2]

1 FB5 Geosciences, University of Bremen, Klagenfurterstraße, 28359 Bremen, Germany

2 DFG Research Center Ocean Margins University of Bremen, Klagenfurterstraße, 28359 Bremen, Germany

Abstract

We combined the analysis of sediment trap data and satellite derived sea surface chlorophyll-*a* to quantify the amount of organic carbon export to the deep-sea in the upwelling induced high production area off Northwest Africa. In contrast to the generally global or basin-wide adaption of export models, we used a regionally fitted empirical model. Furthermore, the application of our model was restricted to a dynamically defined region of high chlorophyll-*a* concentration. This was done to restrict the model application to an environment of more homogeneous export processes. We developed a correlation-based approximation to estimate the surface source area for a sediment trap deployed from 11.06.1998 to 07.11.1999 at 21.25N latitude and 20.64W longitude. We also developed a regression model of chlorophyll-*a* and export of organic carbon to the 1000 m depth level. The working area for this application was 5 – 36 deg latitude and 5 – 36 deg longitude. Carbon export was calculated for an area of high chlorophyll-*a* concentration (> 1 mg m^{-3}) on a daily basis. The resulting zone of high chlorophyll-*a* concentration was 20,000 – 800,000 km^2 in extend and yielded a yearly export of 1.123 to 2.620 Tg organic carbon. The average organic carbon export within the area of high chlorophyll-*a* concentration was 20.6 mg m^{-2} d^{-1} comparable to 13.3 mg m^{-2} d^{-1} as found in the sediment trap results if normalized to the 1000 m level. We found strong interannual variability in export. The period fall 1998 to summer 1999 was exceeding the mean of the other three comparable periods by a factor of 2.25. This excess was caused by an unusual extension of the high chlorophyll-*a* concentration area in that period rather than from an extreme increase of the mean export per unit area.

We believe that this approach can be successfully transferred even to different oceanographic regions by selecting appropriate definition criteria for the working area.

1. Introduction

The 'biological pump' plays an important role in the global ocean carbon cycle. Carbon dioxide (CO_2) dissolved in sea water, is transformed to particulate organic carbon during photosynthesis. Organic carbon (C_{org}) produced near the surface can be transferred to deeper parts of the water column by sedimentation and convection [*Longhurst and Harrison*, 1989]. As soon as the C_{org} leaves the surface mixed layer it is no longer available for remineralization and gas exchange at the ocean-atmosphere boundary layer. While sinking through the water column, a substantial part of C_{org} is remineralized by microbial respiration which converts it back to dissolved carbon dioxide.

The time-scale of exchange of CO_2 with the atmosphere depends on the remineralization depth. The ventilation of subphotic ocean waters typically takes up to one hundred years in the upper and mid ocean and up to several hundred years in the deep ocean therefore the biological pump in conjunction with CO_2 liberated by carbonate precipitation substantially controls the CO_2 concentration of the euphotic zone. Gas exchange at the ocean-atmosphere boundary layer couples the oceanic with the atmospheric CO_2 concentration. Regarding the pathways of marine carbon, two points are of particular importance to eastern boundary upwelling areas: (I) production is high in relation to the total upwelling area and (II) due to their wind-driven forcing, upwelling systems react quickly and sensitively to climate changes. Hence, understanding the export of C_{org} in upwelling regions is essential for the comprehension of climate change and its interrelation with atmospheric and oceanic CO_2 concentration.

In order to determine the temporal and spatial variations of particle flux, numerous investigations with sediment traps, accumulation rates from sediment cores or oxygen saturation at the sediment-ocean interface have been conducted worldwide during the last decades [*Jahnke*, 1996]. Observations of surface primary production and chlorophyll-*a* concentration as well as particle flux to the deep-sea reveal a series of complex, overlapping processes. Nutrient availability, plankton community, food web structure and the hydrodynamic regime have an impact on particle export efficiency [*Antia et al.*, 2001; *Bory et al.*, 2001; *Doval et al.*, 2001; *Fischer et al.*, 2000; *Jahnke*, 1996; *Lutz et al.*, 2002; *Martin et al.*, 1987; *Neuer et al.*, 2002; *Sauter et al.*, 2001; *Schlüter et al.*, 2000]. There have been several attempts to find relationships between sea surface parameters and sediment trap results. For example *Deuser et al.* [1990], *Asper et al.* [1992] and *Bory et al.* [2001] have shown that variations in primary production can

be reproduced in trap results. *Müller and Fischer* [2001] found good coherence of surface water temperature deduced from alkenone analysis of trap material and remotely sensed sea surface temperature. Faunal composition in sediment trap samples can indicate oceanic, upwelling or fresh-water provenance [*Romero et al.*, 2002]. Additionally, particle export was estimated by numerous models [e.g. *Bacastow and Maier-Reimer*, 1990; *Buesseler*, 1998; *Lutz et al.*, 2002; *Najjar et al.*, 1992; *Palmer and Totterdell*, 2001; *Sarmiento et al.*, 1995; *Schlitzer*, 2002; *Six and Maier-Reimer*, 1996; *Toggweiler et al.*, in press (2003)]. Although the qualitative relationship between surface parameters and the deep-sea record has been shown in several cases, it is still difficult to predict the amount of particle transfer from the surface to the deep-ocean [*Boyd and Newton*, 1999]. Recent studies suggest a link of deep sea C_{org} flux to ballast and especially carbonate than to surface production [*Armstrong et al.*, 2002; *Francois et al.*, 2002].
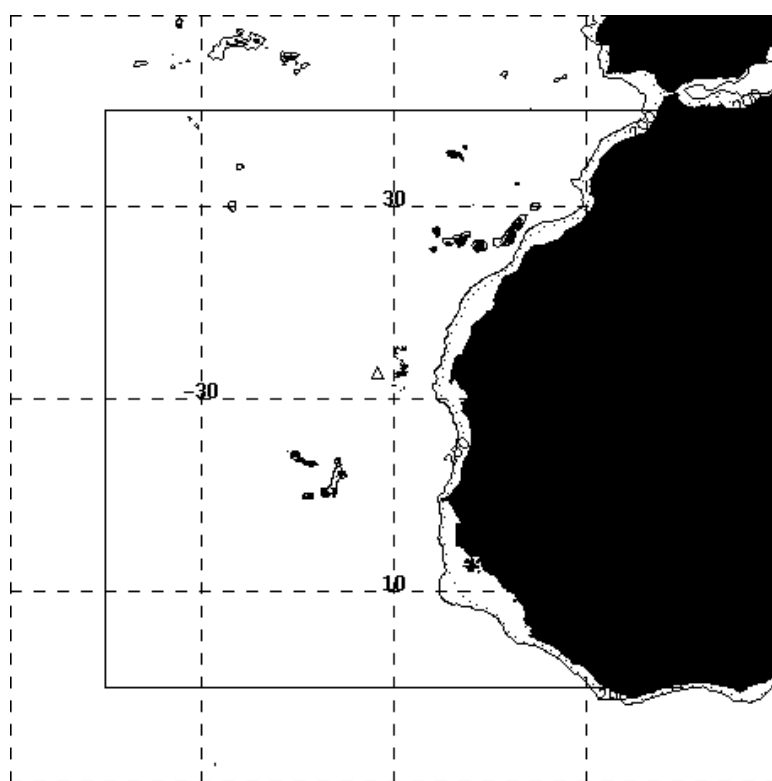
Figure 1. Study area off NW Africa with sediment trap location (full triangle), 200 m isobath (dotted line) and 1000 m isobath (solid line). The square (5° - 35°N and 6° - 35°W) shows the area for which C_{org} export was calculated.

Here we determine the empirical relationship of remotely sensed sea surface chlorophyll-*a* concentration in upwelling induced high chlorophyll-*a* areas and resulting deep-sea C_{org} flux. The C_{org} flux was recorded by a bottom tethered sediment trap deployed in 3850 m depth aproximately 200 km off Cape Blanc, NW Africa. Chlorophyll-*a* concentration for the working area from 5 – 36 deg latitude and 5 – 36 deg longitude as measured with the Sea-Viewing Wide-

Field-of-View Sensor (SeaWiFS) was provided by the Goddard Space Flight Center Distributed Active Archive Center. We carried out a lag-correlation analysis of the sediment trap record and surface chlorophyll-*a* to better determine the source area of deep-sea trapped C_{org}. The linear regression of the chlorophyll-*a* biomass in the source area and lagged trap signal was used as a simple empirical export model for the whole investigation area. The estimation of C_{org} export to the deep-sea from satellite-born chlorophyll-*a* data was restricted to the high productivity area (>1 mg Chl m^{-3}) off NW Africa to confine the model application to a more homogeneous working area. Shelf and upper ocean margin regions up to 1000 m depth were excluded to determine true export away from sea floor remineralization during deep winter mixing.

2. Regional settings

This study was carried out in the NW-African upwelling area, one of the prominent eastern boundary upwelling systems located at the eastern border of the North Atlantic Subtropical Gyre (Figure 1). The seasonal variation of NE trade wind position and intensity controls the westward directed Ekman transport of near shore surface waters. Upwelling of subsurface waters compensates for the surface mass deficit. The appearance and zonal width of the upwelling zone depends also on the shelf width and sea floor topography along NW Africa. The 50-70 km broad coastal band of "primary upwelling" is separated by a front from the Canary Current [*Hagen*, 1981] where "secondary upwelling" occurs [*Mittelstaedt*, 1991]. Along the coast, upwelled waters interact with the Canary Current and are deflected southward and westward. Upwelling is most persistent throughout the year near Cape Blanc at 20°N. Higher and lower latitudes show a more seasonal upwelling pattern, following the migration of the Intertropical Convergence Zone (ITCZ) [*Mittelstaedt*, 1991; *Nykjær and Van Camp*, 1994; *Schemainda et al.*, 1975; *Van Camp et al.*, 1991]. Along the NW-African coast, highest upwelling intensity is located at capes such as Cape Ghir, Cape Yubi, Cape Blanc and Cape Verde. Especially off Cape Blanc, "giant filaments" with chlorophyll-*a* concentrations above 1 mg m^{-3} persist year-round, spreading from the coast to several hundred kilometers offshore [*Van Camp et al.*, 1991]. North of Cape Blanc the upwelled water which originates from the North Atlantic Central Water mixes with South Atlantic Central Water towards the south [*Mittelstaedt*, 1983]. Increasing nutrient concentration south of Cape Blanc due to upwelling of nutrient rich South Atlantic Central Water promotes phytoplankton growth between Cape Blanc and Cape Verde. Towards 12°N upwelling is also fed by the North Equatorial Under Current [*Hagen and Schemainda*, 1984]. A further likely source of nutrients is the deposition of significant amounts of Saharan dust into the northern Atlantic by

the mid-tropospheric Harmattan winds originating from the central Sahara [*Mittelstaedt*, 1983; *Swap et al.*, 1996; *Torres-Padrón et al.*, 2002].

3. Data and Methods

3.1. Sediment trap data

Off the coast of Mauritania, NW Africa, particle flux was determined using sediment traps of type SMT 234 Aquatec Meerestechnik, Kiel. A sediment trap was deployed at 21.25°N; 20.70°W from 11.06.1998 through 07.11.1999 at a depth of 3580 m (trap ID: CB9). It was deployed 541 m above the seafloor to avoid input from particle resuspension. The sampling interval was 1x7.5, 18x27.5, 1x11.5 days [*Balzer et al.*, 2000; *Fischer and crew-members*, 1999]. To minimize biological activity, sampling cups were poisoned with $HgCl_2$ prior to and after deployment. Particles were water sieved using 1 mm mesh-width. Organic carbon was determined with a CHN-analyzer (HERAEUS) using a few milligrams of freeze-dried material (< 1 mm), which was decalcified with 6 N HCl in silver boats and dried on a hot plate at 80°C prior to the analysis. Organic carbon fluxes must be regarded as the lowest values due to degradation of organic matter in the sample cups [*Fischer et al.*, 2000; *Fischer and Wefer*, 1991].

3.2. SeaWiFS chlorophyll-*a* data

Satellite-born chlorophyll-*a* data derived from SeaWiFS measurements were used to evaluate the relationship of surface phytoplankton biomass and export to the deep-sea. Daily standard images mapped to an equidistant cylindrical projection with an equatorial resolution of 9x9 km [*Campbell et al.*, 1995] were used from the third reprocessing which used the OC4v4 algorithm [*O'Reilly et al.*, 1998].

Cloud coverage, aerosols, dust load in the atmosphere and suspended sediment in surface water impair the accuracy of space-born chlorophyll-*a* sensing. As far as possible, corrections for these influences are applied during data processing, otherwise corresponding data point were masked as invalid (NASA/GSFC SeaWiFS Data Processing Center). Recent changes in data processing have improved the yield of valid data significantly (For details see http://seawifs.gsfc.nasa.gov/SEAWIFS/RECAL/Repro4/changes.html). Orbital parameters and swath width of the SeaWiFS sensor result in bi-daily coverage at lower latitudes. The effective daily data coverage in the investigation area varied from 5 to 30%. The four-year mean was 14.2%. We created a rolling composite over 11 days, similar to those applied at the Goddard

Space Flight Center (http://seawifs.gsfc.nasa.gov/cgi/level3.pl), to obtain a compromise between data coverage, artifacts introduced by interpolation and CPU time. An inverse distance weighted mean (IDWM) to the center of the 11 day time-span was used to interpolate missing data. Afterwards we applied a circular IDWM in space with a diameter of 11 pixels. After the interpolation procedure some data gaps still remained at positions of persistent cloud coverage. We determined the area of best correlation of surface chlorophyll-*a* and sedimentation patterns to achieve a better approximation to the sediment trap source region. This was done by using the most likely statistical and hydrographical catchment area. As remaining gaps do not significantly disturb the calculations, we left these unfilled in order to avoid the use of imprecise data. However, to derive the C_{org} export quantitatively from chlorophyll-*a* data, missing data had to be estimated. Remaining data gaps were therefore filled with monthly SeaWiFS chlorophyll-*a* climatologies. The monthly climatologies were produced by calculating the mean of valid data for each coordinate of the corresponding month. The available monthly SeaWiFS chlorophyll-*a* time series ranged from September 1997 through to February 2002. The time span of available data leads to a monthly mean originated from four and five year observation. September - February means comprise a five year data range whereas the March to August means comprise a period of four years. (Since recently such climatologies are available at

http://seawifs.gsfc.nasa.gov/cgi/monthly_climatologies.pl).

3.3. Definition of upwelling zone

It is possible to define the area of upwelling by different parameters. Sea surface temperature, ocean color, and corresponding chlorophyll-*a* concentration, primary production as well as density, salinity or nutrient concentration can be used to discriminate upwelled water. Thus, the definition of the extent of upwelling influence is subject to the threshold of the respective parameter. Due to turbulent mixing of surface water and upwelled subsurface water there is no clear boundary but a transition zone between them. In this work, the high chlorophyll-*a* zone (HCZ) is studied and in accordance with preceding studies, a threshold of 1 mg chlorophyll-*a* m^{-3} is used for the HCZ [*Carr*, 2002; *Deuser et al.*, 1990; *Nixon and Thomas*, 2001; *Strub et al.*, 1991]. This perspective focuses more on the biological response to the higher nutrient supply and the resulting export of organic carbon than on the physical upwelling itself; a distinction is not made between elevated nutrient concentration in upwelled water and that resulting from winter mixing of near surface waters.

4. Results and Discussion

4.1. The sediment trap record

From June 1998 through to November 1999 total particle flux to the sediment trap at 3850 m shows three maxima: The strongest peak occurs in August – September 1998 (390 mg m^{-2} d^{-1}) and two lesser ones in February – April 1999 and July 1999 (345, 247 mg m^{-2} d^{-1}; Table 1, Figure 2). A longer period of reduced sedimentation (~ 100 mg m^{-2} d^{-1}) from mid October 1998 through to mid January 1999 separates the first two maxima. Over the 515 days of trap deployment, the mean total particle flux was 175 mg m^{-2} d^{-1}, and the mean C_{org} flux 6.2 mg m^{-2} d^{-1}. The C_{org} variability reflected that of the total flux, with maxima in August 1998 (12.3 mg m^{-2} d^{-1}), March 1999 (10.5 mg m^{-2} d^{-1}) and June 1999 (7.3 mg m^{-2} d^{-1}). The coefficient of variation was slightly higher for total flux (Cv=0.55) than for C_{org} flux (Cv=0.50). The average input of lithogenic material to the trap was 48.6 mg m^{-2} d^{-1}. The absolute maximum was reached in March 1999 with 115 mg m^{-2} d^{-1}. All peaks of organic carbon flux were accompanied by elevated lithogenic flux (Figure 2). The relationship of lithogenic and organic carbon flux is twofold; strong winds intensify upwelling induced phytoplankton growth as well as dust transport from the Saharan-Sahelian region [*Chomette et al.*, 1999]. Additionally, dust input to surface waters promotes formation of fast settling aggregates [*Buat-Ménard et al.*, 1989; *Ratmeyer et al.*, 1999]. The flux of $CaCO_3$ contributed 38% - 81% to the total flux and largely resamples the total flux pattern. *Armstrong* [2002] stated that mineral ballast is quantitatively accociated with C_{org} at least for depths > 1800 m. We found correlations for C_{org} and $CaCO_3$ r=0.75; C_{org} and lithogen r=0.3 and for C_{org} and total mineral ballast (opal, $CaCO_3$, lithogen) r=0.89.

The accuracy of sediment trap results may be impaired by the effects of lateral particle advection within the nepheloid layer [*Freudenthal et al.*, 2001] strong currents have also been identified to have a lasting influence on trapping efficiency [*Baker et al.*, 1988]. To evaluate this effect, Aanderaa current meters were deployed in the same mooring during May to November 1991 at 3600 m depth. A critical value of > 10 - 12 cm s^{-1} [*Knauer and Asper*, 1989] was reached for only one hour while the mean velocity for the period May to November 1991 was at 2.9 cm s^{-1}. Therefore, we assume that the CB9 trap was not disturbed by high current velocities.

Sample no.	Trap cup open	close	Duration (days)	Fluxes (mg m^{-2} day^{-1}) Total	C_{org}	Lithogen	% of Total	C_{org}	Lithogen	predicted C_{org} flux to 3850 m (mg m^{-2} day^{-1})
1	11.06.1998	18.06.1998	7.5	221.47	3.52	30.28		1.59	13.67	4.35
2	18.06.1998	16.07.1998	27.5	112.44	3.04	26.73		2.71	23.77	4.78
3	16.07.1998	12.08.1998	27.5	139.29	5.82	34.96		4.18	25.10	4.83
4	12.08.1998	09.09.1998	27.5	390.98	12.28	59.59		3.14	15.24	6.81
5	09.09.1998	06.10.1998	27.5	284.87	11.42	66.85		4.01	23.47	9.93
6	06.10.1998	03.11.1998	27.5	125.05	6.01	41.42		4.80	33.12	7.40
7	03.11.1998	30.11.1998	27.5	103.62	5.22	39.37		5.04	37.99	4.00
8	30.11.1998	28.12.1998	27.5	106.80	5.17	39.64		4.84	37.11	3.94
9	28.12.1998	24.01.1999	27.5	112.25	3.83	36.01		3.42	32.08	6.84
10	24.01.1999	21.02.1999	27.5	207.93	9.07	93.40		4.36	44.92	11.03
11	21.02.1999	20.03.1999	27.5	273.58	9.71	114.71		3.55	41.93	10.18
12	20.03.1999	17.04.1999	27.5	344.56	10.49	88.30		3.04	25.63	6.88
13	17.04.1999	14.05.1999	27.5	203.33	7.99	64.80		3.93	31.87	5.59
14	14.05.1999	11.06.1999	27.5	163.16	5.26	43.23		3.22	26.49	6.03
15	11.06.1999	08.07.1999	27.5	247.13	7.28	47.45		2.95	19.20	6.61
16	08.07.1999	05.08.1999	27.5	161.76	5.24	30.83		3.24	19.06	7.57
17	05.08.1999	01.09.1999	27.5	108.18	3.91	17.95		3.61	16.60	6.66
18	01.09.1999	29.09.1999	27.5	96.64	4.13	28.67		4.28	29.67	5.58
19	29.09.1999	26.10.1999	27.5	52.85	2.39	21.44		4.52	40.56	4.36
20	26.10.1999	07.11.1999	11.5	33.57	1.29	11.02		3.85	32.84	4.38
		av. mg m^{-2} day^{-1}		177.0	6.4	48.6	av. % 3.8		29.0	6.52
		av. g m^{-2} year^{-1}		64.6	2.3	17.7				2.38

Table 1. Sampling intervals, flues, percentages of total flux, organic carbon and lithogen for sediment trap CB9 (3850 m depth). All data refer to the <1 mm size fraction. The last column shows the regression model output for export to the trap-depth.

To evaluate trapping efficiency, natural radionuclide measurements were applied in preceding studies [*Bacon*, 1996; *Scholten et al.*, 2001; *Yu et al.*, 2001]. For this method, the ratio of 230Th flux measured in the traps to the expected 230Th flux from the production rate of 230Th in the overlaying water column was taken as a measure for trapping efficiency. While the Th flux in shallow traps (< 1000 m) was generally lower than predicted, the results of meso- to bathypelagic traps were validated [*Yu et al.*, 2001]. Hence, our trap results were not corrected for radionuclide trapping efficiency.
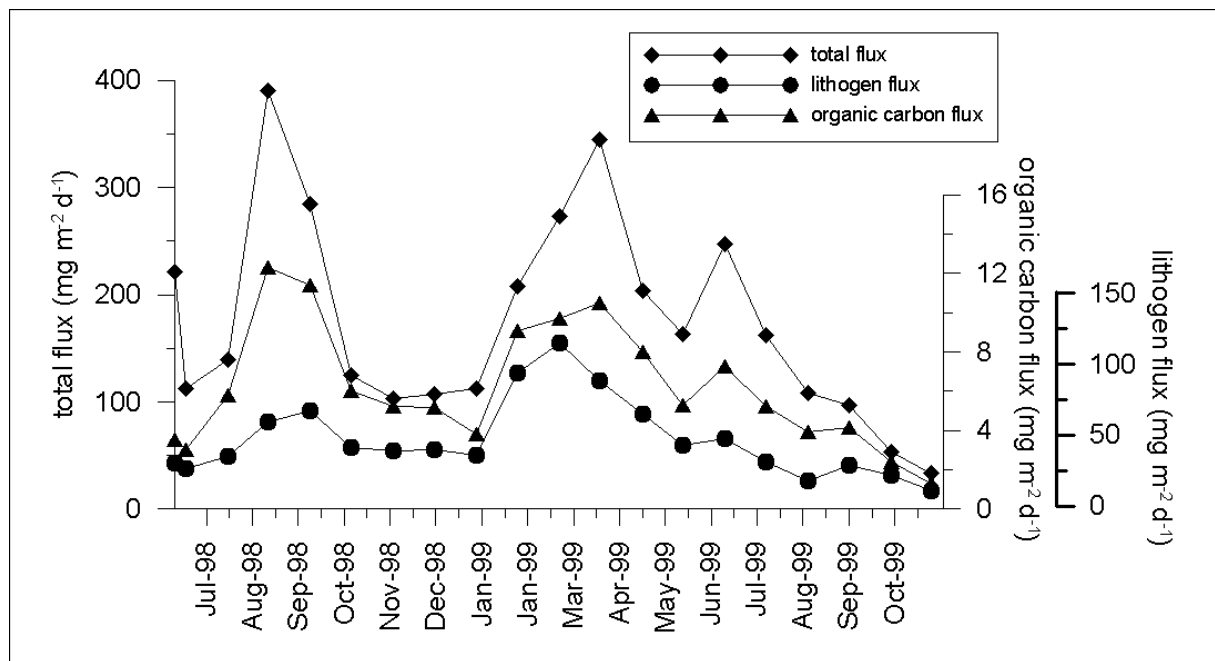

Figure 2. Fluxes of total particle (mg m^{-2} d^{-1}, full diamond), lithogenic material (mg m^{-2} d^{-1}, full circle) and organic carbon (mg m^{-2} d^{-1}, full triangle) at CB9 mooring site from June 1998 through November 1999.

To validate the CB9 trap usability as a basis for an later export model, is was indispensable to identify possible source regions for the sample material. In addition to a statistical determination of a possible surface source region described below, sample composition gives evidence for upwelling influence into the trap: The surface transport off the Cape Blanc area is strongly dominated by trade wind driven Ekman transport and the coastal branch of the Canary Current. Although this makes difficult to find out the exact origin of material collected by sediment traps, long-time sediment trap studies at the CB site allow recognition of a good relationship between the seasonal and interannual variability of the siliceous phytoplankton signal collected at the CB site, and the interplay of water masses and the large off-shore transport off Mauritania. Romero et al. [2002] related the strong contribution of neritic, coastal upwelling-associated diatoms during spring/summer into the pelagic realm to seaward transport of coastal waters. Higher fluxes of silicoflagellates and the dominance of pelagic diatoms, mainly in

winter, reflect the intermingling of open-ocean, nutrient-poorer waters in coincidence with periods of wind relaxation. Additionally, strong interannual variations of the diatom flux were associated with the reduction of coastal upwelling intensity and the seaward spreading of the chlorophyll-*a* filament [*Romero et al.*, 2002].

4.4. Temporal evolution of phytoplankton biomass from coast to trap station

A time-series of surface chlorophyll-*a* was extracted at five positions equidistantly placed between the sediment trap mooring and the adjacent African coast due east to track the signal of phytoplankton growth (Figure 3). Assuming a mainly upwelling driven off-shore transport of surface water, one might expect to see pulses of high chlorophyll-*a* concentration passing over some of the locations. At least one chlorophyll-*a* maximum was clearly tracked from the coast to the trap position and was recorded subsequently in the trap itself. It was first seen near the coast at 18.10.1998 and migrated the 360 km distance towards to the trap location in the west with an average velocity of 0.07 m s^{-1}. Small-scale internal velocities within off-shore transported upwelled water may be substantially larger. For example, *Kostianoy and Zatsepin* [1996] analyzed satellite images and in situ sea surface temperature to determine cross frontal water exchange. They observed an average off-shore development of fast cold-water injections of 0.91 m s^{-1} between 15° and 25°N off NW Africa. Our observation of a bloom at all five positions should therefore be considered exceptional taking into account the highly turbulent nature of off-shore waters (e.g. meandering, eddy formation) and conditions unfavorable for optical remote sensing.

The surface motion of chlorophyll-*a* blooms prior to other peaks in particle flux in mid- to late summer 1998 and 1999 can not be detected in the surface chlorophyll-*a* time-series. A possible explanation is that chlorophyll-*a* measurements in both periods suffer from weak data coverage in the non-interpolated daily source data. The seasonally migrating ITCZ has its northernmost position in the late boreal summer and prevents continuous ocean color sensing due to increased cloud cover. While the average data coverage for the whole trapping period is about 12.6%, it decreased to 4.5% and 3.7% in June to September 1998 and 1999, respectively. A high coverage of 24.6% is reached from 21.11.1998 to 12.5.1999 which included the tracked chlorophyll-*a* maximum.
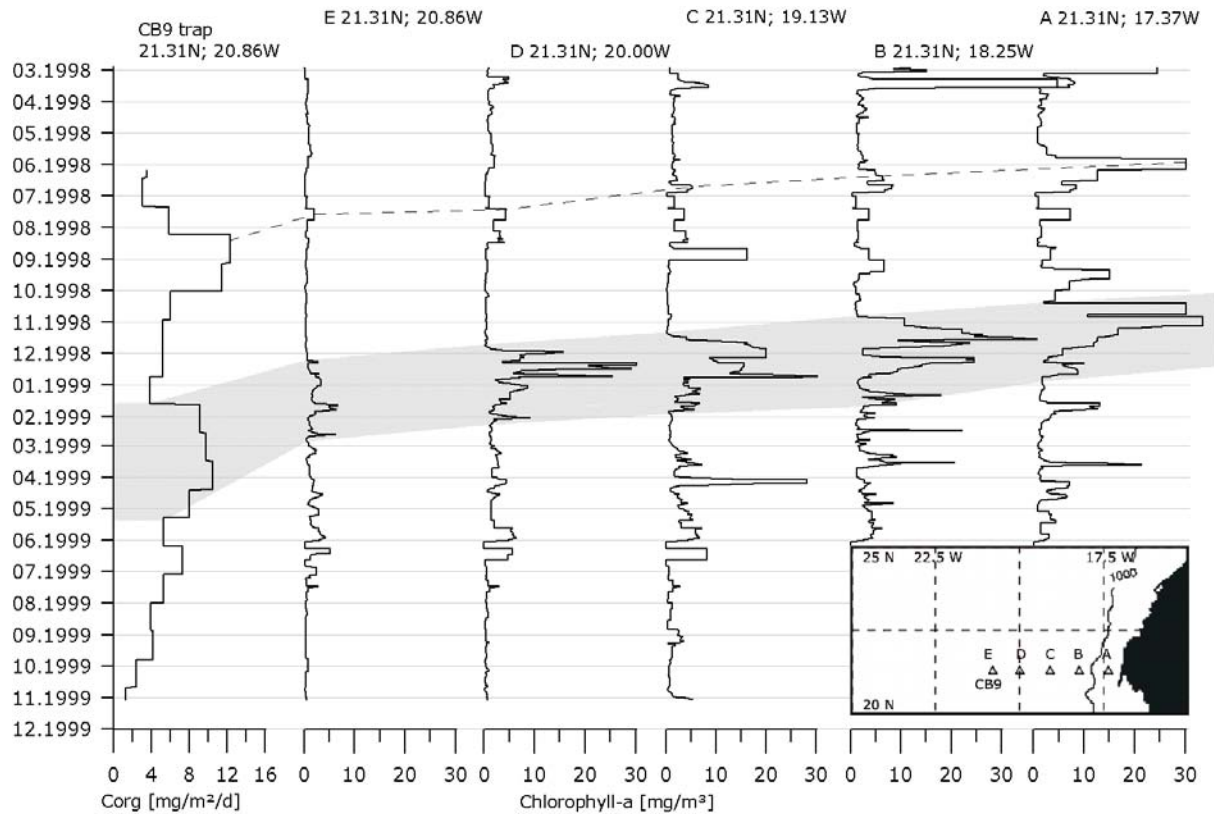
Figure 3. Surface chlorophyll-*a* time-series for the CB9 trapping period. Equidistantly placed time-series on a zonal transect between 35 km off the African coast (A) and the trap position (E) were extracted to identify single events of high chlorophyll-*a* concentration near the coast and to track their offshore westward transport towards the trap position. One chlorophyll-*a* maximum can be clearly followed from the coast to the trap position (A-E) and into the trap (E-CB9) (gray shaded). A less-pronounced maximum detected in June 1998 at 17.37°W is assumed to arrive in the trap ~ 80 days later (dashed line). (E) matches the CB trap location.

The rate at which particles sink is very much dependent on the nature of the particle [*Siegel et al.*, 1990]. Ultraplankton, for example, sink at <0.1-2 m d^{-1} [*Bienfang*, 1980], algal aggregates 40-150 m d^{-1} [*Smetacek*, 1985] and mesozooplankton fecal pellets 20-900 m d^{-1} [*Fowler and Small*, 1972].

The delay between chlorophyll-*a* peaks at the sea surface and the corresponding sedimentation peaks in the trap show an average lag of 47.6 days varying between 21 and 61 days. With a trap deployment depth of 3580 m, this reveals a mean downward particle flux velocity of 88 m d^{-1} with absolute values between 59 and 170 m d^{-1}. This is comparable to results from previous studies [*Deuser et al.*, 1990; *Fischer et al.*, 1996; *Müller and Fischer*, 2001; *Ratmeyer et al.*, 1999]. High sinking speeds of 280 m d^{-1} found in 1990-1991 at the CB position are interpreted as a consequence of high lithogen input [*Fischer et al.*, 1996].

4.6. **Spatial correlation of surface chlorophyll-*a* with export flux**

The approach of best correlation fit was chosen to estimate the trap source region. The following steps were performed to determine the spatial correlation and the source of material:

I. The C_{org}-flux measured in the trap was interpolated to daily values using a cube spline interpolation [*Deuser et al.*, 1990].

II. A time-series of average chlorophyll-*a* data was extracted over an area of 99 by 99 km (11 by 11 pixel) to the east of the trap position. This area was used as a first approximation of the source area. Matching patterns of maxima in C_{org}-flux and surface chlorophyll-*a* exhibited an average time shift of 47 days. A 47-days lagged correlation of C_{org}-flux and a daily mean over the 99 by 99 km box revealed a moderate correlation of r=0.52.

III. A 47-days lagged correlation of C_{org}-flux at each pixel of the chlorophyll-*a* field served as a better approximation for the source region. A series of lagged correlations with an increasing lag from 0 to 100 days at a ten day interval was produced to study the temporal evolution of the relationship between surface chlorophyll-*a* and interpolated C_{org} flux (a selection is shown in Figure 4).

IV. In order to meet the requirement that the source area be located within the 'statistical funnel' [*Siegel and Armstrong* 2002; *Siegel and Deuser*, 1997] or 'catchment area', [*Waniek et al.*, 2000] and within a hydrographically sensible vicinity to the trap, a semicircle of 800 km radius to the east of the trap location was selected. Within the semicircle, the zone of correlation r > 0.5 at 47 days lag was taken as the trap-signal source region. These selection parameters resulted in an area of about 6000 km^2 bounded by latitudes 20.3° and 22.8°N, and longitudes 19.2° and 20.2°W. The center of this area is at 21.76°N and 19.74°W, 116 km to the northeast of the trap position (Figure 4). The empirical relation of lagged chlorophyll-*a* concentration and C_{org}-flux improved from r=0.52 (for the 99 by 99 km box) to r=0.74 for the source region defined here.
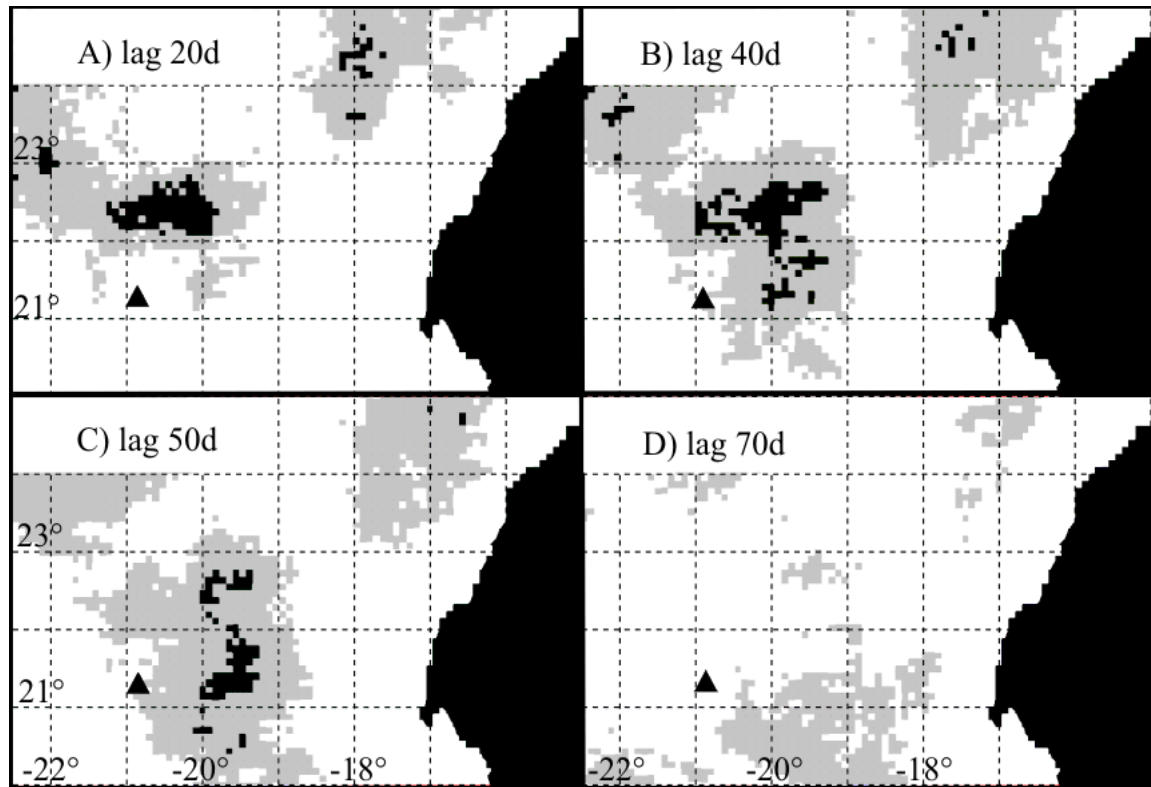
Figure 4. Correlation pattern between surface chlorophyll-*a* and sediment trap C_{org} flux at lags of 20, 40, 50 and 70 days. The development of the shaded area of correlation (gray, $r > 0.3$; black, $r > 0.5$) indicates the influence of more southeasterly and more distant source regions to the trap (full triangle) with increasing lag.

The development of the spatial correlation was analyzed to identify particle transport towards the trap. At zero lag, only a narrow area east of the trap position reflected positive correlation. With increasing lag, the area of positive correlation expanded towards the coast in the east and the south, while the degree of correlation itself increased. The near-shore region showed positive correlation only when the lag exceeded 60 days. This migrating pattern of the relationship with increasing lag from the trap position towards the east can be interpreted as an impact of different particle sources. Autochthonous, near surface grown biomass may contribute to the deep-sea flux within a few days. Distantly-grown material, which mainly contributes to the flux, is transported in the surface flow field for days to weeks before settling. Hence, the distance between trap position and good correlation to surface signal growths with increasing lag. This near surface transport is not necessarily restricted to the euphotic zone and is therefore within the sensitive depth for the SeaWiFS sensor.

Rapid particle settling may occur during aeolian input of Saharan dust [*Chiapello et al.*, 1995; *Swap et al.*, 1996] and the ensuing formation of high density aggregates [*Ittekkot*, 1996]. This observation has been confirmed by good correlation of C_{org} and lithogenic flux (r=0.83) Even previous trap experiments at the Cape Blanc location have shown this relationship [*Fischer*

et al., 1996; *Ratmeyer et al.*, 1999]. At a nearby position (18.5°N; 21.0°W) *Bory et al.* [2001] found sinking speeds of up to 800 m d^{-1}. The fast transport of the surface chlorophyll-*a* signal down to the deep sea faciliates the good correlation and contributes to the good fit of the later regression model.

With this correlation of surface chlorophyll-*a* and flux signal we attempted to approximate the real source region of the trap signal better than the selection of rectangular boxes around the trap. However, even this method is just an approximation of the source because the correlation analysis can not resolve displacements of the source region due to e.g. seasonal current changes [*Siegel and Deuser*, 1997; *Waniek et al.*, 2000]. Furthermore, it must be considered that each trap sample is likely to be composed of particles of different sizes, density and hydrodynamic properties and, therefore, different transport durations, leading to different source regions.

The development of the correlation pattern confirms previous findings about the direction and velocity of upwelling driven lateral particle transport and vertical particle flux in the Cape Blanc region [*Kostianoy and Zatsepin*, 1996; *Mittelstaedt*, 1983]. Therefore, the more sensible correlation analysis appears to be a reliable approximation of the trap signal source region.

4.7. Relationship of chlorophyll-*a* to export flux

Several attempts have been made to link export flux to surface production either from in situ measurements or from satellite derived primary production [*Antia et al.*, 2001; *Fischer et al.*, 2000]. Both methods have their specific advantages and disadvantages. Although in situ measurements may be inherently more reliable, despite ongoing discussion regarding accuracy and compatibility of the different methods used, it is nevertheless extremely difficult to get sufficient spatial/temporal resolution. Computations of primary production from satellite sensors provide unique resolution in time and space; the algorithms, however, are mostly globally fitted [*Behrenfeld and Falkowski*, 1997; *Howard and Yoder*, 1997]. Hence, regional characteristics might be neglected or even misinterpreted. The approach of linking deep-sea fluxes directly to remotely sensed sea surface pigment concentration was first used by *Deuser et al.* [1990]. They investigated the relationship of seven years of organic carbon flux at 3200 m in the Sargasso Sea and Coastal Zone Color Scanner ocean color. A lag of 45 days revealed a correlation of r=0.81 for the mean cycles of surface pigment concentration and organic carbon flux to 3200 m. In this study, a linear regression model was chosen to examine the relationship of sea surface chlorophyll-*a* and trap signals. We extracted the daily mean from the source region, previously defined by the degree of correlation. As a preparation for the regression analysis five main maxima in the C_{org} flux curve were fitted to the corresponding five chlorophyll-*a* time series

maxima with a pre-selected time shift of 47 days, using the software program AnalySeries [*Paillard et al.*, 1996]. The fitting is reasonable to avoid apparently low correlation and regression caused by displaced maxima. It is equivalent to a normalization of the average transport duration. A test of different smoothing factors applied to the chlorophyll-*a* concentration reveals the best correlation with a 50 days running average. The smoothing of the chlorophyll-*a* signal reflects the turbulent mixing during the vertical transport to the trap. Additional sedimentation pulses can be smoothed out due to stimulation of mid-water biological activity as a response to elevated food supply [*Lampitt and Antia*, 1997]. The smoothing and broadening of surface primary productivity peaks with increasing depth has also been documented by *Asper et al.* [1992] during the oligotrophic Oceanic Flux Program 80 km southeast of Bermuda in 1989-1990. Applying the smoothing to the lagged chlorophyll-*a* data for the source region proposed in this study, the best linear fit between sea surface chlorophyll-*a* and C_{org} flux at 3850 m ($FC_{org(trap)}$) is

$$FC_{org(trap)} = 3.52 + 1.06C_{Chl} \text{ , } r = 0.74 \text{ .} \tag{1}$$

The scattering of data in Figure 5 (inlay) may suggest a non-linear part in the low chlorophyll-*a* region. However, we applied the linear model because (a) only one sediment trap sample is responsible for low C_{org} flux values (< 2 mg C_{org} m^{-2} d^{-1}) and (b) for the application of the data model only HCZ were examined, which have a chlorophyll-*a* concentration by definition > 1 mg chlorophyll-*a* m^{-3}, within the more linear section of the relationship (Figure 5, inlay). The relatively small number of 20 trap samples does not permit a reliable fit to a higher order polynomial function. Although the direct relation of surface chlorophyll-*a* concentration and organic carbon flux in the deep-sea has been questioned [*Boyd and Newton*, 1999], the regional approach and use of concurrent data in this study clearly support this connection.
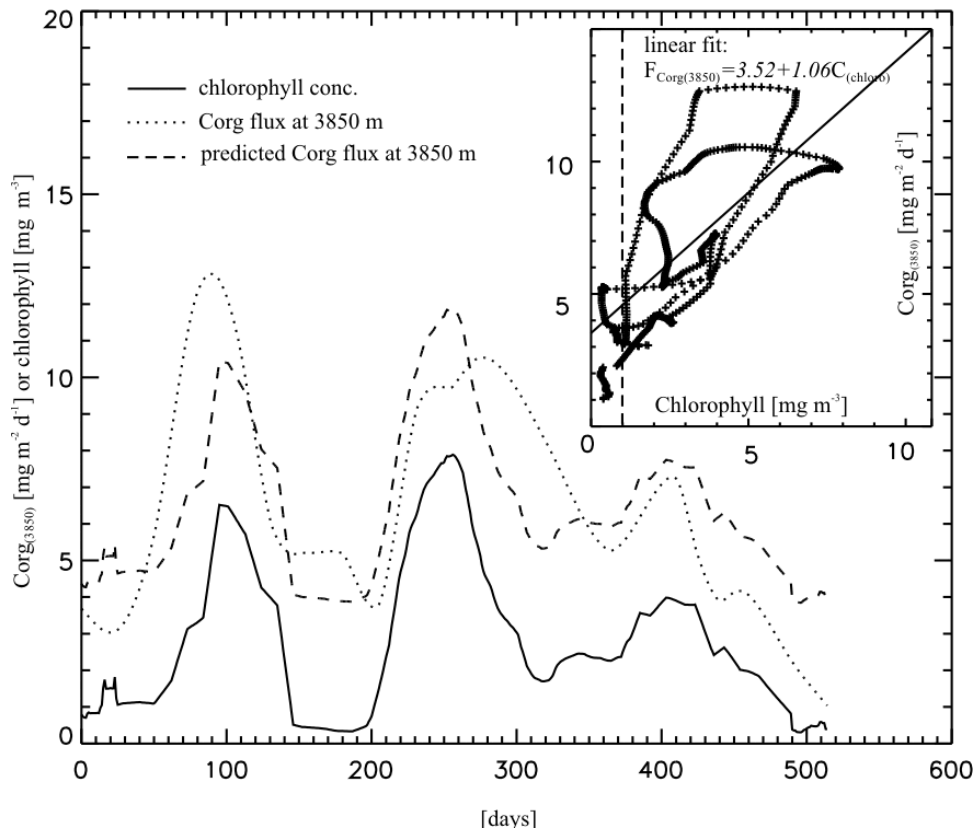
Figure 5. Chlorophyll-*a* concentration in the source region (mg chlorophyll-*a* m^{-3}, solid line), C$_{org}$ flux at 3850m (mg C$_{org}$ m^{-2} d^{-1}, dotted line), predicted C$_{org}$ flux at 3850 m (mg C$_{org}$ m^{-2} d^{-1}, dashed line). The inlay shows the scattering of C$_{org}$ flux at 3850 m against the lagged surface chlorophyll-*a* for the trapping period (Jun '89 - Nov '99) and the linear fit. The threshold for the export calculation is also shown (dashed line).

4.8. Calculated export to the deep-sea in the HCZ

The linear regression model was applied to HCZ along the NW African coast, where the SeaWiFS chlorophyll-*a* concentration is > 1 mg m^{-3}. Data from August/September 1997 to the end of 2001 were used to calculate C$_{org}$ export from the photic layer to the deep-sea. The export to the deep-sea is an estimate within a box region covering the NW-African upwelling from 5 – 36 deg latitude and 5 – 36 deg longitude that includes far offshore drifting plankton blooms, but excludes signals of the Azores front in the north or equatorial upwelling in the south. These prerequisites were chosen to restrict the calculations to a sufficiently homogeneous environment for which the export function was assumed to be valid. For the export calculation, shelf and upper ocean margin regions up to 1000 m depth were excluded. According to JGOFS protocols [*Ducklow and Dickson*, 1996], 1000 m depth is established as an international reference for mid-depth sediment trap deployments. Flux at 1000 m depth is considered true export since it is below the depth of deepest mixing. We normalized the calculated export to 1000 m using the

formula developed by *Martin et al.* [1987] so as to utilize the outcomes in comparisons with other results referring to the 1000 m reference depth.

$$FC_{org(1000)} = FC_{org(trap)} / (Z_{trap}/1000)b .$$ (2)

Where $FC_{org(1000)}$ is the C_{org} flux at 1000 m, $FC_{org(trap)}$ is the C_{org} flux at trap depth and Z_{trap} is the trap depth (3850 m) and the exponent b describes the depth dependence of flux. *Martin et al.* [1987] derived an exponent of b=-0.858 from six free-floating particle interceptor traps from 1980 to 1984 in the oligotrophic northeast Pacific. This "open-ocean composite" was used in several export studies [e.g. *Buesseler et al.*, 2000; *Emerson et al.*, 1997; *Fischer et al.*, 2000; *Sarmiento et al.*, 1998]. The shape of the particle flux profile depends mainly on vertical transport velocity and microbiological remineralization efficiency. Since these factors vary with space and time, the shape of the particle profile and hence the exponent b is variable [*Francois et al.*, 2002; *Schlitzer*, 2002; *Usbeck*, 1999]. In our study an exponent fitted to high production areas is more appropriate. Hence a composition of exponents from California and Peru upwelling stations was used (VERTEX Stat. 1 and PERU; [*Martin et al.*, 1987]). For the given trap depth of 3850 m the high production composite exponent (b=-0.576) yield a 46% higher export to 1000 m than the oligotrophic exponent (b=-0.858). Combining export function (1) and depth normalization (2) results in the following relationship for surface chlorophyll-*a* and C_{org} flux to 1000 m:

$$FC_{org(1000)} = (3.52+1.06C_{Chl}) / (Z_{trap}/1000)b .$$ (3)

Applying the relationship to the chlorophyll-*a* field, all four years (1998 – 2001) were characterized by a clear, recurring seasonal export pattern (Figure 6). From a minimum in August-September, the export increased up to the April-May maximum the following year, but with superimposed short-term spikes of intensified export. Cross-shelf transport of nutrients due to deep mixing during periods of increased trade wind strength supports the growth of phytoplankton in the off-shore area in spring. The area of high chlorophyll-*a* concentration decreased rapidly from May to August (Figure 6 a) and consequently the calculated export did (Figure 6 b). The period from August 1998 to July 1999, which was covered by the CB9 trap deployment, developed remarkably differently. An exceptional increase of export of up to 19.2 Gg C_{org} d^{-1} from the HCZ was found, which was about three times the maximum of 6.0-7.8 Gg C_{org} d^{-1} in the other three years (Table 2). After a decrease in January 1999, the spring bloom

maximum in 1999 developed much broader and stronger than in 1998, 2000 and 2001. As a result, the accumulated C_{org} export in August 1998 to July 1999 reached 2.25 times the mean yearly export of the other three comparable periods or 1.72 times that of all four years. We lack a definitive explanation for the exceptionally high export in 1998 – 1999. However, the multivariate El Niño/Southern Oscillation index was extraordinary high in February to May 1998 (Climate Diagnostics Center, University of Colorado at Boulder, www.cdc.noaa.gov/ENSO/). Some authors propose teleconnections from ENSO driven anomalies in the Pacific even to the Atlantic region [e.g. *Barton et al.*, 1998; *Dong et al.*, 2000; *Huang et al.*, 1998; *Janicot*, 1997; *Roy and Reason*, 2001].
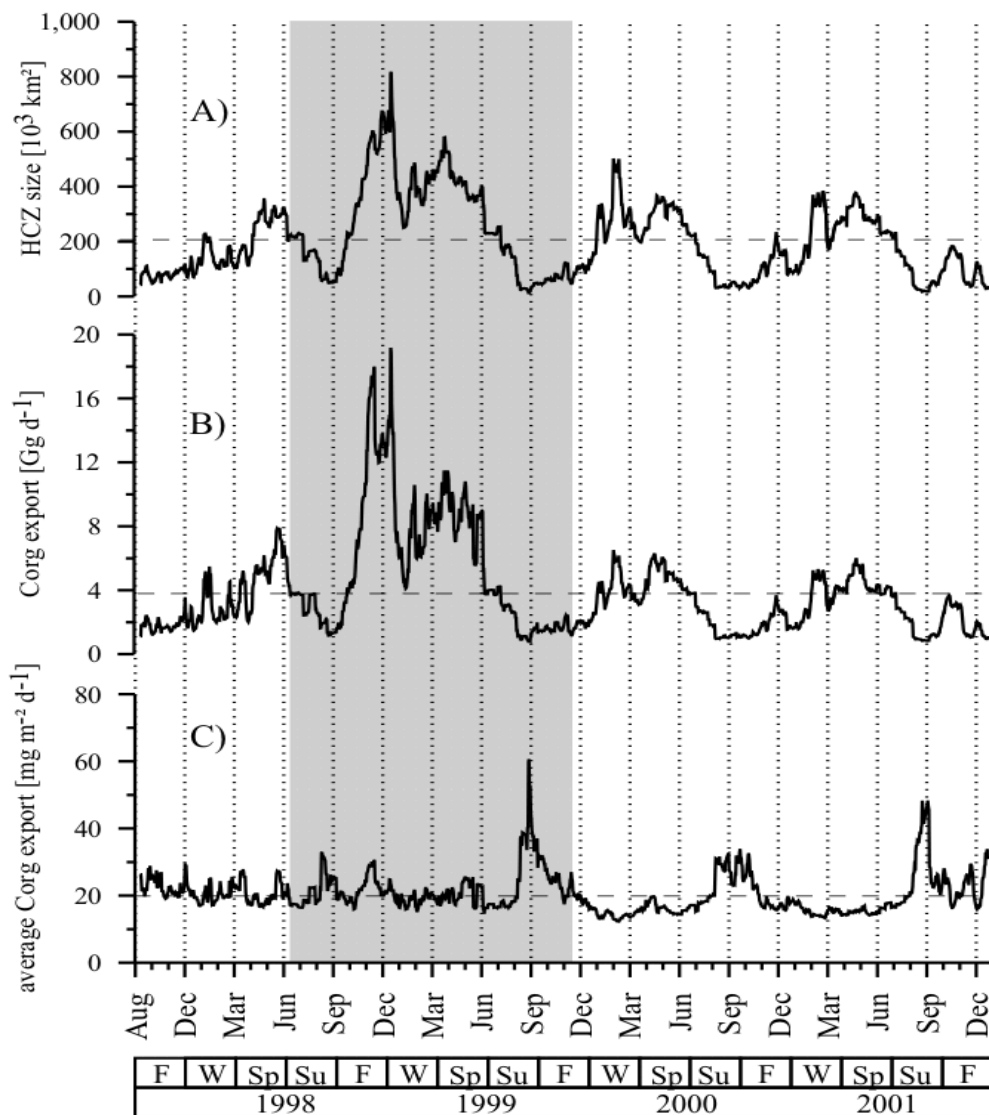

Figure 6. Size of high chlorophyll-*a* zone (HCZ) (A), C_{org} export to 1000 m integrated over the HCZ per day (B), and average C_{org} export per m^{-2} (C) with over-all means (dashed line) is presented. The CB9 deployment period is indicated (gray shaded).

		C_{org} export (Gg / season)	C_{org} export anomaly (Gg / season)	yearly average (period Aug. – Jul.; Tg / year)
1997	fall	162.13	-107.45	
1998	winter	247.81	-104.27	1.12
	spring	441.74	-79.77	
	summer	291.75	28.52	
	fall	717.41	447.83	
1999	winter	789.65	437.56	2.62
	spring	814.63	293.12	
	summer	278.63	15.39	
	fall	149.35	-120.23	
2000	winter	330.64	-21.44	1.15
	spring	430.82	-90.69	
	summer	236.98	-26.26	
	fall	139.31	-130.27	
2001	winter	270.61	-81.48	1.13
	spring	398.86	-122.65	
	summer	245.58	-17.66	
	fall	179.71	-89.87	
	winter	121.72	-230.36	

Table 2. Seasonal and yearly total export of C_{org} in the HCZ and the seasonal export deviation from the four year seasonal mean. The yearly average missing data in 1997, before the onset of SeaWiFS data acquisition, was derived using the mean of the corresponding periods in August 1999 and 2000.

The coherent structure of HCZ size and daily C_{org} export is reflected in the low variability in the average C_{org} export (Figure 6 c). Independent of the size of the HCZ, the average export from August 1997 to July 1999 varied only between 12 and 32 mg m^{-2} d^{-1}. Similar yearly mean C_{org} export values had been reported by *Fischer et al.* [2000] for the CB site in 1988-1991. Locations of higher export are smoothed out by large areas of lower export at the off-shore parts of the HCZ. Momentary peaks of high average export originate from small HCZ patches in upwelling minimum periods around September 1999, 2000 and 2001 which lack the lower chlorophyll-*a* transition zone. In September 1998 this HCZ minimum was not pronounced, hence the transition zone was established and the peak in average export did not occur. While the summer maxima in the 1999 to 2001 average export exceed the maximum in 1998 by up to 100%, the high frequency variation is significantly smaller in the second half of the study period.

The four year average C_{org} export of 20.6 mg m^{-2} d^{-1} is about 1% of the primary production rate calculated from *Longhurst et al.* [1995] for the "Canary Current Coastal" province (2.01 g m^{-2} d^{-1}). Taking into account that at least 2/3 of our HCZ is covered by the "North Atlantic Tropical Gyre" with a low primary production rate of 0.29 g m^{-2} d^{-1}, the resulting export ratio

increases to 0.3 which is within the range found in other studies [*Antia et al.*, 2001; *Berger et al.*, 1988; *Betzer et al.*, 1984; *Pace et al.*, 1987; *Suess*, 1980].

The seasonal variation of the spatial C_{org} export pattern to 1000 m is shown in Figures 7a and 7b. Generally, small variation is observed in summer (June to August) over the years 1998 – 2001 where the zone of HCZ is approximately restricted to 16° - 24°N latitude. The three-month mean for C_{org} export does not exceed 22 mg m^{-2} day-1 in this season. The variability increases in fall (Spt - Nov), when export was strong and extends up to 1300 km westward in 1998, but was weaker and more confined to the coast in 1999 through to 2001. Stripes of enhanced export were recognized in 2000 and 2001 along the coast southwards to 6°N. In winter (Dec – Feb) the export developed a large spatial extension from 6°N to 24°N and, except for 1998, was characterized by elevated export patterns extending far off shore. The winter variability was dominated by the extraordinary export production in 1999 when the near shore export was much higher and the westward extension exceeded the other three years by up to 1000 km. A 'hot spot' of export was confined to a 250 km wide region centered at 20°N in the southwest of Cape Blanc and near the shelf edge around Cape Verde.

Spring was the season of strongest export in all years except 1999, when the highest export developed in winter. Near-shore C_{org} export values of more than 27 mg m^{-2} d^{-1} in 1998 - 2000 and up to 22 mg m^{-2} d^{-1} in 2001 reflected the main upwelling season. Almost every season showed small patches of enhanced export in the southwest of Cape Ghir and Cape Yubi caused by the pronounced upwelling at cape locations.
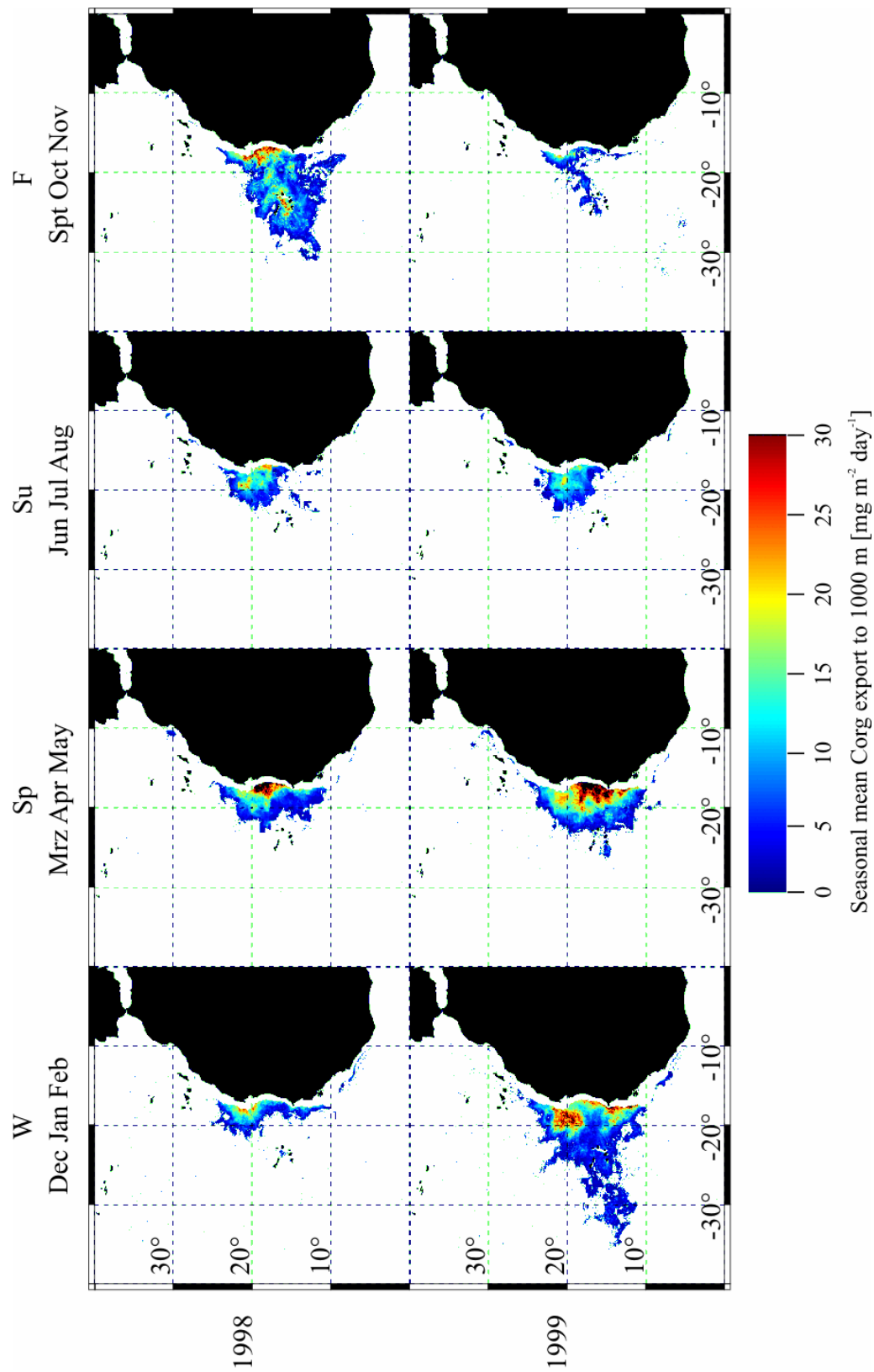
Figure 7a. Seasonally averaged C$_{org}$ export. A spring maximum is visible in all years, additional strong export with exceptionally far westward extension is evident from September 1998 to February 1999. Interannual variation is smallest during spring and summer.
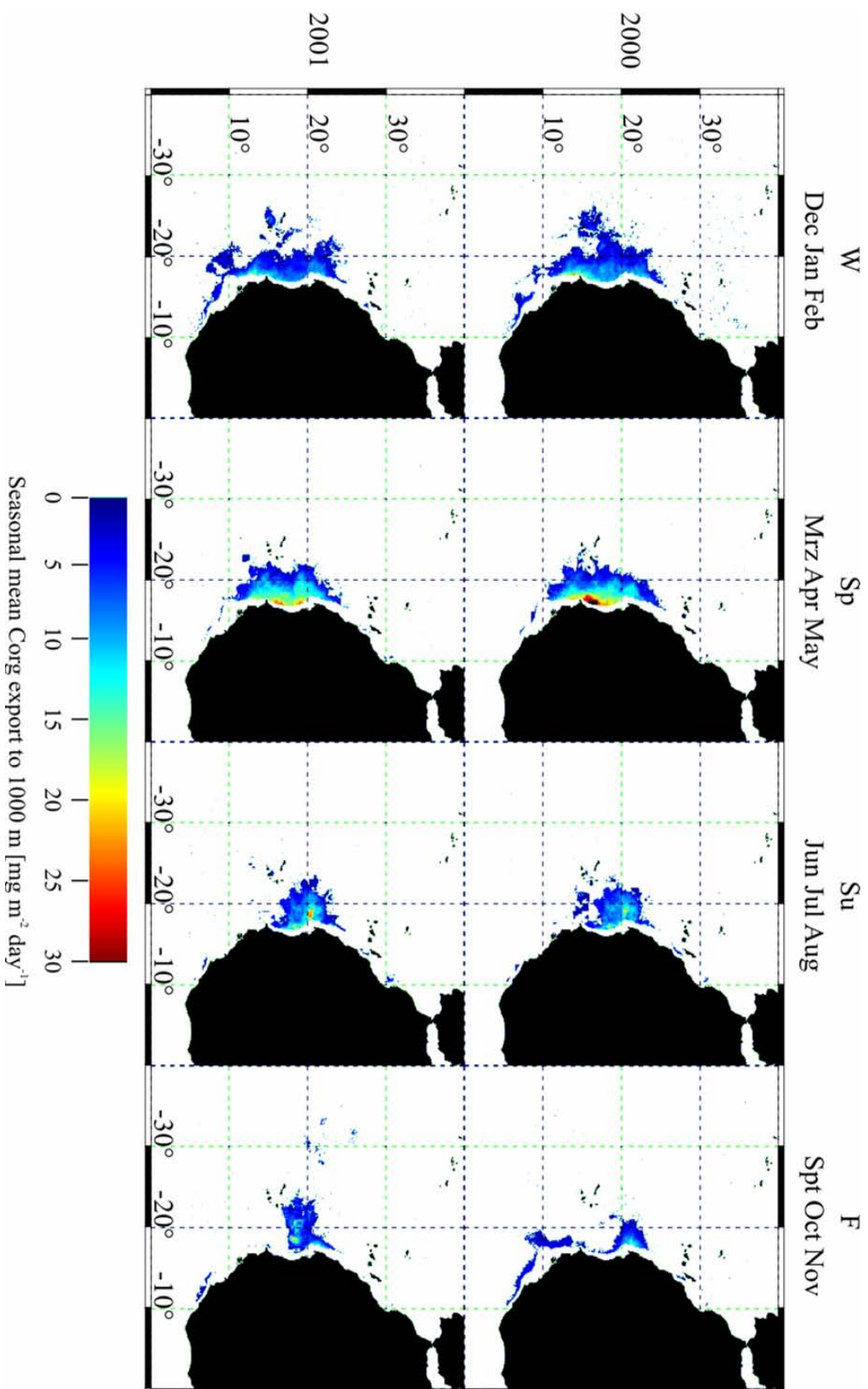
71

Figure 7b. Seasonally averaged C$_{org}$ export as in Figure 7a for the periode 2000-2001

72

5. Concluding remarks

Our approach to determine a statistical source region for material sampled by a bottom tethered sediment trap improved the relationship of surface and deep-sea signal. The application of a derived regression model was restricted to an area within "soft" bounds which are defined by inherent environmental parameters such as chlorophyll-*a* concentration. This restriction was chosen to avoid the model application to areas controlled by a different biological and transport regime. This restriction would be more difficult in a working area defined by fixed geographical borders.

We show here that strong interannual variations exist in C_{org} export out of the upwelling driven high production area off NW Africa. Upwelling variations are not only reflected in biomass production but can even be mirrored in C_{org} export flux to the deep-sea as measured by sediment traps off Cape Blanc. The exceptional period fall 1998 to spring 1999 which followed the strong El Niño/La Niña showed export values exceeding the other years by more than 100%.

The use of a regionally fitted model, and the dynamic definition of a more homogeneous area defined by parameters with major impact on the model results makes us confident that this method may be applied to other biogeochemical regions. This approach would further benefit from longer time-series of continuous trap and chlorophyll-*a* data and the incorporation of multiple trap positions in a multidimensional regression-model.

Acknowledgments.

Conclusion

The studies for the thesis 'Remote sensing of the Northwest African upwelling and its production dynamics' were conducted as part of the Special Research Project SFB 261 'The South Atlantic in the Late Quaternary'. The Northwest African upwelling was investigated by means of remote sensing and *in situ* measurements. The thesis is subdivided into three studies:

a) Upwelling variations on seasonal and interannual scales were recorded for a new period and examined for consequences of climate variations like NAO.

The seasonal fluctuation of the main upwelling area off Northwest Africa follows the northeast trade wind extension. The area of ocean surface under cold water influence – as a measure of upwelling intensity – shows maxima in winter and early spring, while the main minimum is in summer. The spatial distribution of interannual variation is characterized by local upwelling-density anomalies.

In the subtropical open ocean about 50 % of the interannual SST winter variation can be explained by the NAO, whereas this relation does not exist for the local development of near-shore upwelling. Strong ENSO-events, however, seem to interfere with NAO effects and to affect total intensity of upwelling.

b) The distribution of the Cape Ghir Chl-*a* pattern was examined for the ability to serve as an indicator for short-term climate changes and to support the interpretation of sedimentation patterns.

The Cape Ghir chlorophyll-*a* filament was divided into five categories which were assigned to seasonal wind patterns. The correspondence of upwelling-indicating proxies such as G. *bulloides* in the surface-sediments and upwelling-filament distribution confirms that the main occurrence area of upwelling off Northwest Africa was generally in the actual position for the last 500 to 1000 years.

c) Sea surface Chl-*a* distribution, its temporal development and organic matter transport measurements were used to develop a regionally-fitted empirical model for upwelling induced C_{org}-export. The source region for sample material was determined by statistical means. This method improved the statistical relationship of surface Chl-*a* variations to C_{org}-export into the deep sea in contrast to the common method of selecting a rectangular area as a source region.

A C_{org}-export model was developed on the basis of the surface to deep sea relationship and applied to the upwelling area for the period September 1997 – February 2002. An average C_{org}-export of 20.6 mg m^{-2} d^{-1} to a 1000 m depth level, yielded a yearly export of 1,12 Tg (1998) to 2.62 Tg (1999). The interannual variation exceeded the seasonal by a factor of 5.3 (1999).

The period September 1998 – June 1999, preceded by a strong El Niño/La Niña-event, stands out in the observation period through extraordinary strong export.

Outlook

The Department of Geosciences, University Bremen, has begun to integrate near-realtime satellite data into short-term ship cruise planning during marine expeditions. In this context further potential is awaiting discovery: small-scale, *in situ* measurements of *e.g.* fluorescence and particle flux can be put in a synoptic view with remote sensing data. Sampling sites can be selected and guided to meaningful locations through the help of spatial data. The sensors provide a spatial overview which is impossible to obtain from research vessels. Sampling and investigating eddies and upwelling filaments will be possible that way.

Paleoclimate archives such as sediment cores can be interpreted with the help of remote sensing data. The combination of selective sediment data with space-born data eases the understanding of spatial processes. With the help of remote sensing of Chl-*a* and primary production, sedimentation reconstructions can be more precisely linked to ocean surface conditions instead of being solely founded on interpolation between sampling locations.

Primary production in the ocean depends on a several factors. Insolation, wind velocity, nutrient supply, species community, cyclicity and energy level of the system determine the efficiency of primary production (PP). Today, PP is mainly calculated with global-scale models driven by Chl-*a* and SST. These models are rarely or not fitted to regional actualities. The incorporation of different remote sensing data sources combined with *in situ* data in a Geographical Information System (GIS) would provide new possibilities to flexibly define biogeochemical regions, transition zones, and to fit those models regionally.

The Launch of the CALIPSO satellite *(Cloud-Aerosol Lidar and Infrared Pathfinder Satellite Observations)* is scheduled for March 2005. It is planned to extend today's measurement of the atmosphere to vertical profiling detections of clouds and aerosol concentration. So far this has been possible from ground-based measurements and during a 53-hour Space Shuttle mission (www-calipso.larc.nasa.gov and www-lite.larc.nasa.gov). Together with non-profiling but spatial data such as *aerosol optical thickness* as recorded from MODIS and atmospheric transport models the challenge to quantify dust input into the ocean can be tackled.

References

Antia, A.N., W. Koeve, G. Fischer, T. Blanz, D. Schulz-Bull, J. Scholten, S. Neuer, K. Kremling, J. Kuss, R. Peinert, D. Hebbeln, U. Bathmann, M. Conte, U. Fehner, and B. Zeitzschel, Basin-wide particulate carbon flux in the Atlantic Ocean: Regional export patterns and potential for atmospheric CO2 sequestration, *Global Biogeochemical Cycles*, *15* (4), 845-862, 2001.

Armstrong, R.A., C. Lee, J.I. Hedges, S. Honjo, and S.G. Wakeham, A new, mechanistic model for organic carbon fluxes in the ocean based on the quantitative association of POC with ballast minerals, *Deep-Sea Research Part I*, *49* (1-3), 219-236, 2002.

Asper, V.L., W.G. Deuser, G.A. Knauer, and S.E. Lohrenz, Rapid coupling of sinking particle fluxes between surface and deep ocean waters, *Nature*, *357*, 670-672, 1992.

Bacastow, R., and E. Maier-Reimer, Ocean-circulation model of the carbon cycle, *Climate Dynamics*, *4*, 95-125, 1990.

Bacon, M.P., Evaluation of sediment traps with naturally occurring radionuclides, in *Particle Flux in the Ocean*, edited by V. Ittekkot, P. Schäfer, S. Honjo, and P.J. Degens, pp. 85-89, New York, 1996.

Baker, E.T., H.B. Milburn, and D.A. Tennant, Field assessment of sediment trap efficiency under varying flow conditions, *Journal of Marine Research*, *46*, 573-592, 1988.

Bakun, A., Global climate change and intensification of coastal ocean upwelling, *Science*, *247*, 198-201, 1990.

Balzer, W., K.-H. Baumann, W. Bevern, B. Brodherr, H. Buschhoff, A. Deeken, G. Fischer, A. Freesemann, C. Grimmer, M. Gutsch, A. Heuchert, H.-G. Hill, C. Höll, A. Meyer, L.F. Niencheski, W.-T. Ochsenhirt, V. Ratmeyer, G. Ruhland, V. Schlemm, and S. Stregel, Geo Bremen South Atlantic 1999/2000, Part 1, Cruise No. 46, Leg 1, 6 November – 29 November 1999, Las Palmas – Recife, in *METEOR-Berichte 01-1*, 2000.

Barton, E.D., Eastern Boundary of the North Atlantic: Northwest Africa and Iberia, in *The Global Coastal Ocean*, edited by A.R. Robinson, and K. Brink, pp. 29-67, John Wiley & Sons, New York, Chichester, Weinheim, Brisbane, Singapore, Toronto, 1998.

Barton, E.D., J. Arístegui, P. Tett, M. Cantón, J. García-Braun, S. Hernández-León, L. Nykjaer, C. Almeida, J. Almunia, S. Ballesteros, G. Basterretxea, J. Escánez, L. García-Weill, A. Hernández-Guerra, F. López-Laatzen, R. Molina, M.F. Montero, E. Navarro-Pérez, J.M. Rodríguez, K. Van Lenning, H. Vélez, and K. Wild, The transition zone of the Canary Current upwelling region, *Progress in Oceanography*, *41*, 455-504, 1998.

Batteen, M.L., J.R. Martinez, D.W. Bryan, and E.J. Buch, A modeling study of the coastal eastern boundary current system off Iberia and Morocco, *Journal of Geophysical Research*, *105* (C6), 14,173-14,195, 2000.

Behrenfeld, M.J., and P.G. Falkowski, A consumer's guide to phytoplankton primary productivity models, *Limnology and Oceanography*, *42* (7), 1479-1491, 1997.

Berger, W.H., K. Fischer, C. Lai, and G. Wu, Ocean carbon flux: global maps of primary production and export production, in *NOAA National Undersea Research Program, Research Report*, edited by C. Agegian, pp. 131-176, 1988.

Betzer, P.R., W.J. Showers, E.A. Laws, C.D. Winn, G.R. DiTullio, P.M. Kroopnick, and 31:1-11., Primary production and particle fluxes on a transect of the equator at 153° W in the Pacific Ocean, *Deep Sea Research*, *31* (1-11), 1984.

Bienfang, P.K., Phytoplankton sinking rates in oligotrophic waters off Hawaii, USA, *Marine Biology*, *61*, 69-77, 1980.

Bjerknes, L., Atlantic air-sea interaction, *Advances in Geophysics*, *10*, 1-82, 1964.

Bory, A., C. Jeandel, N. Leblond, A. Vangriesheim, A. Khripounoff, L. Beaufort, C. Rabouille, E. Nicolas, K. Tachikawa, H. Etcheber, and P. Buat-Menard, Downward particle fluxes within different productivity regimes off the Mauritanian upwelling zone (EUMELI program), *Deep-Sea Research Part I*, *48* (10), 2251-2282, 2001.

Boyd, P.W., and P.P. Newton, Does plankton community structure determine downward particulate organic carbon flux in different oceanic provinces?, *Deep-Sea Research Part I*, *46*, 63-91, 1999.

Buat-Ménard, P., J.E. Davies, E. Remoudaki, J.-C. Miquel, G. Bergametti, C.E. Lambert, U. Ezat, C. Quétel, J.L. Rosa, and S.W. Fowler, Non-steady-state biological removal of the atmospheric

particles from Mediterranean surface waters, *Nature*, *340*, 131-133, 1989.

Buesseler, K.O., The decoupling of production and particulate export in the surface ocean, *Global Biogeochemical Cycles*, *12* (2), 297-310, 1998.

Buesseler, K.O., D.K. Steinberg, A.F. Michaels, R.J. Johnson, J.E. Andrews, J.R. Valdes, and J.F. Price, A comparison of the quantity and composition of material caught in a neutrally buoyant versus surface-tethered sediment trap, *Deep-Sea Research Part I*, *47* (2), 277-294, 2000.

Campbell, J.W., J.M. Blaisdell, and M. Darzi, *Level-3 SeaWiFS data products: spatial and temporal binning algorithms.*, 73 pp., 1995.

Carr, M.-E., Estimation of potential productivity in Eastern Boundary Currents using remote sensing, *Deep-Sea Research Part I*, *49*, 59-80, 2002.

Casey, K.S., and P. Cornillon, A comparison of satellite and in situ based sea surface temperature climatologies, *Journal of Climate*, *12* (6), 1848-1863, 1999.

Cayan, D.R., Latent and sensible heat flux anomalies over the northern oceans: the connection to monthly atmospheric circulation, *Journal of Climate*, *5*, 354-369, 1992.

Chiang, J.C.H., Y. Kushnir, and S.E. Zebiak, Interdecadal changes in eastern Pacific ITCZ variability and its influence on the Atlantic ITCZ, *Geophysical Research Letters*, *27* (22), 3687-3690, 2000.

Chiapello, I., G. Bergametti, L. Gomes, B. Chatenet, F. Dulac, P. J., and E. Santos-Soares, An additional low layer transport of Sahelian and Saharan dust over the North-Eastern Tropical Atlantic, *Geophysical Research Letters*, *22* (23), 3191-3194, 1995.

Chomette, O., M. Legrand, and B. Marticorena, Determination of the wind speed threshold for the emission of desert dust using satellite remote sensing in the thermal infrared, *Journal of Geophysical Research*, *104*, 31207-31215, 1999.

Davenport, R., S. Neuer, P. Helmke, J. Perez-Marrero, and O. Llinas, Primary productivity in the northern Canary Islands region as inferred from SeaWiFS imagery, *Deep-Sea Research Part I*, *49* (17), 3481-3496, 2002.

Davenport, R., S. Neuer, A. Hernández-Guerra, M.J.L. Rueda, Octavio, G. Fischer, and G. Wefer, Seasonal and interannual pigment concentration in the Canary Islands region from CZCS data and comparison with observations from the ESTOC, *International Journal of Remote Sensing*, *20* (7), 1419-1433, 1999.

Deuser, W.G., F.E. Muller-Karger, R.H. Evans, O.B. Brown, W.E. Esaias, and G.C. Feldman, Surface-ocean color and deep-ocean carbon flux: how close a connection?, *Deep-Sea Research Part A*, *37* (8), 1331-1343, 1990.

Dong, B.W., R.T. Sutton, S.P. Jewson, O.N. A, and J.M. Slingo, Predictable Winter climate in the North Atlantic sector during the 1997-1999 ENSO cycle, *Geophysical Research Letters*, *27* (7), 985-988, 2000.

Doval, M.D., X.A. Alvarez-Salgado, and F.F. Perez, Organic matter distributions in the Eastern North Atlantic-Azores Front region, *Journal of Marine Systems*, *30* (1-2), 33-49, 2001.

Ducklow, H., and A. Dickson, Protocols for the Joint Global Ocean Flux studies (JGOFS) core measurements, pp. 210, 1996.

Emerson, S., P. Quay, D. Karl, C. Winn, L. Tupas, and M. Landry, The carbon pump in the Subtropical Pacific Ocean: Implications for the Global Carbon Cycle, *Nature*, *389*, 951-954, 1997.

Enfield, D.B., and D.A. Mayer, Tropical Atlantic sea surface temperature variability and its relation to El Niño-Southern Oscillation, *Journal of Geophysical Research*, *102* (C1), 929-945, 1997.

Evans, R., and G.P. Podestá, Pathfinder Sea Surface Temperature Algorithm, Version 4.0, *http://www.rsmas.miami.edu/groups/rrsl/pathfinder/Algorithm/algo_index.html*, 1998.

Fairbanks, R.G., A 17,000 year glacio-eustratic sea level record: influence of glacial melting rate on the Younger Dryas event and deep-ocean circulation, *Nature*, *342*, 637-642, 1989.

Fargion, G.S., and J.L. Mueller, Ocean Optics Protocols For Satellite Ocean Color Sensor Validation, Revision 2, in *NASA Tech. Memo.-2000-209966*, pp. 196, National Aeronautical and Space Administration, Goddard Space Flight Space Center, Greenbelt, Maryland, 2000.

Fischer, G., and crew-members, Report and preliminary results of METEOR-cruise M41/4 Salvador da Bahia - Las Palmas, 18.5.-13.6.1998, 1999.

Fischer, G., B. Donner, V. Ratmeyer, R. Davenport, and G. Wefer, Distinct year-to-year particle flux variations off Cape Blanc during 1988-1991: Relations to δ^{18}O-deduced sea-surface temperatures and trade winds, *Journal of Marine Research*, *54* (1), 73-98, 1996.

Fischer, G., V. Ratmeyer, and G. Wefer, Organic carbon fluxes in the Atlantic and the Southern Ocean: relationship to primary production compiled from satellite radiometer data, *Deep-Sea Research Part I*, *47* (9-11), 1961-1997, 2000.

Fischer, G., and G. Wefer, Sampling, preparation and analysis of marine particulate matter, in *Marine Particles: Analysis and Characterization*, edited by D.C. Hurd, and D.W. Spencer, pp. 391-397, Geophysical Monographs, 1991.

Folland, C.K., T.N. Palmer, and D.E. Parker, Sahel rainFall and world-wide sea temperatures, 1901-85, *Nature*, *320*, 602-607, 1986.

Fowler, S.W., and L.F. Small, Sinking rates of euphausiid fecal pellets, *Limnology and Oceanography*, *17*, 293-296, 1972.

Francois, R., S. Honjo, R. Krishfield, and S. Manganini, Factors controlling the flux of organic carbon to the bathypelagic zone of the ocean, *Global Biogeochemical Cycles*, *16* (4), 1087, 2002.

Frankignoulle, C., Sea surface temperature variability in the North Atlantic: Monthly to decadal time scales, in *Beyond El Niño: decadal and interdecadal climate variability*, edited by A. Navarra, pp. 25-48, Springer, Berlin, Heidelberg, New York, 1999.

Freudenthal, T., H. Meggers, J. Henderiks, H. Kuhlmann, A. Moreno, and G. Wefer, Upwelling intensity and filament activity off Morocco during the last 250,000 years, *Deep-Sea Research Part I, 49* (17), 3655-3674, 2002.

Freudenthal, T., S. Neuer, H. Meggers, R. Davenport, and G. Wefer, Influence of lateral particle advection and organic matter degradation on sediment accumulation and stable nitrogen isotope ratios along a productivity gradient in the Canary Island region, *Marine Geologie, 177*, 93-109, 2001.

Gabric, A.J., L. Garcia, L. Van-Camp, L. Nykjaer, W. Eifler, and W. Schrimpf, Offshore export of shelf production in the Cape Blanc (Mauritania) giant filament as derived from coastal zone color scanner imagery, *Journal of Geophysical Research, 98* (C3), 4697-4712, 1993.

Gianinni, A., Y. Kushnir, and M.A. Cane, Interannual Variability of Caribbean RainFall, ENSO, and the Atlantic Ocean, *Journal of Climate, 13*, 297-311, 2000.

Gloor, M., N. Gruber, J. Sarmiento, C.L. Sabine, R.A. Feely, and C. Rödenbeck, A first estimate of present and preindustrial air-sea CO2 flux patterns based on ocean interior carbon measurements and models, *Geophysical Research Letters, 30* (1), 1010, 2003.

Hagen, E., Mesoscale upwelling off the West African coast, in *Coastal Upwelling*, edited by F.A. Richards, pp. 72-78, American Geophysical Union, Washington, 1981.

Hagen, E., Northwest African upwelling scenario, *Oceanologica Acta, 24*, 113-128, 2001.

Hagen, E., and R. Schemainda, Der Guineadom im ostatlantischen Stromsystem, *Beiträge zur Meereskunde, 51*, 5-27, 1984.

Hagen, E., C. Zülicke, and R. Feistel, Near-surface structures in the Cape Ghir filament off Morocco, *Oceanologica Acta, 19* (6), 577-598, 1996.

Halliwell Jr., G.R., Simulation of the North Atlantic Decadal/Multidecadal Winter SST Anomalies Driven by Basin-Scale Atmospheric Circulation Anomalies, *Journal of Physical Oceanography, 28*, 5-21, 1998.

Hameed, S., K.R. Sperber, and A. Meinster, Teleconnections of the Southern Oscillation in the tropical Altantic sector in the OSU coupled upper ocean-atmosphere GCM, *Journal of Climate, 6*, 487-498, 1993.

Henderiks, J., T. Freudenthal, H. Meggers, S. Nave, F. Abrantes, J. Bollmann, and H.R. Thierstein, Glacial-interglacial variability of particle accumulation in the Canary Basin: a time-slice approach, *Deep Sea Research Part II, 49* (17), 3675-3705, 2002.

Hernández-Guerra, A., and L. Nykjær, Sea surface temperature variability off north-west Africa: 1981-1989, *International Journal of Remote Sensing, 18* (12), 2539-2558, 1997.

Horrocks, L.A., B. Candy, T.J. Nightingale, R.W. Saunders, A. O'Carroll, and A.R. Harris, Parameterizations of the ocean skin effect and implications for satellite-based measurement of sea-surface temperature, *Journal of Geophysical Research, 108* (C3), 3096, 2003.

Houghton, J.T., Y. Ding, D.J. Griggs, M. Noguer, P.J.v.d. Linden, and D. Xiaosu, Climate Change 2001: The Scientific Basis, Contribution of Working Group I to the Third Assessment Report of the Intergovernmental Panel on Climate Change (IPCC), pp. 944, Cambridge University Press, Cambridge, UK., 2001.

Howard, K.L., and J.A. Yoder, Contributions of the subtropical oceans to global primary production, in *COSPAR Colloquium on Space Remote Sensing of Subtropical Oceans*, edited by C.-T. Liu, pp. 157-168, Elsevier, Taipai, Taiwan, 1997.

Huang, J., K. Higuchi, and A. Shabbar, The relationship between the North Atlantic Oscillation and El Nino-Southern Oscillation, *Geophysical Research Letters, 25*, 2707-2710, 1998.

Hurrell, J.W., Decadal Trends in the North Atlantic Oscillation: Regional Temperatures and Precipitation, *Science, 269*, 676-679, 1995.

Indermuhle, A., T.F. Stocker, F. Joos, H. Fischer, H.J. Smith, M. Wahlen, B. Deck, D. Mastroianni, J. Tschumi, T. Blunier, R. Meyer, and B. Stauffer, Holocene carbon-cycle dynamics based on CO2 trapped in ice at Taylor Dome, Antarctica, *Nature, 398*, 121-126, 1999.

Ittekkot, V., Particle flux in the ocean: Summary, in *Particle Flux in the Ocean*, edited by V. Ittekkot, P. Schäfer, S. Honjo, and P.J. Degens, pp. 357-366, New York, 1996.

Jahnke, R.A., The global ocean flux of particulate organic carbon: Areal distribution and magnitude, *Global Biogeochemical Cycles, 10* (1), 71-88, 1996.

Janicot, S., Impact of warm ENSO events on atmospheric circulation and convection over the tropical Atlantic and West Africa, *Annales Geophysicae, 15*, 471-475, 1997.

Johnson, J., and I. Stevens, A fine resolution model of the eastern North Atlantic between the Azores, the Canary Islands and the Gibraltar Strait, *Deep-Sea Research Part I, 47* (5), 875-899, 2000.

Knauer, G.A., and V.L. Asper, US GOFS. 1989. Sediment trap technology and sampling. Report of the US GOFS Working Group on sediment trap technology and sampling., 1989.

Kostianoy, A.G., and A.G. Zatsepin, The West African coastal upwelling filaments and cross-frontal water exchange conditioned by them, *Journal of Marine Systems, 7* (2-4), 349-359, 1996.

Lampitt, R.S., and A.N. Antia, Particle flux in deep seas: regional characteristics and temporal variability, *Deep-Sea Research Part I*, *44* (8), 1377-1403, 1997.

Longhurst, A., S. Sathyendranath, T. Platt, and C. Caverhill, An estimate of global primary production in the ocean from satellite radiometer data., *Journal of Plankton Research*, *17* (6), 1245-1271, 1995.

Longhurst, A.R., and W.G. Harrison, The biological pump: profiles of plankton production and consumption in the upper ocean, *Progress in Oceanography*, *22* (1), 47-123, 1989.

Lutz, M., R. Dunbar, and K. Caldeira, Regional variability in the vertical flux of particulate organic carbon in the ocean interior, *Global Biogeochemical Cycles*, *16* (3), 11.1-18, 2002.

Martin, J.H., G.A. Knauer, D.M. Karl, and W. Broenkow, W., VERTEX: carbon cycling in the northeast Pacific, *Deep-Sea Research Part A*, *14* (2), 267-285, 1987.

McClain, C.R., E. Yeh, and G. Fu, An Analysis of GAC Sampling Algorithms: A Case Study, edited by S.B. Hooker, and E.R. Firestone, pp. 22, NASA Goddard Space Flight Center, Greenbelt, Maryland, 1992.

Meggers, H., T. Freudenthal, S. Nave, J. Targarona, F. Abrantes, and P. Helmke, Assessment of geochemical and micropaleontological sedimentary parameters as proxies of surface water properties in the Canary Islands region, *Deep-Sea Research Part I*, *49* (17), 3631-3654, 2002.

Minnett, P., Radiometric measurements of the sea-surface skin temperature: the competing roles of the diurnal thermocline and the cool skin, *International Journal of Remote Sensing*, *24* (24), 5033-5047, 2003.

Mittelstaedt, E., The upwelling area off Africa - a description of Phenomena related to coastal upwelling, *Progress in Oceanography*, *12*, 307-331, 1983.

Mittelstaedt, E., The ocean boundary along the northwest African coast: Circulation and oceanographic properties at the sea surface, *Progress in Oceanography*, *26*, 307-355, 1991.

Moore, J.K., S.C. Doney, D.M. Glover, and I.Y. Fung, Iron cycling and nutrient-limitation patterns in surface waters of the World Ocean, *Deep Sea Research Part II: Topical Studies in Oceanography*, *49*, 463-507, 2002.

Moura, A.D., and J. Shukla, On the dynamics of droughts in northeast Brazil: Observations, theory and numerical experiments with a general circulation model, *Journal of the Atmospheric Sciences*, *38*, 2653-2675, 1981.

Müller, P., and G. Fischer, A 4-year sediment trap record of alkenones from the filamentous upwelling region off Cape Blanc, NW Africa and a comparison with distributions in underlying sediments, *Deep-Sea Research Part I*, *48*, 1877-1903, 2001.

Najjar, R.G., J.L. Sarmiento , and J.R. Toggweiler, Downward transport and fate of organic matter in the ocean: Simulations with a general circulation, *Global Biogeochemical Cycles*, *6*, 45-76, 1992.

Neuer, S., T. Freudenthal, R. Davenport, O. Llinas, and M.-J. Rueda, Seasonality of surface water properties and particle flux along a productivity gradient off NW Africa, *Deep-Sea Research Part I*, *49* (17), 3561-3576, 2002.

Nixon, S., and A. Thomas, On the size of the Peru upwelling ecosystem, *Deep-Sea Research Part I*, *48*, 2521 –2528, 2001.

Nykjær, L., Remote Sensing applied to the Northwest African upwelling area, Thesis, Universität Kopenhagen, 1988.

Nykjær, L., and L. Van Camp, Seasonal and interannual variability of coastal upwelling along northwest Africa and Portugal from 1981 to 1991, *Journal of Geophysical Research*, *99* (C7), 14197-14207, 1994.

O'Reilly, J.E., S. Maritorena, B.G. Mitchell, D.A. Siegel, K.L. Carder, S.A. Garver, M. Kahru, and C. McClain, Ocean Color Algorithms for SeaWiFS, *Journal of Geophysical Research*, *103* (C11), 24937-24953, 1998.

O'Reilly, J.E., S. Maritorena, D. Siegel, M.C. O'Brien, D. Toole, B.G. Mitchell, M. Kahru, F.P. Chavez, P. Strutton, G. Cota, S.B. Hooker, C.R. McClain, K.L. Carder, F. Muller-Karger, Harding, L., A. Magnuson, D. Phinney, G.F. Moore, J. Aiken, K.R. Arrigo, R. Letelier, and M. Culver, Ocean color chlorophyll a algorithms for SeaWiFS, OC2, and OC4: Version 4, in *SeaWiFS Postlaunch Calibration and Validation Analyses, Part 3, NASA Tech. Memo. 2000-206892*, edited by S.B. Hooker, and E.R. Firestone, Goddard Space Flight Center, Greenbelt, Maryland, USA, 2000.

Osborn, T., K.R. Briffa, S.F.B. Tett, P.D. Jones, and R. Trigo, Evaluation of the North Atlantic Oscillation as simulated by a coupled climate model, *Climate Dynamics*, *15*, 685-702, 1999.

Pace, M.L., G.A. Knauer, D.M. Karl, and J.H. Martin, Primary production, new production and vertical flux in the eastern Pacific Ocean, *Nature*, *325*, 803 - 804, 1987.

Paeth, H., M. Latif, and A. Hense, Global SST influence on twentieth century NAO variability, *Climate Dynamics*, *21* (1), 63 - 75, 2003.

Paillard, D., L. Labeyrie, and P. Yiou, Macintosh program performs time-series analysis, *EOS Transactions American Geophysical Union*, *77* (379), 1996.

Palmer, J.R., and I.J. Totterdell, Production and export in a global ocean ecosystem model, *Deep-Sea Research Part I*, *48*, 1169-1198, 2001.

References

Patt, F.S., M. Darzi, J.K. Firestone, B.D. Schieber, L.V. Kumar, and D.A. Ilg, SeaWiFS, Operational Archive Product Specifications, Version 4.0, SeaWiFS Project Code 970.2, NASA Goddard Space Flight Center, 2000.

Peng, S., W.A. Robinson, and S. Li, North Atlantic SST Forcing of the NAO and Relationships with Intrinsic Hemispheric Variability, *Geophysical Research Letters*, *29* (8), 117-1 - 117-4, 2002.

Peters, H., The spreading of the water masses of the Banc d'Arguin in the upwelling area off Northern Mauritanian Coast, *"Meteor" Forschungsergebnisse (A)*, *18*, 78-100, 1976.

Price, J.C., Timing of NOAA afternoon passes, *Internation Journal of Remote Sensing*, *12*, 192-198, 1991.

Rajagopalan, B., Y. Kushnir, and Y.M. Tourre, Observed decadal midlatitude and tropical Atlantic climate variability, *Geophysical Research Letters*, *25* (21), 3967-3970, 1998.

Ramage, C.S., *Monsoon Meteorology*, 296 pp., Academic Press, San Diego, CA, 1971.

Ratmeyer, V., G. Fischer, and G. Wefer, Lithogenic particle fluxes and grain size distributions in the deep ocean off northwest Africa: Implications for seasonal changes of aeolian dust input and downward transport, *Deep-Sea Research Part I*, *46*, 1289-1337, 1999.

Roeckner, E., J.M. Oberhuber, A. Bacher, M. Christoph, and I. Kirchner, ENSO variability and atmospheric response in a global coupled atmosphere-ocean GCM, *Climate Dynamics*, *12*, 737-754, 1996.

Romero, O., C.B. Lange, and G. Wefer, Interannual variability (1988-1991) of siliceous phytoplankton fluxes off northwest Africa, *Journal of Plankton Research*, *24* (9), 2002.

Roy, C., and C. Reason, ENSO related modulation of coastal upwelling in the eastern Atlantic, *Progress in Oceanography*, *49* (1-4), 245-255, 2001.

Saravanan, R., and P. Chang, Interaction between Tropical Atlantic Variability and El Niño–Southern Oscillation, *Journal of Climate*, *13*, 2177-2194, 2000.

Sarmiento, J.L., T.M.C. Hughes, R.J. Stouffer, and S. Manabe, Simulated response of the ocean carbon cycle to anthropogenic climate warming, *Nature*, *393*, 245-249, 1998.

Sarmiento, J.L., R. Murnane, and C. Le Quéré, Air-sea CO2 transfer and the carbon budget of the North Atlantic, *Philosophical Transaction of The Royal Society of London*, *348*, 211-219, 1995.

Sarmiento, J.L., and J.R. Toggweiler, A new model for the role of the oceans in determining atmospheric pCO2, *Nature*, *308*, 621-624, 1984.

Sarnthein, M., J. Thiede, U. Pflaumann, H. Erlenkeuser, D. Fütterer, B. Koopmann, H. Lange, and E. Seibold, Atmospheric and oceanic circulation patterns off Northwest Africa during the past 25 million years, in *Geology of the northwest African continental margin*, edited by U. von Rad, K. Hinz, M. Sarntheim, and E. Seibold, pp. 545-604, Springer-Verlag, Berlin, Heidelberg, 1982.

Sarthou, G., A.R. Baker, S. Blain, E.P. Achterberg, M. Boye, A.R. Bowie, P. Croot, P. Laan, H.J.W. de Baar, T.D. Jickells, and P.J. Worsfold, Atmospheric iron deposition and sea-surface dissolved iron concentrations in the eastern Atlantic Ocean, *Deep Sea Research Part I: Oceanographic Research Papers*, *50* (10-11), 1339-1352, 2003.

Sauter, E., M. Schlüter, and E. Suess, Organic carbon flux and remineralization in surface sediments from the northern North Atlantic derived from pore-water oxygen microprofiles, *Deep-Sea Research Part I*, *48*, 529-553, 2001.

Schemainda, R., D. Nehring, and S. Schulz, Ozeanologische Untersuchungen zum Produktionspotential der nordwestafrikanischen Wasserauftriebsregion 1970 - 1973, *Geodätische und Geophysikalische Veröffentlichungen*, *4* (16), 1-89, 1975.

Schlitzer, R., Carbon export fluxes in the Southern Ocean: results from inverse modeling and comparison with satellite-based estimates, *Deep-Sea Research Part I*, *49*, 1623–1644, 2002.

Schlüter, M., E. Sauter, A. Schäfer, and W. Ritzai, Spatial budget of organic carbon flux to the seafloor of the northern North Atlantic (60°N - 80°N), *Global Biogeochemical Cycles*, *14* (1), 329-340, 2000.

Scholten, J.C., J. Fietzke, S. Vogler, M. Rutgers van der Loeff, A. Mangini, W. Koeve, P. Stoffers, A. Antia, S. Neuer, and J. Waniek, Trapping efficiencies of sediment traps from the deep eastern North Atlantic: The [230]Th calibration, *Deep-Sea Research Part I*, *48*, 2383-2408, 2001.

Siegel, D.A., and R.A. Armstrong Corrigendum to "Siegel, D.A, and W.G. Deuser, 1997: Trajectories of sinking particles in the Sargasso Sea: Modeling of statistical funnels above deep-ocean sediment traps, Deep-Sea Research, I , 44, 1,519-1,541", *Deep-Sea Research Part I*, *49*, 1115-1116, 2002.

Siegel, D.A., and W.G. Deuser, Trajectories of sinking particles in the Sargasso Sea: modeling of statistical funnels above deep-ocean sediment traps, *Deep-Sea Research Part I*, *44* (9-10), 1519-1541, 1997.

Siegel, D.A., T.C. Granata, A.F. Michaels, and T.D. Dickey, Mesoscale Eddy Diffusion, Particle Sinking, and the Interpretation of Sediment Trap Data, *Journal of Geophysical Research*, *95* (C4), 5305-5311, 1990.

Siegenthaler, U., and J.L. Sarmiento, Atmospheric carbon dioxide and the ocean, *Nature*, *365*, 119-125, 1993.

Six, K.D., and E. Maier-Reimer, Effects of plankton dynamics on seasonal carbon fluxes in an ocean general circulation model, *Global Biogeochemical Cycles*, *10* (4), 559-583, 1996.

Smetacek, V.S., Role of sinking diatom life-history cycles: Ecological, evolutionary and geological significance, *Marine Biology*, *84*, 239-251, 1985.

Smith, E., J. Vazquez, A. Tran, and R. Sumagaysay, Satellite-Derived Sea Surface Temperature Data Available From the NOAA/NASA Pathfinder Program, *http://www.agu.org/eos_elec/95274e.html*, 1996.

Speth, P., H. Detlefsen, and H.-W. Sierts, Meteorological influence on upwelling off Northwest Africa, *Deutsche Hydrographische Zeitschrift*, *31*, 95-104, 1978.

Strub, P.T., P.M. Kosro, and A. Huyer, The Nature of the Cold Filaments in the California Current System, *Journal of Geophysical Research*, *96* (C8), 14743-14768, 1991.

Suess, E., Particulate organic flux in the oceans - Surface productivity and oxygen utilization, *Nature*, *288*, 260-262, 1980.

Swap, R., S. Ulanski, M. Cobbett, and M. Garstrang, Temporal and spatial characteristics of Saharan dust outbreaks, *Journal of Geophysical Research*, *101* (D2), 4205-4220, 1996.

Takahashi, T., S.C. Sutherland, C. Sweeney, A. Poisson, N. Metzl, B. Tilbrook, N. Bates, R. Wanninkhof, R.A. Feely, C. Sabine, J. Olafsson, and Y. Nojiri, Global sea–air CO2 flux based on climatological surface ocean pCO2, and seasonal biological and temperatur effects, *Deep-Sea Research, Part II*, *49*, 1601-1622, 2002.

Thorne, M., E.J. Garnero, and S. Grand, Geographic correlation between hot spots and deep mantle lateral shear-wave velocity gradients, *Physics of the Earth and Planetary Interiors (C)*, 2003 in press.

Toggweiler, J.R., R.J. Murnane, S. Carson, A. Gnanadesikan, and J.L. Sarmiento, Representation of the carbon cycle in box models and GCMs, Part 2, the organic carbon pump, *Global Biogeochemical Cycles*, in press (2003).

Torres-Padrón, M.E., M.D. Gelado-Caballero, C. Collado-Sánchez, V.F. Siruela-Matos, P.J. Cardona-Castellano, and J.J. Hernández-Brito, Variability of dust inputs to the CANIGO zone, *Deep-Sea Research Part I*, *49* (17), 3455-3464, 2002.

Usbeck, R., Modeling of marine biogeochemical cycles with an emphasis on vertical particle fluxes, Ph.D. Thesis, Bremen, 1999.

Van Camp, L., L. Nykjaer, E. Mittelstaedt, and P. Schlittenhardt, Upwelling and boundary circulation off northwest Africa as depicted by infrared and visible satellite observations., *Progress in Oceanography*, *26* (4), 357-402, 1991.

Vazquez, J., AVHRR Oceans Pathfinder Sea Surface Temperature Data Sets, *http://podaac.jpl.nasa.gov:2031/ DATASET_DOCS/avhrr_pathfinder_sst.html*, 1999.

Vazquez, J., K. Perry, and K. Kilpatrick, NOAA/NASA AVHRR Oceans Pathfinder Sea Surface Temperature Data Set User's Reference Manual Version 4.0, Jet Propulsion Laboratory, 1998.

Volk, T., and M.I. Hoffert, Ocean carbon pumps: Analysis of relative strengths and efficiencies in ocean-driven atmospheric CO2 changes, in *The Carbon Cycle and Atmospheric CO2: Natural Variations Archean to Present*, edited by E.T. Sundquist, and W.S. Broecker, pp. 99-110, AGU, Washington, D.C, 1985.

Wallace, J.M., C. Smith, and Q. Jing, Spatial patterns of atmosphere-ocean interaction in the northern Winter, *Journal of Climate*, *3*, 990-998, 1990.

Waniek, J., W. Koeve, and R.D. Prien, Trajectories of sinking particles and the catchment areas in the North East Atlantic, *Journal of Marine Research*, *58*, 983-1006, 2000.

Williams, R.G., and M.J. Follows, Eddies make ocean deserts bloom, *Nature*, *394*, 228-229, 1998.

Wooster, W.S., A. Bakun, and D. McLain, The seasonal upwelling cycle along the eastern boundary of the North Atlantic, *Journal of Marine Research*, *34* (2), 131-141, 1976.

Yu, E.-F., R. Francois, M.P. Bacon, S. Honjo, A.P. Fleer, S.J. Manganini, M.M. Rutgers van der Loeff, and V. Ittekot, Trapping efficiency of bottom-tethered sediment traps estimated from the intercepted fluxes of 230Th and 231Pa, *Deep-Sea Research Part I*, *48* (3), 865-889, 2001.

Appendix: further publications

Further publications, to which significant contribution in form of data processing and analysis was made. The final form of the scientific articles may change during revision.

Davenport, R., S. Neuer, P. Helmke, J. Perez-Marrero, and O. Llinas, Primary productivity in the northern Canary Islands region as inferred from SeaWiFS imagery, Deep-Sea Research Part II, 49, 3481-3496, 2002.

Kuhlmann, H., T. Freudenthal, P. Helmke, and H. Meggers, Reconstruction of paleoceanography off NW Africa during the last 40,000 years: influence of local and regional factors on sediment accumulation,,, submitted.

Meggers, H., T. Freudenthal, S. Nave, J. Targarona, F. Abrantes, and P. Helmke, Assessment of geochemical and micropaleontological sedimentary parameters as proxies of surface water properties in the Canary Islands region, Deep-Sea Research Part II, 49, 3631-3654, 2002.

Stuut, J-B., Mattias, M., Ratmeyer, V., Helmke, P., Schefuß, E., Lavik, G. and Schneider, R, Provenance of present-day eolian dust collected off NW Africa; in preparation

Primary productivity in the northern Canary Islands region as inferred from SeaWiFS imagery

by Robert Davenport[1], Susanne Neuer[1,2], Peer Helmke[1], Javier Perez-Marrero[3], and Octavio Llinas[3]

1. *FB5 Geosciences, University of Bremen, Klagenfurterstraße, 28359 Bremen, Germany.*
2. *Present address: Arizona State University, Department of Biology, Tempe, AZ 85287-1501,USA*
3. *Instituto Canario de Ciencias Marinas, Direccion General de Universidades e Investigacion Consejeria de Educacion, Cultura y Deportes, Apartado 56, 35200 Telde, Canary Islands, Spain.*

ABSTRACT

A 19 month record from September 1997 to March 1999 is presented of the productivity gradient at 3 stations that fall along a quasi zonal 29°N transect through the Canary Islands region using the Sea-viewing Wide Field-of view Sensor (SeaWiFS) chlorophyll data and the primary production method of Antoine and Morel (1996). These stations correspond to 3 fixed sediments traps positioned during the same period east of the island of Fuerteventura (Eastern Boundary Current, EBC) and north of the islands of Gran Canaria (European Station for Time-Series in the Ocean, Canary Islands, ESTOC) and La Palma (LP). The mean annual productivity during the 19 month period was observed to steeply decrease westwards along the quasi zonal 29°N transect from 237 g C m^{-2} yr^{-1} at EBC to 164 and 145 g C m^{-2} yr^{-1} at ESTOC and LP, respectively. The high productivity at EBC indicates that this station is strongly influenced by the seasonal coastal upwelling off the adjacent Moroccan coast. This is confirmed by SeaWiFS chlorophyll images showing incursions of the Cape Yubi filament over the EBC station in March, July and October 1998 and January 1999 coincident with a decrease in Sea Surface Temperature (SST) of up to 1.5°C as observed by satellite. In comparison it was observed that although some cooler upwelled water does reach the ESTOC and LP stations in summer 1997 and summer/fall 1998 there was no corresponding increase in productivity indicating that the water was nutrient depleted. It is concluded that the ESTOC and LP stations are more characteristic of oligotrophic ocean with minimal influence of coastal upwelling in near surface waters. Comparison of SeaWiFS chlorophyll values with in situ data at the ESTOC station show that in general the SeaWiFS provided good quality data (within the ±35% accuracy goal targeted for this instrument) for the Canary Island region except for period December 1997–April 1998. Comparison of model productivity estimates with in situ ^{14}C uptake measurements show good agreement for oligotrophic water but that model usage in upwelling regions, in particular filaments, may be problematic. This investigation suggests that the application of the Antoine and Morel model with a limited dataset of satellite images can provide a good insight into relative primary production in the Canary Islands region.

INTRODUCTION

One of the main goals of the Canary Islands Azores Gibraltar Observations (CANIGO) project is to study the carbon global cycle in the pelagic system in nutrient limited (oligotrophic)

and nutrient-rich (productive) waters and to estimate the carbon flow through and from the pelagic system to deep waters (Parrilla et al., in press). Since 1991 long-term moored sediment traps have been deployed in 3600 m water-depth at the European Station for Time-Series in the Ocean, Canary Islands (ESTOC) situated 100 km north of the island of Gran Canaria (Llinás et al., 1994; Neuer and Rueda, 1997). ESTOC is positioned in the transition zone between the oligotrophic open ocean and the north west African upwelling (Neuer et al., 1997; Davenport et al.,1999). An analysis of 8 years (1979-86) of near-surface chlorophyll concentration at the ESTOC station using the Coastal Zone Color Sensor (CZCS) showed the annual late Winter/early spring bloom which is characteristic for this region, but no increased pigment levels associated with water that originated from the coastal upwelling zone (Davenport et al.,1999). Sediment traps at ESTOC though regularly record higher flux levels in the deeper traps than in the upper traps (Neuer et al., 1997, Freudenthal et al., 2001) and it is possible that lateral advection from a coastal upwelling region is the source of such material. As part of the Canigo programme additional traps were therefore moored east of the Canary Islands (Eastern Boundary Current, EBC) and north of the island of La Palma (LP) with the objective to a) characterise the seasonal and interannual carbon fluxes both within the upwelling zone and in the adjacent oligotrophic ocean and b) to improve our understanding of the effects of the coastal upwelling over the shelf region and carbon transport into the deeper ocean in the Canary Island region, (Figure 1) (Neuer et al, in press). All three traps lie along a quasi zonal 29°N latitude transect hereafter referred to as the 29°N transect. Historical CZCS images indicate that EBC is positioned almost in the coastal upwelling regime while LP, together with ESTOC, are in an oligotrophic regime.

The launch of the Sea-viewing Wide Field-of view Sensor (SeaWiFS) ocean colour instrument in August 1997 provided the opportunity to observe the seasonal and interannual changes of chlorophyll concentration at the three stations and to assess the quality of the SeaWiFS algorithm by comparison with the monthly in situ chlorophyll measurements made at ESTOC. To characterise the productivity gradient along the 29°N transect, we investigated the application of a primary production model (Antoine and Morel, 1996) using SeaWiFS chlorophyll concentration and Advanced Very High Resolution Radiometer (AVHRR) sea surface temperature (SST). Several such models have been developed over the last decade and applied to historical CZCS data to assess ocean basin and regional productivity on monthly, seasonal and annual time scales (Sathyendranath et al., 1995; Longhurst et al., 1995; Antoine et al., 1996; Behrenfeld and Falkowski, 1997a, 1997b). With SeaWiFS and AVHRR data available

on almost a daily basis and with a resolution of 1–10 km it is now theoretically possible to apply such models locally and compare the results directly with in situ productivity measurements.

In this study we attempt to characterise the offshore productivity gradient along the 29°N transect by using SeaWiFS chlorophyll concentration, AVHRR SST, and the primary productivity method of Antoine and Morel (1996).

REGIONAL SETTING

The Canary Islands are located off the north west African coast at about 28°N and comprise seven major islands lying between 100 km and 600 km offshore. The islands lie in the weak, southwestwards flowing Canary Current which is one of the eastern arms of the North Atlantic subtropical gyre (Stramma, 1984; Müller and Siedler, 1992). A major feature along the north west African coast is the upwelling of cold, nutrient-rich, North Atlantic Central Water extending as a 50-70 km band along-shore (Mittelstaedt, 1986; Mittelstaedt, 1991). The intensity of this upwelling is generally correlated with the position of the Azores High which migrates north in spring reaching its most northerly position in July-August. North of 25°N the upwelling is strongest in the summer and fall as a result of the strengthened north-east trade winds associated with the Azores High (Wooster et al., 1976; Speth and Detlefsen, 1982; Van Camp et al., 1991). A characteristic feature of the upwelling zone is the formation of filament structures which transport the cooler upwelled water offshore (Van Camp et al., 1991; Nykjaer and Van Camp, 1994). Kostianoy and Zatsepin (1996) identified 60 filaments over 1000 km of coastline from an analysis of satellite SST. Filaments are very variable both in structure and duration and several mechanisms have been proposed for their development (Strub et al., 1991). The growth of the larger, permanent filaments appears to be related to changes in coastal topography such as headlands. These large filaments such as at Cape Ghir, Cape Yubi, and Cape Bojador (Figure 1) and Cape Blanc, Mauritania, (20.8°N) may readily be seen in AVHRR SST images as colder jets and meanders extending several hundred kilometres off-shore (Van Camp et al., 1991; Nykjaer and Van Camp, 1994). The role of filaments in carbon cross-shelf transport and export to the deep ocean has been addressed by several authors (Strub et al.1991; Gabric et al.,1993; Barton et al., 1998). Gabric et al. (1993), from analysis of Coastal Zone Color Scanner (CZCS) pigment images, estimate a net offshore export for the `giant` Cape Blanc filament of 6 x 1012 g C yr^{-1} of which up to half may be exported by sinking to the deep ocean.
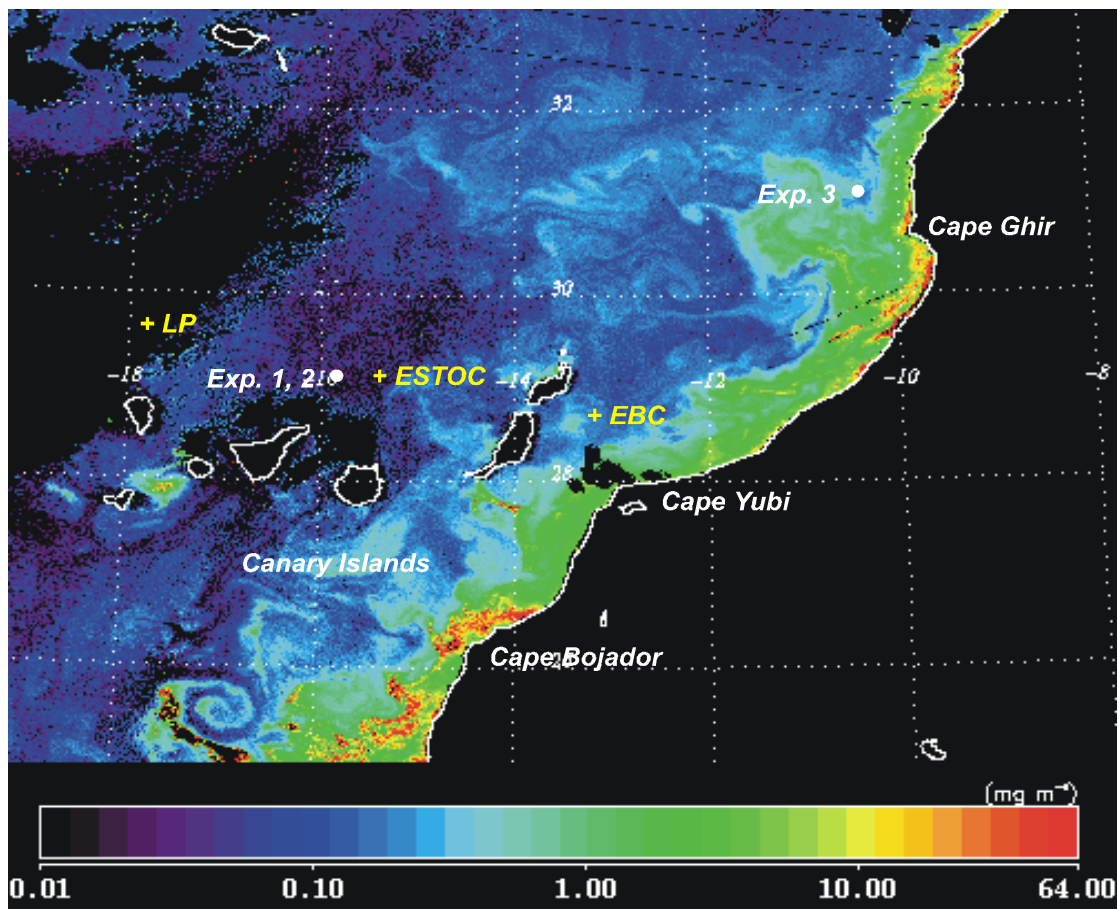
Figure 1. SeaWiFS chlorophyll image from 19 March 1998. The locations of the LP, ESTOC and EBC traps are indicted along the 29°N transect through the Canary Islands. Also shown are the positions where *in situ* primary production was determined using the ^{14}C bicarbonate uptake method. Note the Cape Ghir filament extending some 500 km offshore from the upwelling zone.

Aeolian dust from the Sahara and Sahel is often transported westwards over the north west African continent and the eastern tropical Atlantic sometimes as far as the Caribbean Sea and South America. The main transport mechanism for dust is the westward moving Harmattan or 'Saharan Air Layer' (SAL) at altitudes between 1 and 5 km which reaches its maximum strength and dust load in summer. A northward branch of the SAL forms an anticyclonic flow along the African coast which can transport dust over the Canary Islands (Bergametti, 1989). The input of aeolian dust particles to the ocean has significant implications for water column sedimentation processes. Ratmeyer et al. (1999) observed a strong correlation between mineral particles from aeolian dust and organic matter sedimentation at trap sites in the Canary Islands region, and off Cape Ghir and Cape Verde. The aeolian iron flux may also be a significant factor for phytoplankton growth in this region (Duce and Tindale, 1991).

METHODS

SeaWiFS Data

SeaWiFS was launched on the OrbView-2 polar orbiting satellite in August 1997. SeaWiFS is a spectroradiometer which measures the water-leaving radiance at 6 bands in the visible light (412, 443, 490, 510, 555, and 670 nm) and 2 in the near-IR (765, and 865 nm) (Hooker et al., 1992). The 443 and 510 bands are used for determining the chlorophyll concentration. The other bands are used for atmospheric correction or determination of pigment absorption, Gelbstoff concentration and sediment load in the near-surface water. Remotely sensed determination of the water-leaving radiance caused by photosynthetic pigments is a complex process (Sturm, 1981; Gordon and Wang, 1994). Atmospheric Rayleigh and aerosol scattering can contribute more than 90% of the total radiance observed by the sensor. Also the effect of absorption and scattering of solar illumination by particulate matter in the water column has to be taken into account. The SeaWiFS project set an accuracy goal of ±35% for chlorophyll-*a* retrieval in Case 1 waters (reflectance dominated by phytoplankton optical properties). A major post-launch calibration and validation program involving moored optical buoys and bio-optical cruises has shown that the present SeaWiFS processing algorithm has attained an approximately 10% accuracy for a wide range of open ocean environments (Bailey et al., 2000).

In this study the near-surface chlorophyll concentration (in mg m^{-3}) was determined at the EBC, ESTOC and LP station positions from daily SeaWiFS 1 km resolution Local Area Coverage (LAC) data received directly from the satellite by the University of Las Palmas, Gran Canaria, ground station. The LAC data was first processed to Level 1A calibrated SeaWiFS channel values by the Goddard Spaceflight Center, NASA, USA. We then used the SeaDAS V3.2 application package (compatible with the second SeaWiFS data reprocessing performed by NASA/GSFC) to process the L1A data to Level 2 chlorophyll products. For each station mean chlorophyll values were determined for a square box region of about 120 km^2 centred at the trap positions (11 x 11 pixels). By visually examining all available SeaWiFS pseudo colour browse images, we found 438 L1A files that covered the Canary Island region for the period September 1997 – March 1999. To assure that there were enough valid pixels for the mean chlorophyll computation we selected only those files for which there were no clouds over one or more of the stations. In those cases where no such image was available for more than a one month period we used the next best available with respect to minimum cloudiness (but never more than 50%

cloudiness). We also excluded all days where the SeaWiFS browser images showed clear evidence of aeolian dust over the trap stations (124 days) as there is no atmospheric correction possible for such events with the present SeaWiFS chlorophyll algorithm. As a result of this search we found 33 images providing 14 data points for LP, 25 for ESTOC and 25 for EBC.

We investigated the quality of the SeaWiFS chlorophyll data by comparison with in situ chlorophyll measurements at about 10 m water depth made monthly at the ESTOC time series station for the period September 1997 to December 1998 (the first 16 months of SeaWiFS operations). Water samples for chlorophyll analysis were filtered on GF/F filters and stored in 90% acetone for at least 24 hours in a refrigerator. Chlorophyll was determined fluorometrically with a Turner 10AU fluorometer applying the Welshmeyer (1994) non-acidification method.

Primary Production

Primary production estimates (in g C m^{-2} d^{-1}) computed from SeaWiFS near-surface chlorophyll concentration, Chlsat, were determined using the method of Antoine and Morel (1996) which is based on the following global equation:

$$P = (1/J_c) <Chl>_{tot} PAR(0^+) \Psi^*$$

where <Chl>tot represents the column integrated chlorophyll content (g Chl m^{-2}) and PAR(0+) the photosynthetically available radiant energy (spectral range 400-700 nm) incident at sea level per unit area over a given length of time (daily as in our case, J m^{-2}). Ψ^* is the cross section of algae for photosynthesis per unit areal chlorophyll biomass (m^2(g Chl)$^{-1}$) and incorporates the two processes involved in photosynthesis; radiant energy capture and the transfer of that energy into chemical energy to fix CO_2 into carbohydrates stored in the phytoplankton cells. Jc is the energetic equivalent of photosynthetic assimilate (39 kJ (g C)-1) and Ψ^* is a function of both <Chl>tot and PAR(0+) as well as the temperature. We used lookup tables provided by Antoine and Morel (Antoine, pers. communication) and linear interpolation to compute Ψ^* as a function of date, latitude, cloudiness, temperature and Chlsat. < Chltot> was computed using the two polynomials cited in Appendix B in Antoine and Morel (1996), the choice of polynomial depending on assuming the chlorophyll concentration was the same as Chlsat throughout the productive layer (well mixed) or by assuming a non-linear profile with a deep chlorophyll maximum (DCM) (stratification). It should be noted that with the Antoine and Morel (1996) method the depth of the productive layer is taken as the depth at which PAR is reduced to 0.1% of the surface value to take into account any DCM below the euphotic depth (the '1% light level'). Another lookup table and linear interpolation were used to compute

PAR(0+) as a function of date. For those SeaWiFS images where cloud pixels were present in the 121 km^2 box, PAR(0+) was corrected for cloudiness using the approach of Reed (1997) as modified by Antoine and Morel (1996) such that :

$$PAR(0^+){=}PAR(0^+)_{clear}\left[1-\frac{0.75(0.632c-0.0019\alpha)}{(1-0.25F_{vis})}\right]$$

where c is the cloudiness index varying from 1 for an overcast sky to 0 for a clear sky, α is the solar elevation at noon (degrees) and F_{vis} is the fraction of total radiation which Falls within the 400 – 700 nm range (set at 0.46 after Pinker and Laszlo (1992)). For a cloudiness value less than 0.28, PAR(0+) was reduced by a constant 5%. The cloudiness index c was determined from the number of SeaWiFS image cloud pixels in the 121 km^2 box area at each station position.

We do not intend to review here the various merits and restrictions of the many primary production models based on remotely sensed data described in the literature (see instead Behrenfeld and Falkowski, 1997a.; Behrenfeld and Falkowski, 1997b). There is a broad spectrum of model complexity ranging from simple empirical regression models through complex bio-optical models. At present though there is no consensus model for estimating primary production using remotely-sensed data. Our choice of the Antoine and Morel (1996) method (apart from it being one of the better known models) was primarily based on the availability of the standard lookup tables allowing for fast computation of Ψ *. We recognised though that a possible drawback of such a model for our purposes is that, to quote Antoine and Morel (1996), 'with respect to an ideal use of the model on a daily basis, approximations are inevitable`. The model was developed more to derive basin wide and global estimates of primary production than analyse productivity at a particular site. The advantage of the model for this study though is that it offers through the use of standard lookup tables for computing Ψ * a flexible approach for estimating primary production from remotely sensed data.

SST Data

The AVHRR sensors of the National Oceanic and Atmospheric Administration (NOAA) satellite series were used for SST. Daily AVHRR ascending node SST data with a resolution of about 9 km were extracted from the NASA Physical Oceanography Distributed Active Archive Center (PODAAC) Pathfinder Best SST (V4.1) data set. Because of the lower resolution of the SST data compared with the SeaWiFS chlorophyll data we estimated the SST using a single

pixel at each station position. A 5-day moving average was used to cover those days for which there was a SeaWiFS chlorophyll value but no valid SST pixel.

In situ productivity using the ^{14}C uptake method

We also investigated the quality of the primary production estimates determined from remotely sensed data, by comparing model results with some in situ production measurements conducted on one cruise in October 1999 in the ESTOC and Cape Ghir filament area (Figure 1 and Table 1). Water was inoculated with ^{14}C-bicarbonate (ca. 0.08 µCi/ml) and incubated in situ from dawn to dusk, following the standard Joint Global Ocean Flux Study (JGOFS) protocol (Knap et al., 1996). Bottles were attached to a polyethylene rope and suspended from a surface drifter. Dark bottle values were not subtracted from light bottle values.

RESULTS AND DISCUSSION

Chlorophyll concentration

We determined the near-surface chlorophyll-*a* concentration for the three stations at EBC, ESTOC and LP over the period September 1997 - March 1999 from SeaWiFS data (Figure 2). From September 1997 – November 1998 the chlorophyll concentration ranged from 0.03 – 0.11 mg m^{-3} for LP and 0.04 – 0.17 mg m^{-3} for ESTOC. From December 1998 – February 1999 the ESTOC station showed a significant increase to a peak value of 0.44 mg m^{-3}. LP also displayed enhanced pigment levels but not until March 1999 with a maximum of 0.25 mg m^{-3}. Comparison with historical CZCS data for the ESTOC station (Davenport et al., 1999) shows that these peaks are typical for the late-Winter/early spring bloom in the Canary Islands region. The apparent lack of a Winter bloom in early 1998 at both LP and ESTOC is probably related to the SeaWiFS data processing version used (see discussion below) but is also consistent with the CZCS observations which showed large interannual variability in the Winter bloom intensity.

In contrast with LP and ESTOC, the EBC station displayed significant variability over the whole period with peak events in March 1998 (0.34 mg m^{-3}) July 1998 (0.4 mg m^{-3}), October 1998 (0.44 mg m^{-3}) and January 1999 (0.56 mg m^{-3}). Visual inspection of the SeaWiFS images shows that these peaks are associated with penetration of the Cape Yubi filament over the EBC station. These incursions of the Cape Yubi filament are also correlated with a
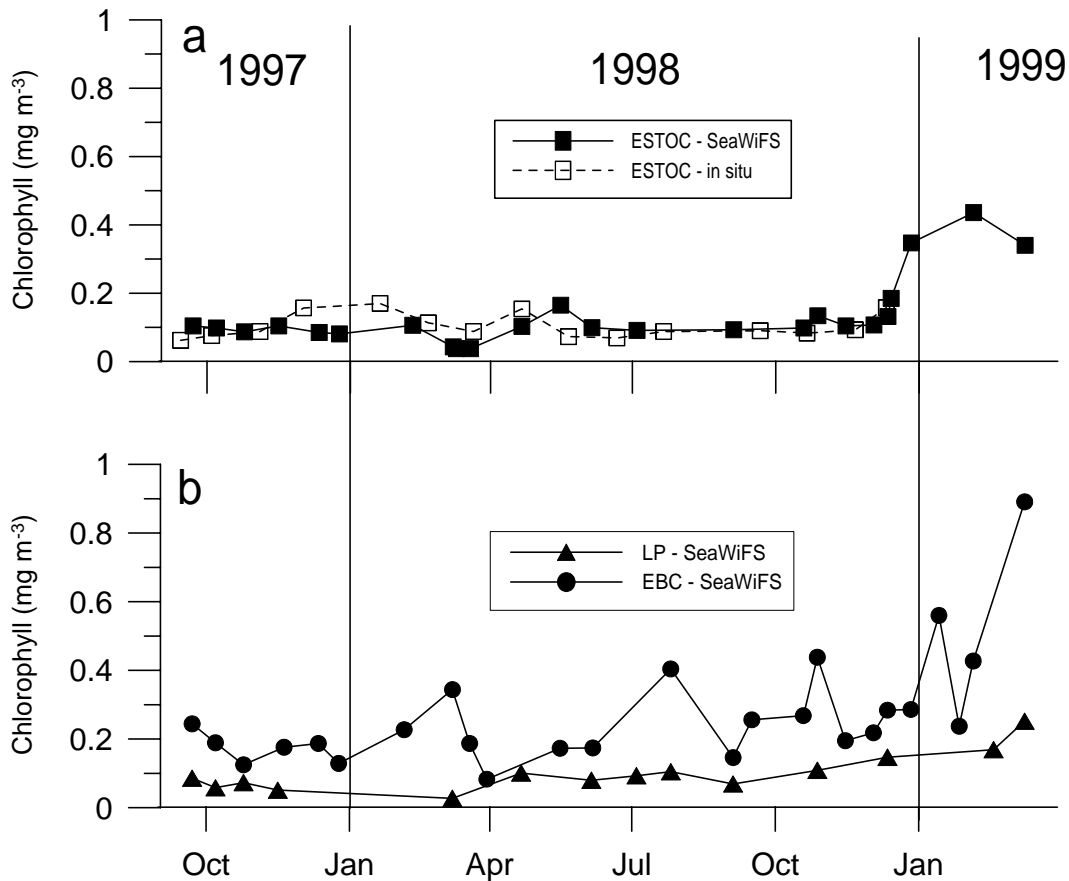
Figure 2. Surface chlorophyll concentration at the a) ESTOC and b) LP and EBC stations for the period September 1997 – March 1999 as determined by SeaWiFS. In a) the *in situ* chlorophyll at ESTOC for the period September 1997-December 1998 is also indicated. Note that SeaWiFS appears to underestimates the chlorophyll concentration for the period December 1997 to April 1998 at the ESTOC station (see text for likely explanation).

decrease in SST of up to 1.5°C indicating the presence at EBC of cooler coastal upwelled water (Figure 3). The peak in March 1999 (0.89 mg m^{-3}) at EBC is the late Winter/early spring bloom signal as discussed previously for the ESTOC and LP stations.

Comparison between SeaWiFS and in situ chlorophyll data

The in situ measured chlorophyll data at ESTOC covers the period September 1997 – December 1998 (Figure 2). For April 1998 – December 1998 the SeaWiFS derived chlorophyll concentration is within the ±35% accuracy goal set by NASA when compared with the in situ data. But for December 1997 – April 1998 there is a significant error in
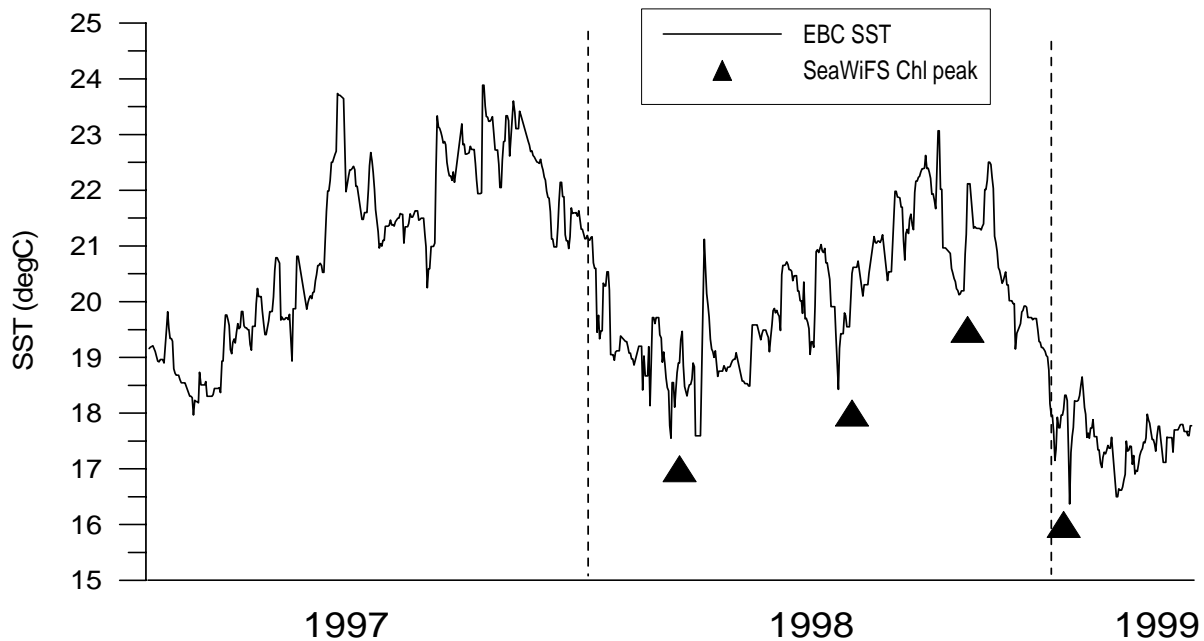
Figure 3. Daily AVHRR SST at the EBC station for the period January 1997-March 1999. The arrows show the days where SeaWiFS chlorophyll images were available showing incursion of the Cape Yubi filament over the EBC station.

the SeaWiFS values. In December 1997 and January 1998 SeaWiFS has underestimated by about 50% and the broad peak between November 1997 – March 1998 observed in situ is completely absent in the SeaWiFS data. Although we are in general comparing non-coincidental dates we believe the discrepancy is real because for the one coincidental date, 21 April 1998, the in situ value was 0.154 mg m^{-3} (standard deviation 5%) compared with a SeaWiFS value of 0.103 mg m^{-3} (standard deviation ± 0.023), i.e. 50% more than that of SeaWiFS. It is therefore unlikely that natural patchiness in the SeaWiFS 11 x 11 pixel box could explain the discrepancy on this date (although it can not be excluded as a possible explanation for other dates). Also on the 21 March 1998 the in situ chlorophyll value is 132% more than the SeaWiFS value measured two days earlier on the 19 March 1998; such a short-term variability has not been observed before at ESTOC (Davenport et al., 1999). We do not believe this discrepancy is related to the second reprocessing by NASA/GSFC of SeaWiFS data in August 1998 (Acker, 1998) as we used a SeaDAS version and channel calibration file compatible with this reprocessing step. We also reject the effects of mineral aerosol, a significant factor in the Canary Island region, which at low concentration reduces the water-leaving radiance in the SeaWiFS 443 nm band and hence increases the apparent pigment concentration. Also the depth of the in situ chlorophyll measurements was 10 m which for such low pigment waters is well within the optical depth of the SeaWiFS sensor. We therefore suggest that remotely sensed pigment concentrations from

December 1997 to April 1998 derived using SeaWiFS data from the second reprocessing by NASA/GSFC, may not be within the SeaWiFS ±35% accuracy goal for the Canary Island region. There are though indications that the problem may largely be solved by using the SeaWiFS data from the third reprocessing (Carr, priv.comm.).

Comparison between productivity estimated by remote sensing and the ^{14}C uptake method

During the M45/5 cruise of the German research vessel FS Meteor in October 1999, productivity estimates were performed at three stations north of the Canary Islands and in the upwelling region off Cape Ghir using the ^{14}C bicarbonate uptake method (Table 1). Exp. 1 and Exp.2 were performed in low surface pigment locations while Exp.3 was within the Cape Ghir filament regime (Figure 1). We also estimated productivity for the same stations and days using SeaWiFS chlorophyll concentration and the production model assuming a deep chlorophyll maximum. For Exp.1 and 2 we used the average chlorophyll concentration of an 11 x 11 pixel box (121 km^2) centred on the ship position at the time of the experiment. For Exp. 3 there was no LAC L1A file available and a 4 km resolution GAC file was used instead with a box size of 3 x 3 pixels. At each station the SeaWiFS chlorophyll values are very close to the actual in situ chlorophyll concentration to a depth of 10 m. The productivity as determined from SeaWiFS chlorophyll concentration for Exp. 2 (0.38 g C m^{-2} d^{-1}) is in good agreement with the ^{14}C measurement (0.35 g C m^{-2} d^{-1}). For Exp. 1 though the model primary production is a factor 1.6 larger than the in situ value. A likely explanation for this discrepancy relates to the cloudiness factor used in the model calculation. At the time of the SeaWiFS pass the area around the station was cloud free and hence the model calculation assumes a cloudiness factor of zero from dawn to dusk. Cloudiness cover observed from the ship though was 75% at 6.00 GMT and 100% with rain at 18.00 GMT. If we assume an average cloudiness factor of 0.75 then the model primary production estimate would be reduced to 0.27 g C m^{-2} d^{-1} compared with the in situ value of 0.25 g C m^{-2} d^{-1}. In comparison for Exp. 2 the cloudiness factor at the time of the SeaWiFS pass of 0.6 was in good agreement with the ship observation of 0.63 for the day. This suggests that the model primary production

values may be too large for some of the dates at the 29°N transect stations since the majority of model estimates were made for cloud free conditions at the time of the SeaWiFS pass and no account was taken of cloud variability during the rest of the daylight period. It would definitely be an improvement in future applications of such a model for daily primary productivity estimates if a statistical approximation of daily cloud was also taken into account.

Table 1. Primary production (g C m^{-2} d^{-1}) and biomass (mg Chl m^{-2}) measured *in situ* by the ^{14}C uptake method compared with production determined using SeaWiFS chlorophyll data and the Antoine and Morel (1996) method.

Exp.	Date	Station	Chl. *in situ*		Biomass (mg Chl m^{-2})	Chl$_{sat}$ (mg Chl m^{-3})	SST *in situ* (°C)	PP ^{14}C (g C m^{-2}d^{-1})	PP$_{sat}$
			Depth (m)	Chl. (mg m^{-3})					
1	24/10/99	29.18°N 15.94°W	10	0.09	28.15	0.109 (0.09)[1]	23.7	0.249	0.388
			25	0.11					
			50	0.19					
			75	0.19					
			100	0.31					
			125	0.13					
			150	0.05					
2	27/10/99	29.08°N 15.99°W	10	0.09	24.28	0.118 (0.118)[1]	23.4	0.35	0.378
			25	0.11					
			50	0.19					
			75	0.21					
			100	0.22					
			125	0.17					
			150	0.06					
3	30/10/97	31.20°N 10.46°W	10	0.31	25.08	0.328[2] (0.325)[3]	20.1	0.913	0.647
			25	0.37					
			50	0.28					
			75	0.15					
			100	0.05					
			125	0.01					
			150	0.00					

(1)   Actual SeaWiFS pixel value at the centre of the 11 x 11 km box.
(2)   No SeaWiFS LAC 1 km resolution image is available for this date. The Chl$_{sat}$ value is from a SeaWiFS Global Area Coverage (GAC) image at 4 km resolution.
(3)   Actual SeaWiFS pixel at the centre of the 12 x 12 km box.

For Exp. 3 in the Cape Ghir filament region, the in situ primary production is a factor 1.4 larger than the model estimate. On the date of Exp. 3 the station was in the coastal upwelling regime as is evidenced by the in situ SST of 20.1°C (Table 1). Also inspection of a SeaWiFS image for this day shows that the station was positioned within the Cape Ghir filament with a surface chlorophyll concentration of about 0.3 mg m^{-3} observed both in situ and by SeaWiFS. The in situ primary production to integrated chlorophyll biomass ratio at the Exp. 3 station is 36 g C g-1 Chl d^{-1} compared with 9 and 14 g C g-1 Chl d^{-1} at the Exp. 1 and Exp. 2, respectively, implying that the algal population in the filament region is more efficient in carbon fixation. Morel (2000) also reported elevated primary production to chlorophyll biomass ratios during the EUMELI (EUtrophic, MEsotrophic and oLIgotrophic regimes) programme for a mesotrophic region in the giant filament off Cape Blanc, Mauritania, and suggested that such enhanced photosynthetic capacity originates from differences in algal photophysiology when compared with an oligotrophic region outside the filament. Barton et al. (1998), observed that the Cape

Bojador filament southeast of the Canary Islands transports higher chlorophyll concentrations to the open ocean but the phytoplankton community composition is not always the same. In October 1991 the filament was transporting mostly cyanobacteria while in March 1991 and August 1993 it was dominated by eukaryotic cells. It should nevertheless be noted that at the Exp. 3 station the observed deep chlorophyll maximum (DCM) at about 25 m depth (Table1) is significantly shallower than the value used by the Antoine and Morel (1996) method for a surface chlorophyll concentration of 0.31 mg Chl m^{-3} (50-75 m). The Antoine and Morel (1996) method uses a standard vertical chlorophyll profile for each near-surface chlorophyll value as derived by Morel and Berthon (1989). It is therefore possible that part of the excess production may simply be related to the DCM receiving more light than is assumed in the model. A shallow DCM was also observed by Barton et al. (1998) for the Cape Bojador filament and this condition may be characteristic of upwelling filaments in general. The EBC station east of the Canary Islands, which is situated in a comparable region to the mesotrophic stations of the EUMELI programme, displayed a similar annual range of chlorophyll concentration in the near surface waters (CANIGO, 0.08-0.89 mg m^{-3}; EUMELI, 0.15-1.4 mg m^{-3}).

Although only three 14C measurements are available (due to the logistical problems associated with this method), these results suggest that for oligotrophic regions the model daily primary productivity estimates are consistent with in situ values provided that the cloudiness factor reflects the actual situation dawn to dusk. But for filaments within upwelling regions, the model estimates are probably too low due to the model assuming a too deep DCM. This suggests that some model primary production estimates at the EBC station may be significantly underestimated when the Cape Yubi filament penetrates the station position.

Primary productivity along the 29°N transect

We have determined the primary productivity (in g C m^{-2}) from the SeaWiFS chlorophyll data shown in Figure 2 and AVHRR SST at the EBC, ESTOC and LP stations for the period September 1997 – March 1999 (Figure 4). At all stations the production time series over this period were similar. At LP and ESTOC production varied from about 0.2 – 0.5 g C m^{-2} d^{-1} for September 1997–April 1998. From May 1998 values were more or less constant ranging from about 0.4 - 0.5 g C m^{-2} d^{-1} through December 1998 for both stations. From January – March 1999 production increased rapidly due to onset of the Winter bloom with peak values of 0.7 g C m^{-2} d^{-1} for both LP and ESTOC. EBC showed a similar variability as at LP and ESTOC but production levels were higher in all seasons. Also the increased chlorophyll concentration due to the

frequent incursion of the Cape Yubi filament at EBC led to enhanced production compared with ambient levels e.g. 0.7 g C m^{-2} d^{-1} in March 1998, 1.2 g C m^{-2} d^{-1} in July 1998. The low production at all stations during the Winter 1997/1998 is primarily caused by the low SeaWiFS chlorophyll values used for the model. As already discussed there is evidence that SeaWiFS underestimated chlorophyll concentration by up to 50% at this time. Nevertheless even correcting the SeaWiFS values by this factor does not lead to the elevated production levels seen in the Winter of 1998/99.
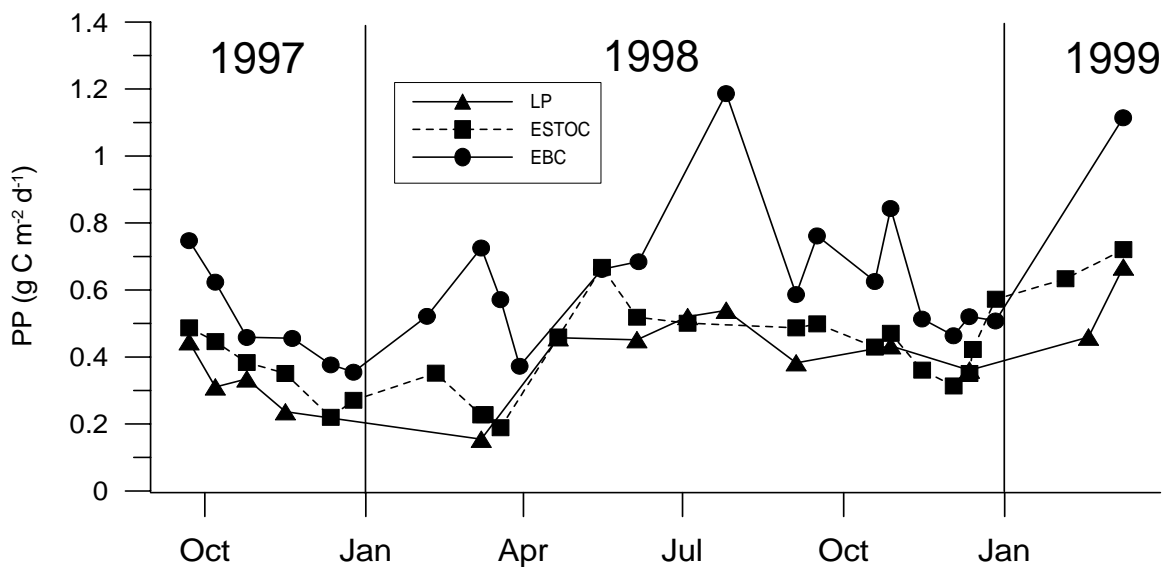

Figure 4. Primary productivity at LP, ESTOC and EBC for the period September 1997-March 1999 as determined by the Antoine and Morel (1996) method using SeaWiFS chlorophyll and AVHRR SST. Note the elevated productivity throughout the period at EBC in comparison with LP and ESTOC and the productivity peaks associated with incursions of the Cape Yubi filament over the EBC station.

The stations along the 29°N transect were chosen to cover (1) a region influenced strongly by coastal upwelling (EBC), (2) a transition zone between coastal upwelling and oligotrophic ocean (ESTOC) and (3) an open ocean, oligotrophic regime (LP). It was expected that the productivity gradient along this transect would decrease away from the coastal upwelling regime at EBC. To provide a better overview of the data we have computed the seasonal productivity for all stations by integrating the average value of all available daily production estimates for each season (Table 2). This averaging approach is valid for most seasons because the productivity estimates are more or less uniformly distributed in time. But it should be noted that the number of estimates available in each season varies significantly, ranging from six in fall 1998 for ESTOC to only one for LP in Winter 1998. Additionally these seasonal values are based on the daily primary productivity derived from SeaWiFS images with more or less clear skies and are

therefore probably overestimated for the LP and ESTOC stations. For the EBC station the influence of coastal upwelling especially from the Cape Yubi filament suggests these values are underestimated as discussed previously. Nevertheless the relative values in the table are useful for the purpose of seasonal and station comparison.

Table 2.   Seasonal primary production (g C m^{-2}) at LP, ESTOC and EBC as determined from SeaWiFS chlorophyll data and the Antoine and Morel (1996) method. Seasonal periods are calculated from 21 September, 21 December, 21 March and 21 June

		LP	ESTOC	EBC
1997	Autumn	30.2	34.4	48.5
1998	Winter	14.0	22.8	48.9
	spring	41.9	50.5	52.7
	summer	44.3	45.6	77.8
	Autumn	36.2	35.6	54.0
1999	Winter	50.8	57.8	73.0

For all seasons except fall 1998 ESTOC has higher productivity than at LP. But apart from Winter 1997/98 (for which only one SeaWiFS LAC image with clear skies was available at LP) the productivity difference between ESTOC and LP is never more than about 20%. In comparison the EBC productivity is always higher than both ESTOC and LP ranging from a minimum difference of 4% in spring 1998 to a maximum of 114% in Winter 1998. These results confirm the expected productivity gradient but they also imply that the gradient decreases sharply between EBC and ESTOC. If we accept that the model productivity values at EBC may be too low as suggested by the ^{14}C experiments, then the gradient fall off is even more dramatic. Indeed the near-surface waters at ESTOC may be characterised as oligotrophic, with the exception of the seasonal bloom, and appear to show no evidence of influence from cooler coastal upwelled water on productivity levels. As indicated previously this observation is supported by historical CZCS data where an 8 year analysis of mean monthly chlorophyll levels at the ESTOC position also showed no indication of coastal upwelling (Davenport *et al*., 1999). Also the mean annual production at ESTOC of 164 g C m^{-2} y^{-1} is comparable with the value of 154 g C m^{-2} y^{-1} from the oligotrophic site in the Bermuda Atlantic Time–series Study (BATS) for the period 1989-1997 (Steinberg *et al*., 2001).
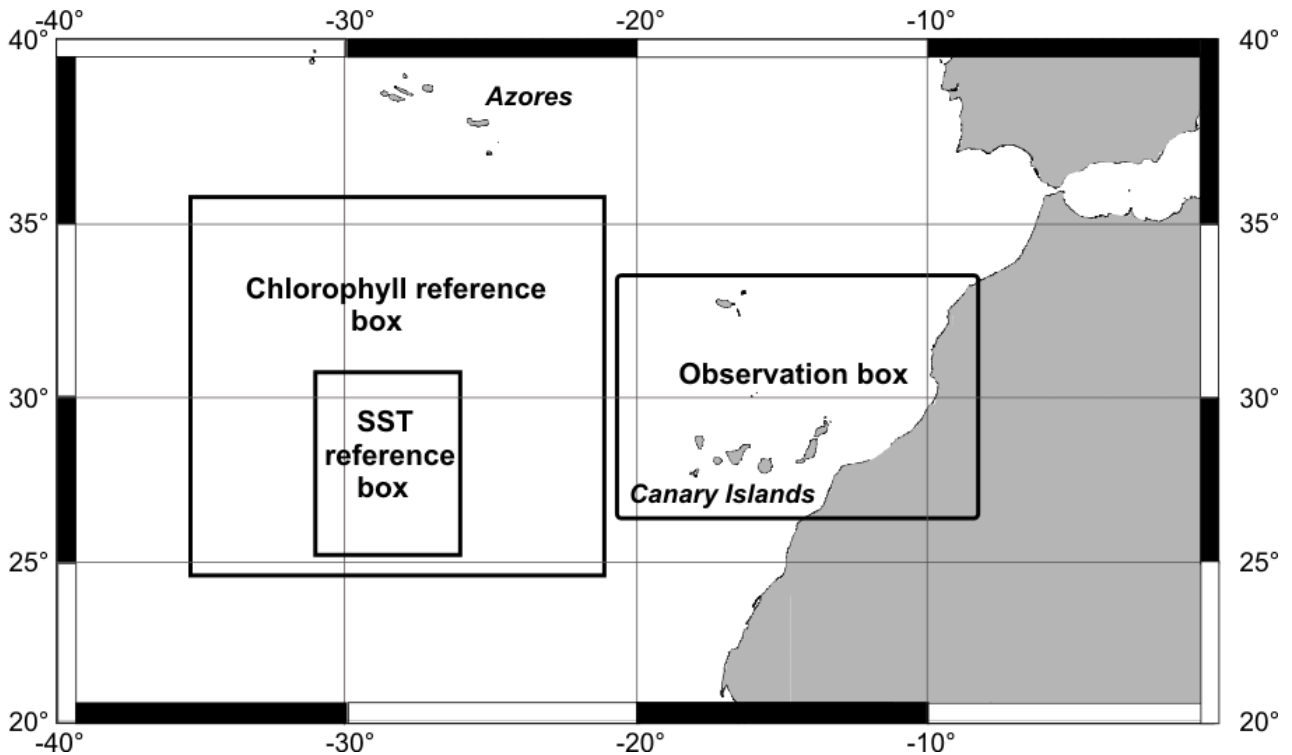
Figure 5. Location of the box region for the Canary Islands used in SST and chlorophyll image analysis to show the seasonal surface distribution of upwelled water in relation to the three stations. The SST and chlorophyll reference boxes to the west of the Canary Islands are also shown (see text for explanation).

To show the seasonal surface distribution of coastal upwelled water in relation to the three station positions, we analysed all available daily 9 km resolution AVHRR SST and SeaWiFS chlorophyll images from the NASA PODAAC covering the Canary Islands region for the period fall 1997 to Winter 1999. For each image the pixel values in a box region centred on the Canary Islands were compared with the mean value for a reference box region west of the islands in oligotrophic water (Figure 5). The size of the chlorophyll reference box was chosen to provide enough valid pixels for each SeaWiFS image; the SST reference box was somewhat smaller to avoid penetrating the cooler water north of the Canary Islands. To display the spatial distribution of upwelled water, for all available SST and chlorophyll images in each season, the percentage of valid pixels at each point in the box region that were respectively more than 2°C cooler or with a chlorophyll concentration > 0.2 mg m^{-3} (maximum ambient chlorophyll concentration) than in the reference boxes have been colour coded and plotted on a seasonal basis (Figure 6). Although the coastal upwelled water can be some 4°C cooler than the ambient water temperature, we chose a delta of 2°C to show the westwards penetration of upwelled water as it moves offshore and warms. The percentage of pixels at each station position fulfilling the above criteria have also been plotted graphically
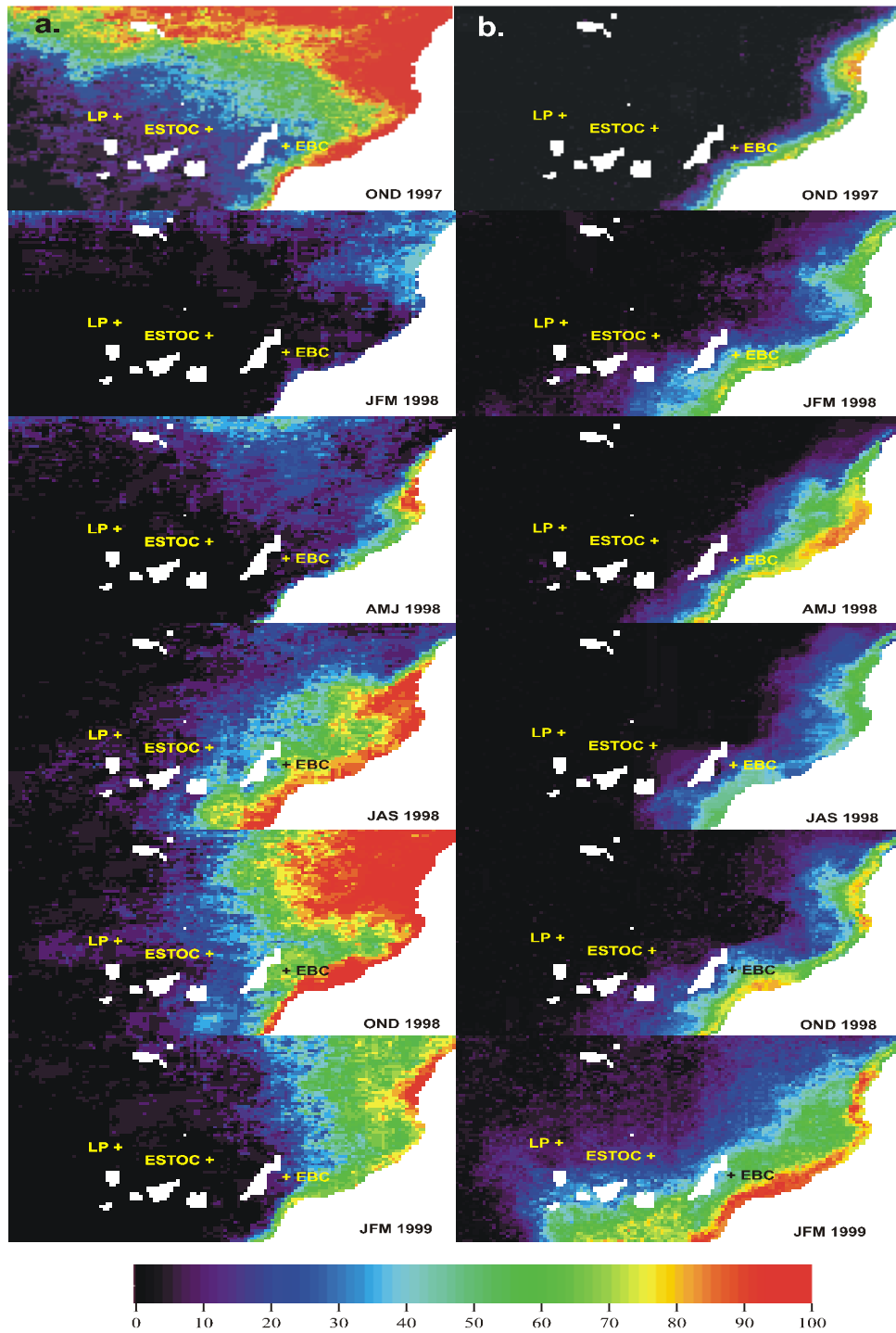
Figure 6. Seasonal patterns in the Canary Islands region of the persistence of (a) low SST and (b) high chlorophyll-*a* concentration from fall (OND) 1997 at the top to Winter (JFM) 1999. The colour scale indicates the temporal density of such conditions for each season according to the definitions given in Figure 7. Note the offshore extent of cooler upwelled water in summer (JAS) 1998 through fall (OND) 1998 in relation to the three stations at EBC, ESTOC and LP.
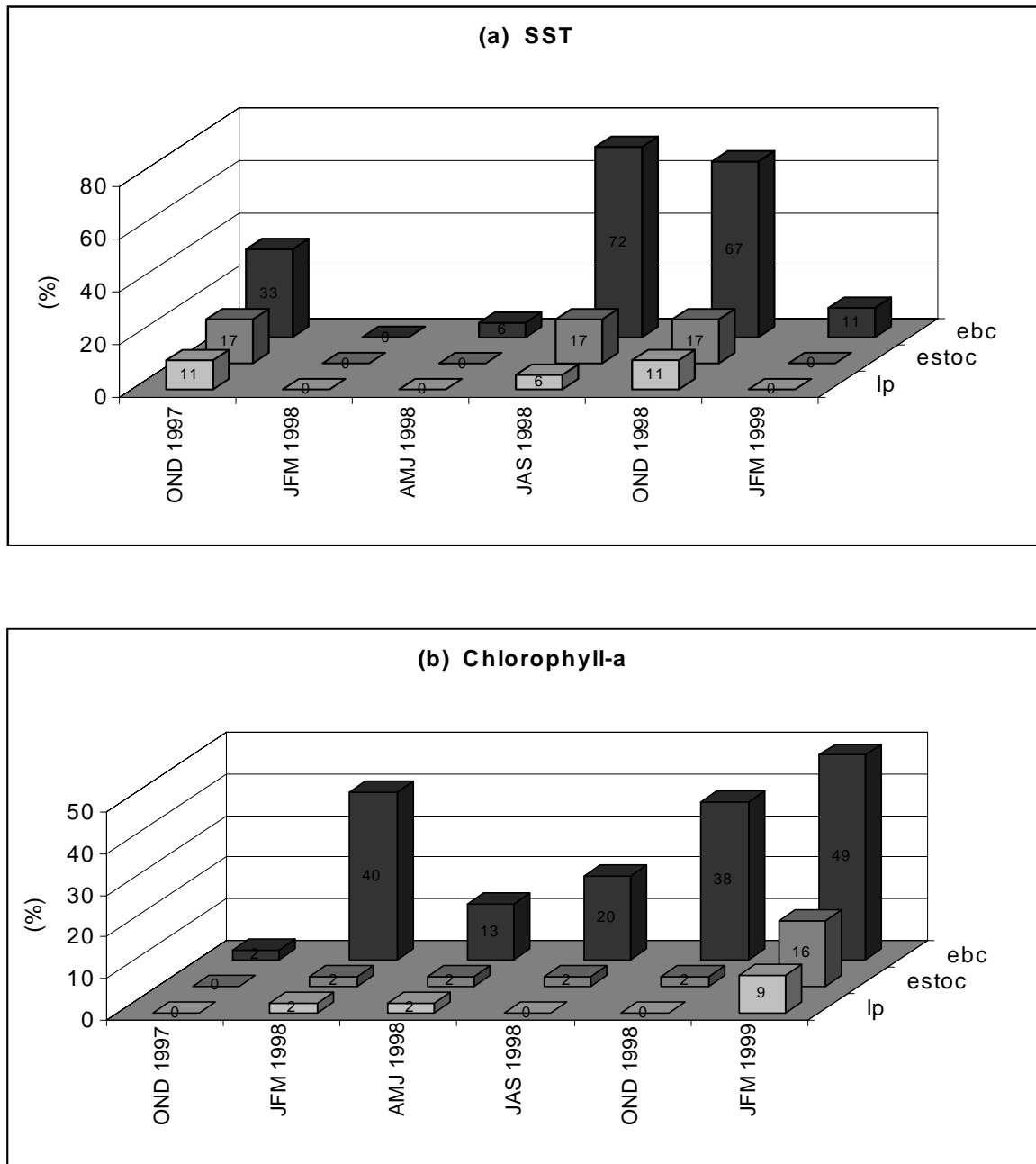
Figure 7. Seasonal SST (a) and chlorophyll-*a* distribution (b) at the LP, ESTOC and EBC stations for the period fall (OND) 1997 to Winter (JFM) 1999 as determined from 9 km AVHRR SST and SeaWiFS chlorophyll-*a* images. In (a) the vertical axis in each SST plot shows the percentage of valid pixels from all available images for each season that were more than 2°C cooler than a reference region west of the Canary Islands in oligotrophic water. Similarly in (b) the chlorophyll-*a* plots show the percentage of valid pixels with a chlorophyll-*a* concentration > 0.2 mg m^{-3} than in the reference region. Note that in the SST data all three stations are affected by coastal upwelled water in summer (JAS) and fall (OND) 1998. But elevated chlorophyll-*a* concentrations are only seen at EBC for the same period. The elevated chlorophyll-*a* concentrations at all three stations in Winter (JFM) 1999 are caused by the late Winter/early spring bloom.

on a seasonal basis (Figure 7). For the SST at all three stations (Figures 6a, 7a) there appears to be evidence of upwelled water both in fall 1997 and summer/fall 1998 corresponding to the period of most intense coastal upwelling. But for the EBC station, the penetration of the upwelled water was much more pronounced than for ESTOC and LP which is expected given the position of the EBC station near the African coast; there is even an indication of upwelled water for spring 1998 and Winter 1999 at EBC. Elevated chlorophyll-*a* concentration (Figures 6b, 7b) though is only evident at EBC in summer/fall 1998 corresponding to the presence of upwelled water seen in the SST data. But in contrast to the SST data there is no evidence of elevated chlorophyll-*a* concentration at the ESTOC and LP stations in summer/fall 1998. The strong chlorophyll-*a* signal at all stations in Winter 1999 is unlikely to be the result of upwelled water being transported offshore as this is the season of least intense upwelling. Instead this is interpreted as the annual Winter/spring bloom in the Canary Island region resulting from deep mixing of near-surface waters; the much weaker seasonal bloom of Winter 1998 was only seen at EBC.

These observations show that although cooler upwelled water did reach the ESTOC and LP stations in fall 1997 and summer/fall 1998, it did not lead to elevated phytoplankton growth which implies that it was nutrient depleted. In contrast the EBC station position displayed both a strong upwelled water signal and elevated chlorophyll-*a* concentration for the same seasons. We may conclude that in near surface waters the LP and ESTOC regions are oligotrophic while the EBC station region is a coastal upwelling zone.

CONCLUSIONS

The primary productivity estimates along the 29°N transect through the Canary Islands show that, as expected, the LP and ESTOC stations are situated in oligotrophic waters. Nevertheless both stations displayed a clear signal from the late Winter/early spring bloom in 1999 and possibly a much weaker spring bloom in 1998. In comparison the EBC station is regularly influenced by cooler, upwelled water especially from the Cape Yubi filament giving rise to much higher primary productivity levels than at ESTOC and LP. Although some cooler upwelled water appears to reach the ESTOC and LP regions during the upwelling season in summer/fall, productivity levels were observed to fall away very steeply between EBC and ESTOC implying that such waters may be nutrient depleted at ESTOC and LP.

The new generation of ocean colour sensors such as SeaWiFS have the potential of providing an unparalled insight into primary productivity changes in the world's oceans at all

time scales from daily to seasonal and annually and at a regional, basin and global scale. In this study we have demonstrated that the application of a simple model together with even a limited data set of satellite images can provide good insight into relative primary production in the Canary Islands region. It is also clear though that much needs to be done to improve models performance if we are to have confidence in regional absolute primary production estimates in an upwelling area.

REFERENCES

Acker, J. G. (Ed.), 1998. GDAAC Ocean Color Newsletter, Spring/Summer 1998, 4(2).

Antoine, D. and Morel. A., 1996. Oceanic primary production. 1. Adaptation of a spectral light-photosynthesis model in view of application to satellite chlorophyll observations. Global Biogeochemical Cycles, 10 (1), 43-55.

Antoine, D., André, J.-M., and Morel. A., 1996. Oceanic primary production. 2. Estimation at global scale from satellite (coastal zone color scanner) chlorophyll. Global Biogeochemical Cycles, 10 (1), 57-69.

Bailey, S. W., McClain, C. R., Werdell, P. J., and Schieber, B. D., 2000. Normalized Water-Leaving Radiance and Chlorophyll a Match-up Analyses. In: NASA Technical Memorandum 2000-206892, Vol. 10, 7, pp 45-52., NASA Goddard Space Flight Center

Barton, E.D., Arístegui, J., Tett, P., Cantón, M., García-Braun, J., Hernández-León, S., Nykjaer, L., Almeida, C., Almunia, J., Ballesteros, S., Basterretxea, G, Escánez, J., García-Weill, L., Hernández-Guerra, A., López-Laatzen, F., Molina, R., Montero, M. F., Navarro-Pérez, E., Rodríguez, J. M., van Lenning, K., Vélez, H., and Wild, K., 1998. The transition zone of the Canary Current upwelling region. Progress in Oceanography, 41, 455-504.

Behrenfeld, J. and Falkowski, P. G., 1997a. Photosynthetic rates derived from satellite-based chlorophyll concentration. Limnological Oceanography, 42(1), 1-20.

Behrenfeld, J. and Falkowski, P. G., 1997b. A consumer's guide to phytoplankton primary productivity models. Limnological Oceanography, 42(7), 1479-1491.

Bergametti, G., Gomes, L., Coude-Gaussen, G., Rognon, P., and Le Coustumer, M. N., 1989. African dust observed over the Canary Islands: Source-regions identification and transport pattern for some summer situations. Journal of Geophysical Research, 94, 14855-14864.

Davenport, R., Neuer S., Hernández-Guerra A., Rueda M. J., Llinás O., Fischer G. and Wefer G., 1999. Seasonal and interannual pigment concentration in the Canary Islands region from CZCS data and comparison with observations from ESTOC. International Journal of Remote Sensing, 20(7), 1419-1433.

Duce, R. A. and Tindale, N. W., 1991. Atmospheric transport of iron and its deposition in the ocean. Limnological Oceanography, 36, 1715-1726.

Freudenthal, T., Neuer, S., Meggers, H., Davenport, R., and Wefer, G., 2001. Comparison of water column particle fluxes, sedimentary accumulation rates, and the stable nitrogen isotope signature along a productivity gradient in the Canary Islands region. Marine Geology, 177, 93-109.

Gabric, A. J., Garcia, L., Van Camp, L., Nykjaer, L.,Eifler, W. and Schrimpf, W., 1993. Offshore Export of Shelf Production in the Cape Blanc (Mauritania) Giant Filament as Derived From Coastal Zone Color Scanner Imagery. Journal of Geophysical Research, 98(C3), 4697-4712.

Gordon, H. R., and Wang, M., 1994. Retrieval of water-leaving radiance and aerosol optical thickness over the oceans with SeaWiFS: a preliminary algorithm. Applied Optics, 33(3), 443-452.

Hooker, S. B., Esaias, W. E., Feldman, G. C., Gregg , W. W. and McClain, C. R.,1992. An overview of SeaWiFS and ocean color. – NASA Technical Memorandum 104566, Vol. 1, 24 pp., NASA Goddard Space Flight Center

Knap, A., Michaels, A., Close, A., Ducklow, H. and Dickson, A., (Eds.), 1996. Protocols for the Joint Global Ocean Flux Study (JGOFS) Core Measurements. JGOFS Report Nr. 19, 170 pp. Reprint of the IOC Manuals and Guides No. 29, UNESCO, 1994.

Kostianoy, A. G., and Zatsepin, A. G. (1996). The West African coastal upwelling filaments and cross-frontal water exchange conditioned by them. Journal of Marine Systems., 7, 349-359.

Llinás, O., Rodríguez de León, A., Siedler, G. and Wefer, G., 1994. The ESTOC time series started operation. International WOCE Newsletter, 17, 20.

Longhurst, A., Sathyendranath, S., Platt, T., and Caverhill, C., 1995. An estimate of global primary production in the ocean from satellite radiometer data. Journal of Plankton Research, 17 (6), 1245-1271.

Mittelstaedt, E., 1986. Upwelling regions. In: Oceanography, Landolt-Börnstein New Series, Group V, vol. 3c, J. Sündermann, editor. Springer-Verlag, New York, pp. 135-163.

Mittelstaedt, E., 1991. The ocean boundary along the northwest African coast: Circulation and oceanographic properties at the sea surface. Progress in Oceanography, 26, 307-355.

Morel, A., and Berthon, J. F., 1989. Surface pigments, algal biomass profiles, and potential production in the euphotic layer : Relationships reinvestigated in view if remote-sensing applications. Limnological Oceanography, 34, 1545-1562.

Morel, A., 2000. Process studies in eutrophic, mesotrophic and oligotrophic oceanic regimes within the tropical northeast Atlantic. In: The Changing Ocean Carbon Cycle. R. B.Hanson, , H. W. Ducklow, and J. G. Field, editors. Cambridge University Press, Cambridge, U.K, pp. 338-374.

Müller, T. J., and Siedler, G., 1992. Multi-year current time series in the eastern North Atlantic Ocean. Journal of Marine Research, 50, 63-98.

Neuer, S., Ratmeyer V., Davenport R., Fischer G. and Wefer G., 1997. Deep water particle flux in the Canary Island region: seasonal trends in relation to long-term satellite derived pigment data and lateral sources. Deep-Sea Research, I, 44(8), 1451-1466.

Neuer, S., Freudenthal, T., Davenport, R., Llinás, O., Rueda, M. J., Wefer, G., (in press). Seasonality of particle flux and surface parameters in the northern Canary Island basin. Deep-Sea Research, II.

Neuer, S., and Rueda M-J., 1997. European Time-Series Station In Operation North Of Canary Islands. – In: Bowles, M. C. (Ed.), U.S. JGOFS NEWS, 8(2), 9 and 15. U.S. Planning Office, Woods Hole Oceanographic Inst., Woods Hole, MA, USA.

Nykjaer, L., and Van Camp, L., 1994. Seasonal and interannual variability of coatal upwelling along northwest Africa and Portugal from 1981 to 1991. Journal of Geophysical Research, 99, 14197-14207.

Parrilla, G., (in press). Deep-Sea Research, II.

Pinker, R. T., and Laszlo, I., 1992. Global distribution of photosynthetically active radiation as observed from satellites. Journal of Climatology, 5, 56-65.

Ratmeyer, V., Fischer, G., and Wefer, G., 1999. Lithogenic particle fluxes and grain size distributions in the deep ocean off northwest Africa: Implications for seasonal changes of aeolian dust input and downward transport. Deep-Sea Research, I, 46, 1289-1337.

Reed, R. K., 1977. On estimating insolation over the ocean. Journal of Physical Oceanography, 7, 482-485.

Sathyendranath, S., Longhurst, A., Caverhill, C. M., and Platt, T., 1995. Regionally and seasonally differentiated primary production in the North Atlantic. Deep-Sea Research, I, 42 (10), 1773-1802.

Speth, P., and Detlefsen, H., 1982. Meteorological influences on upwelling off Northwest Africa. In: Rapports et Procès - Verbaux des Réunions, Conseil International pour l'Exploration de la Mer., Copenhagen, Denmark, 180, 29-35.

Steinberg, D.K., Carlson, C. A., Bates, N. R., Goldthwait, S. A., Madin, L. P., and Michaels, A. F., 2001. Overview of the U.S. JGOFS Bermuda Atlantic Time-series Study (BATS): A decade-scale look at ocean biology and biogeochemistry. Deep-Sea Research, II, 48, 1405-1447.

Stramma, L., 1984. Geostrophic transport in the Warm Water Sphere of the eastern subtropical North Atlantic. Journal of Marine Research, 42, 537-558.

Strub, P. T., Kosro, P. M., and Huyer, A., 1991. The nature of the cold filaments in the California current system. Journal of Geophysical Research, 96, 14743-14768.

Sturm, B., 1981. The atmospheric correction of remotely sensed data and the quantitative determination of suspended matter in marine water surface layers. In: Remote Sensing in Meteorology, Oceanography and Hydrology, A. P. Cracknell, editor. Ellis Horwood, Chichester, U.K., pp 163-197.

Van Camp, L., Nykjaer, L., Mittelstaedt, E., and Schlittenhardt, P., 1991. Upwelling and boundary circulation off Northwest Africa as depicted by infrared and visible satellite observations. Progress in Oceanography, 26, 357-402.

Welshmeyer, N. A., 1994. Fluorometric analysis of chlorophyll a in the presence of chlorophyll b and phaeopigments. Limnological Oceanography, 39, 1985-1992.

Wooster, W. S., Bakun, A., and McLain, D. R., 1976. The seasonal upwelling cycle along the eastern boundary of the North Atlantic. Journal of Marine Research, 34, (2), 131-141

4. Reconstruction of paleoceanography off NW Africa during the last 40,000 years: influence of local and regional factors on sediment accumulation

H. Kuhlmann[*], T. Freudenthal, P. Helmke and H. Meggers

University of Bremen, Department of Geosciences, PO Box 330440, 28334 Bremen, Germany

4.1 Abstract

A set of 43 sediment cores from around the Canary Islands is used to characterize this region, which intersects meridional climatic regimes and zonal productivity gradients with a high spatial resolution. Using rapid and non-destructive core logging techniques we carried out Fe intensity and magnetic susceptibility (MS) measurements and created a stack on the basis of five stratigraphic reference cores, for which a stratigraphic age model was available from $\delta^{18}O$ and ^{14}C analyses on planktic foraminifera. By correlation of the stack with the Fe and MS records of the other cores we were able to develop age depth models at all investigated sites of the region. We present the bulk sediment accumulation rates (AR) of the Canary Islands region as an indicator of shifts in the upwelling-influenced areas for the Holocene (0-12 kyr), the deglaciation (12-18 kyr), and the last glacial (18-40 kyr). As a general observation it can be said that productivity was enhanced during glacial times with highest values during the deglaciation. The main differences between the analysed time intervals we interpret to be the result of the sea-level effects, changes in the geographical extent of high productivity areas, and variations in current intensity.

---

[*] Corresponding author. phone: ++49-421-2182886; fax: ++49-421-2183116; E-mail: kuhlma@uni-bremen.de.

4.2 Introduction

High flux rates between the various atmospheric, oceanic and sedimentary element pools focus research on the climate-relevant carbon cycle in high productivity areas like coastal upwelling regions. The high nutrient content of the upwelled water masses results in enhanced primary productivity in these areas and, depending on the favoured organisms exploiting the high nutrient conditions, accounts for the role as source or sink for carbon. Changes in the upwelling intensity and primary productivity are presumed to have major impact on the variability of the oceanic and atmospheric CO_2 concentrations at glacial/interglacial time scales (Berger and Keir, 1984). In glacial time intervals the atmospheric circulation was enhanced, which is interpreted to have caused generally higher productivity in subtropical eastern boundary-current regions. Higher productivity in combination with increased dust input is presumed to have caused higher sediment accumulation rates (AR) in glacial continental margin sediments off NW Africa (Sarnthein et al., 1988). Recent research indicates that the assumption of enhanced glacial sediment accumulation off NW Africa has to be modified. Various studies point to strong differences in the upwelling-related productivity pattern, with highest productivity partly during glacial times, partly during deglaciation times, and partly during wet intervals like the early Holocene, although the driving force of the upwelling, the seasonal trade winds, are supposed to be of regional significance (Bertrand et al., 1996; Marret and Turon, 1994; Martinez et al., 2000; Zhao et al., 2000). A variety of factors influencing productivity and the sediment accumulation records were identified. Changes of climatic conditions, atmospheric circulation, and sea-level changes act as regional factors influencing environmental conditions, whereas displacement of upwelling cells, sediment transport and seafloor morphology result in local differences. In single-core studies it is not possible to distinguish between these influencing factors, and only regional studies can provide the opportunity to separate these factors and the resulting features in the sediment accumulation.

The modern patterns of upwelling and related primary productivity in the Canary Islands region are manifold, including zonal gradients from the near-coast upwelling areas to oligotrophic conditions further off the coast, as well as coastal morphology-induced filament formation. The upwelling pattern, as recognized from satellite-derived chlorophyll-a concentrations, is known to be an indicator of primary productivity. This pattern, characterizing sea-surface conditions, is mirrored in the

underlying sediments by the AR. Regional studies with a high spatial resolution are necessary to distinguish the various local and regional factors in order to get a better impression of changes in the NW African climate and related upwelling systems (Bertrand et al., 1996). Correlations of the records of 43 sediment cores in the Canary Islands region were made to resolve a detailed picture of even mesoscale processes that affect the sedimentation. We address the question of the sensitivity of sediment accumulation pattern to various oceanographic features such as coastal upwelling, filament structures off the cape locations and more oligotrophic conditions in the Canary Islands region. Our data set will also provide insights into the changes of the upwelling processes and the sedimentary environment over time, i.e. through the last glacial, the deglaciation, and the Holocene. We focus on the causes for shifts and changes in the intensity of upwelling processes mirrored by AR during the last 40 kyr.

4.2.1 Oceanographic setting

The investigation area, located at the NW African continental margin between 27°N and 32°N is shown in Fig. 4.1 with the surface-current direction and chlorophyll-a concentration. The sea-floor morphology is characterized by a shallow (< 150 m) continental shelf that extends offshore to about 25 km at Cape Ghir and up to 75 km north of Cape Yubi (Summerhayes et al., 1976). An important structure on the narrow continental slope at Cape Ghir is the Agadir Canyon system, which consists of several channels draining into the Agadir Basin. By contrast the continental slope at Cape Yubi is comparatively regular and plain (Uchupi et al., 1976; Weaver et al., 2000).

The water column in the region is characterised by subtropical water at the surface, underlain by southward-directed North Atlantic Central Water, with increments of South Atlantic Central Water increasing to the south down to a depth of 600 m, which is the main source of the upwelling water masses. Below this the Mediterranean Outflow Water, with southward-increasing imprints of South Atlantic Intermediate Water, occurs in water depths down to 1700 m, and this is underlain by southward-directed North Atlantic Deep Water (Knoll et al., 2002; Llinás et al., 2002; Sarnthein et al., 1982). The surface water is influenced by the southward-directed Canary Current, which is fed by the eastern branch of the subtropical North Atlantic gyre (Knoll et al., 2002; Mittelstaedt, 1991). During the last glacial the Canary Current is presumedd to have intensified due to the generally enhanced atmospheric and oceanic circulation (Sarnthein et al., 1982). Sea level was lower by 120 m during the last glacial maximum compared to modern values (Fairbanks, 1989) and rose during the

deglaciation up to the present level in several steps (Bard et al., 1989; Bard et al., 1996). These changes caused the exposure of large areas of the continental shelf during the glacial and therefore altered coastal morphology. These changes are believed to have a strong influence on the sediment accumulation, particularly at sites located near the coastline (Bertrand et al., 2000; Martinez et al., 1999).
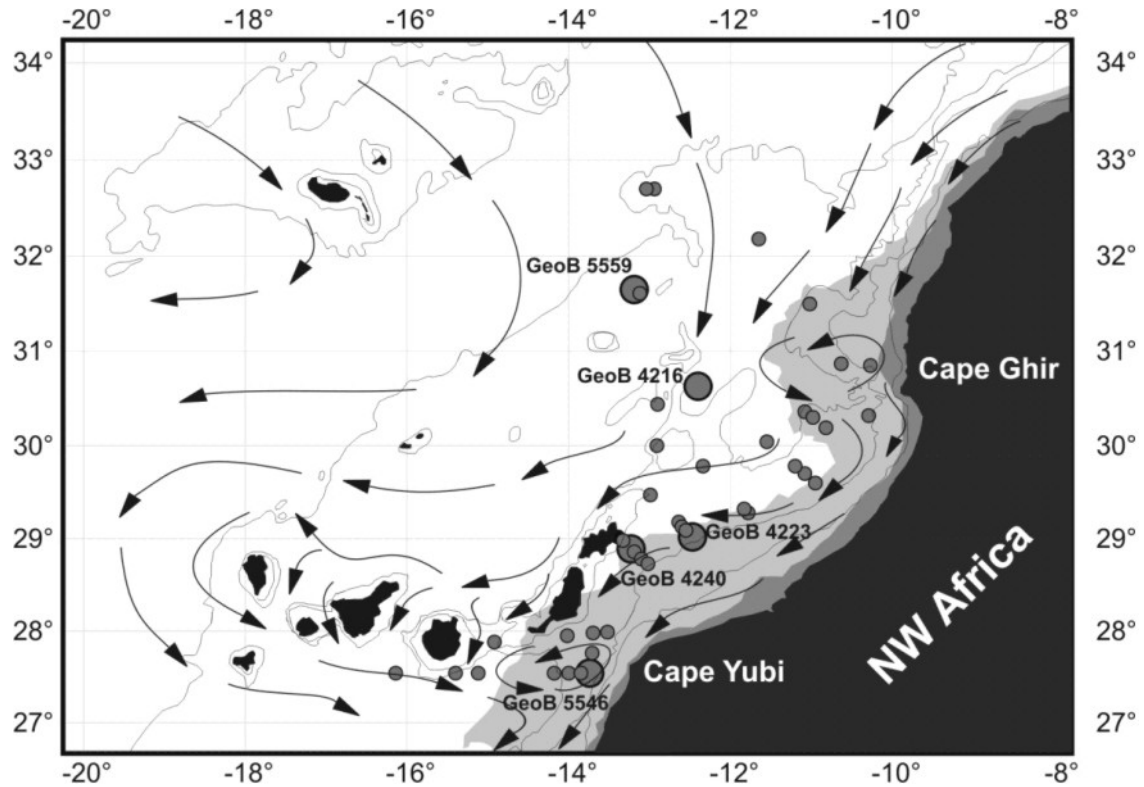
Figure 4.1 Bathymetric map of the investigation area with 100, 1000, 2000 and 4000 m depth contour lines. SeaWiFS derived chlorophyll-a concentrations averaged from 1997 – 2000; areas with > 1 mg m^{-3} are shaded dark grey, 0.25 – 1 mg m^{-3} light grey, < 0.25 mg m^{-3} not shaded. The surface currents are indicated by arrows (after Mittelstaedt, 1991). The filled circles indicate core locations, the larger circles show stratigraphic reference cores GeoB 5559, GeoB 4216, GeoB 4223, GeoB 4240 and GeoB 5546.

Trade-wind-induced coastal upwelling occurs mostly in a narrow 5-km band on the shelf (Mittelstaedt, 1991), while oligotrophic conditions prevail further offshore. In the northern part of the working area, at Cape Ghir (~ 30°N) a strong seasonal upwelling dominates in the summer, whereas at Cape Yubi (~ 27°N) the trend of upwelling conditions throughout the whole year is observed as is also the case further to the south at Cape Blanc (Nykjaer and Van Camp, 1994). Upwelling features deduced from satellite-derived chlorophyll-a concentrations are closely connected to high

primary productivity (Antoine et al., 1996; Behrenfeld and Falkowski, 1997; Davenport et al., 1999). The water masses from the upwelling areas are transported far offshore in filaments (Davenport et al., 2002; Hagen, 2001; Van Camp et al., 1991), which are generated by interaction of the current system and the coastal morphology (cape locations) (Johnson and Stevens, 2000).

S to SW of the Canary Islands a small-scale formation of cyclonic and anticyclonic eddies is reported, which results from the lee-side hydrographic and atmospheric conditions (Arístegui et al., 1994; Barton et al., 1998). The associated up- and downwelling at these sites impacts the ecosystem development in these areas (Arístegui et al., 1997; Basterretxea et al., 2002).

In the northern part of the region, modern oceanography is influenced by river input from the Souss River draining the Atlas Mountains. There has been no significant recent fluvial input south of 30°N, with activity limited to sporadic active wadi systems. During the climate optimum in the early Holocene, the adjacent African continent received more humidity from the monsoon system (Gasse, 2000; Gasse et al., 1990). This may have resulted in a drainage via wadi systems into the ocean. During the glacial time period, dry conditions comparable to the present situation prevailed in NW Africa.

4.3 Material and Methods

4.3.1 Material

This study benefits from a pool of 73 sediment cores recovered during METEOR cruises M37/1 (Wefer et al., 1997), M42/4 (Wefer et al., 1999) and M45/5 (Neuer et al., 2000), all located in the Canary Islands region off NW Africa. From this set 43 cores were selected, for which a confident stratigraphic interpretation was possible. We excluded all cores where turbidites, volcanic gravel and ash layers extended over long intervals of the cores. Additionally, cores where the extent of these layers were uncertain had to be omitted because of the resulting uncertainties in the age control. The cores used in this study are from 800 - 4,000 m waterdepth (Tab. 4.1), representing different areas of enhanced productivity near the coast of Morocco, especially at the cape locations and more oligotrophic conditions further offshore (Fig.4.1).

Core logging methods provide the opportunity to work on a large number of cores with a sufficient resolution in an acceptable length of time. We used two rapid and non-destructive core logging facilities at the University of Bremen: the Multi-Sensor Core Logger (MSCL) and the X-Ray Fluorescence (XRF) Core Scanner.

4.3.2 Multi-Sensor Core Logger (MSCL)

Physical properties (GRAPE-density, p-wave velocity and magnetic susceptibility) were measured non-destructively on the archive halves of the cores using a GEOTEK™ (Surrey, UK) MSCL (Gunn and Best, 1998; Weaver and Schultheiss, 1990) at the Department of Geosciences at the University of Bremen. Here we present the magnetic susceptibility (MS) measurements, carried out using a BARTINGTON™

Table 4.1 Cruise and core number, geographic position, water depth, gear type and recovery of the investigated sediment cores from the Canary Islands Region. (GC = gravity corer, PC = piston corer)

Cruise Meteor	Station GeoB	Latitude (°N)	Longitude (°W)	Geartype	Waterdepth (m)	Recovery (cm)
M37/1	4205-2	32°10.9	11°38.9	GC	3272	501
M37/1	4206-1	31°30.0	11°01.3	GC	1855	571
M37/1	4209-2	30°21.4	11°05.0	GC	2150	970
M37/1	4210-1	30°18.0	10°58.8	GC	1959	424
M37/1	4211-2	30°11.6	10°49.3	GC	1773	650
M37/1	4212-2	29°36.2	10°57.0	GC	1256	857
M37/1	4213-2	29°41.8	11°04.7	GC	1547	754
M37/1	4214-1	29°46.9	11°11.8	GC	1788	952
M37/1	4215-2	30°02.2	11°33.2	GC	2106	766
M37/1	4216-2	30°37.9	12°23.8	GC	2325	1117
M37/1	4217-5	30°26.1	12°53.7	GC	2504	716
M37/1	4218-1	29°57.3	12°54.7	GC	2723	619
M37/1	4221-1	29°46.5	12°20.3	GC	1826	843
M37/1	4223-2	29°01.1	12°28.0	GC	777	779
M37/1	4225-1	29°16.5	11°46.9	GC	1281	725
M37/1	4226-3	29°19.2	11°50.0	GC	1400	907
M37/1	4228-3	29°28.2	12°59.4	PC	1633	1188
M37/1	4229-1	29°10.9	12°38.3	GC	1422	663
M37/1	4230-2	29°07.7	12°35.8	GC	1316	993
M37/1	4231-1	29°05.2	12°33.1	GC	1197	726
M37/1	4232-2	29°01.3	13°23.2	GC	1161	991
M37/1	4233-1	28°58.5	13°19.8	GC	1303	1076
M37/1	4235-2	28°51.4	13°11.4	GC	1247	777
M37/1	4236-1	28°47.0	13°05.7	GC	1030	1084
M37/1	4237-2	28°43.7	13°01.0	GC	800	966
M37/1	4240-2	28°53.3	13°13.5	GC	1358	688
M42/4	5536-2	27°32.2	16°08.1	GC	3456	880
M42/4	5537-3	27°32.1	15°24.1	GC	2362	784
M42/4	5538-1	27°32.2	15°07.0	GC	2537	1080
M42/4	5540-2	27°32.1	14°10.5	GC	2035	920
M42/4	5541-4	27°32.2	13°59.7	PC	1748	1252
M42/4	5545-1	27°32.2'	13°50.8	PC	1431	1156
M42/4	5546-2	27°32.2	13°44.2	PC	1071	851
M42/4	5547-3	27°45.6	13°42.6	GC	1310	1066
M42/4	5548-2	27°59.5	13°31.1	GC	1162	755
M42/4	5549-3	27°58.7	13°41.7	GC	1454	890
M42/4	5550-2	27°57.1	14°00.9	GC	1738	1056
M42/4	5551-3	27°52.6	14°54.9	GC	1885	1027
M42/4	5559-2	31°38.7	13°11.2	GC	3178	585
M42/4	5560-1	31°36.6	13°07.1	GC	3944	469

M42/4	5561-2	32°42.2	12°56.1	GC	3500	434
M45/5	6006-1	30°52.1	10°37.8	GC	1275	908
M45/5	6011-1	30°18.9	10°17.3	GC	993	477

measurements were made in 1-cm steps over an area of 1 cm^2. The resulting data are the volume specific magnetic susceptibilities in 10^{-5} SI units.

4.3.3 X-Ray Fluorescence (XRF) Core Scanner analysis

The XRF Core Scanner at the University of Bremen is a non-destructive analysis system for scanning the surface of archive halves of sediment cores. It was developed and built at the Royal Netherlands Institute for Sea Research (NIOZ), Texel, Netherlands (Jansen et al., 1998). The central sensor unit consists of a molybdenum X-ray source (3-50kV), a Peltier-cooled PSI detector (KEVEX^{TM}) with 125 μm beryllium window, and a multichannel analyser with a 20 eV spectral resolution. The system configuration (X-ray tube energy, detector sensibility) at the University of Bremen allows the analyses of elements from K (atomic no. 19) to Sr (atomic no. 38) (X-ray tube voltage: 20 kV). We analysed element intensities at 1-cm intervals, each measurement over an area of 1 cm^2. In this study we present the elements Fe and Ti, using 30-s count time and an X-ray current of 0.087 mA. The acquired XRF spectrum for each measurement was processed by the KEVEX^{TM} software Toolbox$^{©}$. The resulting data are element intensities in counts per second (cps). Detection limits of the device as well as accuracy experiments were carried out by Jansen et al., 1998.

4.3.4 Density measurements and accumulation rates

Density calculations were carried out following Weber et al., (1997). We measured wet weight (WW) and dry weight (DW) of discrete samples of 10 cm^3 volume at 5-cm spacing for all cores used in this study. The salt weight (SW) was calculated assuming 35 ‰ pore water salinity.

$$SW~(g) = WW~(g) - DW~(g) \times 0.035) \times (1 - 0.035)^{-1}. \qquad (1)$$

The dry bulk density (DBD) was calculated following the equation:

$$DBD~(g \times cm^{-3}) = (DW~(g) - SW~(g) \times volume^{-1}~(cm^3), \qquad (2)$$

DBD was used to calculate average AR in combination with sedimentation rates (SR) that were inferred from stratigraphic investigations following the equation:

$$AR \ (g \times cm^{-2} \times kyr^{-1}) = SR \ (cm \times kyr^{-1}) \times DBD \ (g \times cm^{-3}). \qquad (3)$$

4.4 Stratigraphy

The well established but time and cost intensive oxygen isotope stratigraphy technique is not appropriate for the investigation of a large number of sediment cores as were used in this study. Therefore we used Fe intensities and MS records, obtained by rapid and non-destructive core logging tools to transfer the age models of five reference cores with reasonable age control to the remainder of the cores. These reference cores cover the various environmental and sedimentary conditions representing offshore and nearshore locations as well as northern and southern locations in the Canary Islands region. Their age-depth relationships (Fig. 4.2) were established by correlating the $\delta^{18}O$ records of planktic foraminifera with the SPECMAP stack (Imbrie et al., 1984) and the higher-resolution records of Martinson et al. (1987) and Raymo (1997) in combination with ^{14}C measurements. The age models of the cores GeoB 4216, GeoB 4223, and GeoB 4240 were adopted from Freudenthal et al. (2002), the age model of core GeoB 5559 from Moreno et al. (2001). These age models were slightly modified within oxygen isotope stage (OIS) 3 based on six additional ^{14}C-AMS dates (Freudenthal, et al. subm.). The age model of core GeoB 5546 will be published elsewhere (Meggers et al., in prep.).

MS and Fe intensity of the five reference cores are shown versus age in Fig. 4.2. Generally we observe a rough coincidence of the two parameters, with higher values during interglacial periods as compared to glacial conditions. The change from the penultimate glacial to the following interglacial period is characterised by a strong increase from minimum glacial values to higher values during OIS 5.5. The high values at OIS 5.3 (represented by a characteristic double peak) and 5.1 are interrupted by significantly lower values during the interstadials 5.2 and 5.4. The following glacial time interval is characterised by relatively low values of both parameters with minimum values in OIS 3 at about 40 kyr and during OIS 2 at 18 and 12 kyr.

Comparing the Fe intensity and MS records of the different stratigraphic reference cores, we see that the pattern is time equivalent at all sites as demonstrated in the Fe and MS stacks (Fig. 4.2).

4.4.1 Canary Stacks (CAFE, CAMS)

The iron intensity (CAFE Stack) and MS (CAMS Stack) records of the stratigraphic reference cores GeoB 4216, GeoB 4223, GeoB 4240, GeoB 5546 and GeoB 5559 were used to create a stack following Imbrie et al. (1984) and von Dobeneck and Schmieder (1999)(Fig. 4.2). After the removal of a few turbidite,
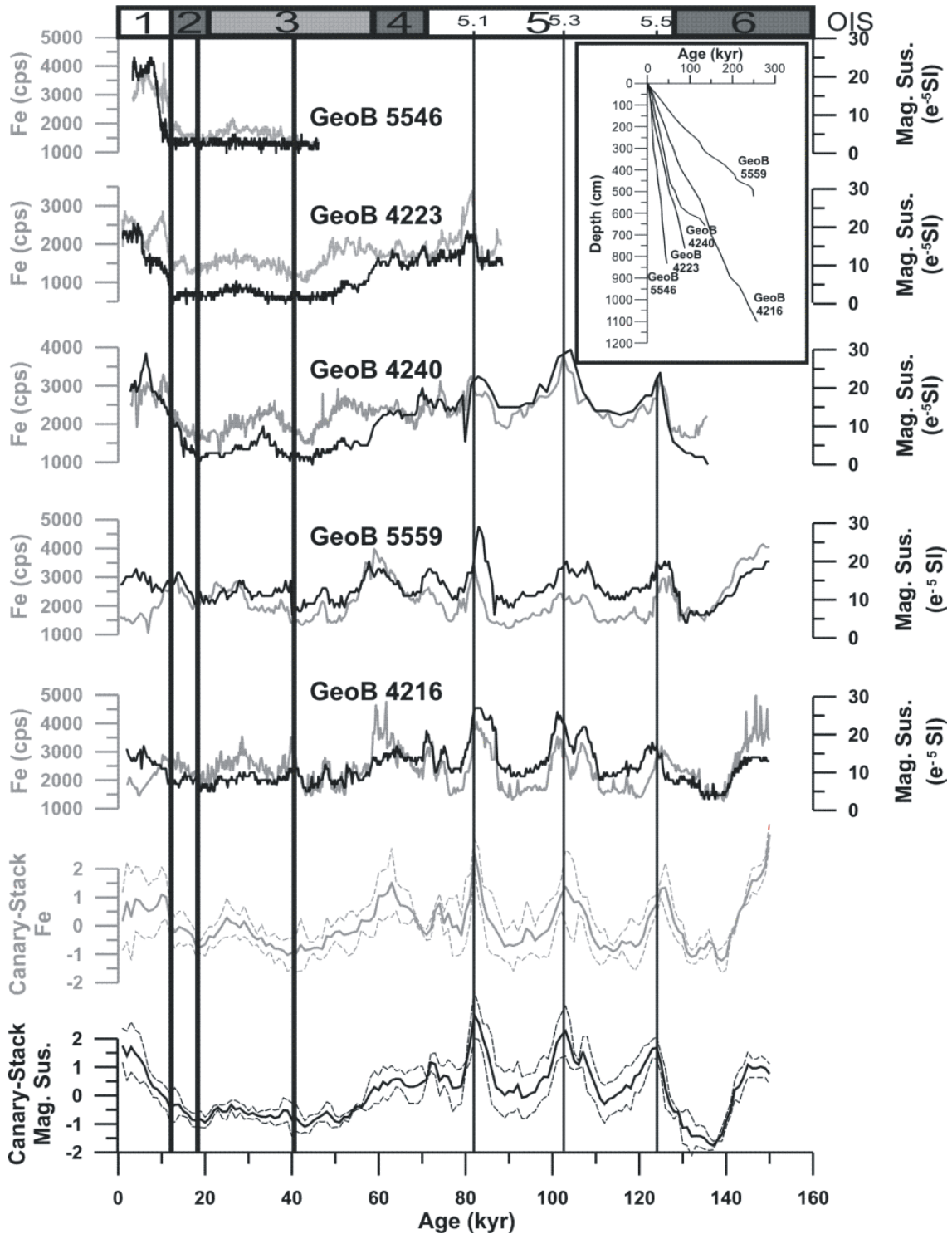

Figure 4.2 Canary **Fe** (CAFE) (grey) and **Ca**nary **m**agnetic **s**usceptibility (CAMS) (black) records (arithmetic mean with standard deviation band) resulting from the records of the

stratigraphic reference cores. Vertical lines indicate the tie points at 12, 18, 40 kyr (bold lines) and 80, 100, 122 kyr. Oxygen isotope stages are indicated at the top and in the upper right edge the age versus depth plots of the five reference cores are shown.

volcanic gravel and ash layers (all < 10 cm that were identified by visual core description), MS and density records of the stacked curves show the characteristic pattern observed in the reference cores. To compensate for different amplitudes, each record was subtracted by its mean, divided by the standard deviation and resampled in 1 kyr intervals (Imbrie et al., 1984). The resulting stack records exhibit the similarities to the five reference cores, in particular, relative minima during glacial and deglacial times at 12, 18, and 40 kyr and well-pronounced maxima during the last interglacial at 80, 100 and 122 kyr.

Diagenetic processes may have a significant influence on the Fe and MS data. The MS record is partly altered during glacial times at sites influenced by upwelling and enhanced primary productivity. This effect is documented in Fig. 4.2 for the cores GeoB 5546 and GeoB 4223. This is interpreted to be caused by dissolution of fine grained magnetite as a result of carbon oxidation (Bloemendal et al., 1992; Haag, 2000). Therefore, where available we chose the Fe-intensity record for the age transfer, especially at the near-coast sites. The iron intensity records are quite robust against diagenesis, because the X-ray fluorescence analysis detects Fe atoms irrespective of their oxidation state. To ensure that the diagenetic transport of iron does not affect the records significantly we compared the Fe records with those for Ti, which is known to be much less subject to diagenetic alteration than iron. We found that the Ti records show a pattern that is nearly identical to the Fe records, and the Fe/Ti ratio is quite constant throughout the cores, giving no obvious indication for a diagenetic displacement of iron (Kuhlmann et al., subm.). Summing up the influence of diagenetic effects, we decided to use the CAFE stack preferentially for stratigraphic correlation. In cases where Fe data were not available we used the CAMS stack.

We successfully transferred the age model of the stacks to the other cores in the region by correlation. Even detailed characteristics like the double peak at about 100 kyr could be detected in most records. For the comparison of AR at different time intervals we have chosen three tie points that were easily detected in most of the cores. These selected tie points are 12, 18 and 40 kyr, enabling us to define three time intervals representing full glacial conditions (18 – 40 kyr), the deglaciation (12 – 18 kyr) and the Holocene starting at 12 kyr. Now we are able to calculate the average SR for the time intervals. We used the AR, where SR and DBD are included to avoid the

influences of density changes through the cores, for the comparison of different time intervals. To obtain the average Holocene AR, we assumed that the core top is the sediment surface and has an age of 0 kyr. It should be mentioned that the core tops generally do not reflect the sediment surface, because of the sampling procedure using gravity corer. This effect is more pronounced in cores with lower sedimentation rates but from the reference cores it is obvious that the maximum loss is 3 kyr (Fig. 4.2). Therefore, the Holocene accumulation rates may be slightly overestimated, but do not significantly change the results.

4.5 Holocene sediment accumulation rates

The most prominent feature of the Holocene time interval is the wide range of AR from the lowest values (1.65 g cm^{-2} kyr^{-1}) at offshore sites to the highest values (17.17 g cm^{-2} kyr^{-1}) at nearshore sites. Among the near coastal sites we observe the highest AR at Cape Yubi. This is less pronounced at Cape Ghir except for an exceptional result at site GeoB 6007, which is excluded from Figures 4.3-4.5. This site is located in a small sedimentation trough, where sediment focusing results in a SR of about 80 cm kyr^{-1}. The lowest nearshore values are observed between these two cape locations (Fig. 4.3). The zonal productivity gradient, as a major feature in the region, is slightly modified on the transect off Cape Yubi (27°32´N). Here we observe a higher sediment accumulation rate at the site GeoB 5536 than at the two adjacent sites GeoB 5537 and GeoB 5538, which are located nearer to the coast (SE of Gran Canaria).

The scenario depicted by the Holocene AR reflects the pattern observed in satellite derived chlorophyll-a concentrations in surface waters of the area (Fig. 4.3), which is known to be an indicator of primary productivity (Antoine et al., 1996; Behrenfeld and Falkowski, 1997; Hoepffner et al., 1999). The relationship of AR and productivity is expressed by a linear regression between AR and chlorophyll-a concentrations at the core locations with a coefficient of determination of $r^2 = 0.41$. The calculated *F* of the statistical correspondence test exceeds the critical *F* (Swan and Sandilands, 1995). This tendency is additionally supported by analyses of productivity proxies in surface sediments of the Canary Islands region, which show a highly comparable distribution with the AR reported in this study (Meggers et al., 2002).

The particle export from surface waters includes eolian dust, which is known to be an important particle source in this area (Ratmeyer et al., 1999; Sarnthein et al., 1981; Schütz et al., 1981). The results of sediment-trap studies indicate that the particle flux of lithogenic material is strongly related to biological processes by scavenging and

incorporation into faecal pellets (Neuer et al., 1997; Wefer and Fischer, 1993). This could explain the close relationship between primary production and AR even if a similar atmospheric dust input into high and low productivity regions is assumed.

Sediment trap studies indicate that lateral particle transport exists in the Canary Islands region (Freudenthal et al., 2001). However, the good correlation of chlorophyll-a concentration in surface water with the AR indicates that lateral particle transport as reported from trap studies in this area may shift and smooth the filament pattern known from the sea surface, but does not disturb the general signal (Freudenthal et al., 2002). We therefore conclude that particle export to the sediment in the Canary Islands region is strongly influenced by processes that are closely connected to the primary productivity.

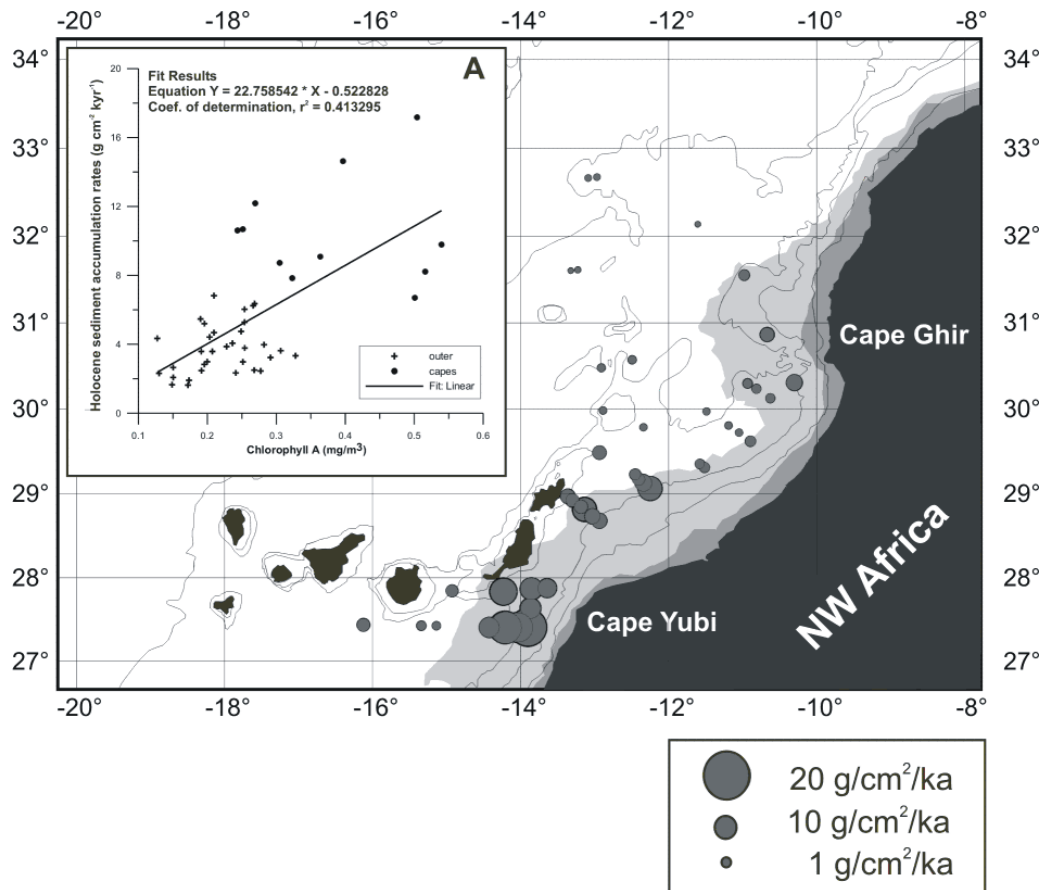**Figure 4.3** Holocene (0-12 kyr) bulk sediment accumulation rates (g cm^{-2} kyr[-1]) for each investigation site. Chlorophyll-a concentrations are indicated as in Fig. 4.1. **A**: Linear regression of Holocene bulk sediment accumulation rates and chlorophyll-a (same source as Fig. 4.1) resulting in a coefficient of determination $r^2 = 0.41$.

We interpret the higher AR at Cape Yubi compared to Cape Ghir to be the result of sediment transport influenced by differences in sea-floor morphology. The Agadir Canyon is known to be an important pathway of sediment to the Agadir Basin and the Madeira Abyssal Plain (de Lange et al., 1987; Ercilla et al., 1998; Weaver et al., 1992). The narrow shelf area and relatively steep continental slope at Cape Ghir as compared to Cape Yubi may also sustain the transport of material to the deep sea plains further off the coast. Another reason for the differences between the two cape locations may be the seasonality of the upwelling at Cape Ghir as detected by the Ekman upwelling index, whereas at Cape Yubi the duration of the upwelling season lasts three times as long as at Cape Ghir (Nykjaer and Van Camp, 1994). This would result in enhanced primary productivity values averaged over a year, but it is not reflected in the average chlorophyll-a concentration shown in Fig. 4.3b.

In contrast to the zonal pattern of decreasing AR further off the coast, the outermost core of the Cape Yubi transect (GeoB 5536) shows higher values. This site is influenced by a mesoscale stationary cyclonic and anticyclonic eddy system, which is caused by the location of the Canary Islands in the atmospheric and oceanic current systems. Lee-side effects on the SW side of Gran Canaria cause a stationary cyclonic and anticyclonic eddy system, which induces up- and downwelling with the associated impacts on productivity (Arístegui et al., 1994; Arístegui et al., 1997; Barton et al., 1998; Basterretxea et al., 2002). These sea-surface conditions might also have influenced also the surface sediment (Meggers et al., 2002). We may speculate that the observed Holocene AR pattern is a result of these island-generated eddies on the lee side of the Canary Islands, which caused upwelling, enhanced primary productivity and, therefore, higher AR at site GeoB 5536. At any rate, this high-spatial-resolution study indicates that the Holocene AR pattern is compatible with present oceanographic characteristics of the Canary Islands region. With this actualistic assessment we will now focus on the differences of AR between Holocene, deglaciation and the last glacial.

4.6 Variability of sediment accumulation through time

The general scenario in the Canary Islands region during all the investigated time intervals is characterized by low AR offshore and high AR nearshore, with pronounced high accumulation at the cape locations (Fig. 4.3, 4.4a, 4.4b). Another common effect seen in all the time intervals is the higher AR at Cape Yubi when compared to Cape Ghir. In contrast to these findings, strong differences in the intensity, size and position of high-accumulation areas are shown in Figures 4a-c. The

time interval of the deglaciation (12 – 18 kyr) generally shows the highest AR (max. 22.6 g cm^{-2} kyr^{-1}), except for a small area north of Cape Yubi, where the AR during the glacial time interval is higher (Fig. 4.5a, c). The high-accumulation area at Cape Ghir is expanded to the southwest during deglaciation (Fig. 4.5a). In contrast, the high-accumulation area of Cape Yubi is extended in a northerly direction (Fig. 4.5a). The pattern of enhanced accumulation SW of Cape Ghir is less pronounced, but also present in the time interval representing full glacial conditions (18 – 40 kyr) (Fig. 4.5b).
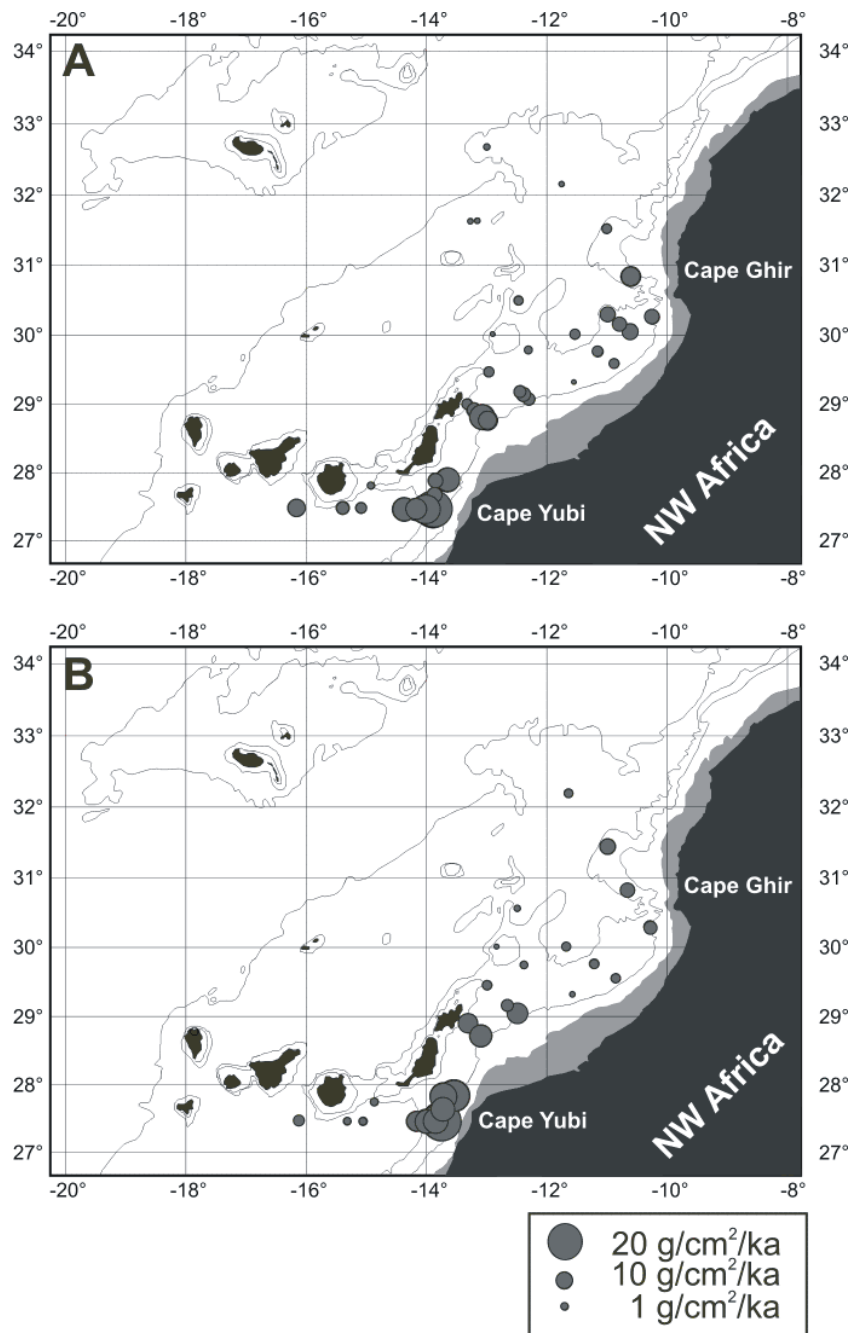
Figure 4.4 Bulk sediment accumulation rates (g cm^{-2} kyr^{-1}) for the time intervals of (**a**) deglaciation (12 – 18 kyr) and (**b**) the last glacial (18 – 40 kyr). The depth interval 0 – 100 m is shaded grey to indicate the coastline during sea-level lowstand.

The most prominent differences in the AR during the glacial period compared to the other time intervals are observed in the area between Fuerteventura and the coast of Morocco. This area of high sediment accumulation adjacent to Cape Yubi shows its widest extent and reaches up to 50 km further to the north during the glacial period (Fig. 4.5b, c).

The general trend of enhanced accumulation during the last glacial and deglaciation may result from higher productivity of the Atlantic Ocean during glacials, which is frequently described and discussed in the literature (e.g., Mix, 1989). For the region off NW Africa Sarnthein et al. (1988) report the same trend of enhanced primary productivity. The enhanced atmospheric circulation with stronger trade winds during glacial times may have intensified coastal upwelling and therefore caused higher productivity in the upwelling-influenced parts of the working area. This would explain the generally higher AR in the Canary Islands region during deglaciation and the glacial as compared to the Holocene.

The current system is an important factor influencing the filament formation (Johnson and Stevens, 2000) independent of the upwelling intensity. The intensity of the Canary Current is assumed to have been stronger during the glacial and deglaciation intervals (Sarnthein et al., 1982; Zahn et al., 1997). This corresponds with findings of an intensified filament activity detected by total organic carbon (TOC) measurements at specific sites off NW Africa (Freudenthal et al., 2002; Moreno et al., 2002). We conclude that the enhanced accumulation in the filament-influenced area off Cape Ghir result from the even more intensified filament formation during the deglaciation. The differences in AR indicate that the direction of the Cape Ghir filament during the Holocene (westerly) was different during glacial (south-westerly) and even more pronounced during deglaciation, as is illustrated in Fig. 4.5a, b. In recent descriptions of filament structures off Cape Ghir, Helmke et al. (subm.) report a comparable pattern. In general they describe filaments directed to the west, but also a south-westerly filament direction prevails at times of very strong wind intensities. Therefore, we conclude that the enhanced atmospheric circulation during deglaciation and the last glacial caused a south-westerly shift of the high-accumulation area of Cape Ghir. The pattern of increased AR described for the three easternmost cores on the transect south

of Gran Canaria is pronounced, and may be an effect of the enhanced surface circulation (Sarnthein et al., 1982) and stronger throughflow through the Canary Islands.

The larger extension of the high-accumulation area north of Cape Yubi we interpret to result from sea-level changes. In the working area ,the continental shelf lies, for the most part under less than 150 m of water and was therefore widely exposed during sea-level lowstands at the last glacial (Bard et al., 1989; Bard et al., 1996; Fairbanks, 1989). The morphological cape characteristics, which cause the upwelling and especially the formation of filaments were situated about 50 km to the N during sea-level lowstand.
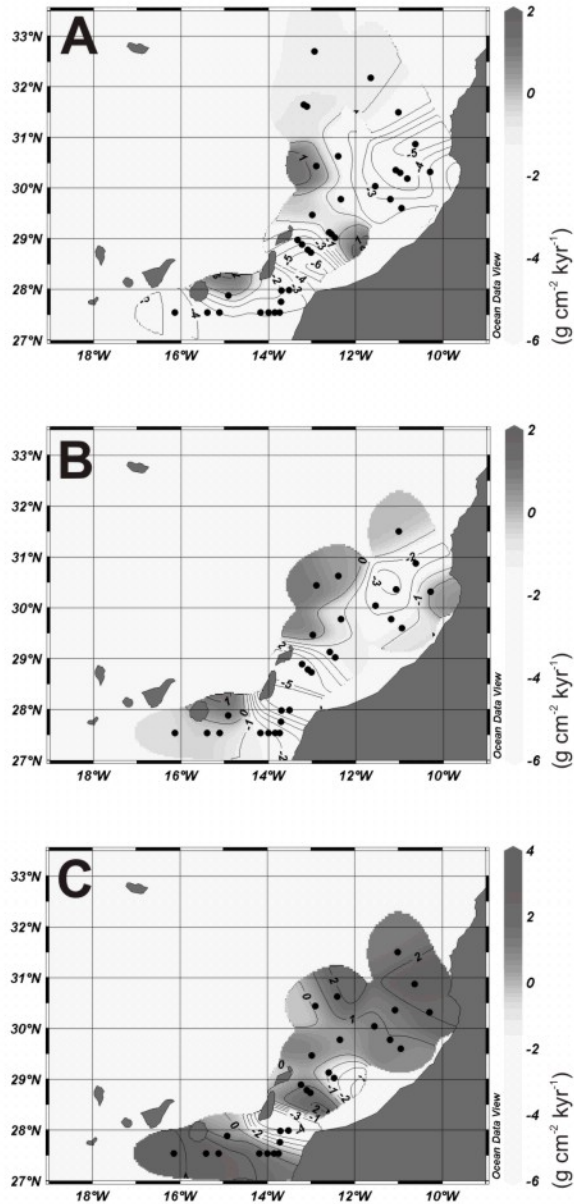
Figure 4.5 Differences (g cm^{-2} kyr^{-1}) in bulk sediment accumulation rates of the time intervals between (**a**) Holocene and deglaciation, (**b**) Holocene and glacial and (**c**) deglaciation and glacial (negative values indicate higher AR in the Holocene (a, b) and the deglaciation (c)). The interpolated contour line maps were generated with Ocean Data View (Schlitzer, 2002).

We conclude that as a consequence, the upwelling area extended further to the N at times of sea-level lowstand. The size of this upwelling area decreased with rising sea-level. The time interval of the deglaciation represents an intermediate state on the way to Holocene conditions.

The possible influence of temporal variations in river discharge on the AR is not clearly reflected. During the glacial and deglaciation based on paleohydrological data, the adjacent African continent has been characterized as dominated by dry conditions. At the boundary to the Holocene a generally wet climate was established. This persisted until the mid-Holocene transition at about 5 kyr, after which dry conditions again prevailed (Gasse, 2000; Gasse et al., 1990). An interval of more humid conditions within the Holocene, including enhanced river discharge to the ocean is not reflected in the AR, possibly because these are averaged over the entire Holocene.

It has been suggested that eolian dust input was enhanced during glacial and deglacial times due to greater wind stress (Bozzano et al., 2002; Moreno et al., 2001; Tiedemann et al., 1989). The transport mechanism to the sediments is assumed to be closely connected to scavenging effects as discussed in the previous chapter. Assuming the same close relationship between primary production and AR as for the Holocene, we think that enhanced eolian dust input may have strengthened the AR pattern, but not significantly modified its distribution.

The regional features as claimed by Bertrand et al. (1996) in the Canary Islands region resulting from the AR of the last 40 kyr exhibit higher values during the glacial and deglaciation as compared to the Holocene. But we observed additional local features such as enhanced differences in the AR between different time intervals in areas influenced by upwelling filaments, and effects of varying coastal morphology due to sea-level changes, which modify the general pattern locally.

4.7 Conclusion

The comparison of Holocene AR and satellite-derived chlorophyll-a concentrations representing present-day primary productivity revealed strong similarities. The features of coastal upwelling and filament formation pattern are well

mirrored in the underlying sediment by the AR. Even small-scale features such as an eddy system at the lee-side of Gran Canaria have left their imprint on the sediment accumulation pattern.

We conclude that the higher sediment accumulation rates at Cape Yubi, as compared to the northern area at Cape Ghir, primarily reflect the topographic conditions, which favour sediment transport to the open ocean at the northern site. Additionally, the duration of intense upwelling in the seasonal cycle is much shorter at Cape Ghir, which is interpreted to be the reason for lower particle production.

In comparing the Holocene with the deglaciation time interval the most prominent enhancement of sediment accumulation is observed at the outer filament-influenced area of Cape Ghir. These findings are interpreted to indicate a stronger filament activity due to enhanced oceanic circulation during the glacial and especially the deglaciation.

The differences in AR between the glacial time interval and the Holocene are greatest to the north of Cape Yubi, where the continental shelf is very wide. We conclude that lower sea-level is responsible for the northward enlargement of the upwelling-influenced area of Cape Yubi, where the highest AR occur during the glacial time interval.

The results of this study show that the heterogeneity of even a small scale region like the Canary Islands region indicates the need for studies with high spatial resolution to detect and understand the processes responsible for the observed regional pattern in contrast to local features and their related processes.

Acknowledgements

References

Antoine, D., André, J.-M., Morel, A., 1996. Oceanic primary production, 2. Estimation at global scale from satellite (coastal zone color scanner) chlorophyll. Global Biogeochemical Cycles, 10(1), pp. 57-69.

Arístegui, J., Sangrá, P., Hernámdez-Leon, S., Cantón, M., Hernández-Guerra, A., Kerling, J.L., 1994. Island-induced eddies in the Canary Islands. Deep-Sea Research, Part I, 41(10), pp. 1509-1525.

Arístegui, J., Tett, P., Hernández-Guerra, A., Basterretxea, G., Montero, M.F., K.Wild, Sangrá, P., Hernández-León, S., Cantón, M., García-Braun, J.A., Pacheco, M., Barton, E.D., 1997. The influence of island-generated eddies on chlorophyll distribution: a study of mesoscale variation around Gran Canaria. Deep Sea Research Part I, 44(1), pp. 71-96.

Bard, E., Fairbanks, R., Arnold, M., Maurice, P., Duprat, J., Moyes, J., Duplessy, J.-C., 1989. Sea-level estimates during the last deglaciation based on d18O and accelerator mass spectrometry 14C ages measured in Globigerina bulloides. Quaternary Research, 31, pp. 381-391.

Bard, E., Hamelin, B., Arnold, M., Montaggioni, L., Cabioch, G., Faure, G., Rougerie, F., 1996. Deglacial sea-level record from Thahiti corals and the timing of global meltwater discharge. Nature, 382, pp. 241-244.

Barton, E.D., Arístegui, J., Tett, P., Cantón, M., García-Braun, J., Hernández-León, S., Nykjaer, L., Almeida, C., Almunia, J., Ballesteros, S., Basterretxea, G., Escánez, J., García-Weill, L., Hernández-Guerra, A., López-Laatzen, F., Molina, R., Montero, M.F., Navarro-Pérez, E., Rodríguez, J.M., Van Lenning, K., Vélez, H., Wild, K., 1998. The transition zone of the Canary Current upwelling region. Progress in Oceanography, 41, pp. 455-504.

Basterretxea, G., Barton, E.D., Tett, P., Sangrá, P., Navarro-Perez, E., Arístegui, J., 2002. Eddy and deep chlorophyl maximum response to wind-shear in the lee of Gran Canaria. Deep Sea Research Part I, 49(6), pp. 1087-1101.

Behrenfeld, M.J., Falkowski, P.G., 1997. Photosynthetic rates derived from satellite-based chlorophyll concentration. Limnology and Oceanography, 42(1), pp. 1-20.

Berger, W.H., Keir, R.S., 1984. Glacial-Holocene changes in atmospheric CO2 and the deep-sea record. In: J.E. Hansen, T. Takahashi (Editors), Climate Processes and Climate Sensitivity. Geophysical Monographs. American Geophysical Union, Washington, DC, pp. 337-351.

Bertrand, P., Shimmield, G., Martinez, P., Grousset, F., Jorissen, F., Paterne, M., Pujol, C., Bouloubassi, I., Buat-Menard, P., Peypouquet, J.P., Beaufort, L., Sicre, M.-A., Lallier-Verges, E., Foster, J.M., Tenois, Y., Program, O.p.o.t.S., 1996. The Glacial ocean productivity hypothesis: the importance of regional temporal and spatial studies. Marine Geology, 130, pp. 1-9.

Bertrand, P., Pdersen, T.F., Martinez, P., Calvert, S., Shimmield, G., 2000. Sea level impact on nutrient cycling in coastal upwelling areas during deglaciation: Evidence from nitrogen isotopes. Global Biogeochemical Cycles, 14(1), pp. 341-355.

Bloemendal, J., King, J.W., Hall, F.R., Doh, S.-J., 1992. Rock magnetism of late Neogene and Pleistocene deep-sea sediments: Relationship to sediment source , diagenetic processes, and sediment lithology. Journal of Geophysical Research, 97(B4), pp. 4361-4375.

Bozzano, G., Kuhlmann, H., Alonso, B., 2002. Storminess control over African dust input to the Moroccan Atlantic margin (NW Africa) at the time of maxima

boreal summer insolation: a record of the last 220 kyr. Palaeogeography, Palaeoclimatology, Palaeoecology, 183(1-2), pp. 155-168.

Davenport, R., Neuer, S., Hernández-Guerra, A., Rueda, M.J.L., Octavio, Fischer, G., Wefer, G., 1999. Seasonal and interannual pigment concentration in the Canary Islands region from CZCS data and comparison with observations from the ESTOC. International Journal of Remote Sensing, 20(7), pp. 1419-1433.

Davenport, R., Neuer, S., Helmke, P., Perez-Marrero, J., Llinas, O., 2002. Primary productivity in the northern Canary Islands region as inferred from SeaWiFS imagery. Deep Sea Research Part II, 49(17), pp. 3481-3496.

de Lange, G.J., Jarvis, I., Kujpers, A., 1987. Geochemical characteristics and provenance of late Quaternary sediments from the Madeira Abyssal Plain. In: P.P.E. Weaver, J. Thomson (Editors), Geology and geochemistry of abyssal plains. Geological Society Special Publications. Blackwell Scientific Publications, Oxford, pp. 147-165.

Ercilla, G., Alonso, B., Perez-Belzuz, F., Estrada, F., Baraza, J., Farran, M., Canals, M., Masson, D., 1998. Origin, sedimentary processes and depositional evolution of the Agadir turbidite system, central eastern Atlantic. Journal of the Geological Society London, 155(6), pp. 929-939.

Fairbanks, R.G., 1989. A 17,000 year glacio-eustratic sea level record: influence of glacial melting rate on the Younger Dryas event and deep-ocean circulation. Nature, 342, pp. 637-642.

Freudenthal, T., Neuer, S., Meggers, H., Davenport, R., Wefer, G., 2001. Influence of lateral particle advection and organic matter degradation on sediment accumulation and stable nitrogen isotope ratios along a productivity gradient in the Canary Islands region. Marine Geology, 177(1-2), pp. 93-109.

Freudenthal, T., Meggers, H., Henderiks, J., Kuhlmann, H., Moreno, A., Wefer, G., 2002. Upwelling intensity and filament activity off Morocco during the last 250,000 years. Deep Sea Research Part II, 49(17), pp. 3655-3674.

Freudenthal, T., Kasten, S., Meggers, H., subm.. Glacial trade wind intensity controlled by latitudinal sea surface temperature gradients. Geology

Gasse, F., Téhet, R., Durand, A., Gilbert, E., Fontes, J.-C., 1990. The arid-humid transition in the Sahara and the Sahel during the last deglaciation. Nature, 346, pp. 141-146.

Gasse, F., 2000. Hydrological changes in the African tropics since the Last Glacial Maximum. Quaternary Science Reviews, 19(1-5), pp. 189-211.

Gunn, D.E., Best, A.I., 1998. A new automated nondestructive system for high resolution multi-sensor core logging of open sediment cores. Geo-Marine Letters, 18(1), pp. 70-77.

Haag, M., 2000. Reliability of relative palaeointensities of a sediment core with climatically-triggered strong magnetisation changes. Earth and Planetary Science Letters, 180(1-2), pp. 49-59.

Hagen, E., 2001. Northwest African upwelling scenario. Oceanologica Acta, 24(1), pp. 113-128.

Helmke, P., Davenport, R., Kuhlmann, H., (subm.). Wind stress-related filament structures off Cape Ghir, NW Africa. (subm. to Deep-Sea Research).

Hoepffner, N., Sturm, B., Finenko, Z., Larkin, D., 1999. Depth-integrated primary production in the eastern tropical and subtropical North Atlantic basin from ocean colour imagery. International Journal of Remote Sensing, 20(7), pp. 1435-1456.

Imbrie, J., Hays, J.D., Martinson, D.G., McIntyre, A., Mix, A.C., Morley, J.J., Pisias, N.G., Prell, W.L., Shackleton, N.J., 1984. The orbtal theory of Pleistocene

climate: Support from a revised chronology of the marine d18O record. In: W.H. Berger, J. Imbrie, J.D. Hays, J. Kukla, J. Saltzmann (Editors), Milankovitch and Climate, Part 1. Reidel, Hingham, Mass., pp. 269-305.

Jansen, J.H.F., Gaast, S.J.V.d., Koster, B., Vaars, A.J., 1998. CORTEX, a shipboard XRF-scanner for element analyses in split sediment cores. Marine Geology, 151(1-4), pp. 143-153.

Johnson, J., Stevens, I., 2000. A fine resolution model of the eastern North Atlantic between the Azores, the Canary Islands and the Gibraltar Strait. Deep Sea Research Part I, 47(5), pp. 875-899.

Knoll, M., Hernández-Guerra, A., Lenz, B., Laatzen, F.L., Machín, F., Müller, T.J., Siedler, G., 2002. The Eastern Boundary Current system between the Canary Islands and the African Coast. Deep Sea Research Part II, 49(17), pp. 3427-3440.

Kuhlmann, H., Meggers, H., Moreno, A., Freudenthal, T., Kasten S., Hensen, C., von Oppen, C. (subm.). Meridional shifts of the Mediterranean and the monsoonal climate system off NW Africa during the last 130,000 years: implications from river discharge. (subm. to Quaternary Research).

Llinás, O., Rueda, M.J., Marrero, J.P., Pérez-Martell, E., Santana, R., Villagarcía, M.G., Cianca, A., Godoy, J., Maroto, L., 2002. Variability of the Antarctic intermediate waters in the Northern Canary Box. Deep Sea Research Part II, 49(17), pp. 3441-3453.

Marret, F., Turon, J.-L., 1994. Paleohydrology and paleoclimatology off Northwest Africa during the last glacial-interglacial transition and the Holocene: Palynological evidences. Marine Geology, 118, pp. 107-117.

Martinez, P., Bertrand, P., Shimmield, G.B., Cochrane, K., Jorissen, F.J., Foster, J., Dignan, M., 1999. Upwelling intensity and ocean productivity changes off Cape Blanc (northwest Africa) during the last 70,000 years: geochemical and micropalaeontological evidence. Marine Geology, 158(1-4), pp. 57-74.

Martinez, P., Bertrand, P., Calvert, S.E., Pedersen, T.F., Shimmield, G.B., Lallier-Vergès, E., Fontugne, M.R., 2000. Spatial variations in nutrient utilization, production and diagenesis in the sediments of a coastal upwelling regime (NW Africa): Implications for the paleoceanographic record. Journal of Marine Research, 58, pp. 809-835.

Martinson, D.G., Pisias, N.G., Hays, J.D., Imbrie, J., Moore, T.C., Shackleton, N.J., 1987. Age dating and the orbital theory of the ice ages: development of a high-resolution 0 to 300.000 year chronostratigraphy. Quarternary Research, 27, pp. 1-29.

Meggers, H., Freudenthal, T., Nave, S., Targarona, J., Abrantes, F., Helmke, P., 2002. Assessment of geochemical and micropaleontological sedimentary parameters as proxies of surface water properties in the Canary Islands region. Deep Sea Research Part II, 49(17), pp. 3631-3654.

Meggers, H., Freudenthal, T., Hensen, C., Kuhlmann, H., (in prep.). Climate variability in the eastern boundary current region off NW Africa (Cape Yubi, Morocco)

Mittelstaedt, E., 1991. The ocean boundary along the northwest African coast: Circulation and oceanographic properties at the sea surface. Progess in Oceanography, 26, pp. 307-355.

Mix, A.C., 1989. Pleistocene paleoproductivity: Evidence from organic carbon and foraminiferal species. In: W.H. Berger, V.S. Smetacek, G. Wefer (Editors), Productivity of the Ocean: Present and Past. Wiley-Interscience, Bath, pp. 313-340.

Moreno, A., Nave, S., Kuhlmann, H., Canals, M., Targarona, J., Freudenthal, T., Abrantes, F., 2002. Productivity response in the North Canary Basin to climate changes during the last 250000 yr: a multi-proxy approach. Earth and Planetary Science Letters, 196(3-4), pp. 147-159.

Moreno, A., Targarona, J., Henderiks, J., Canals, M., Freudenthal, T., Meggers, H., 2001. Orbtial forcing of dust supply to the North Canary Basin over the last 250 kyr. Quaternary Science Reviews, 20, pp. 1327-1339.

Neuer, S., Ratmeyer, V., Davenport, R., Fischer, G., Wefer, G., 1997. Deep water particle flux in the Canary Island region: seasonal trends in relation to long-term satellite derived pigment data and lateral sources. Deep Sea Research Part I, 44(8), pp. 1451-1466.

Neuer, S., Alfke, R., Bergenthal, M., Bittkau, A., Böhme, L., Bothmer, H., Cianca, A., Diekamp, V., Freudenthal, T., Gerdes, A., Godoy, J., Grimm, G., Hayn, C., Hebbeln, D., Huebner, H., Kahl, G., Klein, T., Köster, J., Laglera, L., Langer, J., Benz, B., Meggers, H., Meinecke, G., Metzler, W., Moroto, L., Nave, S., Ochsenhirt, W., Ratmeyer, V., Rosiak, U., Rueda, M.-J., Ruhland, G., Schiebel, R., Schüssler, U., Struck, U., Themann, S., Villagarcia, M., von Oppen, C., Waldmann, C., 2000. Report and preliminary results of METEOR cruise M 45/5, Bremen - Las Palmas, October 1 - November 3, 1999. Berichte aus dem Fachbereich Geowissenschaften der Universität Bremen, 163, pp. 93.

Nykjaer, L., Van Camp, L., 1994. Seasonal and interannual variability of coastal upwelling along northwest Africa and Portugal from 1981 to 1991. Journal of Geophysical Research, 99(C7), pp. 14197-14207.

Ratmeyer, V., Fischer, G., Wefer, G., 1999. Lithogenic particle fluxes and grain size distributions in the deep ocean off northwest Africa: Implications for seasonal changes of aeolian dust input and downward transport. Deep Sea Research, 46(8), pp. 1289-1337.

Raymo, M.E., 1997. The timing of major climate terminations. Paleoceanography, 12(4), pp. 577-585.

Sarnthein, M., Tetzlaff, G., Koopmann, B., Wolter, K., Pflaumann, U., 1981. Glacial and interglacial wind regimes over the easternsubtropical Atlantic and North-West Africa. Nature, 193, pp. 193-196.

Sarnthein, M., Thiede, J., Pflaumann, U., Erlenkeuser, H., Fütterer, D., Koopmann, B., Lange, H., Seibold, E., 1982. Atmospheric and oceanic circulation patterns off Northwest Africa during the past 25 million years. In: U. von Rad, K. Hinz, M. Sarnthein, E. Seibold (Editors), Geology of the northwest African continental margin. Springer-Verlag, Berlin, Heidelberg, pp. 545-604.

Sarnthein, M., Winn, K., Duplessy, J.-C., Fontugne, M.R., 1988. Global variations of surface ocean productivity in low and mid latitudes: Influence on CO2 reservoirs of the deep ocean and atmosphere during the last 21.000 years. Paleoceanography, 3(3), pp. 361-399.

Schlitzer, R., 2002. Ocean Data View. http://ww.awi-bremenhaven.de/GEO/ODV,2002.

Schütz, L., Jaenicke, R., Pietrek, H., 1981. Saharan dust transport over the North Atlantic Ocean. Geological Society of Amreica Spec. Pap., 186, pp. 87-100.

Summerhayes, C.P., Milliman, J.D., Briggs, S.R., Bee, A.G., Hogan, C., 1976. Northwest African shelf sediments: Influence of climate and sedimentary processes. Journal of Geology, 84, pp. 277-300.

Swan, A.R.H., Sandilands, M., 1995. Introduction to geological data analysis. Blackwell Science, Oxford, 446 pp.

Tiedemann, R., Sarnthein, M., Stein, R., 1989. Climatic changes in the western Sahara: Aeolo-marine sediment record of the last 8 million years (sites 657-661). In: W.

Ruddiman, M. Sarntheim (Editors), Proceedings of the ODP, Scientific Results, pp. 241-261.

Van Camp, L., Nykjaer, L., Mittelstaedt, E., Schlittenhardt, P., 1991. Upwelling and boundary circulation off Northwest Africa as described by infrared and visible satellite observations. Progress in Oceanography, 26, pp. 357-402.

von Dobeneck, T., Schmieder, F., 1999. Using rock magnetic proxy records for orbital tuning and extended time series analysis into the Super- and Sub-Milankovitch bands. In: G. Fischer, G. Wefer (Editors), Use of Proxies in Paleoceanography: Examples from the South Atlantic. Springer, Berlin, Heidelberg, pp. 601-633.

Weaver, P.P.E., Schultheiss, P.J., 1990. Current methods for obtaining, logging and splitting marine sediment cores. Marine Geophysical Researches, 12, pp. 85-100.

Weaver, P.P.E., Wynn, R.B., Kenyon, N.H., Evans, J., 2000. Continental margin sedimentation, with special reference to the north-east Atlantic margin. Sedimentology, 47(Suppl. 1), pp. 239-256.

Weaver, P.P.E., Rothwell, R.G., Ebbing, J., Gunn, D., Hunter, P.M., 1992. Correlation, frequency of emplacement and source directions of megaturbidites ont he Madeira Abyssal Pain. Marine Geology, 109(1-2), pp. 1-20.

Weber, M.E., Niessen, F., Kuhn, G., Wiedicke, M., 1997. Calibration and application of marine sedimentary physical properties using a multi-sensor core logger. Marine Geology, 136(3-4), pp. 151-172.

Wefer, G., Fischer, G., 1993. Seasonal patterns of vertical fluxes in equatorial and coastal upwelling areas of the eastern Atlantic. Deep -Sea Research I, 40(8), pp. 1613-1645.

Wefer, G., Abrantes, F., Bassek, D., Bollmann, J., Bozzano, G., Diekamp, V., Dittert, L., Eberwein, A., Klump, J., Kuhlmann, H., Lindblom, S., Meggers, H., Meinecke, G., Metzler, W., Moustafa, Y., Peters, M., Ratmeyer, V., Rieß, W., Rosiak, U., Segl, M., Skoglund, S., Targarona, J., Vaqueiro, S., Waldmann, C., Wenzhöfer, F., Zabel, M., 1997. Report and preliminary results of METEOR cruise M 37/1 Lisbon - Las Palmas; 04.12.96-23.12.96. Berichte aus dem Fachbereich Geowissenschaften der Universität Bremen, 90, pp. 79.

Wefer, G., Segl, M., Bassek, D., Buhlmann, K., Deeken, A., Dehning, K., Diekamp, V., Drünert, F., Eberwein, A., Franke, P., Freudenthal, T., Geisen, M., Godoy, J., Gonzáles-Davila, M., Günther, L., Hayn, C., Hendriks, J., Irmisch, A., Jeronimo, D., Kotte, N., Koy, U., Kretschmar, F., Langer, J., Makaoui, A., Maroto, L., Meggers, H., Meinecke, G., Metzler, W., Moreno, A., Nave, S., Neuer, S., Nowald, N.R., V., Rieß, W., Rosiak, U., Schroeter, M., Sprengel, C., Targarona, J., Thiele, J., Tierstein, H., von Oppen, C., Waldmann, C., 1999. Report and preliminary results of METEOR cruise M 42/4 Las Palmas - Las Palmas - Vienna do Casstelo; 26.09.1998 - 26.10.1998. Berichte aus dem Fachbereich Geowissenschaften der Universität Bremen, 132, pp. 104.

Zahn, R., Schönfeld, J., Kudrass, H.-R., Park, M.-H., Erlenkeuser, H., Grootes, P., 1997. Thermohaline instability in the North Atlantic during meltwater events: Stable isotope and ice.rafted detritus records from core SO75-26KL, Portuguese margin. Paleoceanography, 12(5), pp. 696-710.

Zhao, M., Eglinton, G., Haslett, S.K., Jordan, R.W., Sarnthein, M., Zhang, Z., 2000. Marine and terrestrial biomarker records for the last 35,000 years at ODP site 658C off NW Africa. Organic Geochemistry, 31(9), pp. 919-930.

Assessment of geochemical and micropaleontological sedimentary parameters as proxies of surface water properties in the Canary Islands region

Helge Meggers[1*], Tim Freudenthal[1], Silvia Nave[2], Jordi Targarona[3], Fatima Abrantes[2], Peer Helmke[1]

1. Department of Geosciences, University of Bremen, Post-box 330440, D-28334 Bremen, Germany

2. Departamento de Geologico Marinha, Instituto Geologico e Mineiro, P-2720 Alfragide, Portugal

3. Departamento Estratigrafia i Paleontologia, Universitat de Barcelona, E-08071 Barcelona, Spain

*Corresponding Author:Helge Meggers, e-mail: meggers@allgeo.uni-bremen.de, phone: + 49 (0)421 218 7760, fax: + 49 (0)421 218 3116

Abstract

The Canary Islands region occupies a key position with respect to biogeochemical cycles, with the zonal transition from oligotrophic to nutrient-rich waters and the contribution of Saharan dust to the particle flux. We present the distribution of geochemical proxies (TOC, carbonate, δ^{15}N, δ^{13}C$_{org}$, C/N-ratio) and micropaleontological parameters (diatoms, dinoflagellates, foraminifera, pteropods), in 80 surface sediment samples in order to characterise the influence of coastally upwelled water on the domain of the subtropical gyre.

Results of the surface sediment analyses confirmed the high biomass gradient from the coast to the open ocean inferred from satellite data of surface chlorophyll or SST. The distribution of total dinoflagellate cysts, the planktic foraminifera species *Globigerina bulloides*, the diatom resting spore *Chaetoceros spp.* and the TOC concentration coincided well with the areas of strong filament production off Cape Ghir and Cape Yubi. The warm-water planktic foraminifera *Globigerinoides ruber* (white), the diatom *Nitzschia spp.* and the δ^{15}N-values showed the opposite trend with high values in the open ocean. Factor analyses on the planktic foraminifera species distribution indicated 3 major assemblages in the Canary Islands region that represent the present surface water conditions from the upwelling influenced region via a mixing area towards the subtropical gyre.

Introduction

Upwelling regions are of strong importance for the global atmospheric CO_2-budget, since they are both CO_2-source areas through the upwelling of water masses that are enriched in dissolved inorganic carbon (carbonate/physical pump) and CO_2-sinks through organic carbon production and resulting burial of organic carbon in the underlying sediments (biological pump) (Broecker, 1982; Berger, 1982; Berger and Keir, 1984; Berger and Wefer, 1990). One major coastal upwelling area is situated off NW Africa in the area of the Canary Islands. This region intersects the boundary between eutrophic NW African upwelling waters and oligotrophic oceanic waters of the eastern boundary of the North Atlantic subtropical gyre.
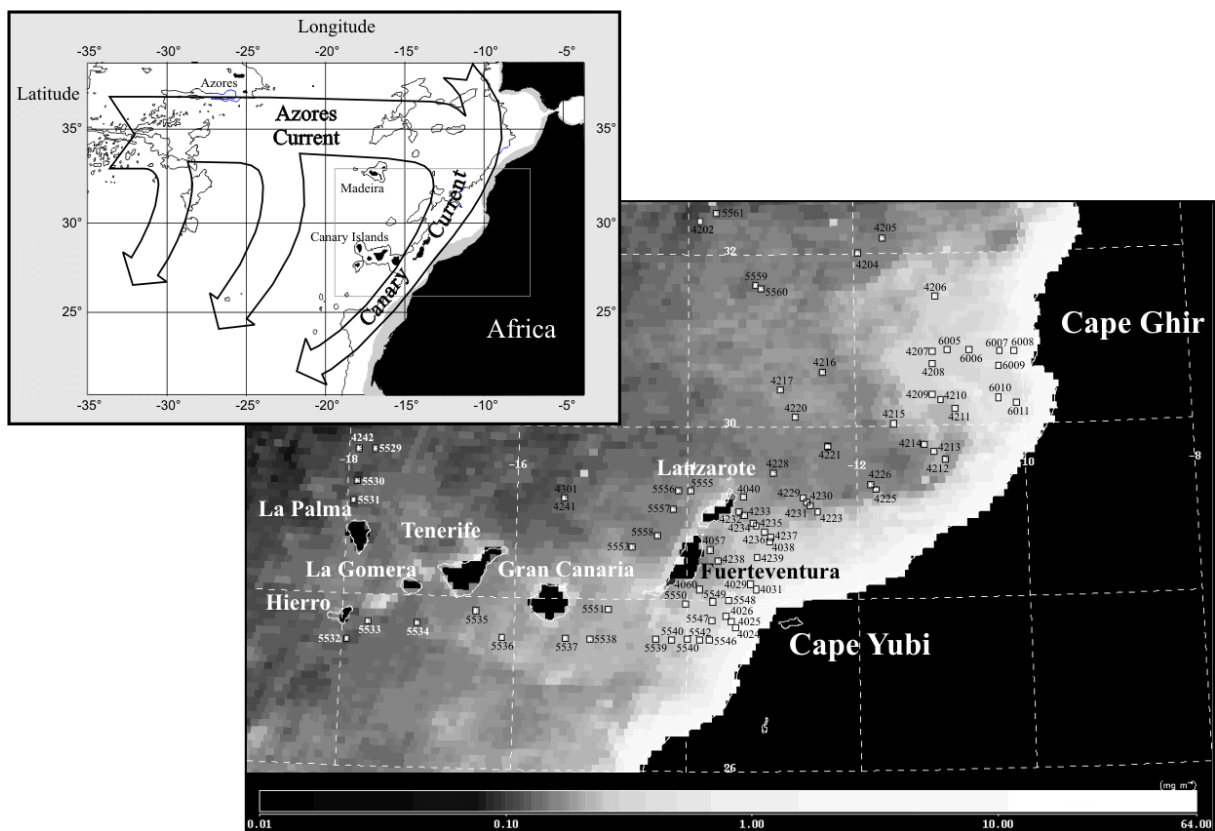
Figure 1: Main geostrophic transport and topography in the subtropical East Atlantic (modified after Siedler and Onken, 1996) and annual mean chlorophyll concentration in the Canary Islands region as observed by SeaWiFS. Data provided by the SeaWiFS Project, NASA/Goddard Space Flight Center. Squares represent surface sediment sites that have been investigated in this study.

The Azores current located at the northern boundary of the subtropical gyre seperates into three bands that flow southward; a first one east of the Mid-Atlantic Ridge, a second one in the Central Canary Basin and a third one, the Canary Current, flows equatorward close to NW Africa`s coast line (Stramma and Siedler, 1988) (Fig. 1). Along the coast, where the upwelling zone off NW Africa is restricted to a coastal band of about 50-70 km width, upwelling and related currents interact with the Canary Current (Mittelstaedt, 1991). Off NW Africa, coastal

upwelling is the response of the shelf waters to the alongshore wind stress (Mittelstaedt, 1991) and the strength and persistence of upwelling is coupled with the seasonal variation of the trade winds, which itself is coupled with the meridional shift of the Azores High. During summer the Azores High is situated at its northernmost position, and trade winds blow mainly between 32°N and 20°N. In winter the Azores High is in its southernmost position with the trade wind belt located between 25°N and 10°N. Thus, upwelling is strong throughout the year between 25°N and 20°N, while north of 25°N upwelling occurs only in summer (Speth et al., 1978; Mittelstaedt, 1991; Hernández-Guerra and Nykjaer, 1997).

Upwelling and its main impact on the marine environment are usually restricted to the waters over the shelf and the upper slope region (Mittelstaedt, 1991). However, satellite images of SST or ocean colour reveal filaments of upwelled waters far extending into the open ocean. The most striking filament is the giant filament off Cape Blanc, where cool and pigment-rich waters extend several hundred kilometres offshore (van Camp et al., 1991; Nykjaer and van Camp, 1994). Smaller filaments are also found north of this region in the area of the Canary Islands at Cape Ghir (Hagen et al., 1996; Head et al., 1996) and Cape Yubi (Arístegui et al., 1994; Barton, 1998) (Fig. 1). In addition, unusual surface temperature patterns are found in the shadow zone of winds and currents south of Cape Ghir (van Camp et al., 1991, Mittelstaedt, 1991) and south of the Canary Islands where current flow perturbations lead to eddy formation (Arístegui et al., 1994, 1997).

Stronger upwelling and enhanced productivity have often been proposed to explain lower atmospheric CO_2-contents during the last glacial periods (e.g. Sarnthein et al., 1988). Variations in atmospheric CO_2 in the Quaternary are well known from ice core studies, and glacial to interglacial CO_2 changes have been a strong amplifier of climate variability (Neftel et al., 1982; Lorius et al., 1990). The NW African upwelling area has often been cited as the type-example of the glacial high productivity (Sarnthein et al., 1988). Interestingly, Bertrand et al. (1996) and Guichard et al. (1997, 1999) documented that stronger productivity could exist in both glacial periods and interglacial periods in the NW Africa upwelling system depending on the local hydrographic situation. Accordingly, the detailed assessment of regional ecosystems as sources or sinks of carbon and their quantitative CO_2-contributions to the global carbon cycle needs further refinement. Surface sediment studies are a first step and a basis for actualistic approaches to understand both the present-day conditions and, consequently, past climatic variations.

Therefore major questions of this and other studies (compare with Freudenthal et al., this volume; Henderiks et al., this volume) are: 1.) How is the present day oceanographic condition

reflected in the surface sediment? 2.) Can a seasonal signal be identified and quantified in the surface sediment composition? 3.) Could knowledge of the connection between present oceanographic conditions and subsequent sediment composition act as an actualistic tool to decipher the past?

Within this study we will compare monthly and annual SST and chlorophyll satellite data of the years 1997 and 1998 as one proxy for surface ocean productivity together with the distribution of various other proxies within the underlying sediments with the goal to understand if a special season could be determinant for the surface sediment record.

An overview of sedimentary components most widely used as proxies for estimating upwelling intensity and productivity of surface water masses is provided by Brink et al. (1995) and Wefer et al. (1999). In this study we will concentrate on the concentrations of total organic carbon (TOC), nitrogen and carbonate, organic carbon stable isotope ratios ($\delta^{13}C_{org}$), bulk nitrogen stable isotopes ($\delta^{15}N$) and changes in the assemblages of diatoms including key-species, dinoflagellates, foraminifera (planktic foraminifera including key-species) and pteropods. All of these paleoceanographic proxies are subject to changes during sinking through the water column, upon reaching the seafloor, and after burial in the sediments, which can impose major complications in productivity reconstructions (Jahnke and Shimmield, 1995). However, lack of preservation and other changes rarely affect different components in the same fashion and therefore a multiproxy-approach is the preferred method to gain a better understanding of upwelling and related filament production in the Canary Islands region.

Material and Methods

80 surface sediment samples were recovered with multicorer and giant boxcorer during 5 cruises with RV "Meteor" (M 37/1, M 38/1, M 42/4, M 45/5) and RV "Victor Hensen" (VH 96/1) from 1996 to 1999 (Neuer et al., 1997a, 2000; Wefer et al., 1997, 1999; Fischer et al., 1998) (Fig. 1, Tab. 1).

As an actualistic approach surface sediment investigations of geochemical parameters and microfossils were performed on the 0-1 cm sample of each multicorer/giant boxcorer to describe the spatial variability of these parameters. These samples represent approximately 500 years in the open ocean and 100 or less years in the upwelling-influenced area (compare with Freudenthal et al., this volume and Henderiks et al., this volume).

Core GeoB	Latitude (N)	Longitude (W)	Water-Depth (m)	Device	Cruise	Geo-chemistry	Foraminifera/ Pteropoda	Diatoms	Dino-flagellates
4024-3	27°40.7	13°25.9	95	GBC	VH 96/1	x	x	x	
4025-2	27°44.9	13°29.2	496	GBC	VH 96/1	x	x	x	
4026-1	27°48.5	13°32.6	990	GBC	VH 96/1	x	x	x	
4029-2	28°10.8	13°15.8	680	GBC	VH 96/1	x	x	x	
4031-1	28°07.7	13°11.3	100	GBC	VH 96/1	x	x	x	
4038-2	28°40.6	13°02.2	695	GBC	VH 96/1	x	x	x	
4040-2	29°11.6	13°20.1	1000	GBC	VH 96/1	x	x	x	
4057-2	28°35.0	13°44.1	1000	GBC	VH 96/1	x	x	x	
4060-2	28°07.5	13°50.9	1000	GBC	VH 96/1	x	x	x	
4202-1	32°28.6	13°39.8	4289	GBC	M37/1	x	x	x	x
4204-1	32°01.1	11°56.7	3213	GBC	M37/1	x	x	x	x
4205-1	32°10.9	11°38.9	3272	GBC	M37/1	x	x	x	x
4206-2	31°30.0	11°01.3	1855	GBC	M37/1	x	x	x	x
4207-1	30°51.8	11°04.3	2123	GBC	M37/1	x	x	x	x
4208-1	30°42.8	11°04.7	2724	GBC	M37/1	x	x	x	
4209-1	30°21.4	11°05.0	2150	GBC	M37/1	x	x	x	x
4210-2	30°18.0	10°58.8	1959	MUC	M37/1	x	x	x	
4211-1	30°11.6	10°49.3	1773	MUC	M37/1	x	x	x	x
4212-3	29°36.2	10°57.0	1256	MUC	M37/1	x	x	x	x
4213-1	29°41.8	11°04.7	1547	MUC	M37/1	x	x	x	
4214-3	29°46.9	11°11.8	1788	MUC	M37/1	x	x	x	x
4215-1	30°02.2	11°33.2	2106	MUC	M37/1	x	x	x	x
4216-2	30°37.9	12°23.8	2325	MUC	M37/1	x	x	x	
4217-1	30°26.1	12°53.7	2504	MUC	M37/1	x	x	x	
4220-2	30°06.9	12°43.4	404	GBC	M37/1	x	x		
4221-2	29°46.5	12°20.3	1826	MUC	M37/1				x
4223-1	29°01.1	12°28.0	777	MUC	M37/1	x	x	x	x
4225-3	29°16.5	11°46.9	1281	MUC	M37/1	x	x	x	
4226-1	29°19.2	11°50.0	1400	MUC	M37/1	x	x	x	
4227-1	29°46.1	12°20.2	1826	MUC	M37/1	x	x	x	
4228-1	29°28.2	12°59.4	1633	MUC	M37/1	x	x	x	x
4229-2	29°10.9	12°38.3	1422	MUC	M37/1	x	x	x	
4230-1	29°07.7	12°35.8	1316	MUC	M37/1	x	x	x	
4231-2	29°05.2	12°33.1	1197	MUC	M37/1	x	x	x	
4232-1	29°01.3	13°23.2	1161	MUC	M37/1	x	x	x	
4233-2	28°58.5	13°19.8	1303	MUC	M37/1	x	x	x	
4234-1	28°53.4	13°13.6	1360	MUC	M37/1	x	x	x	
4235-1	28°51.4	13°11.4	1247	MUC	M37/1	x	x	x	
4236-2	28°47.0	13°05.7	1030	MUC	M37/1	x	x	x	
4237-1	28°43.7	13°01.0	800	MUC	M37/1	x	x	x	x
4238-2	28°27.1	13°38.1	1185	MUC	M37/1	x	x	x	
4239-1	28°29.6	13°10.8	881	MUC	M37/1	x	x	x	x
4241-5	29°10.0	15°27.2	3610	GBC	M37/1				x
4242-4	29°40.9	17°53.4	4292	GBC	M37/1	x	x		

Core GeoB	Latitude (N)	Longitude (W)	Water-Depth (m)	Device	Cruise	Geo-chemistry	Foraminifera/Pteropoda	Diatoms	Dino-flagellates
4301-1	29°10.0	15°27.2	3610	MUC	M38/1	x	x	x	
5529-1	29°41.4	17°41.9	4166	MUC	M42/4	x	x	x	
5530-3	29°18.2	17°53.8	3985	MUC	M42/4	x	x		
5531-1	29°04.8	17°55.5	3301	MUC	M42/4	x	x		
5532-2	27°28.3	17°56.0	3150	MUC	M42/4	x	x		
5533-1	27°40.9	17°41.6	3251	MUC	M42/4	x	x		
5534-2	27°40.7	17°07.8	2832	MUC	M42/4	x	x		
5535-1	27°50.6	16°27.2	2690	MUC	M42/4	x	x		
5536-3	27°32.2	16°08.1	3456	MUC	M42/4	x	x		
5537-2	27°32.1	15°24.1	2362	MUC	M42/4	x	x		
5538-2	27°32.2	15°07.0	2537	MUC	M42/4	x	x		
5539-2	27°32.2	14°21.3	2202	MUC	M42/4	x	x		
5540-3	27°32.1	14°10.5	2035	MUC	M42/4	x	x		
5541-2	27°32.2	13°59.7	1748	MUC	M42/4	x	x		
5542-3	27°32.2	13°50.8	1431	MUC	M42/4	x	x		
5546-3	27°32.2	13°44.2	1071	MUC	M42/4	x	x		
5547-2	27°45.6	13°42.6	1310	MUC	M42/4	x	x		
5548-3	27°59.5	13°31.1	1162	MUC	M42/4	x	x		
5549-2	27°58.7	13°41.7	1454	MUC	M42/4	x	x		
5550-3	27°57.1	14°00.9	1738	MUC	M42/4	x	x		
5551-2	27°52.6	14°54.9	1885	MUC	M42/4	x	x		
5553-2	28°36.6	14°38.7	3397	MUC	M42/4	x	x		
5555-2	29°16.0	13°57.4	2837	MUC	M42/4	x	x		
5556-3	29°15.9	14°06.6	3170	MUC	M42/4	x	x		
5557-2	29°02.7	14°09.9	2949	MUC	M42/4	x	x		
5558-2	28°44.7	14°21.2	2471	MUC	M42/4	x	x		
5559-1	31°38.7	13°11.2	3178	MUC	M42/4	x	x		
5560-2	31°36.6	13°07.1	3944	MUC	M42/4	x	x		
5561-1	32°42.2	12°56.1	3500	MUC	M42/4	x	x		
6005-1	30°52.8	10°53.8	1781	MUC	M45/5	x	x		
6006-2	30°52.1	10°37.8	1275	MUC	M45/5	x	x		
6007-1	30°51.1	10°16.0	899	MUC	M45/5	x	x		
6008-2	30°50.7	10°05.9	355	MUC	M45/5	x	x		
6009-1	30°40.9	10°16.5	579	MUC	M45/5	x	x		
6010-1	30°15.0	10°05.0	406	MUC	M45/5	x	x		
6011-2	30°18.9	10°17.3	993	MUC	M45/5	x	x		

Table 1: List of surface samples used in this study. Referred are cruise identifications and the analyses performed for each sample.

Various geochemical parameters (e.g. concentrations of TOC, carbonate and nitrogen and $\delta^{15}N$ values) that are known from previous research as good upwelling indicators have been used (e.g. Müller et al., 1983; Brink et al, 1995; Hebbeln et al., 2000). Upwelling is also reflected in the micropaleontology and is characterised by dominance of indicator diatom species (Abrantes,

1988; Bárcena and Abrantes, 1998; Abrantes and Moita, 1999), a dominance of special planktic foraminifera species (Bé and Tolderlund, 1971; Thiede, 1971, 1975; Hilbrecht, 1996) and certain dinoflagellate cysts (Zonneveld, 1996; Targarona et al., 1999), a decrease in pteropods (Thiede, 1975; Ganssen and Lutze, 1982), and a high standing stock of benthic foraminifera (Lutze, 1980; Lutze and Coulbourn, 1984). With respect to the various micropaleontological proxies, different numbers of samples have been investigated for species composition in this study.

The regional distribution of all investigated parameters were plotted using the PC-program OceanDataView (Schlitzer, 2000). The method used a variable grid with increased resolution and smaller averaging length scales in the upwelling-influenced positions where most sampling sites are situated.

Geochemical analyses

Prior to the geochemical analyses, sediment samples were freeze-dried and homogenized. Total carbon (TC) and total nitrogen (TN) concentrations were measured on non-acidified samples while TOC was measured on acidified samples using a CHN-Analyzer (Haereus). Analytical standard deviation calculated for repeated measurements was 1.6 % for carbon and 2.0 % for nitrogen concentration. Carbonate content was calculated assuming that calcium carbonate was the only carbonate-bearing mineral ($CaCO_3$ = (TC − TOC) * 8.33). The carbon/nitrogen-ratio (C/N ratio) we employ is the weight ratio of organic carbon and total nitrogen.

For the determination of $\delta^{15}N$ and $\delta^{13}C_{org}$, sediment samples were combusted at 1050 °C in a NC 2500 Elemental Analyzer (CE Instruments). The $\delta^{15}N$ and $\delta^{13}C$ of the gas thus formed was measured using a Finnigan MAT Delta Plus mass spectrometer. The stable nitrogen isotope ratio of TN was measured on non-decalcified samples. Nitrogen isotope ratios are reported with reference to air nitrogen ($\delta^{15}N$ (‰) = (($^{15}N/^{14}N_{sample}$) / ($^{15}N/^{14}N_{air}$) - 1) * 1000). $\delta^{13}C_{org}$ samples of METEOR cruises M 37/1, M 38/1 and VH 96/1 were decalcified with 1M HCl and washed with pure water. Samples from METEOR cruises M 42/4 and M 45/5 were decalcified with 6M HCl in silver boats. No significant differences of the $\delta^{13}C_{org}$ using the two decalcification methods have been observed (Rühlemann, 1996). For carbon isotope measurements we used a working standard (Burgbrohl CO_2 gas), which has been calibrated with NBS 18, 19, and 20 standards against PDB. Precision calculated from repeated measurements on laboratory sediment standard was about ± 0.1 ‰ for $\delta^{13}C_{org}$ and ± 0.2 ‰ for $\delta^{15}N$.

Micropaleontological analyses

Diatoms

The presence of diatoms was first evaluated by smear-slide analyses of each sample. For quantitative analysis 2 cm^3 of fresh sediment was taken from each sample, weighed, dried, weighed again and cleaned according to the method of Fenner (1982). Slides were prepared using the evaporation tray method of Battarbee (1973), and mounted with Permount medium. These slides were examined under a Nikon Labophot 2 microscope equipped with Differential Interference Contrast. Diatoms were counted in three of the four slides prepared from each sample following Abrantes et al. (1994). Siliceous microfossils were counted in 100 randomly selected fields of view per slide. Absolute abundances are expressed as number of valves per g of dry sediment (valv./g). The relative abundance of diatom species was determined for each sample following the counting procedures of Schrader and Schuette (1968). In general, for each sample about 300 specimens were identified and raw counts were then converted to percent abundance.

Planktic and benthic foraminifera and pteropods

Sediment samples for coarse fraction analyses were freeze-dried, weighed, and washed on a sieve with 63 μm mesh size. After splitting in further subfractions, the coarse fraction >125 μm was split into aliquots of at least 400-600 particles and quantified. Planktic foraminifera species and various other particles including benthic foraminifera and pteropods were identified within the coarse fraction (>125 μm) with a light microscope. Absolute abundances are expressed as specimen per g of dry sediment (spec./g).

As an indicator for carbonate preservation the number of fragmented planktic foraminifera species were counted and expressed as percentages of the total number of planktic foraminifera (Thunell, 1976).

Correlation of SST and micropaleontology data within surface sediments was first successfully used by Imbrie and Kipp (1971) and Kipp (1976) for reconstruction of past SST changes in sediment cores by factor analyses and transfer functions. Accordingly, we have used factor analyses to combine planktic foraminifera species in assemblages to compare these with the present-day satellite-derived SST and chlorophyll concentration of the region. Since two species (*Globigerina bulloides* and *Globigerinoides ruber* (white)) dominate within surface sediments of the Canary Islands region, we have used the natural logarithm of the percentages of each planktic foraminifera species to represent species assemblages.

The planktic foraminifera taxonomy follows Hemleben et al. (1989) with the exception that we have named the species *Neogloboquadrina pachyderma* dextral *Neogloboquadrina incompta*

following Cifelli (1961) and Meggers and Baumann (1997). In addition, we have differentiated *N. incompta* in species with 4 and with ≥4.5 chambers. Since species of the *Globorotalia menardii* group are very rare in the surface sediments of the Canary Islands region they were grouped together. Factor analyses were calculated with the program package CAPFAC (Imbrie and Kipp, 1971).

Dinoflagellates

For counting of total dinoflagellate cysts 1.5-2 g of dried sediment sample was treated with 10 % HCl for carbonate removal. Subsequently, 38 % HF was added and the samples were agitated for two hours. The acid was decanted and the residue was sieved through a 20 μm sieve. The residue remaining on the sieve was transferred to a glass tube and centrifuged. From the glass-tube, the residue was transferred to a reaction vessel with a 0.5 ml scale interval and concentrated to a 1 ml volume. From this vessel, with a pipette, 50 μl of homogenised residue were placed on a slide, embedded with glycerine jelly, and sealed with paraffin wax. The whole slides were counted using a microscope and the counts were expressed quantitatively in cysts per g dry sediment.

Satellite data

Pflaumann et al. (1996) have discussed in detail the importance of densely spaced SST data for surface sediment calibration that is needed especially in regions with strong thermal gradients in the surface waters. The comparison of satellite SST data of the years 1997 and 1998 to the SST data of the climatological atlas in the coastal upwelling area off NW Africa (Levitus and Boyer, 1994) indicated that significant local temperature features like the Cape Yubi filament were not resolved by the 1° * 1° grid of Levitus and Boyer (1994). Consequently, SST has been computed from Advanced Very High Resolution Radar (AVHRR) radiances operational since 1981 for the years 1997 and 1998. Data were mapped into an equal-angle projection of 9 km resolution. Pigment concentration of the year 1998 was derived from the Sea-viewing Wide Field-of-view Sensor (SeaWiFS). SeaWiFS was launched in August 1997 and is a multi-channel scanning spectrometer, which observes the ocean surface in 8 spectral bands with the same 9 km resolution as AVHRR. The satellite-derived hydrographical data were used for correlations with our measured sedimentological proxies.

Results and Discussion

Organic matter and its isotopic composition

The coastal upwelling processes along the Moroccan coast are most pronounced around capes, which are sites of filament production (van Camp et al., 1991; Davenport et al., 1999).

These filaments are exporting substantial biomass into the oligotrophic portions of the NE Atlantic and are likely to superimpose their signal on the sediments. Most geochemical parameters within the surface sediments corresponded well to this gradient of surface water phytoplankton biomass as recorded by historic satellite derived pigment data (Fig. 2). The spatial variability of the TOC content within surface sediments in the Canary Islands region showed a zonal gradient with highest values off the capes and low values in the open ocean (Fig. 2A). Highest TOC values existed at Cape Ghir (1.87 % at site GeoB 6007-1), while Cape Yubi showed contents up to 1.55 % at site GeoB 5546-3. The lowest values (<0.6 %) were found north of La Palma and in the near shore sites GeoB 4024-3 (shelf-sample) or GeoB 4220-2 (seamount-sample).
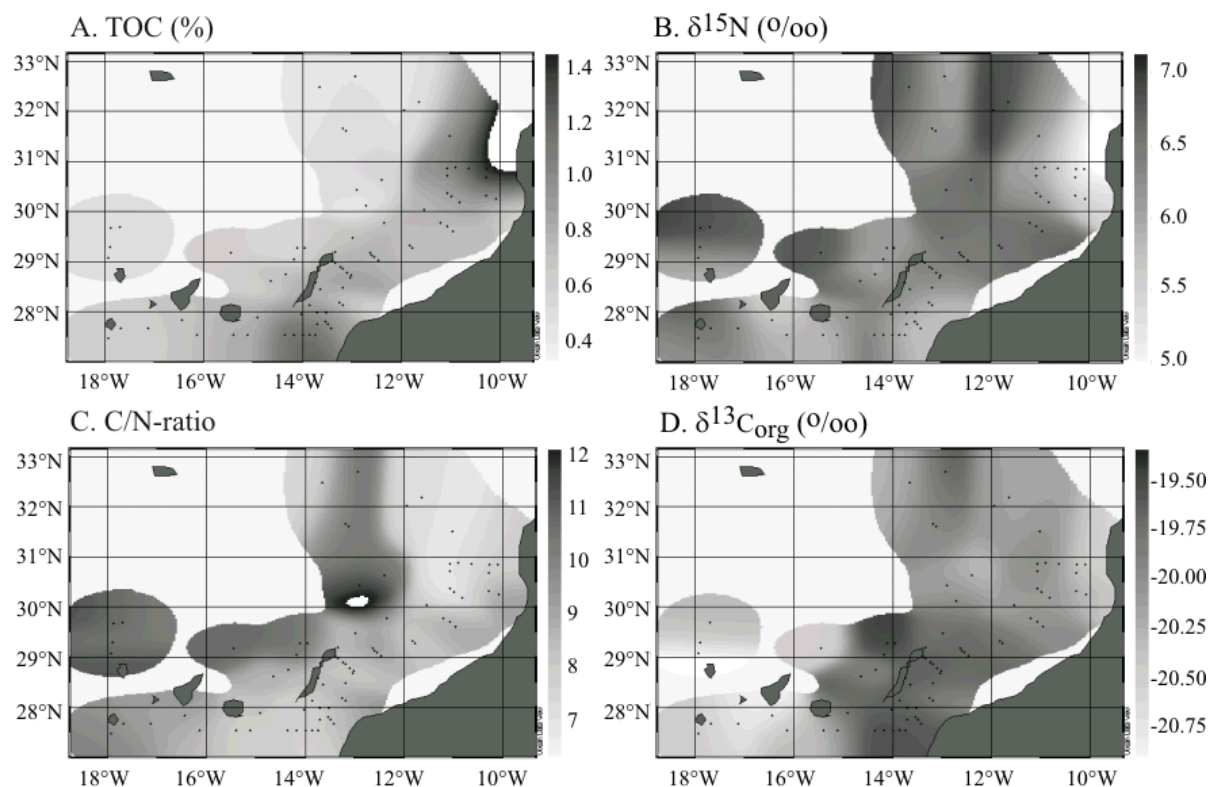
Figure 2: Spatial distribution of geochemical parameters in the surface sediments from the Canary Islands region (A: Total organic carbon (TOC) in %; B: $\delta^{15}N$ of bulk sediment in ‰; C: Organic carbon/total nitrogen weight-%-ratio (C/N-ratio); D: $\delta^{13}C$ of the organic fraction in ‰).

The preservation of TOC is strongly dependent on the water-depth in which particles are finally sedimented, since strong decay of TOC occurs during settling through the water-column (Suess, 1980; Martin et al., 1987). This raises the question whether the strong zonal gradient in TOC concentration reflects the primary signal of surface water productivity or the increasing water-depths towards the open ocean. Generally, TOC concentrations decreased with increasing

water-depth (Fig. 3). Both, increased preservation and higher supply of organic matter at the upwelling influenced sites could explain this relationship. However, it was obvious that especially sediment samples between the two capes reveal relatively low TOC concentrations despite shallow water-depths. This observation was in correspondence with relatively low productivity indicated by lower chlorophyll concentrations compared to the filament areas off the capes (Fig. 1). Therefore we concluded that it is variability in organic matter supply and not water-depth related organic matter preservation that was responsible for the observed spatial TOC distribution.
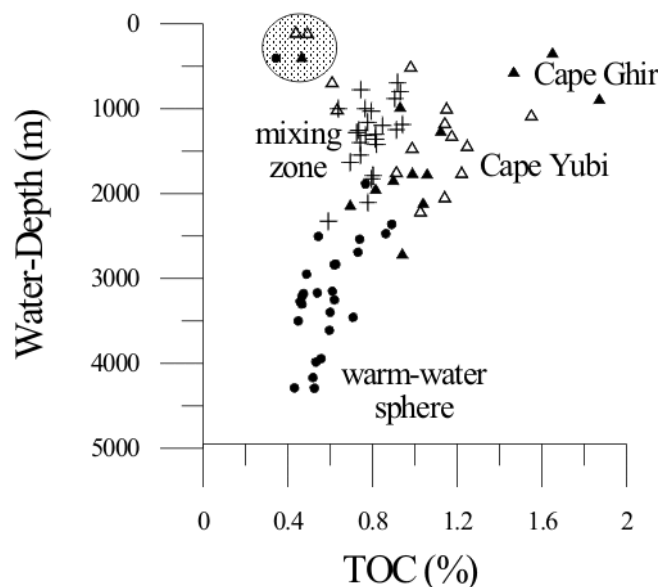
Figure 3: Correlation of total organic carbon content (TOC) to the water-depth. Three major domains in the research area were shown with different signatures (triangles for the capes, which are influenced by upwelling and filament production (filled: Cape Ghir; not filled: Cape Yubi), crosses for the area between the capes and dots for the warm-water sphere of the subtropical open ocean). The shaded area indicated four samples that are characterised by "unusual" conditions (GeoB 4024-3 and GeoB 4031-1 (shelf area); GeoB 6010-1 (possibly turbidite influence), GeoB 4220-2 (seamount position).

The spatial variability of the $\delta^{15}N$ as a nutrient indicator showed a distribution inversely related to the TOC content, thus, lowest $\delta^{15}N$-values were measured off the capes (Fig. 2B), with the lowermost values off Cape Ghir. From site GeoB 6007-1 to GeoB 6010-1 values ranged between 4.59 and 5.17 ‰. Cape Yubi sediments showed also light $\delta^{15}N$-values at sites GeoB 4025-2 (5.23 ‰), GeoB 5546-3 (5.40 ‰) and GeoB 5547-2 (5.44 ‰). Highest $\delta^{15}N$-values were found in far offshore positions such as GeoB 4242-4 north of La Palma (7.14 ‰), GeoB 4204-2 (6.99 ‰) and GeoB 5533-1 (6.97 ‰) east of Hierro. Overall the $\delta^{15}N$-values increased from east to west along the productivity gradient. Results from shallow traps of a sediment trap transect north of the Canary Islands reflect also the strong gradient from light to heavy values of $\delta^{15}N$

from an upwelling-influenced site towards the subtropical gyre (Freudenthal et al., in press). Similary, surface sediments in other coastal upwelling areas have lowest $\delta^{15}N$-values near to the coast, where nutrient availability is highest (Holmes et al., 1999; Hebbeln et al., 2000). This indicates that the $\delta^{15}N$ from surface sediments could be interpreted as a good proxy for Holocene nutrient availability in surface waters (Altabet and Francois, 1994). However, opposite to the TOC distribution, a clearly marked far offshore NNE-SSW-belt within the surface sediments with $\delta^{15}N$-values <6 ‰ was also observed. This belt from positions north of the Canary Islands (e.g. GeoB 5561-1 (5.92 ‰)), to an area west of Fuerteventura/Lanzarote (e.g. GeoB 5558-2 (5.58 ‰)), and towards an area south of Tenerife and Gran Canaria (e.g. GeoB 5535-1 (5.48 ‰) or GeoB 5536-3 (5.94 ‰)) could reflect locally enhanced nutrient availability (Fig. 2B). We can only speculate on the reasons for "anomalous" $\delta^{15}N$-values in this more offshore region and we can not exclude the effects of diagenesis for the mentioned sites (compare with Altabet and Francois, 1994; Holmes et al., 1999). However, if we are looking in detail at the sites with "anomalous" light $\delta^{15}N$ values far offshore, we recognise that the northernmost samples are taken on or near to seamounts. These topographic features are known to introduce anticyclonic eddies and associated higher nutrient availability in the surface waters (Genin and Boehlert, 1985; Dower et al., 1992; Odate and Furuya, 1998). The sites further south, west of Fuerteventura and Lanzarote, are known to be temporally affected by the Cape Yubi filament (Davenport et al., 1999) or by episodic west coast upwelling (Hernández-Guerra et al., 1993; Johnson and Stevens, 2000) introducing a higher nutrient content. Finally, the minimum in $\delta^{15}N$ south of the Canary Islands could be best explained by the island`s anticyclonic eddy formation, which is known to occur mainly in the current shadow of the islands (Arístegui et al., 1994; 1997). Despite these possible causes for the lighter $\delta^{15}N$ values in the NNE-SSW belt, the other proxies for higher surface water productivity, such as enhanced TOC, did not confirm the trend in $\delta^{15}N$. Possible future investigations using e.g. an increased spatial resolution of other proxies could bring new insights to this topic.

The Canary Islands region is affected by repeated inputs of atmospheric dust that are a source of additional terrigenous organic particles within the marine sediments (Koopmann, 1981; Coude-Gaussen et al., 1987; Hooghiemstra, 1988; Bergametti et al., 1989). Accordingly, the marine and the terrigenous fraction have to be distinguished when applying TOC as a marine productivity proxy (Müller et al., 1983; Meyers, 1994; Wagner and Dupont, 1999). For that purpose, we determined the C/N-ratio and the $\delta^{13}C_{org}$-values of the surface sediment samples. In the entire research area, C/N-ratios were between 6.3 and 12 indicating dominance of marine organic matter (compare with Tyson, 1995) (Fig. 2C). Lowest values were found off Cape Ghir.

However, we observed a gradient from values of about 8 at sites GeoB 6007-1 and GeoB 6008-2 nearest to Cape Ghir towards ratios of 6.3 at site GeoB 4211-1. Highest C/N-ratios between 11 and 12 were analysed north of La Palma at site GeoB 4242-4 (12.06) and GeoB 5531-1 (11.24). Only the C/N-ratio at GeoB 4220-2 on the Conception Seamount is extraordinary with a value of 13.95.

$\delta^{13}C_{org}$-values ranged between –21.16 ‰ at GeoB 5531-1 north of La Palma and –19.55 ‰ at GeoB 5555-2 west of Lanzarote, also fairly typical for marine organic matter (Wagner and Dupont, 1999). The $\delta^{13}C_{org}$-dataset reflected both, a strong zonal gradient, and a meridional gradient in the Canary Islands region (Fig. 2D). Heaviest values were found in the area off Cape Yubi with a decreasing towards the north, which points to a relative increase of terrigenous organic matter towards Cape Ghir.

Carbonate concentration and carbonate dissolution proxies

To interpret the distribution of carbonate bearing organisms (see below) and assess organic particle dilution within the surface sediment, we need information on the sediment carbonate content. Carbonate concentrations were, in contrast to the TOC, lowest in the vicinity of the capes (Fig. 4A). Overall, the carbonate content ranged from values of 24.91 % at site GeoB 6008-2 off Cape Ghir towards 71.72 % at site GeoB 5561-1. The highest values in sites GeoB 4024-3 and GeoB 4031-1 (shelf-samples) and GeoB 4220-2 (seamount-sample) (>75 %) could be explained by accumulation of shelf- and seamount-derived carbonate particles.

The fragmentation index of planktic foraminifera species helps to detect areas where carbonate dissolution takes place (Fig. 4B). The percentages of fragments within the planktic foraminifera assemblages ranged from 4.0 % at GeoB 4217-1 to 65.5 % at GeoB 6010-1 off Cape Ghir. Overall, the highest percentages of fragmented planktic foraminifera tests were found in the areas off the capes, pointing to stronger carbonate dissolution at these sites. Pteropods consist of aragonite that is more easily dissolved in the water column or within the surface sediments. Thus, there was a strong negative correlation between the occurrence of pteropod tests and fragmented planktic foraminifera (Fig. 4). Highest numbers were observed in a distinct region between the two capes with contents up to 12,300 spec./g in site GeoB 4212-3 (Fig. 4C). The samples north of La Palma and off the capes were barren of pteropods. Thus, it appears reasonable to relate the rareness and absence of pteropod tests and the higher fragmentation of planktic foraminifera off the capes to the local formation of a more carbonate-dissolving bottom and pore water, caused by increased degradation of organic matter at the seafloor (Milliman et al., 1999). In the filament area the aragonite compensation depth (ACD) rises up to a water-depth of 355 m off Cape Ghir and 1300 m off Cape Yubi as determined from the spatial distribution of

aragonite (pteropod) free surface sediments. Offshore, in the domain of the subtropical gyre, the ACD is located much deeper in 3,200 m water-depth. This is in agreement with findings of Ganssen and Lutze (1982), who documented an ACD-rising from 3,100 m to 400 m water-depth in the higher productivity zone off Cape Blanc at 20°N.
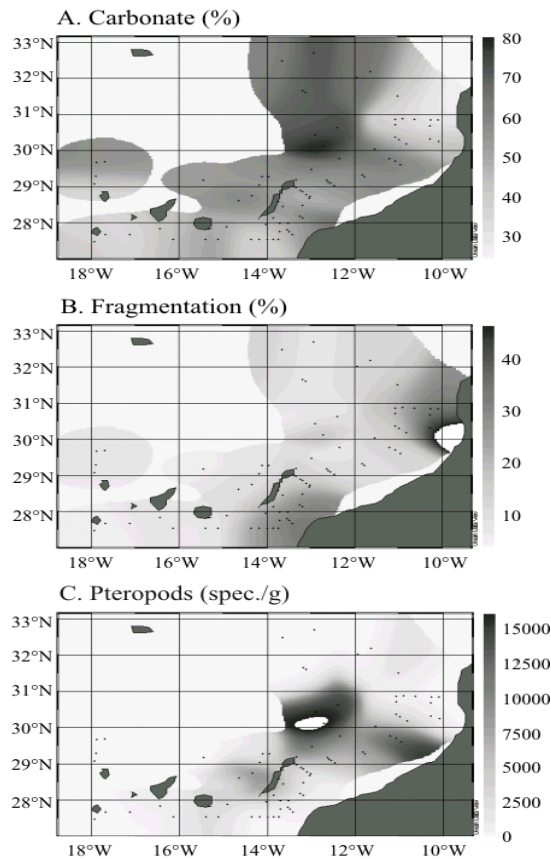

Figure 4: Spatial distribution of carbonate preservation indicating proxies in the surface sediments from the Canary Islands region (A: Carbonate content in %; B: Fragments of planktic foraminifera in % of the total number of planktic foraminifera; C: Pteropods in specimen per g dry sediment).

Thus, carbonate preservation proxies can be used as indirect indicators of the surface water properties, as high productivity produces high TOC signals in the underlying sediments. The accompanying increasing of pCO_2 and lowering of the pH within the sediments may be responsible for complete aragonite dissolution and slight calcite dissolution. However, no preferential dissolution of susceptible planktic foraminifera species was observed neither near shore nor offshore. This was confirmed by the occurrence of the same species in seasonal plankton tows, sediment trap time-series and surface sediments (see below, Abrantes et al., this volume; Meggers, unpublished data).

Planktic foraminifera distribution

Planktic foraminiferal faunas exhibit strong seasonality and are sensitive to changes of hydrographic properties (Bé and Tolderlund, 1971; Hemleben et al., 1989). Latitudinal and geographic restrictions of species groups are largely imposed by their dependence on particular water masses and their productivity. Thus, planktic foraminifera could also be used as indicators of the influence of water originating from the upwelling zone on the oligotrophic regime of the Canary Islands region. The total planktic foraminifera content in the Canary Islands region ranged from values of 84 spec./g at GeoB 6008-1 off Cape Ghir to values of >16,000 spec./g at GeoB 5560-2 (Fig. 5A). An exceptionally high value of >30,000 spec./g was observed at the shallow-water seamount position at GeoB 4220-2.

One more supporting evidence for a parallel variation of productivity and TOC concentration in surface sediments comes from the relative abundance of *G. bulloides*, a planktic foraminifera indicator species for more productive water-masses (Thiede, 1975; Naidu, 1990; Conan and Brummer, 1999). High relative abundances of *G. bulloides* were found at both capes with maxima at site GeoB 6008-2 (61.4 %) for Cape Ghir and at site GeoB 5546-3 (46.3 %) for Cape Yubi (Fig. 5B). High relative abundances of *G. bulloides* occurred in the two shelf samples GeoB 4031-1 (60.0%) and GeoB 4024-3 (55.9%), which are both situated in the Cape Yubi domain. Intermediate relative abundances of *G. bulloides* (20 to 30 %) were observed between the two capes east of the Canary Islands. The lowest relative abundances of *G. bulloides* were found at site GeoB 5533-1 (1.5 %) east of Hierro and GeoB 5530-13 (1.5 %) north of La Palma. In both cases, north and south of the Canary Islands, a strong zonal decrease from the capes towards the subtropical gyre is reflected within the surface sediment.

The second investigated important planktic foraminifera *G. ruber* (white) that serves as an indicator for warmer water masses (Hemleben et al., 1989) revealed a spatial distribution opposite to *G. bulloides* (Fig. 5C), with maximum relative abundances in the open ocean south of the Canary Islands (29.6 % at site GeoB 5534-2) and north of the Canary Islands (33.8 % at site GeoB 5558-2). Minima were observed in both cape regions, at site GeoB 6008-2 (2.5 %) off Cape Ghir and at site GeoB 5546-3 (7.6 %) off Cape Yubi. *G. ruber* (white) was also found in the shelf samples GeoB 4031-1 (2.0 %) and GeoB 4024-3 (5.9 %) nearby Cape Yubi, albeit with low relative abundances.
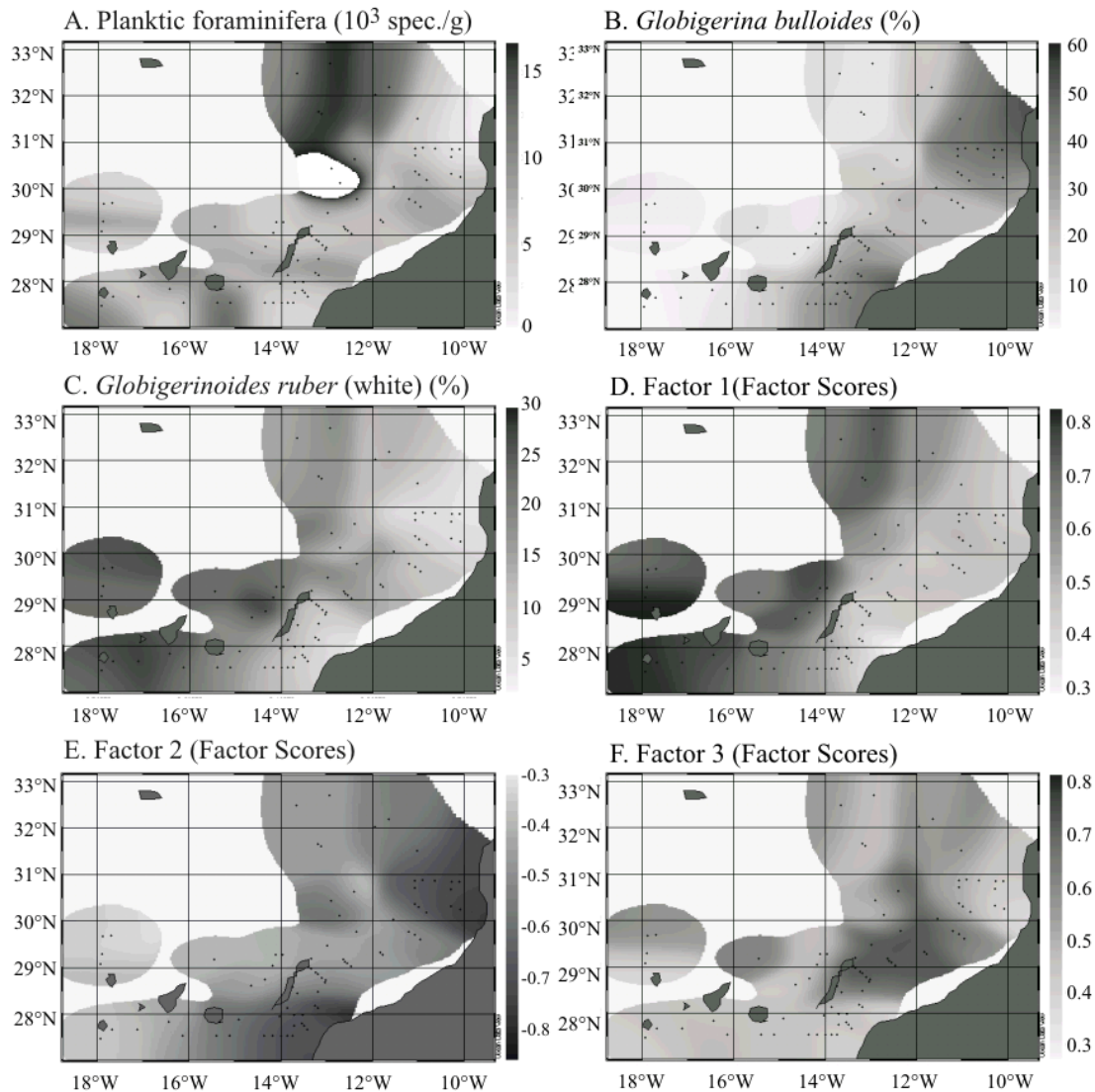
Figure 5: Spatial distribution of absolute abundance of planktic foraminifera, relative abundances of planktic foraminifera species and of factor scores derived from a factor analyses on the planktic foraminifera assemblage in surface sediments from the Canary Islands region (A: Planktic foraminifera in specimen per g dry sediment; B: Planktic foraminifera *G. bulloides* in %; C: Planktic foraminifera *G. ruber* (white) in %; D: Factor 1 "warm-water factor"; E: Factor 2 "upwelling/filament factor"; F: Factor 3 "mixing factor").

To assess the planktic foraminifera data statistically a factor analyses was carried out on the total planktic foraminifera assemblage. A Q-mode principal component analysis including 78 surface sediment samples and 25 planktic foraminifera taxa/groups from the Canary Islands region was calculated in order to combine 25 planktic foraminifera species (natural logarithm of percentages) into factors. 3 factors explained 94.2 % of the total variance (Tab. 2). The model provided high communality values (>0.83) for all samples except the site GeoB 4024-3 (shelf-sample) with a communality value of 0.65.

Factor 1 (Fig. 5D) explained 32.0 % of the total variance and was mainly composed of *Globigerina falconensis*, *G. ruber* (white), *Globoturborotalita rubescens* and *Globigerinita*

glutinata (Tab. 2). *G. bulloides* was anticorrelated to this assemblage. This factor was therefore called the "warm-water factor" and represented the water masses of the subtropical gyre. The spatial distribution of the varimax-rotated Q-mode principal component scores was similar to the distribution of the relative abundance of *G. ruber* (white) (Fig. 5). Highest scores were found north of La Palma at site GeoB 5531-1 (0.83) and south and east of Hierro at sites GeoB 5532-2 and GeoB 5533-1 (both 0.81).

Species	Factor 1	Factor 2	Factor 3
G. bulloides	**-0.33**	**-0.766**	**0.341**
G. falconensis	**0.451**	-0.106	-0.172
T. quinqueloba	0.11	**-0.258**	-0.141
T. humilis	0.243	0.137	**0.327**
G. rubescens	**0.371**	-0.166	-0.055
G. calida	0.042	-0.043	**0.285**
G. siphonifera	-0.096	0.144	**0.487**
G. ruber pink	0.135	0.01	0.031
G. ruber white	**0.412**	-0.01	0.246
G. sacculifer	0.138	0.029	**0.302**
G. conglobatus	-0.071	0.087	0.227
G. tenellus	0.146	-0.022	0.097
O. universa	0.071	-0.077	0.038
N. dutertrei	0.038	0.044	0.089
N. pachyderma	-0.016	-0.162	-0.055
N. incompta	0.123	**-0.301**	-0.097
N. incompta (≥4 chambers)	0.177	-0.149	-0.052
P. obliquiloculata	0.03	0.015	**0.252**
G. glutinata	**0.331**	-0.034	0.141
G. hirsuta	0.135	0.016	-0.005
G. theyeri	-0.037	-0.034	0.019
G. crassaformis	-0.078	0.084	0.248
G. inflata	0.122	**-0.294**	0.007
G. truncatulinoides	0.155	-0.098	0.025
G. scitula	0.083	0.063	0.147

Table 2: Factor loadings of the 3 factors as determined from factor analyses of the relative abundances of the planktic foraminfera in the Canary Islands region. The relevant species are marked in bold.

Lowest scores were present in a coastal band from Cape Ghir to Cape Yubi. The "warm-water factor" (factor 1) represented a planktic foraminifera assemblage that is known to be associated with higher SST. The most obvious species that was determining this factor is *G. ruber* (white) (see above). But also *G. falconensis* is known to have a distinct preference for physical conditions in subtropical regions with highest abundances in summer (Bé and Tolderlund, 1971; Hilbrecht, 1996). The worldwide relationship between relative abundance of *G. glutinata* and SST resembles those of *G. bulloides* (Thiede, 1975; Hilbrecht, 1996). However,

G. glutinata is most abundant in higher latitudes and adjacent to upwelling zones and may occur in a late stage of the bloom succession and at the margins of productive areas (Hilbrecht, 1996). Thus, relative abundances of *G. glutinata* in the Canary Islands region show some inverse correlation with relative abundances of *G. bulloides*.

Factor 2 (Fig. 5E) explained 31.2 % of the total variance and was dominated by *G. bulloides*. In addition, *N. incompta*, *Globorotalia inflata* and *Turborotalita quinqueloba* were represented in this "upwelling/filament factor" (Tab. 2). The spatial distribution of the factor scores indicated highest scores exclusively off Cape Ghir and Cape Yubi. Sites GeoB 6009-1 (-0.78) and GeoB 6010-1 (-0.77) were representing Cape Ghir and sites GeoB 5546-3 (-0.77) and GeoB 4029-2 (-0.73) Cape Yubi. Lowest scores were present north of La Palma at site GeoB 5529-1 with a value of –0.30. All species of the "upwelling/filament factor" (factor 2) are known to reflect colder SST conditions (Bé and Tolderlund, 1971; Thiede, 1975; Bé, 1977). In other upwelling regions like the Benguela upwelling *G. bulloides* is present together with *N. incompta* in the highly productive intermediate zone between the oligotrophic and the upwelling waters (Giraudeau, 1993), while the upwelling zone proper is reflected by high numbers of *Neogloboquadrina pachyderma*, *N. incompta* and *T. quinqueloba* (Giraudeau and Rogers, 1994). Unfortunately we have investigated only few samples directly influenced by upwelling, .since upwelling of North Atlantic Central Water off NW Africa is restricted to an area of 50-70 km width on the shelf (Mittelstaedt, 1991). However, these samples revealed the same assemblage and resulted in the same factor as the filament samples. Therefore the name "upwelling/filament factor" for factor 2 seems to be reasonable.

Factor 3 (Fig. 5F) was filling in the gap between highest scores of factor 2 at the capes and highest scores of factor 1 far offshore. Factor 3 explained 31.0 % of the total variance and is dominated by an assemblage consisting out of *Globigerinella siphonifera*, *G. bulloides*, *Turborotalia humilis*, *Globigerinoides sacculifer*, *Globigerinella calida* and *Pulleniatina obliquiloculata* (Tab. 2). We termed this factor the "mixing factor". The spatial distribution of factor scores showed highest values east of the Canary Islands. The length-axis of the eastern Canary Islands Fuerteventura and Lanzarote represented a direct boundary to factor 1. Highest scores of factor 3 were present in site GeoB 4232-1 (0.82) and lowest scores off Cape Ghir and Cape Yubi (e.g. in site GeoB 6009-1 (0.28) or GeoB 5542-3 (0.33)). The factor 3 assemblage is a mixture of planktic foraminifera species that are known to be associated with warmer conditions and to have a tolerance to a temporal increase in productivity (like *P. obliquiloculata* and *G. siphonifera*) and species that have a preference for high productivity (like *G. bulloides*). *G. siphonifera* is known to be abundant in the subtropical province, but is also associated to

upwelling regions and boundary currents (Bé, 1977). *P. obliquiloculata*, which also shows some relations to productive water masses (Hilbrecht, 1996), together with *G. sacculifer* is frequently encountered in the subtropical province but normally belongs to the tropical province (Bé, 1977). Little is known in the literature about the ecological preference of *T. humilis*, however seasonal plankton tow results indicate that this species is one of the most abundant planktic foraminifera in the region in winter regardless of the distance to the coast (Meggers, unpublished data). The "mixing factor" assemblage is present in an oceanographic realm that is characterised by essentially conditions other than found off the capes or in the open ocean. Mittelstaedt (1991) for instance shows that southeast of Cape Ghir, within the Bay of Agadir, which located in the spatial distribution of factor 3, the seas are generally calm during strong northerly trade winds, because this area is sheltered by the Atlas mountains, and therefore upwelling is subdued. Between Cape Ghir and Cape Yubi and the warm-water sphere in the "battlefield" between the two major regimes/factors "upwelling/filament" and "warm-water", an upwelling influence occurs during summer and fall while oligotrophic open ocean conditions prevail during winter and spring. Although "upwelling-fingerprints" could be recognised during the whole year within the open ocean off the capes due to a more or less annual stability of the filament structure, the extent of the filaments was most pronounced during the summer months, influencing the entire region between Cape Ghir and Cape Yubi (Davenport et al., 1999).

Other micropaleontological proxies

Additional supporting evidence for roughly parallel variations in surface water productivity and surface sediment properties are derived from the absolute abundances of diatoms (including the relative abundance of two diatom key-species), benthic foraminifera and dinoflagellates. All these groups are known to reflect specific oceanographic conditions like coastal upwelling or filament production (Lutze, 1980; Abrantes, 1988; Targarona et al., 1999).

Diatom abundances were highest in two samples, one at site GeoB 4228-1 ($11.1*10^6$ valv./g) north of Lanzarote and another north of La Palma in site GeoB 5529-1 ($6.0*10^6$ valv./g) (Fig. 6A). No diatoms were found at sites GeoB 4029-2, GeoB 4060-1 and GeoB 4231-2 and in the shelf positions GeoB 4024-3 and 4031-1. However, a significant decrease in the amount of diatoms from $3.2*10^6$ valv./g (GeoB 4207-1) to $0.2*10^6$ valv./g (GeoB 4217-1) was observed within the surface sediments possibly reflecting the filament extension off Cape Ghir. Also the distribution of *Chaetoceros spp.* resting spores as a well known indicator for higher productivity in the surface water (Abrantes and Moita, 1999) showed highest relative abundances (>50 %) off Cape Ghir at sites GeoB 4208-1 (62.1 %) and GeoB 4207-1 (52.2 %) (Fig. 6B), and lowest at site GeoB 4223-2 (3.4 %). The Cape Yubi filament was not mirrored, probably due to the fact

that only a few samples were counted for diatoms in this area (Tab. 1). Another maximum in relative abundances of *Chaetoceros spp.* was located north of La Palma at site GeoB 5529-1 (34.9 %).
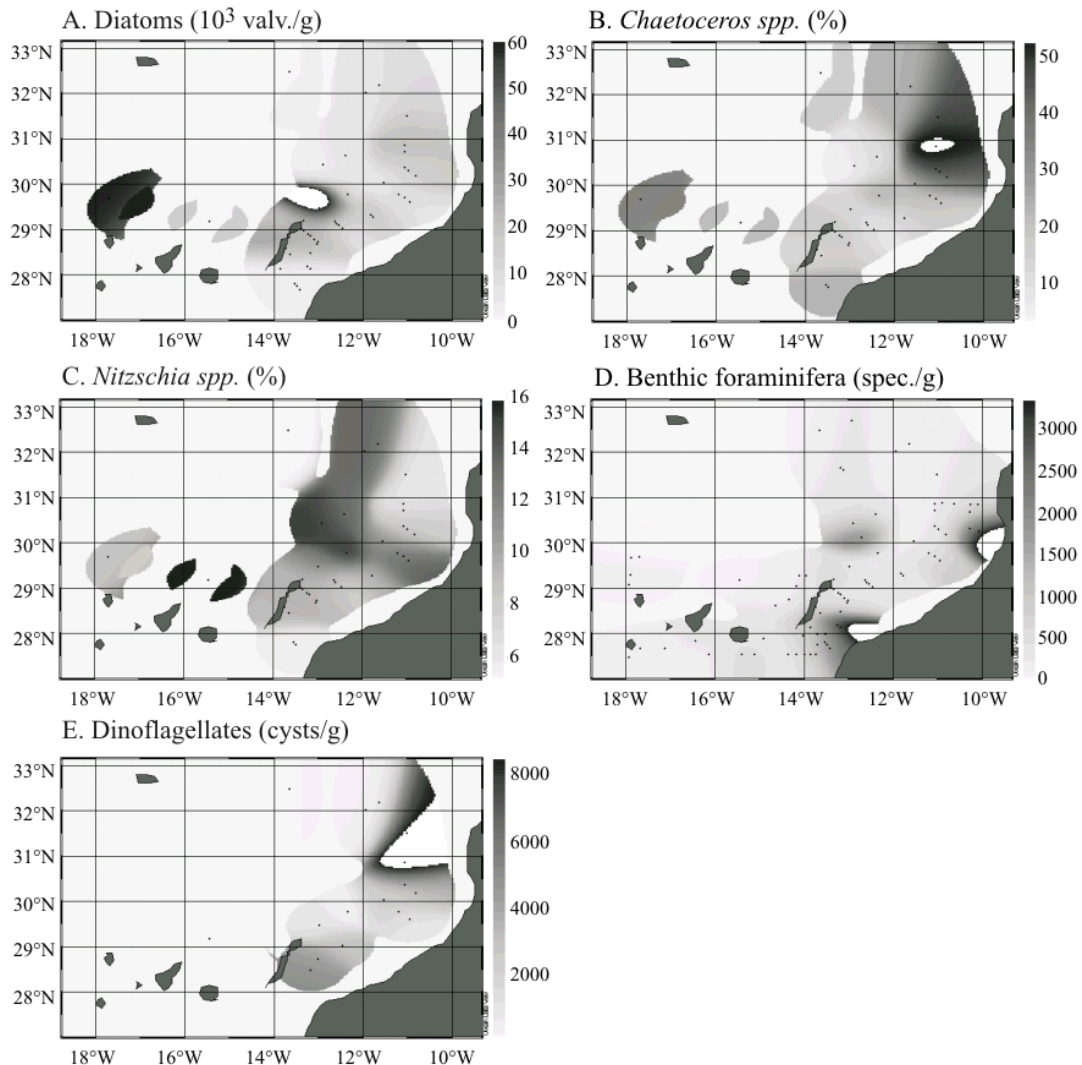

Figure 6: Spatial distribution of various micropaleontological parameters in surface sediments from the Canary Islands region (A: Diatoms in valves per g dry sediment; B: Diatom *Chaetoceros spp.* resting spores in %; C: Diatom *Nitzschia spp.* in %; D: Benthic foraminifera in specimen per g dry sediment; E: Dinoflagellates in cysts per g dry sediment).

An opposite trend was shown by the relative abundances of *Nitzschia spp.* (Fig. 6C). This open ocean species had lowest relative abundances in the area nearby Cape Ghir (e.g. site GeoB 4207-1 with 5.7 %) and higher abundances in a belt 60 nm offshore (e.g. site GeoB 4227-1 (15.2 %) and GeoB 4217-1 (15.2 %)) similar to the open ocean planktic foraminifera species *G. ruber* (white) (Fig. 5C). The maximum relative abundance was found north of Gran Canaria at site GeoB 4301-1 (15.8 %).

The spatial distribution of benthic foraminifera as another indicator for higher surface water productivity showed two clear maxima off Cape Ghir and Cape Yubi (Fig. 6D). Maximal contents were recognised at site GeoB 6010-1 (7,100 spec./g) and site GeoB 4025-2 (4,300 spec./g) for Cape Ghir and Cape Yubi, respectively. Benthic foraminifera were absent at site GeoB 5558-2 and rare north of La Palma (<20 spec./g). The high standing stock of benthic foraminifera off Cape Ghir and Cape Yubi was linked to the high TOC content of the surface sediment in that area (Fig. 2A).

A similar distribution pattern in spite of the lower sample resolution was seen in the dinoflagellate cyst distribution (Fig. 6E). Highest numbers of dinoflagellate cysts occurred again off Cape Ghir at site GeoB 4207-1 (13,000 cysts/g) and lowest numbers were observed north of Gran Canaria at site GeoB 4241-5 (192 cysts/g). Samples closest to Cape Ghir were dominated by *Lingulodinium machaerophorum*, *Gymnodinium spp.* and *Protoperidinium spp*. These dinoflagellate cysts are usually found in high productive upwelling regions (Dale and Fjellså, 1994). A detailed description of the species distribution in the research area is given by Targarona et al. (1999).

Statistical correlation of geochemical and micropaleontological parameters to the present oceanographic conditions

High numbers of shelf-derived carbonate particles like fragments of molluscs, bryozoans and corals were found in two shelf samples (GeoB 4024-3 and GeoB 4031-1). These samples and the sample GeoB 4220-2 taken from the Conception Bank Seamount were not used for correlations with surface water SST and chlorophyll since the geochemical/micropaleontological characteristics in these samples were masked by the dilution of non-pelagic allochthonous (shelf-samples) or autochthonous (seamount-sample) particles (see above).

We have shown that the surface sediment in the research area mirror the productivity gradient as observed in present day satellite data, even resolving mesoscale features like the Cape Ghir and the Cape Yubi filaments. By comparing surface sediment proxies with the SST and chlorophyll concentration of the years 1997 and 1998, we are now able to establish the influence of a particular season on the seafloor sediments of the Canary Islands region. Assessing the relation between what is produced in the photic zone and what accumulates on the seafloor is an important aspect in the evaluation of paleoceanographic proxies. It is well known that e.g. the use of transfer functions in upwelling regions suffer by the extreme contrasts in SST, salinity, nutrient availability and productivity on seasonal time scales. However, synthesizing the detailed descriptions based on multiproxy approaches in upwelling regions (e.g. Naidu, 1990; Giraudeau and Rogers, 1994; Hebbeln et al., 2000; this study) will hopefully enable us to reach a

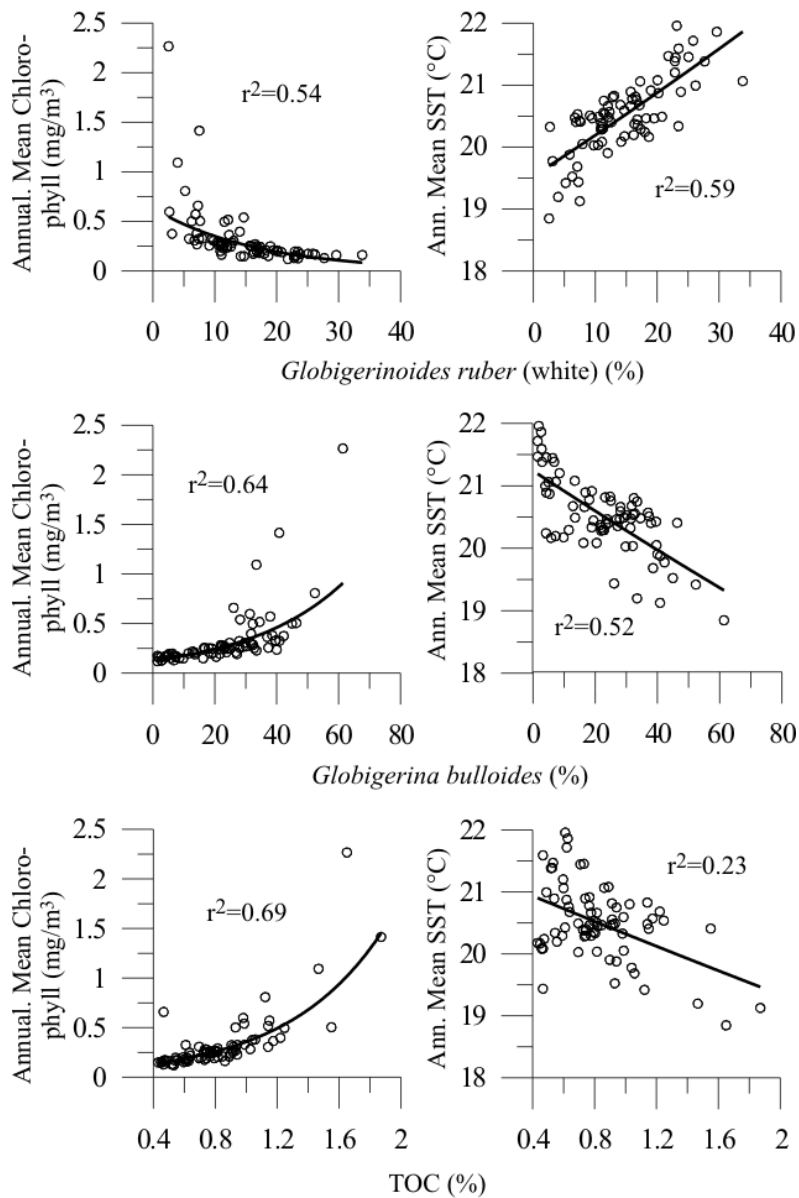better paleocenographic reconstruction of coastal upwelling systems in the future.

Figure 7: Correlation of the relative abundances of planktic foraminifera species *G. ruber* (white), *G. bulloides* and the TOC concentration on the annual mean SST of the years 1997 and 1998 and the annual mean chlorophyll content of the year 1998 in the Canary Islands region. The correlation coefficients (r^2) were also indicated. The calculated F in a statistical correspondence test exceeds the critical F indicating a linear relationship between ln (Chlorophyll/SST) and all proxies except for the relationship between TOC and SST.

Despite of the restrictions mentioned above, relatively good correlation coefficients were found for the relative abundance of planktic foraminifera species *G. bulloides* and *G. ruber* (white) on the satellite SST and chlorophyll data (Fig. 7). The significance of all regressions were tested using analysis of variance (F-test) (Swan and Sandilands, 1995). A negative correlation was observed between *G. bulloides* and SST, while *G. ruber* (white) had a positive correlation with this parameter. The opposite correlation existed between these two species and

the chlorophyll content of the surface waters (Fig. 7). Also, the TOC concentration in the surface sediments was positively correlated to the concentration of chlorophyll in surface waters (Fig. 7). A correlation between TOC concentration and SST was less pronounced, pointing to the fact that the surface sediment TOC concentration was rather determined by the chlorophyll- or the phytoplankton concentration in the surface water, while SST was more decisive for the planktic foraminifera distribution. When looking to the most important species of the near shore area, *G. bulloides*, it is striking that the best correlation coefficient (>0.7) on SST was found for August, which is known to be the month with strongest upwelling (Fig. 8) (van Camp et al., 1991; Davenport et al., 1999). This correlation agreed with the surface sediment oxygen isotope data of *G. bulloides* off NW Africa that were consistent with temperatures from the upwelling season (Ganssen, 1983; Ganssen and Sarnthein, 1983). Best correlation coefficients were also calculated for TOC and the percentage of *G. ruber* (white) in August (Fig. 8). It is known from remote sensing and sediment trap data that the winter time shows a less established gradient in surface water productivity and SST (Davenport et al., 1999; Abrantes et al., this volume; Meggers, unpublished data). Accordingly, deep-mixing in the NE Atlantic and an associated winter-bloom produces similar planktic foraminifera assemblages over the whole productivity gradient from the coastal upwelling influenced area towards the subtropical gyre (Abrantes et al., this volume, Meggers, unpublished data). The time with strongest contrasts in surface water properties between the coastal area and the oligotrophic open ocean is the upwelling season in summer when both upwelling and filament production are most intense. Thus, the surface sediment characteristic of the Canary Islands region is determined by the summer time through strongest zonal contrasts in the faunal and floral properties of the water column. This is confirmed by multiple regressions of the factor analysis results to the monthly mean SST. We saw a fairly good correlation between factors 1 ("warm-water factor" with positive correlation) and 2 ("upwelling/filament factor" with negative correlation) to the monthly mean SST (Fig. 9). No correlation was observed in comparing the "mixing factor" (factor 3) scores to the annual mean SST (Fig. 9), since this factor is mixing up planktic foraminifera species with different ecological preferences like *G. bulloides* (summer species) and *T. humilis* (winter species).
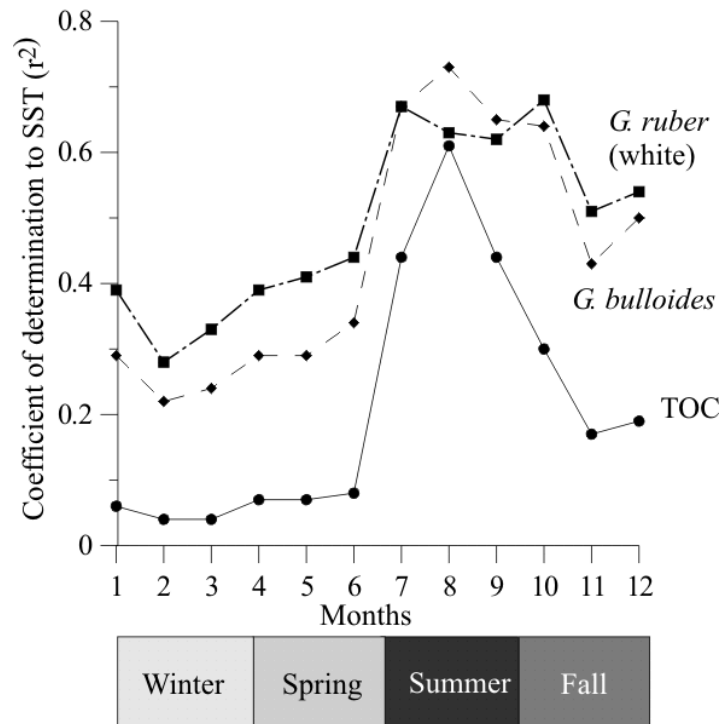
Figure 8: Correlation coefficients (r^2) derived from regression analysis of surface sediment proxies on the monthly average SST in the Canary Islands region. The SST data from January (1) to December (12) were based on an average of the years 1997 and 1998. Relative abundances of *G. ruber* (white) are indicated with squares, relative abundances of *G. bulloides* with rhombs and the TOC concentration with dots.

The good correlation between present day surface water characteristics and surface sediment properties is somewhat surprising, having in mind that in addition to the processes "dust input" and "preservation" (see above) displacement processes influence and alter the surface sediment composition. An important factor determining the surface sediment is the effect of bioturbation at the seafloor that leads to mixing of the sediment. The mixed layer in the Atlantic is about 2 to 12 cm thick depending on the organic carbon flux (Trauth et al., 1997). Consequently, the geochemical and micropaleontological characteristics of the surface sediments are averaged over thousands of years. Comparisons between the present hydrographical conditions and proxies within the sediment will therefore never produce ideal correlations. However, since Holocene climatic conditions were +/- stable during the last 6000 years in the marine environment (e.g. Sarnthein et al., 1982; Marret and Turon, 1994) and in the terrestrial environment (e.g. Lamb et al., 1989; Cheddadi et al., 1998), a comparison of the surface sediment composition to the present hydrography is reasonable.

In addition to bioturbation, turbidity currents at the seafloor and lateral advection within the intermediate and the deep nepheloid layers could transport allochthonous material to the site of interest. A strong influence of turbidity currents is known to occur at the submarine slopes of the western Canary Islands (Weaver and Thomson, 1993; Wynn et al., 2000). However, the effect of

turbidity currents influence is nearly negligible in the investigated sediments, since the core description (conducted shortly after recovery) did not indicate a strong turbidity influence with possibly one exception at site GeoB 6010-1 (see Fig. 3) (Neuer et al., 1997a, 2000; Wefer et al., 1997, 1999; Fischer et al., 1998).
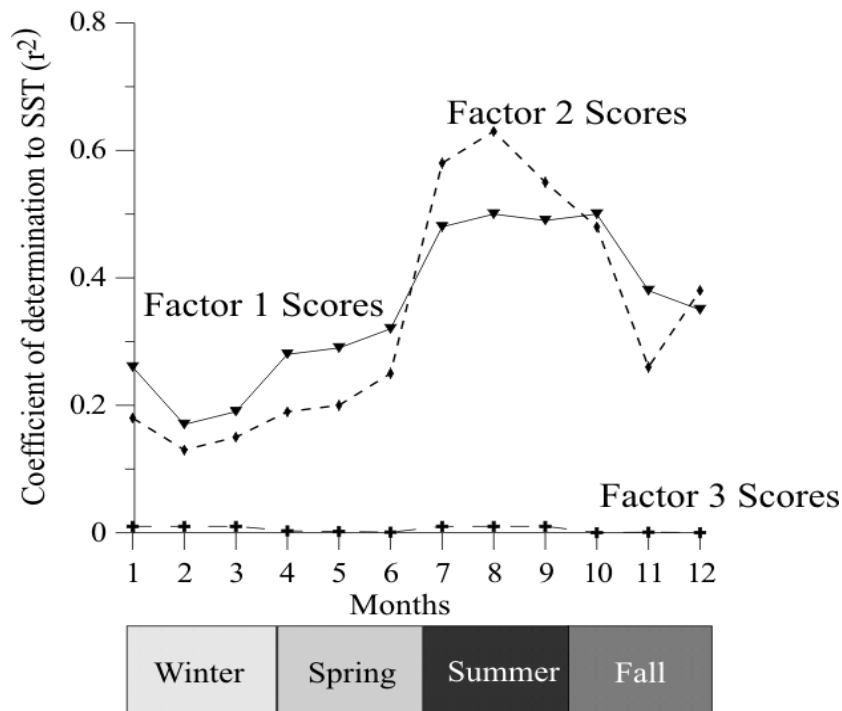

Figure 9: Correlation coefficients (r^2) derived from regression analysis of planktic foraminifera factor scores on the monthly average SST in the Canary Islands region. The SST data from January (1) to December (12) were based on an average of the years 1997 and 1998. Factor 1 ("warm-water factor") is presented with triangles, factor 2 ("upwelling/filament factor") with rhombs and factor 3 with crosses.

Much more difficult is it to discern the influence of lateral advection processes within the surface sediments. Sinking velocities of empty tests of planktic foraminifera are in the order of hundreds of meters per day (Fok-Pun and Komar, 1983; Takahashi and Bé, 1984) leading to deposition within days or weeks in water-depths ranging from 90 m to 4200 m. In this time a lateral transport of the sinking tests could lead to differences between living and sedimented assemblages of planktic foraminifera. This effect is much more pronounced within the diatom or the calcareous nannoplankton groups, since these organisms are mostly much smaller and thus have slower sinking speeds (Berger, 1976). North of the Canary Islands, sediment trap studies and a comparison of biogenic fluxes in sediment traps and surface sediments showed upwelling-derived particles to impact on the sedimentation far offshore (Neuer et al, 1997b; Ratmeyer et al, 1999; Freudenthal et al., in press). Accordingly, lateral advection influences not only the continental slope sedimentation, but has also a strong impact on the sediment accumulation and

the geochemical signature in the open ocean. However, most of the investigated proxies in this study indicated a well-established gradient in their spatial distribution from the upwelling-influenced coastal area towards the subtropical gyre domain. This points to the fact that in spite of strong lateral advection north of the Canary Islands the E-W productivity contrast is still reflected (probably smoothed) within the surface sediments.

Conclusions

Geochemical and microfossil data from surface sediments of the Canary Islands region mirror the high biomass and SST-gradient from the coast towards the oligotrophic subtropical gyre (Fig. 10). Despite the evidence of influence of lateral advection in the region, the surface sediment reflected the strong contrast between the upwelling influenced area and the subtropical gyre. A decrease in TOC, an increase in the C/N-ratio (if we assume that the terrigenous input is +/- constant in the Canary Islands region), decreasing numbers of benthic foraminifera and decreasing relative abundances of *G. bulloides,* and the opposite trend for *G. ruber* (white) were typical representatives of several valuable proxies mirroring the E-W-productivity gradient (Fig. 10). Factor analyses of the planktic foraminifera assemblage indicated three major factors in the Canary Islands region: A "warm-water factor" that characterised the subtropical water masses of the oligotrophic ocean, an "upwelling/filament factor" that clearly reflected the recent filament positions and a third "mixing-factor" that mixed the signatures of the first and the second factor populations together in an area between Cape Ghir and Cape Yubi. Multiple regressions showed a good correlation between chlorophyll concentration and the TOC content and between SST and the planktic foraminifera factor loadings (for factor 1 and 2).

Overall, the multiproxy approach used in this study reflected well the present day conditions in many details (e.g. a mixing zone between the capes and the subtropical gyre domain; islands-generated eddies in the shadow of the Canary Islands). The signals within the surface sediments are therefore good averages of the present day oceanographic conditions and can be applied for future paleoceanographic reconstructions.
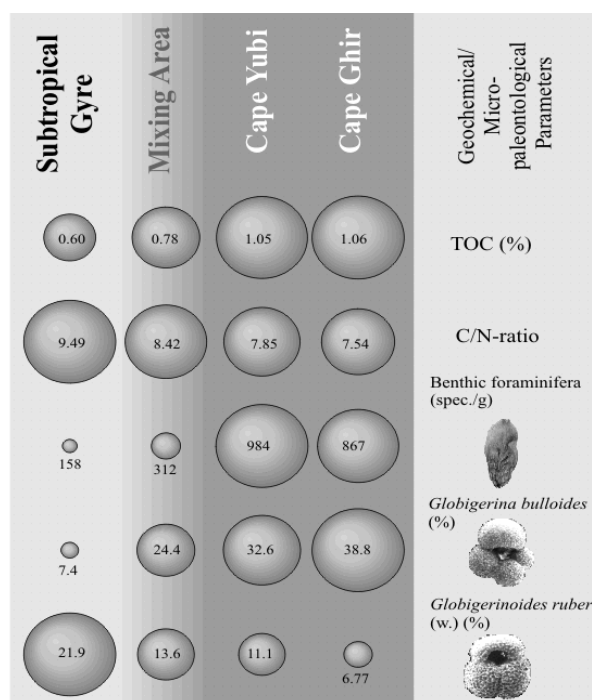
Figure 10: Schematic summary of the 3 domains in the research area of the Canary Islands region (the subtropical gyre, the filament areas off Cape Yubi and Cape Ghir and the mixing zone that is seasonally influenced by the two other areas) indicating in all proxies a well established zonal productivity gradient. The domains were derived from the planktic foraminifera factor analyses. Contents or percentages were mean values for each area.

Acknowledgements

References

Abrantes, F., 1988. Diatom assemblages as upwelling indicators in surface sediments in Portugal. Marine Geology 85, 15-39.

Abrantes, F., Winn, K., Sarnthein, M., 1994. Late Quaternary paleoproductivity variations in the NE and Equatorial Atlantic: diatom and C_{org} evidence. In: Zahn, R., Pedersen, T.F., Kaminski, M.A., Labeyrie, L. (Eds.), Carbon Cycling in the Glacial Oceans. 17, Springer-Verlag, Berlin, pp. 425-439.

Abrantes, F., Moita, M.T., 1999. Water column and recent sediment data on diatoms and coccolithophorids, off Portugal, confirm sediment record of upwelling events. Oceanologica Acta. 22, 67-84.

Abrantes, F., Meggers, H., Nave, S., Bollmann, J., Palma, S., Sprengel, C., Henderiks, J., Spies, A., Salgueiro, E., Moita, T., Neuer, S. this volume. Flux of microorganisms along a productivity gradient in the Canary Islands region (29°N): Implications for paleoreconstructions. submitted to Deep-Sea Research Part II.

Altabet, M.A., Francois, R., 1994. Sedimentary nitrogen isotopic ratio as a recorder for surface ocean nitrate utilization. Global Biogeochemical Cycles 8 (1), 103-116.

Arístegui, J., Sangrá, P., Hernández-León, S., Cantón, M., Hernández-Guerra, A., Kerling, J.L., 1994. Island-induced eddies in the Canary Islands. Deep-Sea Research Part I 41 (10), 1509-1525.

Arístegui, J., Tett, P., Hernández-Guerra, A., Basterretxea, G., Montero, M.F., Wild, K., Sangrá, P., Hernández-León, S., Cantón, M., Garcia-Braun, J.A., Pacheco, M., Barton, E.D., 1997. The influence of island-generated eddies on chlorophyll distribution: a study of mesoscale variation around Gran Canaria. Deep-Sea Research Part I 44 (1), 71-96.

Bárcena, M.A., Abrantes, F., 1998. Evidence of a high-productivity area off the coast of Málaga from studies of diatoms in surface sediments. Marine Micropaleontology 35, 91-103.

Barton, E.D., 1998. Eastern boundary of the North Atlantic: Northwest Africa and Iberia coastal segment. In: Robinson, A.R., Brink, K.H. (Eds.), The sea. 11, John Wiley & Sons, New York, pp. 633-657,

Battarbee, R., 1973. A new method for estimating absolute microfossil numbers with special reference to diatoms. Limnology Oceanography 18, 647-653.

Bé, A.W.H., Tolderlund, D.S., 1971. Distribution and ecology of living planktonic foraminifera in surface waters of the Atlantic and Indian Oceans. In: Funnell, B.M., Riedel, W.R. (Eds.), Micropaleontology of Oceans. Cambridge University Press, London: pp. 105-149.

Bé, A.W.H., 1977. An ecological, zoogeographic and taxonomic review of recent planktonic foraminifera. In: Ramsey, A.T.S. (Ed.), Oceanic Micropaleontology, Academic Press, London, pp.1-100.

Bergametti, G., Gomes, L., Coude-Gaussen, G., Rognon, P., Le Coustumer, M.-N., 1989. African dust observed over Canary Islands: Source-regions identification and transport pattern for some summer situations. Journal of Geophysical Research 94, 14855-14864.

Berger, W.H., 1976. Biogenous deep sea sediments: Production, preservation and interpretation. In: Riley, J.P., Chester, R. (Eds.), Chemical Oceanography. Academic Press, London, New York, San Francisco, pp. 265-389.

Berger, W.H., 1982. Increase of carbon dioxide in the atmosphere during deglaciation, the coral reef hypothesis. Naturwissenschaften 69, 87-88.

Berger, W.H., Keir, R.S., 1984. Glacial-Holocene changes in atmospheric CO_2 and the deep-sea record. In: Hansen, J.E., Takahashi, T. (Eds.), Climate processes and climate sensitivity. American Geophysical Union, Geophysical Monographs 29, Maurice Ewing Series, Washington DC, pp. 337-351.

Berger, W.H., Wefer, G., 1990. Export production: seasonality and intermittency, and paleoceanographic implications. Palaeogeography, Palaeoclimatology, Palaeoecology 89, 245-254.

Bertrand, P., Shimmield, G., Martinez, P., Grousset, F., Jorissen, F., Paterne, M., Pujol, C., Bouloubassi, I., Buat Menard, P., Peypouquet, J.-P., Beaufort, L., Sicre, M.-A., Lallier-Verges, E., Foster, J.M., Ternois, Y., and the other participants of the Sedorqua Program, 1996. The glacial ocean productivity hypothesis: the importance of regional temporal and spatial studies. Marine Geology 130, 1-9.

Brink, K.H., Abrantes, F., Bernal, P.A., Dugdale, R.C., Estrada, M., Hutchings, L., Jahnke, R.A., Müller, P.J., Smith, R.L., 1995. Group report: How do coastal upwelling systems operate as integrated physical, chemical, and biological systems and influence the geological record? The role of physical processes in defining the spatial structures of biological and chemical variables. In: Summerhayes, C.P., Emeis, K.C., Angel, M.V.,

Smith, R.L., Zeitschel, B., (Eds.), Upwelling in the Ocean: Modern Processes and Ancient Records. John Wiley and Sons Ltd., New York, pp. 103-124.

Broecker, W.S., 1982. Ocean chemistry during glacial time. Geochimica et Cosmochimica Acta 46, 1689-1705.

Cifelli, R., 1961. *Globigerina incompta*, a new species of pelagic foraminifera from the North Atlantic. Cushman Foundation Foraminiferal Research, Contributions 12, 83-86.

Cheddadi, R., Lamb, H.F. Guiot, J., van der Kaars, S., 1998. Holocene climatic change in Morocco: a quantitative reconstruction from pollen data. Climate Dynamics 14, 883-890.

Conan, S.M.-H. and Brummer, G.J.A., 2000. Fluxes of planktic foraminifera in response to monsoonal upwelling on the Somalia Basin margin. Deep-Sea Research Part II 47 (9-11), 2207-2227.

Coude-Gaussen, G., Rognon, P., Bergametti, G., Gomes, L. Strauss, B., Gros, J.M., Le Coustumer, M.N., 1987. Saharan dust on Fuerteventura Island (Canaries): Chemical and mineralogical characteristics, air mass trajectories, and probable sources. Journal of Geophysical Research 92, 9753-9771.

Dale, B., Fjellså, A., 1994. Dinoflagellate cysts as productivity indicators: state of the art, potential and limits. In: Zahn, R. (Ed.), Carbon cycling in the glacial ocean: constraints in the ocean's role in global change Springer-Verlag, Berlin, pp. 521-537.

Davenport, R., Neuer, S., Hernández-Guerra, A., Rueda, M.J., Llinas, O., Fischer, G., Wefer, G., 1999. Seasonal and interannual pigment concentration in the Canary Islands region from CZCS data and comparison with observations from the ESTOC. International Journal of Remote Sensing 20 (7), 1419-1433.

Dower, J., Freeland, H., Juniper, K., 1992. A strong biological response to oceanic flow past Cobb Seamount. Deep-Sea Research Part I, 39 (7-8), 1139-1145.

Fenner, J., 1982. Diatoms in the Eocene and Oligocene sediments off NW Africa, their stratigraphic and paleogeographic occurrences. Ph.D. Thesis, University of Kiel.

Fischer, G. and cruise participants, 1998. Report and preliminary results of FS "METEOR"-Cruise M 38/1, Las Palmas - Recife, 25.01.-01.03.1997. Berichte Fachbereich Geowissenschaften, Universität Bremen, 94, 178 pp.

Fok-Pun, L., Komar, P.D., 1983. Settling velocities of planktonic foraminifera: Density variations and shape effects. Journal of Foraminiferal Research 13, 60-68.

Freudenthal, T., Meggers, H., Moreno, A., Henderiks, J., Wefer, G., this volume. Variability of upwelling intensity and filament activity during the last 250 kyr. submitted to Deep-Sea Research Part II.

Freudenthal, T., Neuer, S., Meggers, H., Davenport, R., Wefer, G., in press. Influence of lateral particle advection and organic matter degradation on sediment accumulation and stable nitrogen isotope ratios along a productivity gradient in the Canary Islands region. Marine Geology, in press.

Ganssen, G., Lutze, G.F., 1982. The aragonite compensation depth at the northeastern Atlantic continental margin. „Meteor" Forschungs-Ergebnisse Reihe C 36, 57-59.

Ganssen, G., 1983. Dokumentation von küstennahem Auftrieb anhand stabiler Isotope in rezenten Foraminiferen vor Nordwest-Afrika. „Meteor" Forschungs-Ergebnisse Reihe C 37, 1-46.

Ganssen, G., Sarnthein, M., 1983. Stable isotope composition of foraminifers: The surface and bottom water record of coastal upwelling. In: Suess, E., Thiede, J. (Eds.), Coastal Upwelling. Its sediment record. Part A: Responses of the sedimentary regime to present coastal upwelling. NATO Conference Series, Series IV: Marine Science 10a, Plenum Press, New York and London, pp. 99-121.

Genin, A., Boehlert, G.W., 1985. Dynamics of temperature and chlorophyll structures above a seamount: an oceanic experiment. Journal of Marine Research, 43 (4), 907-924.

Giraudeau, J., 1993. Planktonic foraminferal assemblages in surface sediments from the southwest African continental margin. Marine Geology 110, 47-62.

Giraudeau, J., Rogers, J., 1994. Phytoplankton biomass and sea-surface temperature estimates from sea-bed distribution of nannofossils and planktonic foraminifera in the Benguela upwelling system. Micropaleontology 40 (3), 275-285.

Guichard, S., Jorissen, F., Bertrand, P., Gervais, A., Martinez, P., Peypouquet, J.-P., Pujol C., Vergnaud-Grazzini, C., 1997. Foraminifères benthiques et paléoproductivité: réflections sur une carotte de l´upwelling (NW african). Comptes Rendus Académie des Sciences, Serie II, Sciences de la terre et des planète / Earth & Planetary Sciences 325, 65-70.

Guichard, S., Jorissen, F., Peypouquet, J.-P., 1999. Late Quaternary benthic foraminiferal records testifying lateral variability of the Cape Blanc upwelling signal. Comptes Rendus Académie des Sciences, Serie II, Sciences de la terre et des planète / Earth & Planetary Sciences 329, 295-301.

Hagen, E., Zulicke, C. Feistel, R., 1996. Near-surface structures in the Cape Ghir filament off Morocco. Oceanologica Acta 19, 557-598.

Head, E.J.H., Harrison, W.G., Irwin, B.I., Horne, E.P.W., Li, W.K.W., 1996. Plankton dynamics and carbon flux in an area of upwelling off the coast of Morocco. Deep-Sea Research Part I 43 (11-12), 1713-1738.

Hebbeln, D., Marchant, M., Freudenthal, T., Wefer, G., 2000. Surface sediment distribution along the Chilean continental slope related to upwelling and productivity. Marine Geology 164, 119-137.

Hemleben, C., Spindler, M., Anderson, O.R., 1989. Modern Planktonic Foraminifera. Springer-Verlag, Berlin, 363 pp.

Henderiks, J., Freudenthal, T., Meggers, H., Abrantes, F., Nave, S., Salqueiro, E., Freitas, P., Bollmann, J., Thierstein, H.R., this volume. Glacial-interglacial variability of particle accumulation in the Canary Basin: A time-slice approach. submitted to Deep-Sea Research Part II.

Hernández-Guerra, A, Arístegui, J., Cantón, M., Nykjaer, L., 1993. Phytoplankton pigment patterns in the Canary Islands area as determined using Coastal Zone Colour Scanner data. International Journal of Remote Sensing 14, 1431-1437.

Hernández-Guerra, A., Nykjaer, L., 1997. Sea surface temperature variability off north-west Africa: 1981-1989. International Journal of Remote Sensing, 18, 2539-2558.

Hilbrecht, H., 1996. Extant planktic foraminifera and the physical environment in the Atlantic and Indian Oceans. Mitteilungen aus dem Geologischen Institut der Eidgen. Technischen Hochschule und der Universität Zürich, Neue Folge, 300, Zürich, 99 pp.

Holmes, M.E., Eichner, C., Struck, U., Wefer, G., 1999. Reconstruction of surface ocean nitrate utilization using stable nitrogen isotopes in sinking particles and sediments. In: Fischer, G., Wefer, G., (Eds.). Use of proxies in paleoceanography: Examples from the South Atlantic. Springer Verlag, Berlin, Heidelberg, 447-468.

Hooghiemstra, H., 1988. Palynological records from northwest African marine sediments: a general outline of the interpretation of the pollen signal. Phil. Trans. Royal Society London, 318, 431-449.

Imbrie, J., Kipp, N.G., 1971. A new micropaleontological method for quantitative paleoclimatology: Application to a late Pleistocene Caribbean core. In: Turekian, K.K. (Ed.), The Late Cenozoic Glacial Ages. Yale University Press, New Haven, pp. 71-181.

Jahnke, R.A., Shimmield, G.B., 1995. Particle flux and its conversion to the sediment record: coastal upwelling systems. In: Summerhayes, C.P., Emeis, K.C., Angel, M.V., Smith, R.L., Zeitschel, B., (Eds.), Upwelling in the Ocean: Modern Processes and Ancient Records. John Wiley and Sons Ltd., New York, pp. 83-100.

Johnson, J., Stevens, I., 2000. A fine resolution model of the eastern North Atlantic between the Azores, the Canary Islands and the Gibraltar Strait. Deep-Sea Research Part I 47, 875-899.

Kipp, N.G., 1976. New transfer function for estimating past sea-surface conditions from sea-bed distribution of planktonic foraminiferal assemblages in the North Atlantic. Geological Society of America, Memoir 145.

Koopmann, B., 1981. Sedimentation von Saharastaub im subtropischen Nordatlantik während der letzten 25.000 Jahre. „Meteor" Forschungs-Ergebnisse Reihe C 35, 23-59.

Lamb, H.F., Eicher, U., Switsur, V.R., 1989. An 18,000-year record of vegetation, lake-level and climatic change from Tigalmamine, Middle Atlas, Morocco. Journal of Biogeography 16, 65-74.

Levitus, S., Boyer, T. 1994. World Ocean Atlas 1994. Volume 4; Temperature. NOAA Atlas NESDIS 4, NOAA Washington DC, USA.

Lorius, C., Jouzel, J., Raynaud, D., Hansen, J., Le Treut, H. 1990. The ice-core record: climate sensitivity and future greenhouse warming. Nature 347, 139-145.

Lutze, G.F., 1980. Depth distribution of benthic foraminifera on the continental margin off NW Africa. „Meteor" Forschungs-Ergebnisse Reihe C 32, 31-80.

Lutze, G.F., Coulbourn, W.T., 1984. Recent benthic foraminifera from the continental margin of Northwest Africa: Community structure and distribution. Marine Micropaleontology 8, 361-401.

Marret, F., Turon, J.-L., 1994. Paleohydrology and paleoclimatology off Northwest Africa during the last glacial-interglacial transition and the Holocene: Palynological evidences. Marine Geology 118, 107-117.

Martin, J.H., Knauer, G.A., Karl, D.M., Broenkow, W.W. 1987. VERTEX: carbon cycling in the nortwest Pacific. Deep-Sea Research Part I 34 (2), 267-285.

Meggers, H., Baumann, K.H. 1997. Late Pliocene/Pleistocene calcareous plankton and paleoceanography of the North Atlantic. In: Hass, H.C., Kaminski, M.A. (Eds.), Contributions to the Micropaleontology and Paleoceanography of the Northern North Atlantic. Grzybowski Foundation Special Publication, pp. 39-50.

Meyers, P.A., 1994. Preservation of elemental and isotopic source identification of sedimentary organic matter. Chemical Geology 114, 289-302.

Milliman, J.D., Troy, P.J., Balch, W.M., Adams, A.K., Li, Y.-H., Mackenzie, F.T., 1999. Biologically mediated dissolution of calcium carbonate above the chemical lysocline? Deep-Sea Research Part I 46, 1653-1669.

Mittelstaedt, E., 1991. The ocean boundary along the Northwest African coast: circulation and oceanographic properties at the sea surface. Progress in Oceanography 26, 307-355.

Müller, P.J., Erlenkeuser, H., von Grafenstein, R., 1983. Glacial-interglacial cycles in oceanic productivity inferred from organic carbon contents in eastern North Atlantic sediment cores. In.: Thiede, J., Suess, E. (Eds.). Coastal Upwelling. Its sediment record. Part B: Sedimentary records of ancient coastal upwelling, NATO Conference Series, Series IV: Marine Science 10b, Plenum Press, New York, London, pp. 365-398.

Naidu, P.D., 1990. Distribution of upwelling index planktonic foraminifera in the sediments of the western continental margin of India. Oceanologica Acta 13, 327-333.

Neftel, A., Oeschger, H., Schwander, J., Stauffer, B., Zumbrunn, R., 1982. Ice core sample atmospheric CO_2 content during the past 40,000 yr. Nature 295, 220-223.

Neuer, S. and cruise participants, 1997a. Report and preliminary results of FS "Victor Hensen" Cruise 96/1, Bremerhaven - Bremerhaven, 10.1.- 4.3.1996. Berichte Fachbereich Geowissenschaften, Universität Bremen 96, 76 pp.

Neuer, S., Ratmeyer, V., Davenport, R., Fischer, G., Wefer, G. 1997b. Deep water particle flux in the Canary Islands region: seasonal trends in relation to long-term satellite derived pigment data and lateral sources. Deep-Sea Research Part I 8, 1451-1466.

Neuer, S. and cruise participants, 2000. Report and preliminary results of FS "METEOR"-Cruise M 45/5, Bremen - Las Palmas, 01.10.1999-03.11.1999. Berichte Fachbereich Geowissenschaften, Universität Bremen 163, 93 pp.

Nykjaer, L., van Camp, L., 1994. Seasonal and interannual variability of coastal upwelling along northwest Africa and Portugal from 1981 to 1991. Journal of Geophysical Research 9 (C7), 197-214.

Odate, T., Furuya, K. 1998. Well-developed subsurface chlorophyll maximum near Komahashi No. 2 seamount in the summer of 1991. Deep-Sea Research Part I 45 (10), 1595-1607.

Pflaumann, U., J. Duprat, C. Pujol and L.D. Labeyrie 1996. SIMMAX: A modern analog technique to deduce Atlantic sea surface temperatures from planktonic foraminifera in deep-sea sediments. Paleoceanography 11 (1), 15-35.

Ratmeyer, V., Fischer, G., Wefer, G. 1999. Lithogenic particle fluxes and grain size distributions in the deep ocean off northwest Africa: Implications for seasonal changes of aeolian dust input and downward transport. Deep-Sea Research Part I 46, 1289-1337.

Rühlemann, C., 1996. Akkumulation von Carbonat und organischem Kohlenstoff im tropischen Atlantik: Spätquartäre Produktivitäts-Variationen und ihre Steuerungsmechanismen. Berichte Fachbereich Geowissenschaften, Universität Bremen 84, 139 pp.

Sarnthein, M., Thiede, J., Pflaumann, U., Erlenkeuser, H., Fütterer, D., Koopmann, B., Lange, H., Seibold, E., 1982. Atmospheric and oceanic circulation patterns off Northwest Africa during the past 25 million years. In: von Rad, U., Hinz, K., Sarnthein, M., Seibold, E. (Eds.). Geology of the northwest african continental margin. Springer-Verlag, Berlin, Heidelberg, New York, pp. 545-604.

Sarnthein, M., Winn, K., Duplessy, J.-C., Fontugne, M.R., 1988. Global variations of surface ocean productivity in low and mid latitudes: influence of CO_2 reservoirs of the deep ocean and atmosphere during the last 21,000 years. Paleoceanography 3, 361-399.

Schlitzer, R., 2000. Ocean Data View. http://www.awi-bremerhaven.de/GPH/ODV, 2000, Version 4.0.15-2000.

Schrader, H.J., Schuette, G., 1968. Marine Diatoms. In: Emiliani, C., (Ed.), The Sea. 7, John Wiley and Sons, New York, pp. 1179-1231.

Siedler, G., Onken, R., 1996. Eastern Recirculation. In: Krauss, W., (Ed.), The Warmwatersphere of the North Atlantic Ocean. Gebrueder Bornträger, Berlin, Stuttgart, pp. 339-364.

Speth, P., Detlefsen, H., Sierts, H.-W., 1978. Meteorological influence on upwelling off Northwest Africa. Deutsche Hydrographische Zeitung 31 (3), 95-104.

Stramma, L., Siedler, G. 1988. Seasonal changes in the North Atlantic subtropical gyre. Journal of Geophysical Research 93 (C7), 8111-8118.

Suess, E., 1980. Particulate organic carbon flux in the oceans; surface productivity and oxygen utilization. Nature 288, 260-263.

Swan, A.R.H., Sandilands, M., 1995. Introduction to geological data analysis. Blackwell Science Ltd.

Takahashi, K., Bé, A.W.E., 1984. Planktonic foraminifera: factors controlling sinking speeds. Deep-Sea Research Part I 31, 1477-1500.

Targarona, J., Warnaar, J., Boessenkool, K.P., Brinkhuis, H., Canals, M., 1999. Recent dinoflagellate cyst distribution in the north Canary basin, NW Africa. Grana 38, 1-9.

Thiede, J., 1971. Planktonische Foraminiferen in Sedimenten vom ibero-marokkanischen Kontinentalrand. Ph.D.Thesis, Universität Kiel, 90 pp.

Thiede, J., 1975. Shell- and skeleton-producing plankton and nekton in the eastern North Atlantic Ocean. „Meteor" Forschungs-Ergebnisse Reihe C 20, 33-79.

Thunell, R.C., 1976. Optimum indices of calcium carbonate dissolution in deep-sea sediments. Geology 4, 525-528.

Trauth, M.H., Sarnthein, M., Arnold, M., 1997. Bioturbational mixing depth and carbon flux at the seafloor. Paleoceanography 12 (3), 517-526.

Tyson, R.V., 1995. Sedimentary organic matter. Organic facies and palynofacies. Chapman & Hall, London, 615 pp.

Van Camp, L., Nykjaer, L., Mittelstaedt, E., Schlittenhardt, P.. 1991. Upwelling and boundary circulation off northwest Africa as depicted by infrared and visible satellite observations. Progress in Oceanography 26, 357-402.

Wagner, T., Dupont, L.M., 1999. Terrestrial organic matter in marine sediments: Analytical approaches and eolian-marine records in the Central Equatorial Atlantic. In: Fischer, G., Wefer, G., (Eds.). Use of proxies in paleoceanography: Examples from the South Atlantic. Springer Verlag, Berlin, Heidelberg, 547-574.

Weaver, P.P.E., Thomson, J., 1993. Calculating erosion by deep-sea turbidity currents during inition and flow. Nature 364, 136-138.

Wefer, G. and cruise participants, 1997. Report and preliminary results of FS "METEOR"-Cruise M 37/1, Lisbon - Las Palmas, 04.12.-23.12.1996. Berichte Fachbereich Geowissenschaften, Universität Bremen, 90, 79 pp.

Wefer, G., Berger, W.H., Bijma, J., Fischer, G., 1999. Clues to ocean history: A brief overview of proxies. In: Fischer, G., Wefer, G., (Eds.). Use of proxies in paleoceanography: Examples from the South Atlantic. Springer Verlag, Berlin, Heidelberg, 1-68.

Wefer, G. and cruise participants, 1999. Report and preliminary results of FS "METEOR"-Cruise M 42/4, Las Palmas - Las Palmas – Viena do Castelo, 26.09.-26.10.1998. Berichte Fachbereich Geowissenschaften, Universität Bremen, 132, 104 pp.

Wynn, R.B., Masson, D.G., Stow, D.A.V., Weaver, P.P.E., 2000. Turbidity current sediment waves on the submarine slopes of the western Canary Islands. Marine Geology 163, 185-198.

Zonneveld, K.A.F., 1996. Palaeoclimatic and palaeo-ecologic changes in the Eastern Mediterranean and Arabian Sea regions during the last deglaciation: a palynological approach to land-sea correlation. Ph.D. Thesis, Utrecht University, Utrecht, 197 pp.

Provenance of present-day eolian dust collected off NW Africa

JAN-BEREND STUUT[1], MATTIAS ZABEL[1], VOLKER RATMEYER[1], PEER
HELMKE[1], ENNO SCHEFUß[1], GAUTE LAVIK[2] & RALPH SCHNEIDER[3]

1Research Center Ocean Margins (RCOM), Universität Bremen, Klagenfurterstraße 2,

 28334 Bremen, Germany

2Max Planck Institute for Marine Microbiology, Celciusstrasse 1, 28359 Bremen, Germany

3Département Géologie et Océanographie, UMR-CNRS 5805 EPOC,

 Université Bordeaux I, Avenue des Facultés, 33405 Talence, France

In preparation

Abstract

Atmospheric dust samples collected along a transect off the West African coast have been investigated for their physical (grain-size distribution), mineralogical, and chemical (major elements) composition. On the basis of these data the samples were grouped into sets of samples that most likely originated from the same source area. In addition, shipboard collected atmospheric meteorological data, modeled four-day back trajectories for each sampling day and location, and Total Ozone Mapping Spectrometer (TOMS) Aerosol Index (AI) data for the time period of dust collection (February-March 1998) were combined and used to reconstruct the sources of the groups of dust samples. On the basis of these data we were able to determine the provenance of the various dust samples. It appears that the bulk of the wind-blown sediments that are deposited in the proximal equatorial Atlantic ocean are transported in the lower-level ($\geq$ 900 HPa) NE trade-wind layer, which is a very dominant feature North of the Intertropical Convergence Zone (ITCZ). However, South of the surface expression of the ITCZ, down to 5°S, where surface winds are (South-)westerly, we still collected sediments that originated from the North and East, carried there by the NE trade-wind layer, as well as by Easterly winds from higher altitudes. The fact that the size of the wind-blown dust depends not only on the wind strength of the transporting agent but also on the distance to the source, hampers a direct

comparison of the dust's size distributions and measured wind strengths. However, a comparison between eolian dust and terrigenous sediments collected in three submarine sediment-traps off the West coast of NW Africa shows that knowledge of the composition of eolian dust is a prerequisite for the interpretation of paleo-records obtained from sediment cores in the equatorial Atlantic.

Danksagung

Mein Dank gilt Herrn Prof. Dr. Gerold Wefer für die Möglichkeit, diese Arbeit im Fachbereich Geowissenschaften durchzuführen. Besonderer Dank gebührt Herrn Prof. Dr. Venugopalan Ittekkot als zweitem Gutachter.

Dr. Gerhard Fischer danke ich für seine permanente Diskussionsbereitschaft und für die mir gewährte Freiheit bei der Ausgestaltung meiner Arbeit.

Oscar Romero und Susanne Neuer haben durch viele Ratschläge und konstruktive Kritik viel zur Motivation beigetragen, wofür ich ihnen besonders danken möchte.

Für Rat und Tat, privat und inhaltlich, danke ich Iris Kötter und Ingrid Zondervan.

Ich hätte mir keinen besseren Bürokollegen als Holger Kuhlmann vorstellen können, nicht nur wegen der leckeren Kuchen.

Viele nette Stunden durfte ich mit Boris Dorschel, Sebastian Meyer und Mahyar Mohtade-Hammadani verbringen.

Den Kollegen in der kleinen Dependance der Geologie, dem Gebäude "Zentralbereich", danke ich für die nette Arbeitsatmosphäre zu Land und zu Wasser.

Nicht zuletzt möchte ich den Mitbewohnern des Plendelhofs danken für Toleranz beim Pferdedienst.

Ganz besonderer Dank geht an Britta Munkes.